The author(s) shown below used Federal funds provided by the U.S. Department of Justice and prepared the following final report:

Document Title: Development of Tools for Smoke Residue and Deposition Analysis

Author: Siamak Riahi

Document No.:   238725

Date Received: May 2012

Award Number: 2007-DN-BX-K236

DEVELOPMENT OF TOOLS FOR SMOKE RESIDUE AND DEPOSITION ANALYSIS

by Siamak Riahi

B.S. in Mechanical Engineering, Feb 2000, Tehran Polytechnic University, Tehran, Iran
M.S. in Civil Engineering, May 2004, The George Washington University, Washington, DC

Dissertation submitted to

the Faculty of
The School of Engineering and Applied Science of
The George Washington University
in partial satisfaction of the requirements
for the degree of Doctor of Philosophy

May 16, 2011

Dissertation directed by

Dr. W. M. Kim Roddis
Professor and Chair of Civil and Environmental Engineering Department
and
Dr. Craig L. Beyler, Technical Director
Hughes Associates, Fire Science and Engineering

September 30, 2010

i

The School of Engineering and Applied Science of The George Washington University certifies that Siamak Riahi has passed the Final Examination for the degree of Doctor of Philosophy as of May 24, 2010. This is final and approved form of the dissertation.

Dissertation Research Committee:

W. M. Kim Roddis
Professor and Chair of Civil and Environmental Engineering
Dissertation Director

Craig L. Beyler
Technical Director, Hughes Associates, Inc.
Committee Member

Rumana Riffat
Professor of Civil and Environmental Engineering
Committee Member

Pedro F. Silva
Associate Professor of Civil and Environmental Engineering
Committee Member

Michael Keidar
Assistant Professor of Mechanical and Aerospace Engineering
Committee Member

Peter B. Sunderland
Assistant Professor of Fire Protection Engineering/University of Maryland
Committee Member

To my family for their unconditional love and support

ACKNOWLEDGEMENTS

First and foremost I want to thank both my research (Dr. Craig Beyler) and academic advisors (Dr. W. M. Kim Roddis). Their continuous advice, encouragement, and helpful comments kept me inspired and motivated to work on the project. It was an absolute honor to work with them. Not only did they realize the importance of this work but they also gave me an opportunity to work on this topic.

I want to thank my committee members, Dr. Rumana Riffat, Dr. Pedro Silva, Dr. Peter Sunderland, and Dr. Michael Keidar for their valuable comments that have helped me to improve my work.

I want to thank Dr. Judith Hartman at the United States Naval academy for her contribution. Also, I want to acknowledge the contribution of Dr. Jason Floyd and Dr. Javier Trelles at Hughes Associates. I want to thank Chris Mealy at Hughes Associates for helping me with all the experimental set up and very useful comments for the test procedure. Also I want to thank Ralph Ouellette and Brian Scheffey at Hughes Associates for constructing the parts for the tests apparatus. Special thanks go to William Rutkowski, Willard Morton, and Carl Behnke at SEAS machine shop for their effort in fabricating the parts for the experimental set up.

I want to thank my parents, Minoo and Akbar, for all their unconditional love and support. They have taught me to work hard and be patient in every aspect of life. My sister and her husband, Yasi and Arash, have supported me with their lovely advice. No matter how frustrated I was, my sister always found a way to cheer me up. All the transatlantic phone calls gave me enough confidence that my family has always believed in what I have done towards my education and career.

ABSTRACT

The physics of smoke deposition from a hot layer to a wall has been studied in a hood apparatus. The hood apparatus was specifically designed to study the smoke deposition based on thermophoresis experimentally and analytically in this work. For the first time the optical density method was used to measure the amount of smoke deposited on the surface. By using both gravimetric and optical measurement methods, the correlations between these values were determined for several fuels and test conditions. Solid phase mass specific extinction coefficient values were introduced for the first time for different fuels. Also, the optical properties of the smoke deposited on the surface were determined and compared to the smoke properties in the gas phase. An analytical thermophoretic smoke deposition model was developed using the measured smoke properties. This model is validated using experimental results from this work. This model is suitable for predicting smoke deposition due to a fire.

The physics of smoke deposition from a pan fire to the gypsum wall was studied for different fire sizes and fuels. The optical density method which was developed for the hood tests was used for the wall tests. Solid phase mass specific extinction coefficients were determined for the wall tests. Fire size effect was studied for the wall tests. The effect of fire size and change in the flow regime due to the fire size has been studied in this work. It was noticed that the effect from turbulence changes the values for the solid phase mass specific extinction coefficient. The optical density measurement method was applied to the digital images taken from the smoke patterns against the wall and processed with Image J and developed Matlab code.

Results from the smoke pattern predictions for the wall tests show a very good agreement between the digital images from the smoke deposition in the walls and the processed data. This can be used as a tool for fire investigation purposes to predict the smoke pattern and the amount

of smoke deposited on the surface which was exposed to the fire. The analytical smoke deposition model based on thermophoresis was validated with the experimental data from the wall tests. There was good agreement between the experimental data and the results from the model.

TABLE OF CONTENTS

LIST OF FIGURES

xv

LIST OF TABLES

CHAPTER 1 INTRODUCTION

1.1   Research Objectives

The objective of this research is to develop methods and scientific basis for the use of smoke deposition analysis as a forensic tool. This objective is pursued through a program of experimental and analytical work beginning with small scale testing and progressing through large scale. The basis and interpretive value of smoke deposition patterns is developed to provide a scientific basis for smoke pattern analysis that is lacking today.

Current forensic methods in fire investigation do not make use of the potentially rich information available in smoke deposited on surfaces. While smoke deposition pattern analysis is included in standard fire scene pattern analysis, the chemistry and physics of smoke deposition is poorly understood. This limits the interpretive value of smoke pattern analysis. This work provides scientifically based tools for use by fire investigators and forensic chemists for general fire investigations and arson investigations in particular.

The main components of this research are:

- Develop a scientific understanding of the physics and chemistry of smoke deposition to provide a scientific basis for smoke pattern analysis.
- Develop practical methods for documenting smoke deposition patterns and collecting smoke deposition samples.

1.2   Smoke Definition

The term smoke is defined as the smoke aerosol or condensed phase component of the products of combustion. Some include evolved gases in their definition of smoke (e.g., ASTM). Smoke aerosols vary widely in appearance and structure, from light colored, for droplets produced during smoldering combustion and fuel pyrolysis, to black, for solid, carbonaceous

particulate or soot produced during flaming combustion. A large fraction of the radiant energy emitted from a fire results from the blackbody emission from the soot in the flame [1]. Smoke particles are produced as a result of incomplete combustion and are usually observed to be in the form of spheres and agglomerates. It is also a general term that refers to impure carbon particles resulting from the incomplete combustion of a hydrocarbon. Smoke particles are normally characterized by their optical properties, size, shape, and chemical composition (hydrogen-carbon ratio). From a heat transfer viewpoint, radiation from a soot cloud is predominantly affected by the particle size distribution and can be considered independent of the chemical composition. Soot optical properties are relatively insensitive to temperature changes at elevated temperatures [2]. Deposition is the process in which aerosol particles collect or deposit themselves on solid surfaces. This process will decrease the concentration of particles in the air since they deposit on the surface.

1.3   Research Approach

A small scale apparatus was specifically designed to study certain elements for soot deposition based on thermophoresis, which is the main soot deposition mechanism in fire. The apparatus was designed to generate a smoke layer and all the measurements were performed in the presence of a smoke layer in the hood apparatus. In the hood experiments gravimetric measurements were performed on the filters to study the soot deposition on the surfaces. Optical properties of the smoke deposited on the filters from different fuels (PMMA, PP, gasoline, ABS, and fiber board) were studied and correlated to the gravimetric measurements performed on the filters. The analytical soot deposition model based on thermophoresis was used as a method to calculate the deposition in the hood tests and the model was validated with the experimental data from these tests.

Four important aspects of smoke deposition were addressed in:

- Gas phase mass specific extinction coefficient.

- Soot yields for different fuels used in the tests.

- Optical properties of deposited soot and solid phase mass specific extinction coefficient.

- Validation of thermophoresis analytical model with experimental data.

For the first time in the fire research, smoke has been collected and studied on glass filters attached to surfaces. Soot deposition has been studied for the first time by two different methods; gravimetric measurements and optically by using a gray scale.

The wall tests were performed in order to study the smoke deposition based on thermophoresis for large scale tests as well as studying the soot patterns to study the fire size, fuel source, etc. from the smoke damage evidence. A digital photography method was developed to study the optical properties of the surfaces which were exposed to smoke during the fire scenarios. All the optical properties of the smoke were correlated to the gravimetric measurements for the smoke deposition. Optical properties are representative of the gray scale values and the correlation between these values and gravimetric deposition values are the quantitative analysis on the surface which has been damaged by the smoke.

CHAPTER 2 LITERATURE REVIEW

2.1   Smoke Related Studies

Most research in the area of smoke has been focused on smoke as a dispersion of particles in the air that obscure vision [1]. The main focus has been on the generation of smoke particles, the size range for the agglomerates, and the visibility change due to smoke particles in the air.

There have been a few studies on the light scattering characteristics of smoke aerosols [3]. Weinert et al. measured the differential mass scattering cross section of various non-flaming and flaming fire generated smoke aerosols as well as nuisance aerosols created in the Fire Emulator/Detector Evaluator. Small diameter particles have been separated from large particles using the forward scattering information. The focus has been on the smoke particle size and different measurement methods.

Butler and Mulholland reviewed the characteristics of smoke aerosols in fire [4]. This paper presents the state of knowledge about smoke aerosol phenomena that affects smoke toxicity: soot generation, fractal structure of soot, agglomerate transport via thermophoresis, sedimentation, and diffusion, agglomerate growth through coagulation and condensation, and the potential for the aerosols to transport adsorbed or absorbed toxic gases or vapors into the lungs.

Tewarson [5] has studied properties including: heat of combustion, smoke yield, CO_2 yield, and CO yield for various fuels. Generation of heat and chemical compounds has also been studied [5].

Work on smoke deposition has been limited and focused on damage to electronic components by acid gases produced by burning polyvinylchloride (PVC) and other halogen containing polymers [6]. Quartz crystal microbalance (QCM) was used to measure the smoke deposition. Nuclear power plants rely on digital instrumentation and control systems; however,

the effects of abnormal environments such as fire and smoke on such systems are not known. There are no standard tests for smoke, but previous smoke exposure tests have shown that digital communications can be temporarily interrupted during a smoke exposure. Another concern is the long-term corrosion of metals exposed to the acidic gases produced by a cable fire. The smoke densities in these tests were high enough to cause changes in high impedance (resistance) circuits during exposure, but did not affect most of the other circuits. Conformal coatings and the characteristics of chip technologies should be considered when designing digital circuitry for nuclear power plant safety systems, which must be highly reliable under a variety of operating and accident conditions.

Reagor [7] has studied the smoke generation, impact, detection, and corrosivity. As a result of recent fires worldwide in telecommunications facilities, computer centers, research facilities, and naval vessels, there has been a growing realization that thermal damage may not be the most costly impact to electronic equipment. On the contrary, the real culprit may be exposure of equipment to the by-products of combustion or thermal decomposition. The short-term exposure of equipment to fire gases and smoke particulates can result in massive damage leading to extensive cleaning or replacement in order to regain service.

Ciro et al. [8] used a smoke deposition model based on previous analytical works [9–10]. The model they used successfully predicted smoke deposition on a cold rod placed in pool fire. In this application the smoke deposition based on thermophoresis was studied for an object immersed in the pool fire. In this work, smoke deposition was sufficiently thick that it could be measured directly. However, in most cases of interest the smoke deposition thickness is small and its thickness cannot be readily measured.

Computer fire models have not taken smoke deposition into account. Work done by Gottuk et al. [11] used NIST Fire Dynamics Simulator (FDS) to investigate smoke detector spacing for spaces with deep beam pockets and level ceilings. One configuration evaluated in this research was a corridor configuration with varying beam depth, beam spacing, corridor width, and ceiling height. A subset of the modeled corridor configurations was conducted with full-scale experiments to validate the findings of the modeling study. This work presented the findings of the experimental validation and new discoveries regarding smoke production and loss mechanisms that have an impact on modeling of fires and the spread of smoke. The temperature and velocity measurements along the corridor ceiling were consistent with the modeling results. However, the study showed that FDS significantly over-predicted smoke concentrations compared to the experiments. Exploratory findings indicate that soot deposits to the ceiling above the plume may be as high as 37 percent of the soot produced. Older versions of FDS did not account for this substantial soot loss.

Hamins et al. [12] experienced the same problem with using FDS, which did not correctly predict the optical properties of smoke due to not accounting for smoke deposition. Currently, a smoke deposition model is being added to FDS, and smoke deposition algorithms in the model are being evaluated.

There has also been exploratory work on smoke odor remediation using ozone [13]. Diffuse reflectance was used as a metric for smoke remediation.

Tsuchiya [14] characterized Volatile Organic Compounds (VOC's) and found them to be fuel dependent and their decay rates to correlate with boiling point. Since his concern was odors after fires, he measured gas phase organics up to a month after a fire. The persistence of higher boiling

6

point/less volatile organics demonstrated in his work is encouraging that signature organics adsorbed on soot particles are practical as a forensic tool.

It is widely understood in the general combustion community that soot formation proceeds through polycyclic aromatics (PAH) as intermediates. This results in PAH's found in soot produced by burning fuels. In polymer combustion, these same processes occur and pyrolysis products from the polymer also persistent as part of soluble organic fraction (SOF) of smokes [15].

In the forensic science community there has been some recognition of the possibility of identifying fuels based upon the analysis of smoke deposits. The analysis of smoke for the purpose of identifying the fuel burned (including accelerants) was pursued as early as 1994 [16]. They burned small quantities of 20 liquid fuels and 12 polymer fuels and deposited soot on to glass plates for subsequence analysis. Optical and electron microscopy, gas chromatography-(GC-FID), gas chromatography –mass spectrometry (GC-MS), and Pyrolysis-GC were used to characterize the smoke deposits.

De Vos et al.[17] sought to identify the presence of an accelerant in the vapor from carpet fires. They used charcoal strips suspended above the fire as a collection means. The charcoal was extracted with carbon disulphide and analyzed by GC-MS. They found the accelerants could be identified from the carpet polymers by the relative abundance of PAH's.

2.2   Smoke Deposition

The previously reviewed works in the smoke area demonstrate that there is a lack of fundamental research work on the smoke deposition. There are different smoke deposition mechanisms including: thermophoresis, diffusion, sedimentation, inertial impaction, and turbulent diffusion.

Thermophoresis

Thermophoresis is the term that describes the phenomenon in which particles, such as aerosols or smoke particles, in the presence of temperature gradient migrate from hot to cold regions. A common example of the phenomenon is the blackening of the glass globe of a kerosene lantern. The temperature gradient established between the flame and the globe drives the carbon particles produced in the combustion process towards the globe, where they deposit [18]. One of the practical applications of thermophoresis is in thermal precipitators, which are sometimes more effective than electrostatic precipitators in removing sub-micron particles from gas streams.

Thermophoretic velocity is the speed of the particles due to the thermophoretic force. This velocity is one of the dominant factors in soot deposition on the surface due to the thermophoresis mechanism.

The thermophoretic velocity [18–19] is given by

$$V_{th} = \frac{K_{th}\eta}{\rho T}\frac{\Delta T}{\Delta x} = \frac{k_{th}\eta}{\rho T}(\frac{dT}{dx}) \qquad \text{Equation 2-1}$$

Where η is the viscosity, and ρ, and T are the density and temperature at film temperature. Film temperature is the average between the wall and gas temperature at the surface deposition location. $\frac{\Delta T}{\Delta x}$, is the temperature gradient at the surface. K_{th} is the thermophoretic velocity coefficient (0.55). K_{th} is the thermophoretic velocity coefficient which is derived from the following correlations [20–21].

$$K_{th} = \frac{2C_s(\frac{k_g}{k_s} + C_t K_n)(1 + K_n(A_1 + A_2 \exp(\frac{-2A_3}{K_n})))}{(1 + 3C_m K_n)(1 + 2\frac{k_g}{k_s} + 2C_t K_n)} \qquad \text{Equation 2-2}$$

Where C_s, C_t and C_m are dimensionless coefficients that can be calculated from the kinetic theory [20–22]. A_1, A_2, and A_3 are also dimensionless constants. k_s, k_g are particle and gas thermal conductivity at film temperature. K_n, is Knudsen number which is defined as a dimensionless number as the ratio of the molecular mean free path length to a representative physical length scale (which is smoke particle diameter). Smoke particle diameters less than 1 micron [1] yield very large (10^{12}) Knudsen numbers. Figure 2-1 is a graphical explanation for Equation 2–2. The constants in Equation 2–2 are as follows:

$$\begin{cases} C_t = 2.18, C_m = 1.14, C_s = 1.17 \\ A_1 = 1.257, A_2 = 0.400, A_3 = 0.55 \end{cases}$$

Note that K_{th} approaches 0.55 as K_n (Knudsen number) becomes large. In addition as the particle size becomes small, the thermophoretic velocity coefficient becomes independent of k_g/k_s, which is the ratio of particle thermal conductivity to gas thermal conductivity
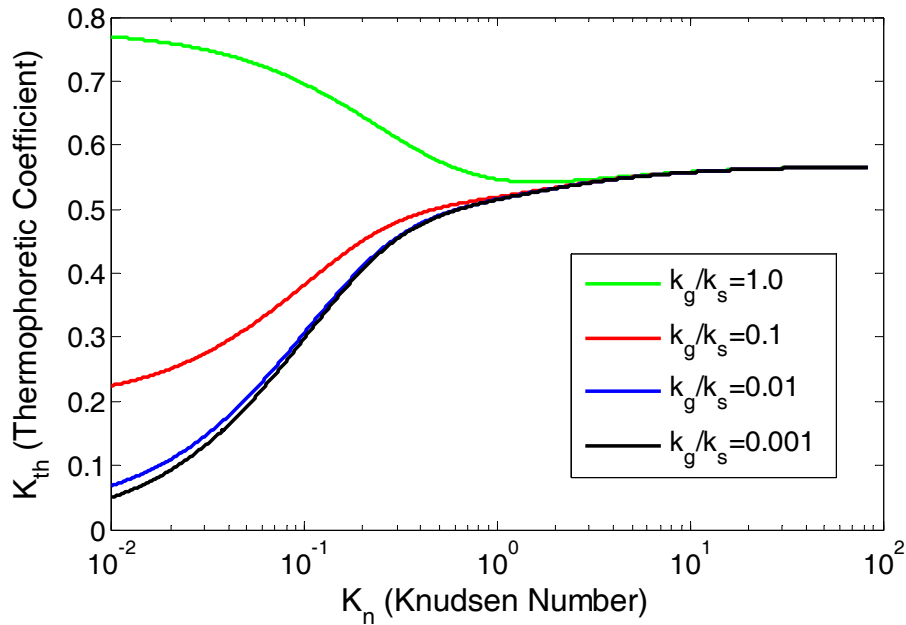
Figure 2-1: Thermophoretic velocity coefficient based on Equation 2-2

9

Thermophoretic velocity coefficient can be derived mathematically to prove that it should be close to 0.55.

$$K_{th} = \frac{2C_s(\frac{k_g}{k_s} + C_t K_n)(1 + K_n(A_1 + A_2 \exp(\frac{-2A_3}{K_n})))}{(1 + 3C_m K_n)(1 + 2\frac{k_g}{k_s} + 2C_t K_n)}$$

$$f(x) = 2C_s(\frac{k_g}{k_s} + C_t K_n)(1 + K_n(A_1 + A_2 \exp(\frac{-2A_3}{K_n}))) \quad g(x) = (1 + 3C_m K_n)(1 + 2\frac{k_g}{k_s} + 2C_t K_n)$$

$$\lim_{K_n \to \infty} K_{th} = \frac{\infty}{\infty} \qquad \text{Using the L'Hoptial's rule:}$$

$$\lim_{K_n \to \infty} K_{th} = \lim_{K_n \to \infty} \frac{f'(x)}{g'(x)}, \quad k = \frac{k_g}{k_s}, \quad \left\{ \begin{array}{l} C_t = 2.18, C_m = 1.14, C_s = 1.17 \\ A_1 = 1.257, A_2 = 0.400, A_3 = 0.55 \end{array} \right\}$$

$$f'(x) = 2C_s \left[A_1 k + A_2 k e^{\frac{-2A_3}{K_n}} + A_2 k(\frac{2A_3}{K_n})e^{\frac{-2A_3}{K_n}} + C_t + 2A_1 C_t K_n + A_2 C_t (2K_n)e^{\frac{-2A_3}{K_n}} + A_2 C_t (2A_3)e^{\frac{-2A_3}{K_n}} \right]$$

$$g'(x) = \left[2C_t + 3C_m + 6C_m k + 12C_m C_t K_n \right]$$

$$\lim_{K_n \to \infty} K_{th} = \lim_{K_n \to \infty} \frac{f'(x)}{g'(x)}$$

$$\lim_{K_n \to \infty} \frac{2C_s \left[A_1 k + A_2 k e^{\frac{-2A_3}{K_n}} + A_2 k(\frac{2A_3}{K_n})e^{\frac{-2A_3}{K_n}} + C_t + 2A_1 C_t K_n + A_2 C_t (2K_n)e^{\frac{-2A_3}{K_n}} + A_2 C_t (2A_3)e^{\frac{-2A_3}{K_n}} \right]}{\left[2C_t + 3C_m + 6C_m k + 12C_m C_t K_n \right]} = \frac{\infty}{\infty}$$

10

Using the L'Hopital's rule one more time:

$$\lim_{K_n \to \infty} K_{th} = \lim_{K_n \to \infty} \frac{f''(x)}{g''(x)}$$

$$f''(x) = 2C_s \left[A_2 k \left(\frac{2A_3}{K_n^2}\right) e^{\frac{-2A_3}{K_n}} - \frac{2A_3 A_2 k}{K_n^2} e^{\frac{-2A_3}{K_n}} + \left(\frac{2A_3 A_2 k}{K_n}\right)\left(\frac{2A_3}{K_n^2}\right) e^{\frac{-2A_3}{K_n}} 2A_1 C_t + 2A_2 C_t e^{\frac{-2A_3}{K_n}} + 2A_2 C_t K_n \left(\frac{2A_3}{K_n^2}\right) e^{\frac{-2A_3}{K_n}} \right.$$

$$\left. + 2A_2 A_3 C_t \left(\frac{2A_3}{K_n^2}\right) e^{\frac{-2A_3}{K_n}} \right] \quad g''(x) = \left[12 C_m C_t \right]$$

$$\lim_{K_n \to \infty} K_{th} = \lim_{K_n \to \infty} \frac{f''(x)}{g''(x)} = \frac{2C_s(2C_t A_1 + 2C_t A_2)}{12 C_m C_t} = \frac{4C_s C_t (A_1 + A_2)}{12 C_m C_t} = \frac{C_s(A1 + A2)}{3Cm}$$

$$K_{th} = \frac{1.17(1.257 + 0.4)}{3(1.14)} = 0.5668 \text{ (Approximately 0.55)}$$

Diffusion

Small particles suspended in a fluid will have a random motion resulting from the fluctuating forces exerted on them by the surrounding molecules. The motion was reported in 1827 by Robert Brown, who made the first detailed studies. As a result of particle's random motion, there is a net migration of particles from regions of high to low concentration, a process known as diffusion [23]. When gaseous molecules in motion hit a wall, the molecules experience a reaction force and rebound. This force is called the gas pressure. In the case of aerosols, when particles hit a wall, they can adhere to the surface. This phenomenon is deposition. Because of particle deposition, the concentrations very close to the wall surface are zero. According to Fick's first law of diffusion, the particles in the higher concentration area move to lower concentration area

11

by diffusion [24]. By continuous diffusive deposition, the particle concentration of the aerosol decreases. The deposition velocity due to diffusion is defined as follows:

If the particles move in y direction and the deposition surface is x-z plane, the velocity due to diffusion is defined as:

$$v_d = \frac{\phi_{y=y_0}}{n(x, y_1, z, t)} \qquad \text{Equation 2-3}$$

Where ϕ is the deposition flux. Φ has the unit of mass per area per time or particle number per area per time (particle number deposited/ cm^2 sec). The deposition flux has been measured at the surface $y=y_0$. n is the concentration at the point (x, y_1, z) and time t. In three dimensional particle deposition, the deposition velocity has three components, one for each direction. If the deposition flux is measured in units of mass per volume and the concentration is measured in units of mass per volume, then the ratio, v_d has units of length per time which is the unit of the velocity. It needs to be noted that the deposition velocity does not represent any velocity of the particles or the flow but instead represents an efficiency of deposition.

Sedimentation

Sedimentation is the tendency for particles in suspension or molecules in solution to settle out of the fluid in which they are entrained, and come to rest against a wall [23]. This is due to their motion through the fluid in response to the forces acting on them. These forces can be due to gravity, centrifugal acceleration, or electromagnetism.

In sedimentation deposition, the applied force accelerates the particles to a terminal velocity, $v_{terminal}$, at which the applied force is exactly canceled by an opposing drag force. For small particles with low velocity, the drag force varies linearly with the terminal velocity, i.e., $F_{drag} = f\, v_{terminal}$, where f depends only on the properties of the particle and the surrounding fluid.

Similarly, the applied force generally varies linearly with some coupling constant (denoted here as q) that depends only on the properties of the particle, $F_{app} = q\, E_{app}$. Hence, it is generally possible to define a sedimentation coefficient $s = q/f$ that depends only on the properties of the particle and the surrounding fluid. Measurements can reveal underlying properties of the particle. In many cases, the motion of the particles is blocked by a hard boundary; the resulting accumulation of particles at the boundary is called sediment. The concentration of particles at the boundary is opposed by the diffusion of the particles.

The sedimentation of particles happens under different forces including: gravity and centrifugal forces. Particles with a charge or dipole moment sediment by an electric field or electric field gradient, respectively. These processes are called electrophoresis and dielectrophoresis.

Inertial Impaction

Inertial impaction deposition occurs when particles do not follow the motion of accelerating gas due to their inertia. Inertial deposition of particles is an important mechanism of filtration [23]. When the flow moves round a fiber the particles start moving relative to the gas, and may deposit on the fiber. If the conditions are constant, there is a certain limiting trajectory separating the trajectories of those particles which are captured from the trajectories of particles which miss the fiber without being captured. The efficiency of inertial deposition E_I is defined as the ratio of the number of captured particles to the number of particles which would be captured if the particles moved permanently in a linear direction. This target efficiency is expressed by

$$E_I = \frac{h}{a}$$

Where h is the distance of the limiting trajectory at infinity from the axis of flow. This quantity has sometimes been referred as the effective diameter or radius of the fiber.

Turbulent Diffusion

In fluid dynamics, turbulence or turbulent flow is a fluid regime characterized by chaotic, stochastic property changes [23]. This includes low momentum diffusion, high momentum convection, and rapid variation of pressure and velocity in space and time. Turbulent diffusion is usually described by a turbulent diffusion coefficient. This turbulent diffusion coefficient is defined in a phenomenological sense, by analogy with the molecular diffusivities, but it does not have a true physical meaning, being dependent on the flow conditions, and is not a property of the fluid itself. In addition, the turbulent diffusivity concept assumes a constitutive relation between a turbulent flux and the gradient of a mean variable similar to the relation between fluxes and gradient that exists for molecular transport. Deposition due to turbulent diffusion occurs when turbulent eddies in the air transfer particles which can collide.

Butler and Mulholland [4] presented the current state of knowledge about smoke aerosol phenomena that affects smoke toxicity: soot generation, fractal structure of soot, agglomerate transport via thermophoresis, sedimentation, diffusion, agglomerate growth through coagulation and condensation, and the potential for the aerosols to transport adsorbed or absorbed toxic gases or vapors into the lungs. This research is focused on the deposition on thermophoresis which is the dominant smoke deposition mechanism.

Table 2-1: Comparison of calculated particle deposition modes [4]

Particle Diameter, μm	Thermophoresis	Diffusion	Sedimentation
0.01	2.8×10^6	2.6×10^5	6.7×10^2
0.1	2.0×10^6	2.9×10^4	8.6×10^3
1.0	1.3×10^6	5.9×10^3	3.5×10^5
10.0	7.8×10^5	1.7×10^3	3.1×10^7

Particles sticking to a 1 cm^2 surface during a 100seconds period for a suspended particle density of 10^6 particles/cm^3.

Table 2-1 shows the particle deposition modes for different particle sizes. It is evident that for smaller particles the number of the particles deposited due to thermophoresis is higher than the particles deposited due to diffusion. Also, number of the particles deposited due to sedimentation is less than both thermophoresis and diffusion mechanisms. By increasing the particle size the sedimentation deposition mechanism will be more dominant than thermophoresis and diffusion. Deposition due to sedimentation occurs due to the tendency of the particle to settle out from the fluid and come to rest. By having larger particles in the fluid the effectiveness of deposition due to sedimentation will increase. According to the discussions and analysis based on Table 2-1, the most dominant mechanism for the smoke particles deposition is thermophoresis and the main focus of this work is studying the smoke deposition based on thermophoresis.

CHAPTER 3 EXPERIMENTAL METHODS

Experiments were done in two different apparatus: first fire beneath a hood and second fire against a gypsum wall.

3.1   Hood Experiments

The main purpose of the small scale hood apparatus experiments was to study smoke deposition based on the thermophoresis mechanism in the presence of a smoke layer. In compartment fires, the smoke layer in the enclosure has a significant effect on smoke deposition to the walls and surfaces. Smoke layer height in the hood apparatus was controlled by changing the exhaust rate. By design, the smoke properties at each elevation within the smoke layer were uniform. Necessary measurements included gas and wall temperatures, smoke concentration, total heat flux, and radiative heat flux.

3.1.1   Hood Test Apparatus

The small scale hood apparatus consisted of a steel frame (0.6 m x 0.6 m x 0.9 m high) with walls of inorganic fiber board that is manufactured by Fiberfrax. Fiberfrax Duraboard is a family of rigid, high temperature ceramic fiber boards manufactured in a wet forming process using Fiberfrax alumina-silica fibers and binders. HD board (0.5 inch) was used as wall material and its properties are presented in Table 3-1.

Table 3-1: Properties of the Fiberfrax Duraboard

Properties	HD Duraboard
Nominal density (kg/m^3)	258
Temperature grade (º C)	1260
Product melting point (º C)	1760
Recommended operating temperature (º C)	1149
Color	Cream/white
Thickness	0.013 m

16

An exhaust plenum on the right side of the main chamber was connected to a duct. (0.45 m x 0.45 m x 0.31 m) (L x W x H).The exhaust plenum kept the smoke layer interface at a set level below all measurement locations. Figure 3-1 shows the front view of the hood apparatus and the equipment used for the measurements in the hood.

Wall mounted glass filters (9 cm diameter) were used to collect smoke at low and high locations (54 cm and 76 cm from the base of hood). Fischer brand glass filters with Grade G6 were used for these tests. The diameter of the filters was 90 mm and their thickness was 0.32 mm. Because of their white color, it is easy to measure the surface optical density after exposure to smoke. In addition, smoke deposition was gravimetrically measured on the filters. Figure 3-2 shows a glass filter used in the hood tests.
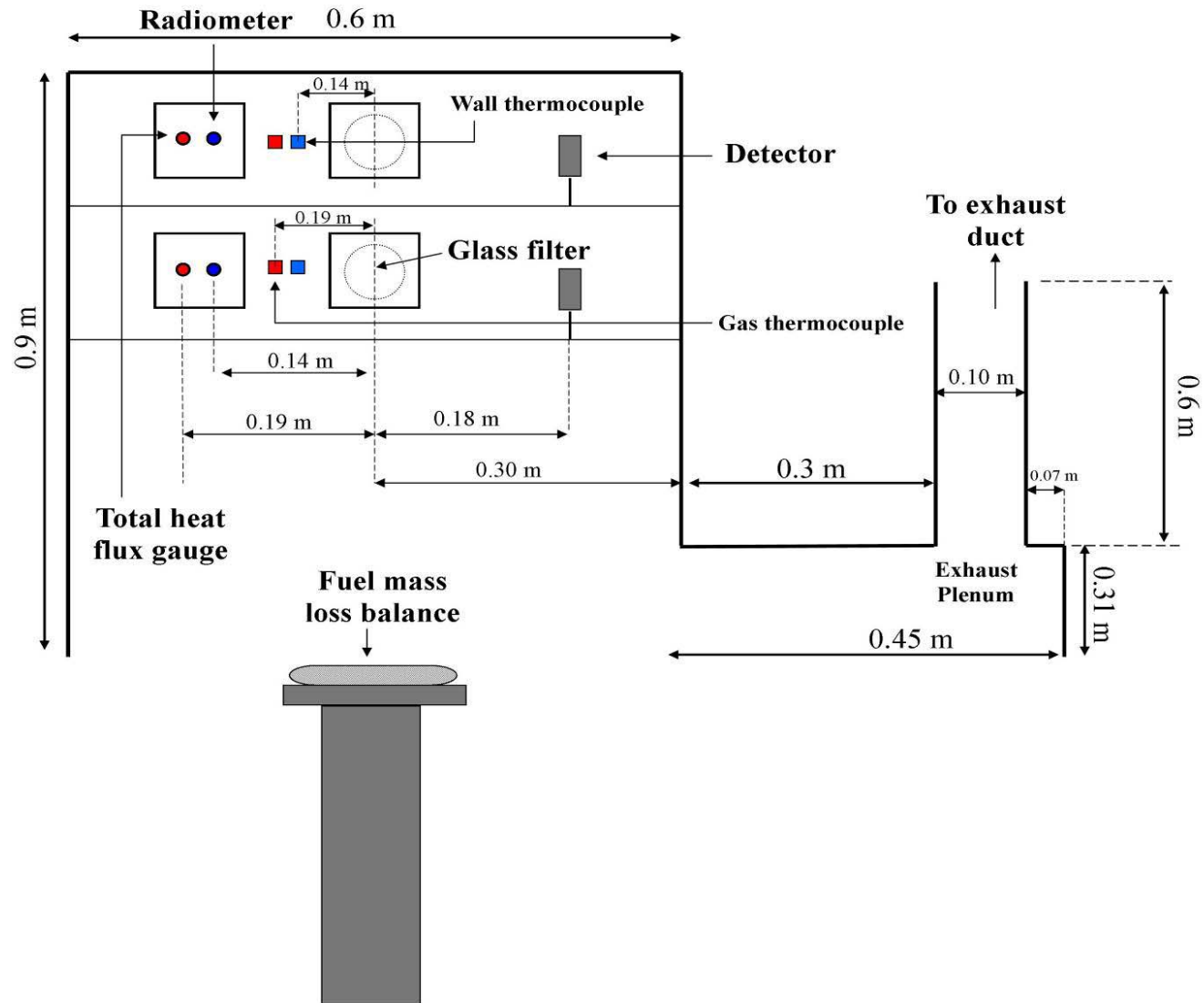
Figure 3-1: Small scale hood apparatus front view

Figure 3-2: Fisher brand glass filter (G6) used in the hood tests

Glass filters were mounted on a sample holder, constructed of wall material (HD Duraboard) with a metal frame around it. The metal frame was made of galvanized steel with a thickness of 0.8 mm. The filters were mounted on the sample holders using 8 small pins (10 mm long) around the circumference of the filter. These pins kept the filters in place and the pins were flush to the wall material. If the filters are not flush to the wall material, smoke will deposit on the wall material beneath the filter and the smoke deposition measurements will not be accurate.
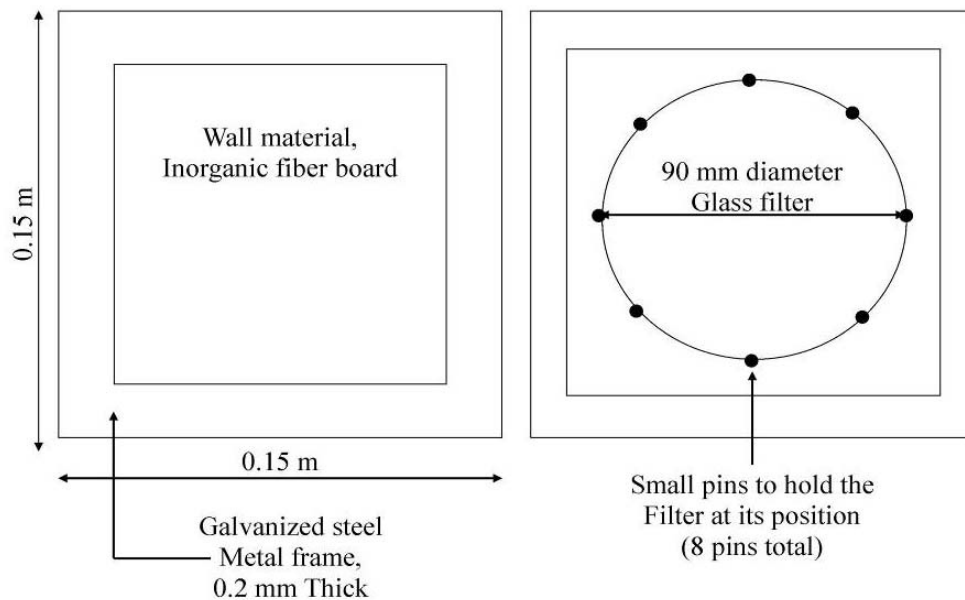
Figure 3-3: Front and back side of the filter holder

Figure 3-3 and Figure 3-4 show the front and back side of the filter holder and the installation
method which was used for the filters on the filter holder.

Figure 3-4: Filter installation

A thermocouple tree was mounted in the corner of the hood (0.1 m from the left and 0.1 m
from the back side of the hood apparatus). Thermocouples were five inches apart and total of
eighteen thermocouples were used. All the thermocouples were bare bead, K type, and 24 gauge.

Heat flux gauges and radiometers were used next to each glass filter to measure the total and
radiative heat fluxes (19 cm and 14 cm from the filters as shown in Figure 3-1).

Total heat flux was measured by using a Schmidt-Boelter total heat flux gauge. The
temperature of the gauge was kept constant using water to cool the gauge. The heat flux gauges
were calibrated by the manufacturer and the calibration curve specifies the relation between the
voltage signal and the heat flux. Full scale range for the heat flux gauges was 50 kW/m^2. Figure
3-5 shows a picture of a Schmidt-Boelter heat flux gauge used in the hood apparatus.

Figure 3-5: Schmidt-Boelter heat flux gauge

The Schmidt-Boelter radiometer operates on the same as a total heat flux gauge. The radiometer has a window made of sapphire which needs to be kept clean of smoke deposition during the test. In order to avoid deposition on this window, a purge air line is used in the Schmidt-Boelter radiometer. Calibration sheets were provided by the manufacturer for the radiometers. Full scale range for the radiometers was $10kW/m^2$. Figure 3-6 shows a picture of a Schmidt-Boelter radiometer.

Figure 3-6: Schmidt-Boelter radiometer

Gas and wall temperatures were measured using K type, bare bead, 24 gauge thermocouples. Thermocouples were mounted next to each filter (7.6 cm and 5 cm from the filters as shown in Figure 3-1). The gas thermocouple was 2.0 cm away from the wall material. The wall thermocouple was mounted by bending it towards the wall such that the thermocouple bead was in contact with wall surface. The thermocouple was fixed in the location by using the tension

behind the thermocouple wire. Figure 3-7 shows a schematic of thermocouple installation for both gas and wall thermocouples.
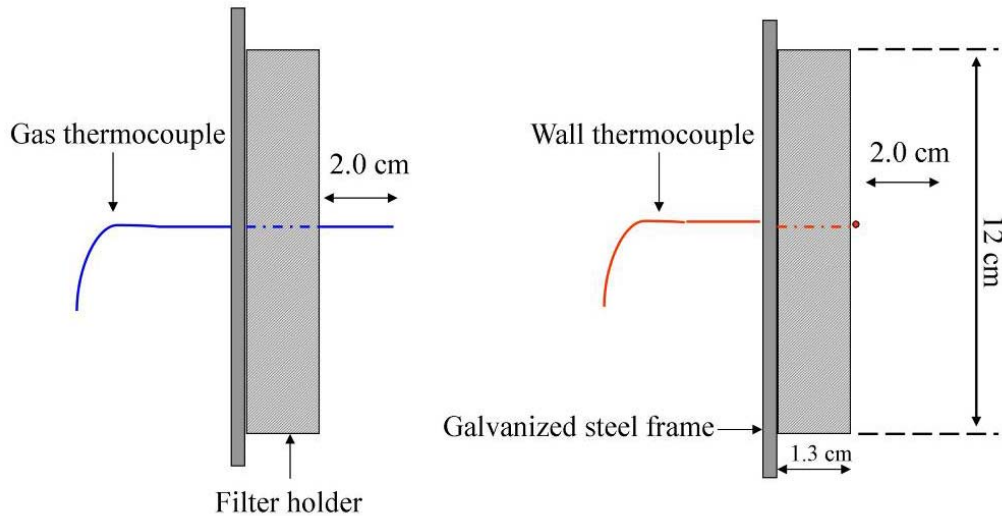
Figure 3-7: Gas and wall thermocouple installation

Optical density of smoke was measured using 4 mW, Coherent, HE NE a laser (wavelength 632.8 nm) across the hood at the same elevation as the glass filters were mounted (18 cm from the filters). Figure 3-8 shows a picture of the laser which was used in the hood apparatus as well as the exhaust duct.
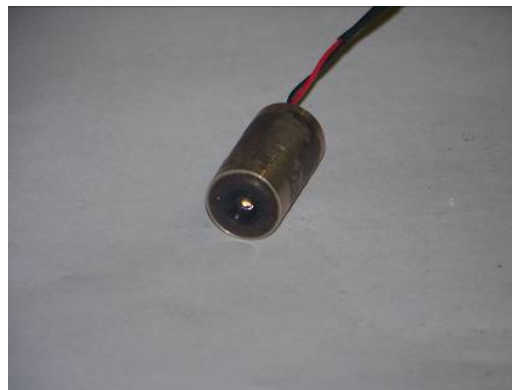
Figure 3-8: Laser used in the hood apparatus for smoke concentration measurement

Detectors (Thorlabs PDA 36A) used in the hood had the following specification; low-noise, wide band amplifiers, wavelength ranges from 150 to 4800 nm, bandwidth up to 150 MHz,

High-Speed PIN photodiodes, 0 to 10 V output. The detectors had a variable gain for voltage output which could be varied from 1 to 10. Figure 3-9 shows a picture of the detector.

Figure 3-9: Detector used in the hood apparatus for smoke concentration measurement

Lasers were mounted by using a variable angle stand from Coherent (0221-448-00). Detectors were mounted by using stainless steel posts. Figure 3-10 shows the detector installation.

Figure 3-10: Detector installation by using stainless steel posts

The installation of the laser extinction measurement system in the hood apparatus was designed to measure smoke concentration at both high and low locations. A glass piece (10 mm thick) was attached to a copper tube. (25 mm diameter, 50 mm length) and the laser and detector were

attached to the other side of a glass piece. Air was used with a low flow rate (0.05 L/min) to avoid smoke deposition on the surface of glass piece which was exposed to smoke. Figure 3-11 and Figure 3-12 show the laser and detector installation in the hood apparatus.
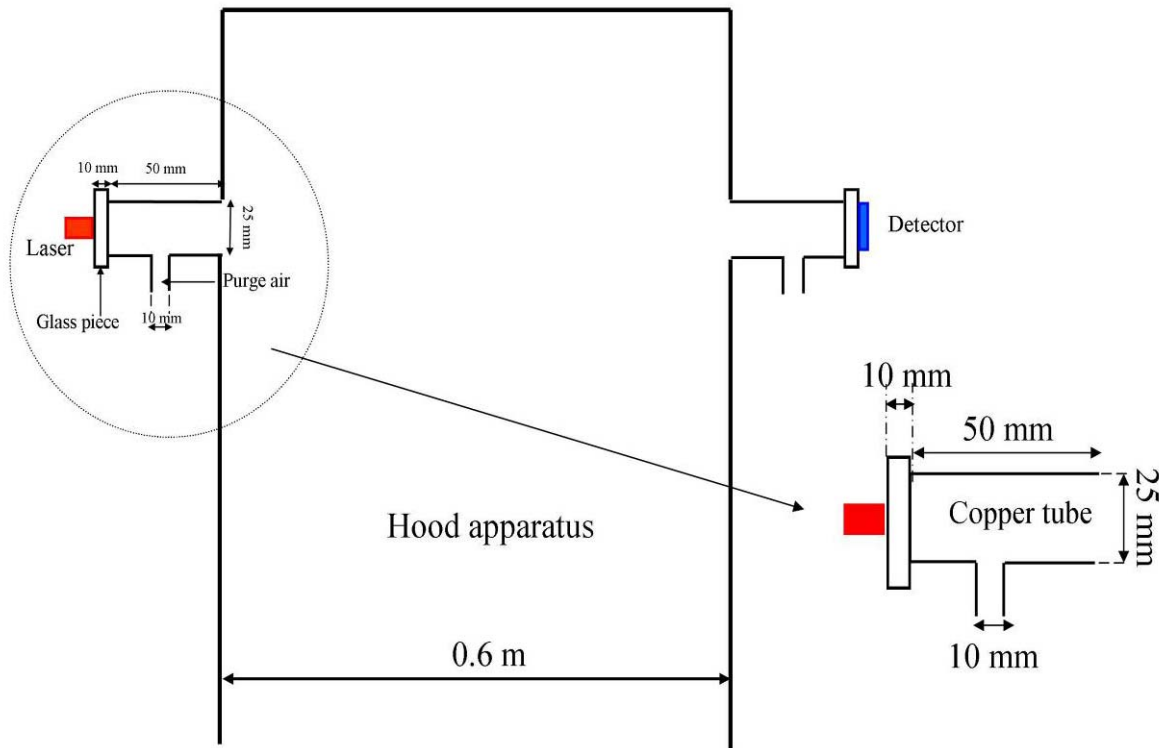
Figure 3-11: Laser and detector installation in the hood apparatus for smoke concentration measurements

Figure 3-12: Detector with purge air installation

Exhaust rate was controlled by use of orifice plates as well as controlling the blower speed. Orifice plates were made of stainless steel with 1 mm thickness. Exhaust flow rate calculations were performed based on ASME PTC 19.5-2004 code. Pressure difference was measured before

and after the orifice plate and pressure taps were located at 10 cm upstream and 2 cm downstream of the orifice plate. The pressure was measured using a Setra pressure gauge, model 264, 0.5 " WC, 0.5 VDC output as shown in Figure 3-15. The equations used in the ASME code for flow measurement are valid for a certain range of Reynolds number. Since the flow in the exhaust duct was laminar, the flow rate equations were modified. Three different orifice plates (3/4", 1 ¼", 2 ¼") with square edges were used in the hood tests to achieve different exhaust flow rates.

In order to find the modified flow rate equations the following tests were performed. A plastic cylinder (1meter diameter, 10 meter long (7.85 m^3)) was made and filled with the exhaust from the duct. The cylinder, a collapsed flexible plastic tube, unrolled as it was filled. The plastic cylinder's volume was constant and the filling time for the cylinder was measured with a stop watch. Flow rates for each orifice plate were measured three times before changing the flow rate by changing the blower's speed. Full scale range on the blower (Dayton, 4YJ33) was 326 CFM. Figure 3-13 shows a picture of the blower used in the hood apparatus.

Figure 3-13: Blower used in the hood apparatus
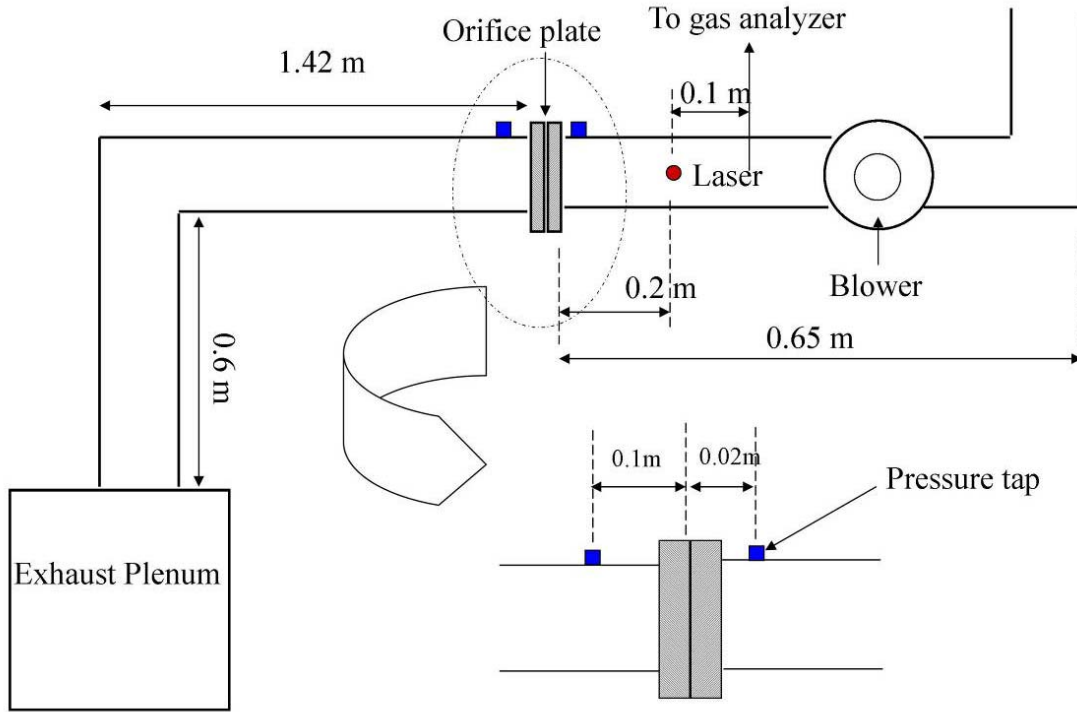
Figure 3-14: Exhaust duct
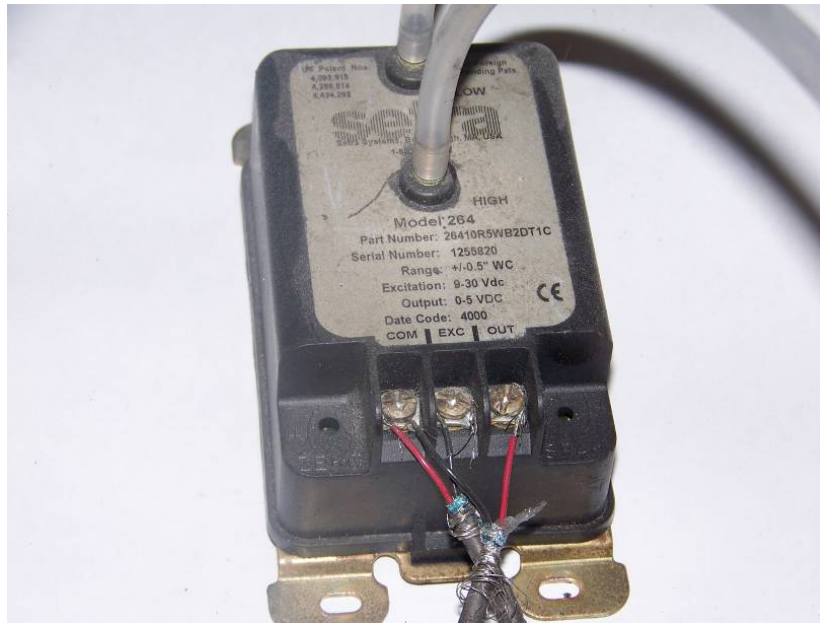
Figure 3-15: Pressure transducer used for flow measurement in the exhaust duct

26
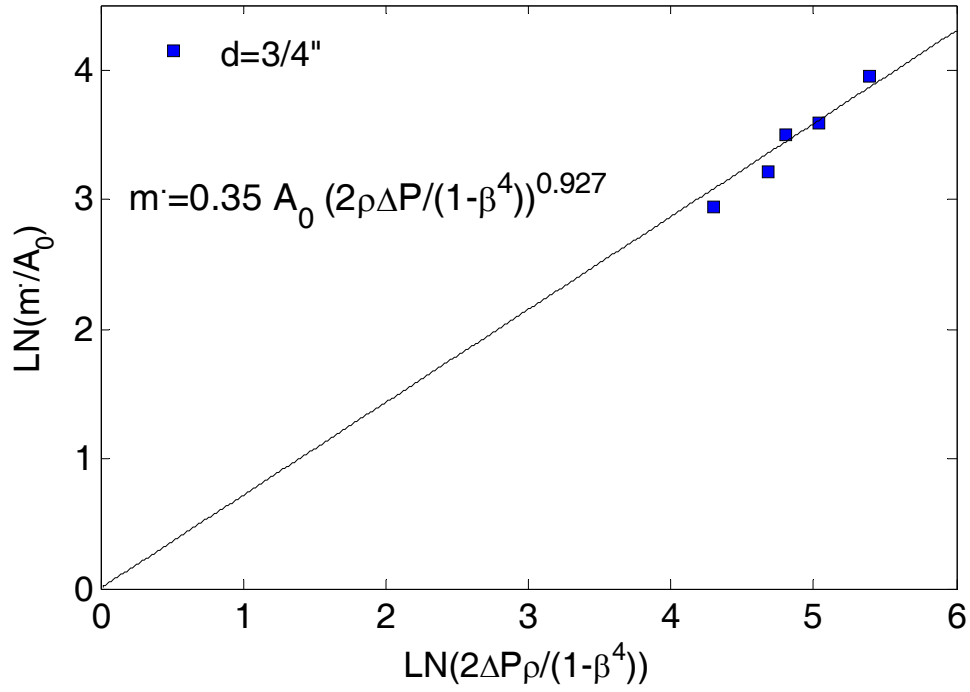
Figure 3-16: Mass flow rate for ¾ " orifice plate
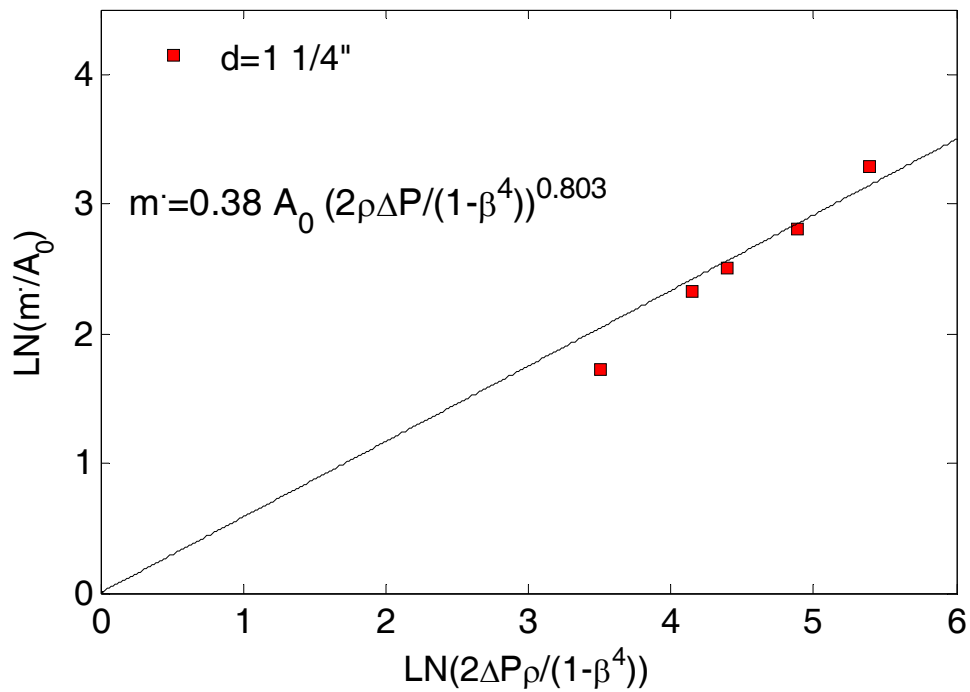
Figure 3-17: Mass flow rate for 1 ¼ " orifice plate
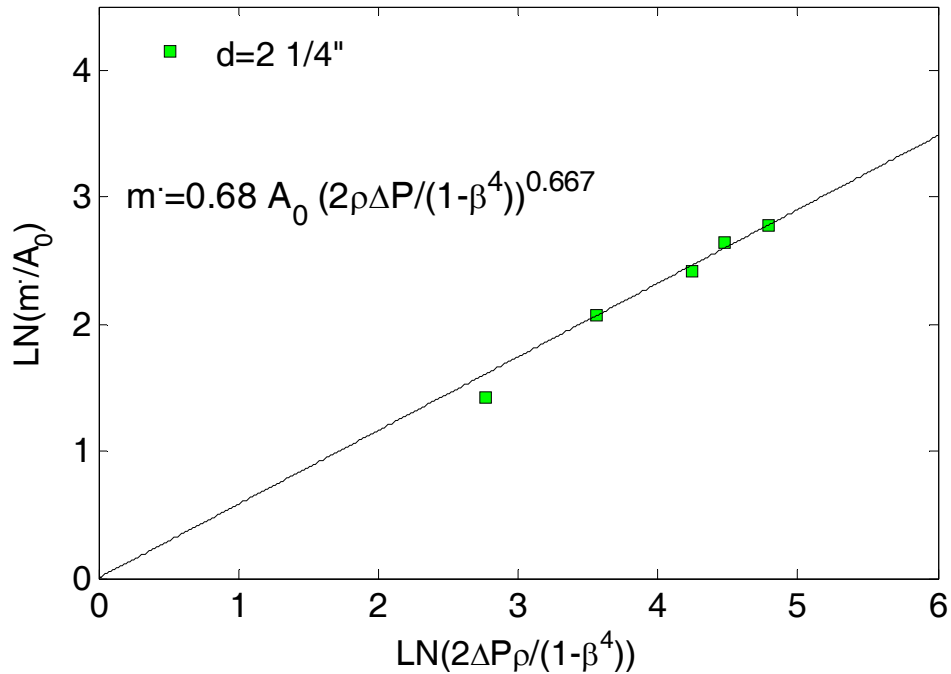
Figure 3-18: Mass flow rate for 2 ¼" orifice plate

Figure 3-16, Figure 3-17, Figure 3-18 and show the equations for calculating the exhaust flow rate for the different orifice plate sizes.

The parameters used for the mass flow rate equations were:

$\dot{m}$, mass flow rate (kg/s)

ΔP, pressure difference (kPa)

ρ, density (kg/m^3)

β, the ratio of the orifice plate diameter to duct diameter (d/D)

A_0, orifice plate area (m^2)

Smoke concentration was measured in the duct using the same type laser and detector. Measurement of O_2, CO_2, and CO concentrations of the exhaust were made at the end of the exhaust duct. Exhaust samples were extracted (0.3 m from the orifice plate) and sent to the gas analyzers.

A Servonex 4100 gas purity analyzer was used to measure O_2 concentration. Its accuracy was ¼ % full scale. A Horiba VA-3000 analyzer was used to measure CO_2 and CO concentrations. The accuracy of the analyzer was ½ % full scale. The measurement ranges for each gas are as follows:

O_2 0-20.95 %

CO_2 0-10 %

CO   0-10000 ppm

The O_2, CO_2, and CO concentrations were used along with the exhaust rate to calculate the heat release rate as well as the heat of combustion (See data reduction section).

Smoke was extracted from the hot layer at a known flow rate and used to determine the gas phase mass specific extinction coefficient. A particulate filter (Fischer brand filter grade G6) 42.5 mm in diameter was placed at 76 cm above the hood base and 5 cm away from each wall in the left corner. An aluminum filter holder (SKC, model 225-4704) which resists high temperatures was used as a filter holder. The extraction rate was controlled by a Dwyer flow meter, which was connected to a pump as shown in Figure 3-19. The flow rate on the flow meter was set to 4.6 L/min. Figure 3-20 shows the aluminum filter holder used in the test.
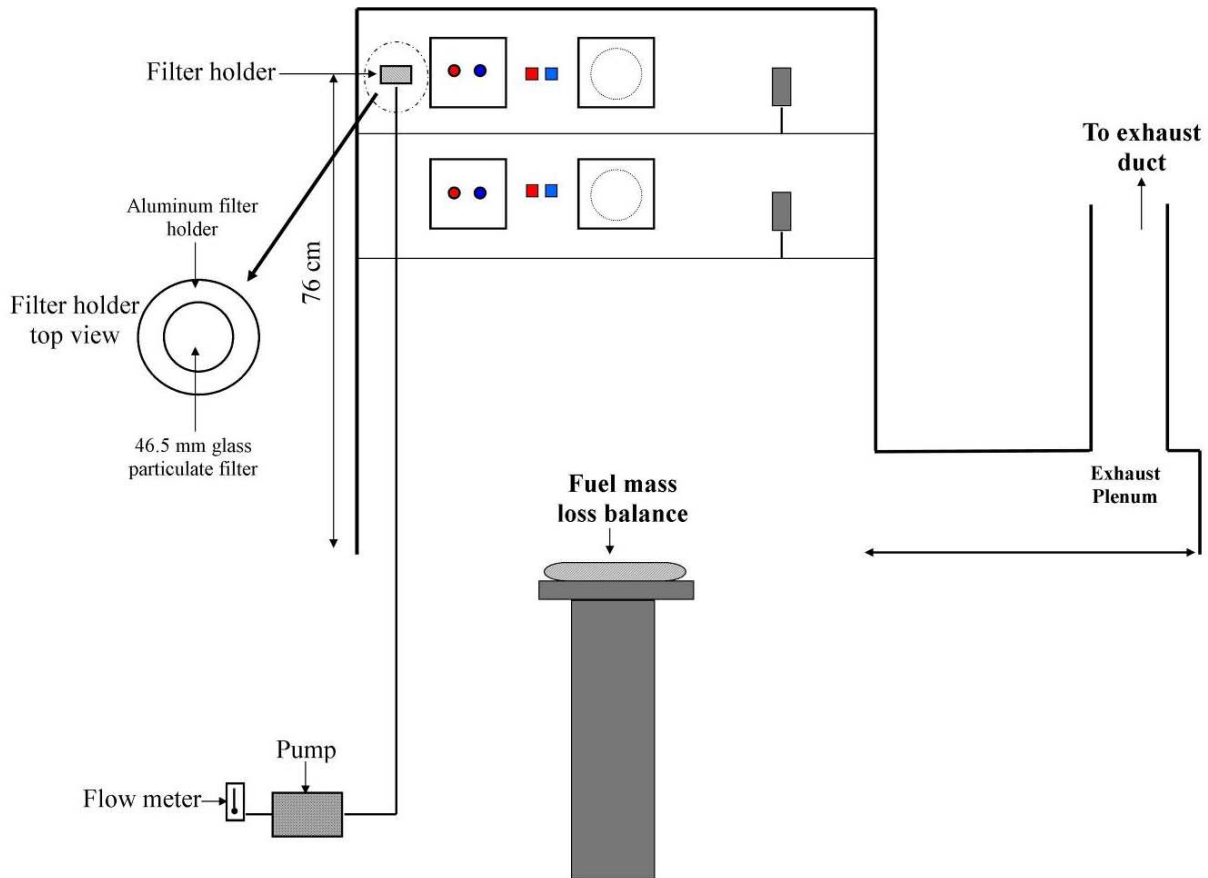
Figure 3-19: Particulate filter installation for smoke concentration measurement

Figure 3-20: Aluminum filter holder

Smoke was extracted from the hot layer at 4.6 L/min. The collected smoke on the filter was measured by using a high accuracy scale (0.1 mg). The optical density per meter in the hood at the location which smoke was collected was measured by using the laser extinction assembly already discussed. All the measurements were used to determine the gas phase mass specific extinction coefficient, which is discussed in the data reduction section.

A variety of fuels were burned in the hood apparatus in order to study the smoke deposition based on thermophoresis. Different polymers (polymethylmethacrylate (PMMA)), polypropylene (PP), acrylonitrile butadiene styrene (ABS)) as well as gasoline and wood fiberboard were burned in the hood apparatus.

PMMA ($C_5H_9O_2$) is often used as an alternative to glass, and in competition with polycarbonate (PC). It is often preferred because of its moderate properties, easy handling and processing, and low cost. It can be found in black and clear colors.

Polypropylene (C_3H_6) is a thermoplastic polymer used in a wide variety of applications, including packaging, textiles, stationery, plastic parts and reusable containers of various types, laboratory equipment, loudspeakers, and automotive components. An addition polymer made from the monomer propylene, it is rugged and unusually resistant to many chemical solvents, bases and acids.

ABS ($C_{15}H_{17}N$) is a common thermoplastic used to make light, rigid, molded products such as piping (for example plastic pressure pipe systems), musical instruments (most notably recorders and plastic clarinets), golf club heads (used for its good shock absorbance), automotive body parts, wheel covers, enclosures, protective headgear, buffer edging for furniture and joinery panels, and toys, including Lego bricks.

These fuels were chosen because of their different properties and smoke yield. ABS generates smoke more than PMMA and PP. Gasoline was chosen as an accelerant and to study the effects of liquid fuel on smoke deposition. Fiber board was chosen as fuel containing cellulose. Normally a combination of polymers and wood are present in a room fire. Sometimes the fire includes the presence of an accelerant. Figure 3-21– Figure 3-24 show PMMA, PP, ABS, and fiber board samples used in the hood tests.

31
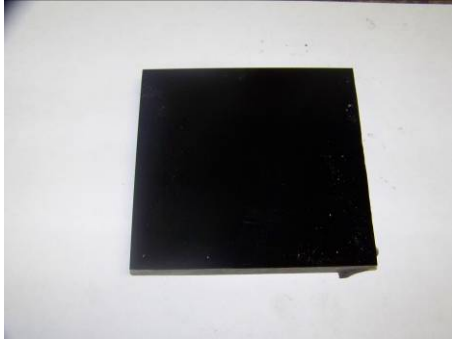
Figure 3-21 : 4" x 4" PMMA sample

Figure 3-22: 4" x 4" PP sample

Figure 3-23: 4" x 4" ABS sample
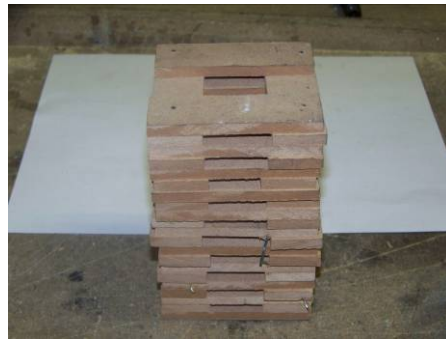
Figure 3-24: 4" x 4" fiber board wood crib

3.1.2 Test Procedure

3.1.2.1 Data Acquisition Set Up and Parameters

Experimental data was collected using a National Instruments SCXI-1000 data acquisition chassis with one SCXI-1303, 32-channel isothermal terminal block, and three SCXI-1327, 8-channel high-voltage attenuator terminal blocks. The National Instruments hardware was interfaced with Labview 8.1 data acquisition software using a 16-bit PCMCIA converter. The data acquisition system was set to a sampling rate of 1 Hz.

3.1.2.2 Wall Filter Preparation and Installation

Glass filters were placed in the filter holders after weighting them with the high accuracy scale (0.1 mg) prior to each test. The installation method for the filters was using eight pins around the circumference of the filter as explained in Section 3.1.1. In addition, a particulate

filter was placed in the filter holder and positioned 76 cm from the base of the hood. The particulate filter's weight was also measured using the high accuracy scale (0.1 mg).

3.1.2.3 Fuel Setup and Ignition

Different pan sizes were used for each fuel to vary the fire size. For PMMA a 5"x5" steel pan was used with a PMMA sample size was 4"x4". Test duration was changed by increasing the number of the PMMA samples. For PP, a different pan size from PMMA was used since PP melts and fills the pan first and after melting it starts to burn. Therefore, the fuel sample size does not matter for PP and the pan size dictates the fire size. A circle pan (4 " diameter) was chosen and the PP samples were melted by holding a propane torch on top of the PP sample for 6 minutes. Test duration was also changed for PP tests by changing the number of the samples. The ABS samples were relatively smaller than both PMMA and PP samples, since ABS generates more smoke than other fuels tested. In order to decrease the smoke generation, smaller ABS samples (1"x1", 2"x2", and 3"x3") were used. ABS samples were burned in the hood apparatus. The pan size for the ABS tests was 5"x5". Gasoline was burned in a smaller round shape pan (2" diameter). 15 ml, 25 ml, 45 ml, 65 ml, and 90 ml of gasoline was burned to achieve different test durations. Fiber board was cut into 2" x 1.5" and 4" x 1.5" sticks, and stacked in fiber board wood cribs. The cross section of these cribs varied from 2"x2" to 4"x4" and their heights varied from 2" to 4". In order to burn fiber board, the entrainment rate needed to be increased. Construction of cribs increased the air entrainment rate and helped the ignition process. For PMMA and ABS, the propane torch was held on top of the sample for 1 minute. A propane torch was applied to PP samples for 6 minutes to maintain a steady fully developed burning. When multiple samples were used for PMMA, PP, and ABS, the samples were layered. Gasoline was ignited by using a lighter. Fiber board cribs were placed in a pan that

33

had 30 ml methanol. Methanol was chosen as an accelerator since it does not generate smoke. The methanol combustion provided rapid and full involvement of the crib.

Data collection was continued until the fuel sample was completely burned, measured properties were back to ambient conditions, and there was no evidence of a smoke layer in the hood apparatus.

3.1.2.4 Recovering sample line filter and wall filters

The sample line filter and wall filters were collected after each test. These filters needed to be handled carefully because gravimetric and optical measurements needed to be done on them. The filters were picked up when they were hot. As there was no noticeable amount of water in the sample, the mass gain is properly interpreted as smoke deposition.

3.1.2.5 Gravimetric and optical measurements on the filters

Two different methods were used to measure the smoke deposition on the filters in this research; gravimetric and optical.

Gravimetric Measurement

Before starting the test, the filter's weight was measured by using a high accuracy (0.1 mg) scale. Total smoke deposition per unit area was calculated from the mass difference between the beginning and end of the test.

$$m'' = \frac{\Delta m}{A} = \frac{m_2 - m_1}{A} \qquad \text{Equation 3-1}$$

m_2 and m_1 are the mass of the filter before and after test and A is the total area of the filter.

Optical Density Measurement

Measuring the smoke deposition on a surface gravimetrically is a straightforward method in the laboratory but is not practical for field measurement. In order to develop a more practical

method of smoke deposition measurement for fire investigation, optical density measurement has been used in this work.

In photography and computing, a grayscale or gray scale digital image is an image in which the value of each pixel is a single sample, that is, it carries only intensity information. Images of this sort, also known as black-and-white, are composed exclusively of shades of gray, varying from black at the weakest intensity to white at the strongest [25]. The intensity of a pixel is expressed within a given range between a minimum and a maximum, inclusive. No matter what pixel depth is used, the binary representations assume that zero is black and the maximum value (255) is white, if not otherwise noted.

After each test, smoke deposition was measured on the filter gravimetrically. In addition, filters were scanned next to a Kodak gray scale by using a Canon flat bed scanner. Kodak gray scale was used every time the filters were scanned in order to calibrate the digital image based on the gray scale values. For calibration, Image J software was used, which is an open source package from the National Institute of Health [26]. Figure 3-25 is an image from an actual gray scale that was used in this work
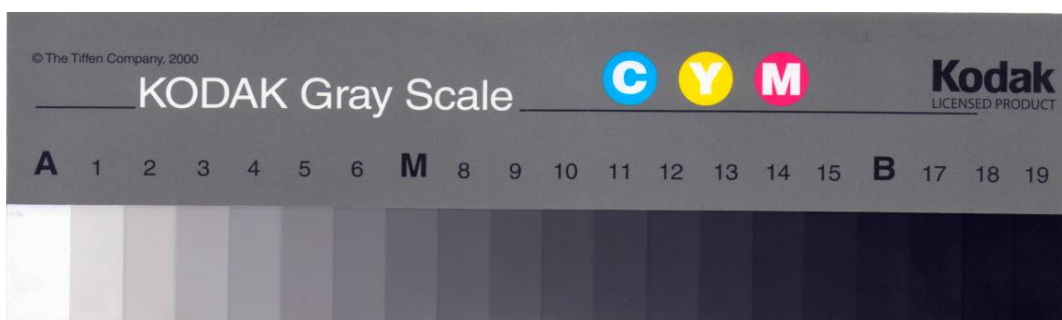
Figure 3-25: Kodak gray scale

Calibration begins with measuring the gray scale values for every step of the Kodak gray scale from white to black, 20 steps. Next, these gray scale numbers are matched to the actual values given by Kodak for the gray scale (optical densities start from 0.05 to 1.95 with 0.10

35

increments). Table 3-2 shows the gray scale values (0-255) measured on a Kodak gray scale for a test. The first column is the step number. The second column is gray scale value. The third column is the optical density value. The calibration function for the measured gray scale values is now computed. The calibration function suggested by Image J for optical density is "Rodbard." Rodbard calibration function has the general form of:

$$O.D. = d + \frac{(a-d)}{1+(\frac{G.S.}{c})^b} \qquad \text{Equation 3-2}$$

a, b, c, and d are constants. O.D. is the optical density and G.S. is the gray scale value measured by Image J.

Table 3-2: Measured gray scale values vs. optical density values

Step Number	Gray Scale Value	Optical Density Number
1	250.55	0.05
2	223.357	0.15
3	200.059	0.25
4	173.901	0.35
5	154.109	0.45
6	135.45	0.55
7	119.965	0.65
8	104.179	0.75
9	93.39	0.85
10	81.562	0.95
11	72.067	1.05
12	61.239	1.15
13	54.204	1.25
14	45.631	1.35
15	37.203	1.45
16	30.033	1.55
17	24.233	1.65
18	19.793	1.75

Step Number	Gray Scale Value	Optical Density Number
19	15.716	1.85
20	15.482	1.95

After calibration, optical density values were measured by using the measurement function in the Image J software to convert the gray scale values to optical density values based on the calibration function.

Figure 3-26 shows the calibration curve and the measured gray scale values. This is an exemplar representative of a family of curves. The calibration parameters varied from sample to sample but the variation was within 10% of the presented values. All the digital images from the filters were calibrated with a Kodak gray scale using the same calibration method as explained.
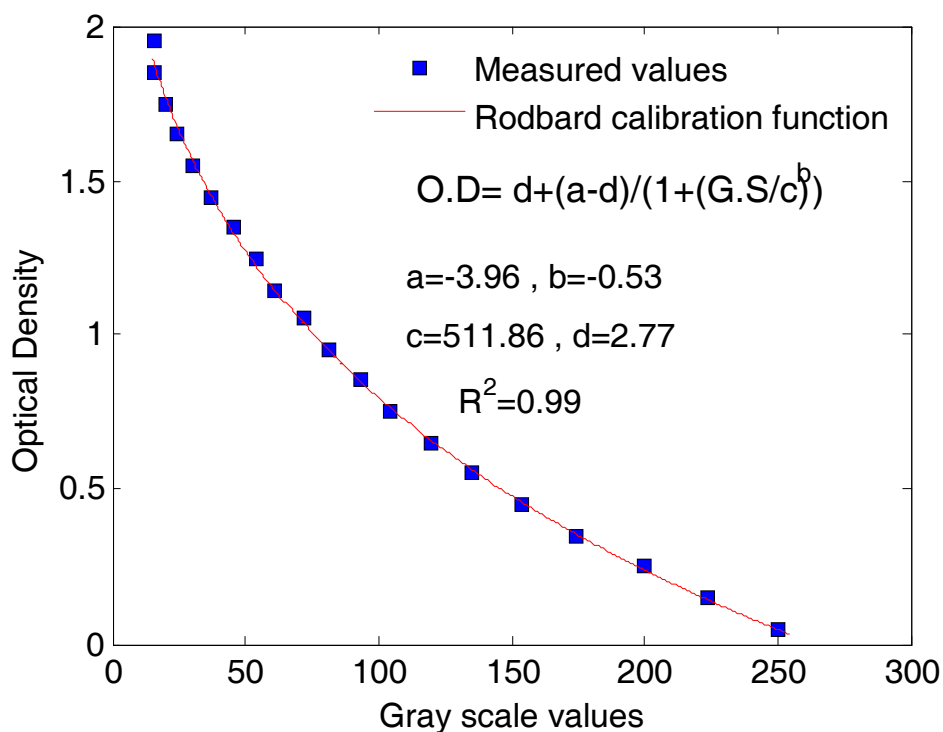
Figure 3-26: Rodbard calibration for the measured gray scale values

3.1.3   Data Reduction

Data reduction was performed in Matlab code in order to determine the following parameters:

- Thermophoretic velocity.

- Extinction optical density.

- Gas phase mass specific extinction coefficient.

- Smoke deposition based on thermophoretic velocity.

- Heat release rate for different fuels.

- Heat of combustion for different fuels.

3.1.3.1   Thermophoretic Velocity

As developed in Chapter 2, the thermophoretic velocity is given by

$$V_{th} = \frac{k_{th}\eta}{\rho T}\frac{\Delta T}{\Delta x} = \frac{k_{th}\eta}{\rho T}(\frac{dT}{dx}) \qquad\qquad \text{Equation 3-3}$$

The only parameter in Equation 3-3 that needs to be calculated is the temperature gradient. Viscosity and density in Equation 3-3 were calculated based on the following equations:

$$\rho = 366.91T^{-1.00669} \qquad\qquad \text{Equation 3-4}$$

$$\eta = 0.0000001861T^{0.80011} \qquad\qquad \text{Equation 3-5}$$
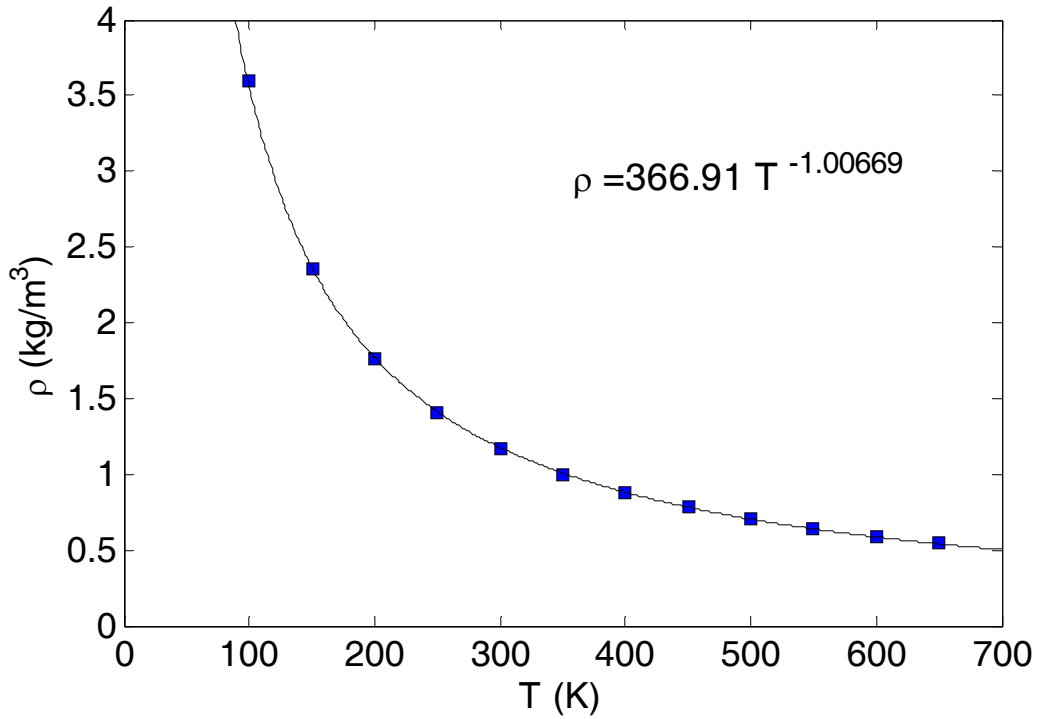
Figure 3-27: Density equation derived from charts for air [27]

$$\rho = 366.91\, T^{-1.00669}$$
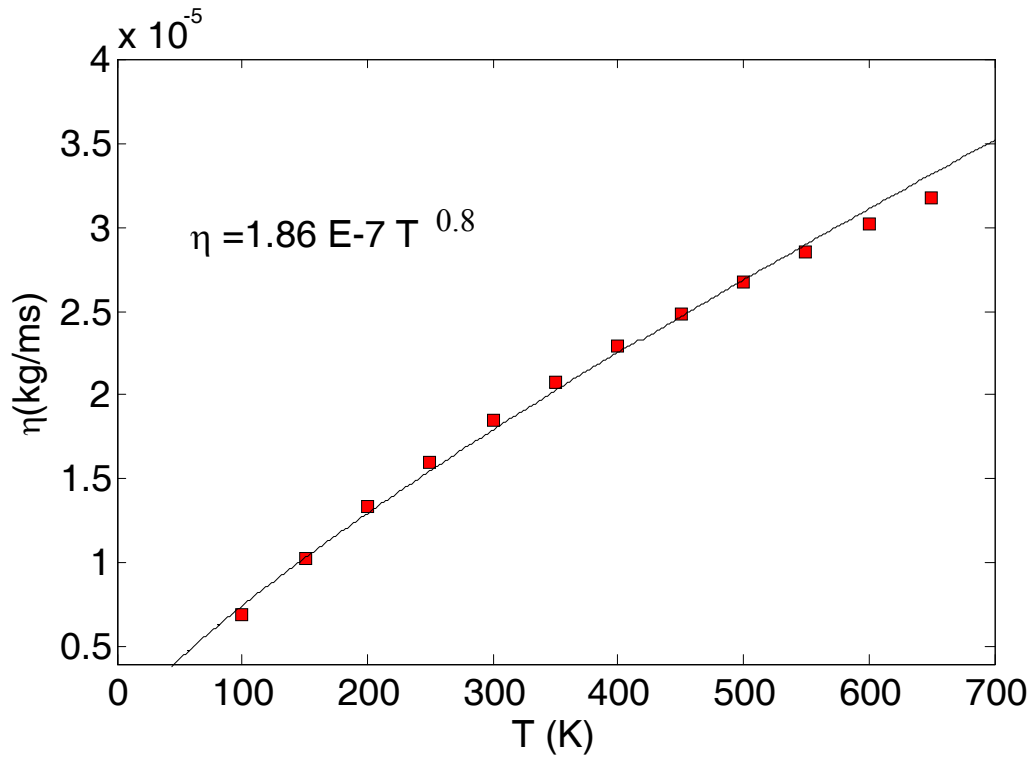
Figure 3-28: Viscosity equation derived from charts for air [27]

$$\eta = 1.86\,E\text{-}7\, T^{0.8}$$

The equations for air density and viscosity were calculated from air property tables [27].

The following method was applied to calculate the temperature gradient. Total heat flux $(\dot{q}''_{total})$ was measured by using a Schmidt-Boelter heat flux gauge and radiative heat flux $(\dot{q}''_{rad})$ was measured by a Schmidt-Boelter radiometer. Convective heat flux $(\dot{q}''_{conv})$ was calculated by:

$$\dot{q}''_{conv} = \dot{q}''_{total} - \dot{q}''_{rad} \qquad \text{Equation 3-6}$$

Convective heat transfer coefficient (h) was calculated by:

$$h = \frac{\dot{q}''_{total} - \dot{q}''_{rad}}{T_{gas} - T_{water}} \qquad \text{Equation 3-7}$$

It was assumed that the surface temperature on the Schmidt-Boelter heat flux gauge is close to the water temperature that was used to make the heat flux gauge's surface temperature constant. The thermal gradient can be determined using conservation of energy at the surface.
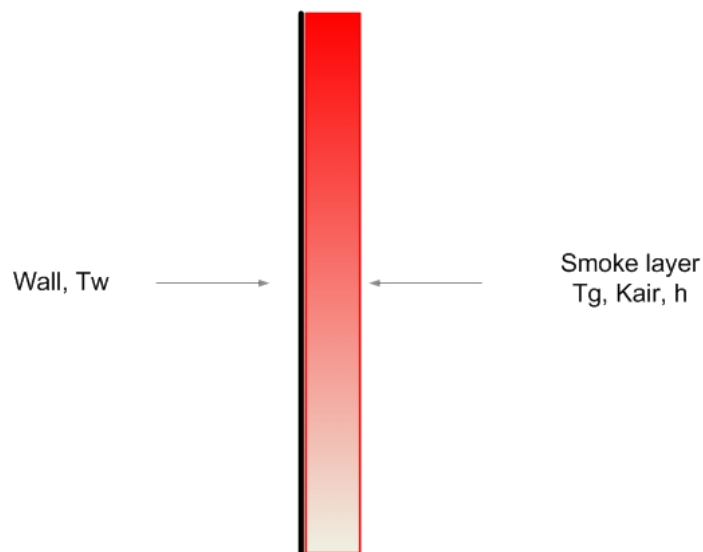
Figure 3-29: Smoke layer and wall interaction

$$\dot{q}''_{conduction} = \dot{q}''_{convection} \qquad \text{Equation 3-8}$$

$$k_{air} \frac{dT}{dx} = h(T_{gas} - T_{wall}) \qquad \text{Equation 3-9}$$

$$\frac{dT}{dx} = h(T_{gas} - T_{wall}) \qquad \text{Equation 3-10}$$

k_{air}, is the air conductivity at the film temperature and was calculated from the following equation:

$$k = 1.1641E\text{-}11 \ T^3 - 4.579E\text{-}8 \ T^2 + 1.0182E\text{-}4 \ T - 5.1609E\text{-}4 \qquad \text{Equation 3-11}$$
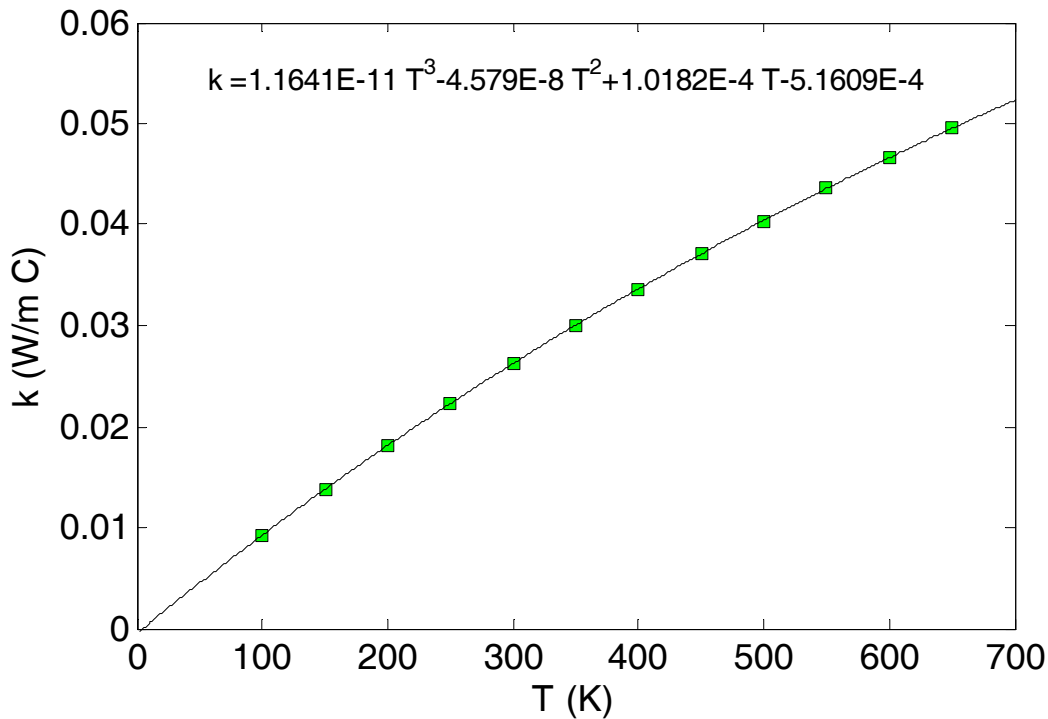
Figure 3-30: Thermal conductivity equation derived from charts for air [27]

The equation for air thermal conductivity is calculated from air property tables [27].

By using the convective heat transfer coefficient from Equation 3–7, thermal gradient is derived

41

as follow:

$$\frac{\Delta T}{\Delta x} = \frac{dT}{dx} = \frac{(\dot{q}''_{total} - \dot{q}''_{rad})(T_{gas} - T_{wall})}{k_{air}(T_{gas} - T_{water})} \qquad \text{Equation 3-12}$$

By employing temperature gradient derived in Equation 3-13, the thermophoretic velocity is derived as follows:

$$V_{th} = \frac{(0.55)\eta}{\rho T} \frac{(\dot{q}''_{total} - \dot{q}''_{rad})(T_{gas} - T_{wall})}{k_{air}(T_{gas} - T_{water})} \qquad \text{Equation 3-13}$$

3.1.3.2 Extinction Optical Density

Smoke concentrations in the air were determined by using a laser and detectors. The extinction optical density is defined as [28]

$$OD = \ln(\frac{I_0}{I}) \qquad \text{Equation 3-14}$$

I_0 is the intensity of incident light and I is the intensity of transmitted light. I_0 was measured during a three minute background data collection. I is the output signal from the detector. Another parameter which was used for data reduction was optical density per meter, which is defined as the extinction optical density divided by the path length between laser and detector source.

$$OD / meter = \frac{\ln(\frac{I_0}{I})}{L} \qquad \text{Equation 3-15}$$

3.1.3.3 Gas Phase Mass Specific Extinction Coefficient

$\sigma_{s,g}$, the gas phase mass specific extinction coefficient, was determined by using a particulate filter 76 cm above the hood base and sampling at 4.6 L/min. Test apparatus and procedure for gas phase mass specific extinction coefficient were discussed in Section 3.1.1. After each test,

42

the particulate filter was recovered and the amount of smoke which was extracted from the smoke layer was measured using a scale (0.1 mg accuracy).

Mass concentration of smoke was determined by:

$$C_{smoke} = \frac{m_{collected}}{V} \qquad \text{Equation 3-16}$$

$m_{collected}$ is the total mass collected on the particulate filter and V, is the volume of gases sampled.

Gas phase mass specific extinction coefficient is defined by [28]

$$\sigma_{s,g} = \frac{OD/meter}{C_{smoke}} \qquad \text{Equation 3-17}$$

By using Equation 3-17 and Equation 3-18, the gas phase mass specific extinction coefficient was calculated as follow:

$$\sigma_{s,g} = \frac{1}{m_{collected}} \int OD/meter \quad \dot{V} \quad dt \qquad \text{Equation 3-18}$$

Since flow meter reading is at ambient temperature and smoke extraction is at the measured gas layer temperature, flow rate needs to be corrected for the temperature.

$$\sigma_{s,g} = \frac{1}{m_{collected}} \int (OD/meter) \quad \dot{V} \quad (\frac{T_{ambient}}{T_g}) dt \qquad \text{Equation 3-19}$$

Gas phase mass specific extinction coefficient is normally taken as $8.7 \pm 1.1 (m^2/g)$ as reported by Mulholland [28].

3.1.3.4 Smoke Deposition Based on Thermophoretic Velocity

Smoke deposition based on thermophoresis is dependent on thermophoretic velocity and smoke concentration.

$$m'' = \int_0^t V_{th}\{t\} \quad C_{smoke}\{t\} \quad dt \qquad \text{Equation 3-20}$$

In order to calculate the smoke deposition per unit area, two important parameters needed to be determined in the data reduction section from the experimental raw data.

1. Thermophoretic velocity V_{th}

2. Smoke concentration C_{smoke}

Thermophoretic velocity was determined by Equation 3-14. Smoke concentration (C_s) is defined as:

$$C_s = \frac{OD/meter}{\sigma_{s,g}} \qquad \text{Equation 3-21}$$

By using Equation 3-14 and Equation 3-22 smoke deposition per unit area is defined as:

$$m'' = \int_0^t \left(\frac{(0.55)\eta}{\rho T} \frac{(\dot{q}''_{total} - \dot{q}''_{rad})(T_{gas} - T_{wall})}{k_{air}(T_{gas} - T_{water})} \right) \left(\frac{OD/meter}{\sigma_{s,g}} \right) dt \qquad \text{Equation 3-22}$$

3.1.3.5 Heat Release Rate for Different Fuels

Heat release rate was calculated at each time step based on O_2, CO_2, and CO concentrations from the gas analyzer and exhaust rate. [29] Water was removed from the gas sample and gas concentrations were corrected to wet concentrations for the calculations.

$$HRR = \left[E\phi - (E_{CO} - E)\frac{1-\phi}{2}\frac{X_{CO}^{A^e}}{X_{O_2}^{A^e}} \right] \cdot \frac{\dot{m}_e}{1+\phi(\alpha-1)} \frac{M_{O_2}}{M_a}(1-X_{H_2O}^a)X_{O_2}^{A^a}$$

$$\phi = \frac{X_{O_2}^{A^a}(1-X_{CO_2}^{A^e}-X_{CO}^{A^e}) - X_{O_2}^{A^e}(1-X_{CO_2}^{A^e})}{(1-X_{O_2}^{A^e}-X_{CO_2}^{A^a}-X_{CO}^{A^e})X_{O_2}^{A^a}}$$

Where

ϕ = oxygen depletion factor

α = volumetric expansion factor (1.105)

M_{O_2} = molecular mass of oxygen (28 g/mol)

44

M_a = molecular mass of the combustion air (29g/mol)

$X_{H_2O}^a$ = actual mole fraction of water vapor in the combustion air which is calculated based on humidity readings in the lab.

$X_{CO_2}^{A^a}$ = actual mole fraction of carbon dioxide in the combustion air

$X_{O_2}^{A^a}$ = measured mole fraction of oxygen in the combustion air

$X_{O_2}^{A^e}$ = measured mole fraction of oxygen in the exhaust flow

E = heat release per mass unit of oxygen consumed (~13.1 kJ/g)

E_{CO} = heat release per mass unit of oxygen consumed for combustion of CO to CO_2 (~17.6 kJ/g)

$X_{CO}^{A^e}$ = measured mole fraction of carbon monoxide in the exhaust flow

$\dot{m}_e$ = exhaust rate (kg/s)

Performing above data reduction on the raw data will calculate the heat release rate at each time step.

3.1.3.6   Heat of Combustion for Different Fuels

By knowing the heat release rate (calculated at each time step) and mass loss rate (measured with a mass balance), the heat of combustion was determined:

$$\Delta H_c = \frac{HRR}{\dot{m}_{fuel}} \qquad\qquad \text{Equation 3-23}$$

The heat of combustion was averaged over the steady state part of the combustion process and was compared with the heat of combustion reported in the handbook [5].

3.2   Wall Experiments

The main purpose of the wall tests was to study the smoke deposition based on thermophoresis mechanism against a vertical wall. In most of the common fire scenarios,

studying the smoke damage on the walls gives the fire investigator information about the location that fire started and the fire size and the fuel source. Each wall test was performed twice. The first test was for measuring the necessary data, and the second test was performed to study the smoke pattern on the wall and development of a practical method for fire investigation based on the optical properties of the walls which were exposed to smoke. These wall tests were performed with three different fire sizes and four different fuels. Measurements were taken including gas and wall temperatures, total heat flux, and radiative heat flux.

3.2.1 Wall Test Apparatus

The wall test apparatus consisted of a gypsum wall (1.2 m x 2.4 m x 0.0127 m). Gypsum is the common material used as drywall in buildings. Drywall is the term used for a common method of constructing interior walls and ceilings using panels made of gypsum plaster pressed between two thick sheets of paper. Gypsum plaster is calcium sulphate hemihydrate, nominally $CaSO_4 \cdot 1/2H_2O$. It is created by heating gypsum to about 150 °C.

$2\ CaSO_4 \cdot 2H_2O \rightarrow 2\ CaSO_4 \cdot 0.5H_2O + 3\ H_2O$ (released as steam) Figure 3-31 shows the wall test set up. Gypsum wall was located under the exhaust hood.
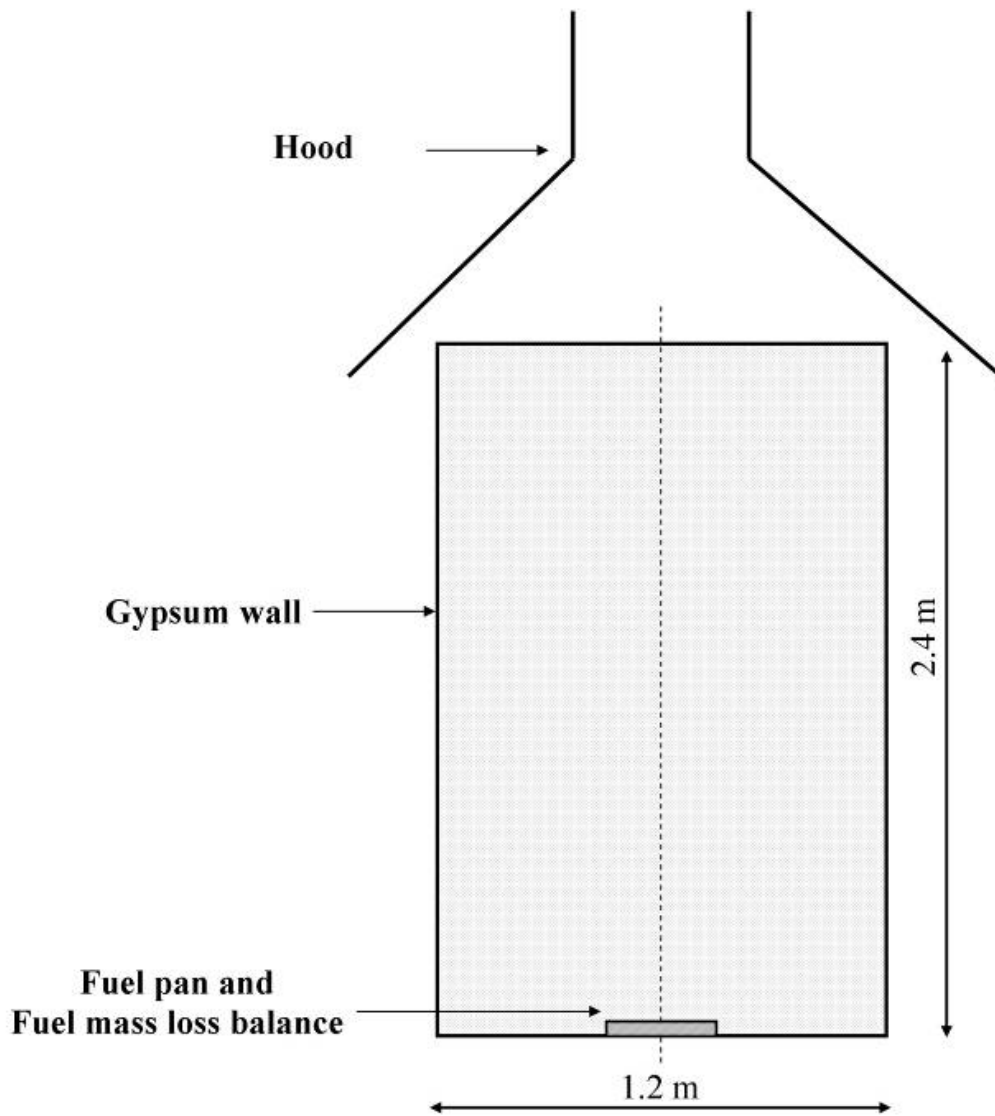
Figure 3-31: Wall test set up front view
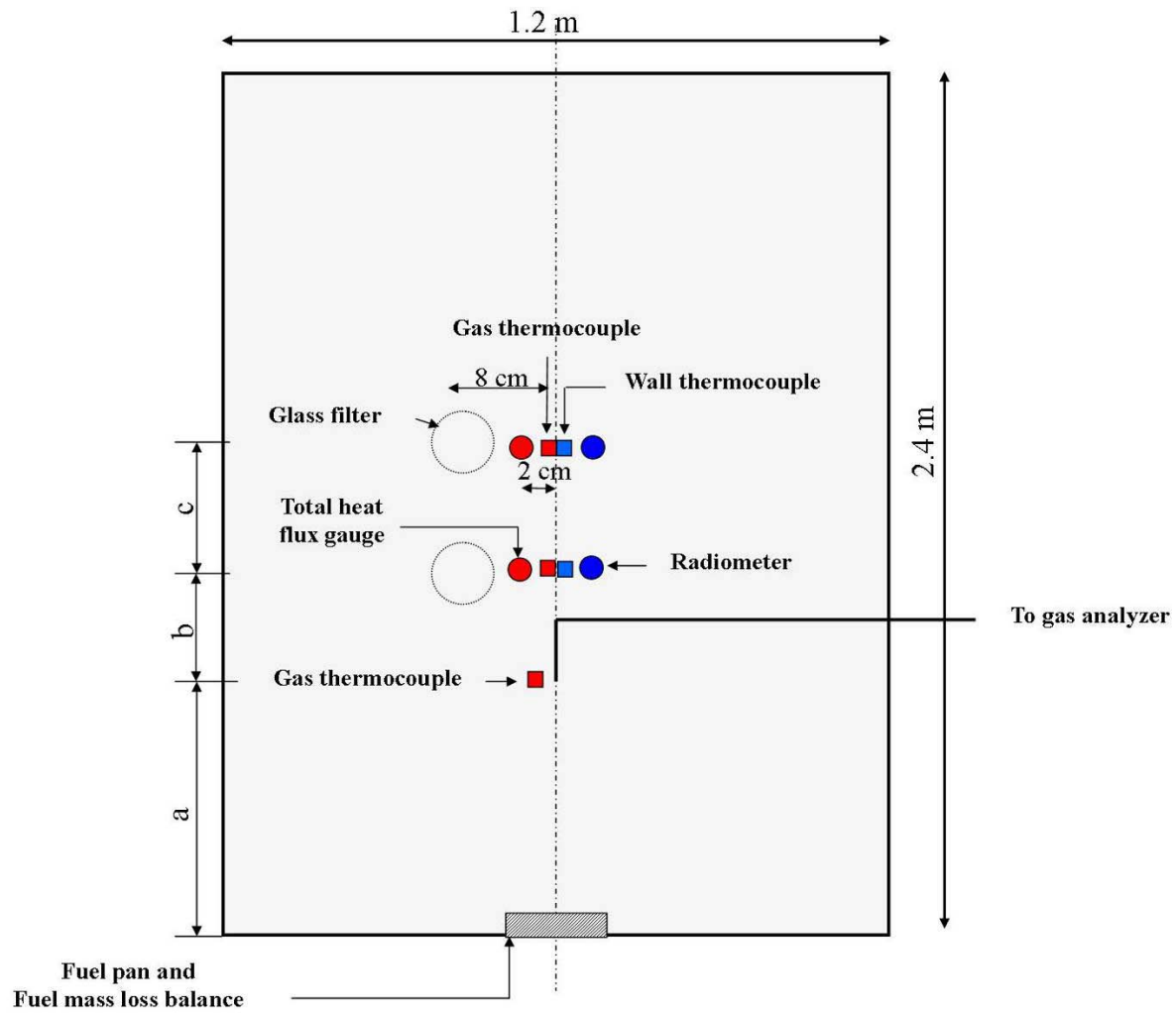
Figure 3-32: Wall test apparatus front view

Wall mounted glass filters (9 cm diameter) were used to collect smoke at low and high locations. These filters were the same filters which were used for the hood tests. Fisher brand glass filters Grade G6 were used for these tests. The diameter of the filters was 90 mm and their thickness was 0.32 mm. Smoke deposition was measured on these filters gravimetrically. The glass filter location which is shown in Figure 3-32 changes based on the wall test. Three different pan sizes were used for the wall tests and for each test filter locations were different. Filters were mounted at different locations for each test series because the flame height for larger fires was larger than smaller fires and filters needed to be outside the flame zone. Glass filters resist temperatures up to 600 ° C and in order to be able to collect smoke on them, they should be outside the flame zone. Table 3-3 shows the filter locations for each test series.

Table 3-3: Filter locations for wall tests

Pan Size	Low Filter Location (a+b)	High Filter Location (b+c)
4" x 4"	0.9 m (3ft)	1.2 m
8" x 8"	1.2 m (4ft)	1.5 m
12" x 12"	1.5 m (5ft)	1.8 m

The filters were mounted on the gypsum wall with the same installation method used for the glass filters in the hood tests. Figure 3-33 shows the filter installation on the gypsum wall.

Figure 3-33: Filter installation on the gypsum wall

49

Heat flux gauges and radiometers were used next to each glass filter to measure the total heat flux and radiative heat flux (2 cm from the center line, heat flux gauges were located on the left side and radiometers were located on the right side). Total heat flux was measured by using a Schmidt-Boelter heat flux gauge. The temperature on the back of the gauge was kept constant by using water to cool the gauge. The heat flux gauges were calibrated by the manufacturer and the calibration curve specifies the relation between the voltage signal output and the heat flux. Full scale for the low location heat flux gauge was $50kW/m^2$ and for the high location heat flux was $25kW/m^2$.

Gas and wall temperatures were measured by using K type thermocouples, bare bead, and 30gauge. Thermocouples were installed at the same elevation as the filter and they were located on the center line of the gypsum wall.

The gas thermocouple was 18 mm away from the wall for the low location and 28 mm away from the wall for the high locations. These values were measured after running exploratory tests to measure the gas thermocouple location due to boundary layer effect. The wall thermocouple was mounted by bending it towards the wall such that thermocouple bead was in contact with the wall surface. The thermocouple was fixed in the location by using the tension on the thermocouple wire. Figure 3-34 shows the thermocouple installation for both gas and wall thermocouples.

Figure 3-34: Gas and wall thermocouple installation, front and side view

Smoke concentration was measured by a different method than the small scale tests. For the wall tests due to small path length, using a laser and detector was not feasible as an optical density measurement method; therefore, smoke concentrations at both low and high locations were determined by measuring the combustion products concentration. This measurement method will be discussed in Section 3.2.3.2.

Measurement of O_2, CO_2, and CO concentrations were made at the location below the low filter location. Sampling location was 4 cm below the low filter location for all the tests. A Servonex 4100 gas purity analyzer was used to measure O_2 concentration and its accuracy was ¼ % full scale. A Horiba VA-3000 analyzer was used to measure CO_2 and CO concentrations the accuracy on the analyzer was ½ % full scale.

Figure 3-35: Gas analyzer used for hood and wall experiments

Figure 3-35 shows the picture of the gas analyzer used for both hood and wall tests. The measurement ranges for each gas are as follows:

O_2 0-20.95 %,

CO_2 0-10 %,

CO   0-10000 ppm

A variety of fuels were burned against the gypsum wall in order to study the smoke deposition based on thermophoresis. Different polymers (polymethylmethacrylate (PMMA)), polypropylene (PP), acrylonitrile butadiene styrene (ABS)) as well as gasoline were burned against the gypsum wall. These fuels were chosen because of their different properties and smoke yields. ABS generates smoke more than PMMA and PP. Gasoline was chosen as an accelerant and to study the effects of liquid fuel on smoke deposition. In the case of fire in the

52

room normally we have combination of polymers and sometimes the fire starts due to presence
of an accelerant.

3.2.2   Test Procedure

3.2.2.1   Data Acquisition Setup and Parameters

Experimental data was collected using the same data acquisition chassis.

3.2.2.2   Wall Filter Preparation and Installation

Glass filters were located in their place on the gypsum wall after weighting them with the
high accuracy scale (0.1 mg) prior to each test. The installation method for the filters was using
eight pins around the circumference of the filter as explained in the previous section.

3.2.2.3   Fuel Setup and Ignition

Different pan sizes were used for each fuel to vary the fire size. Table 3-4 shows the test
matrix for the wall tests.

Table 3-4: Test matrix for the wall tests

Fuel	Pan Size	Test Length
PMMA	4" x 4", 8" x 8", 12" x 12"	73 minutes, 90 minutes for 4" x 4" 50 minutes, 75 minutes for 8" x 8" 45 minutes, 75 minutes for 12" x 12"
PP	4" x 4", 8" x 8", 12" x 12"	26 minutes, 40 minutes for 4" x 4" 28 minutes, 40 minutes for 8" x 8" 35 minutes, 41 minutes for 12" x 12"
ABS	4" x 4", 8" x 8", 12" x 12"	25 minutes, 35 minutes for 4" x 4" 20 minutes, 15 minutes for 8" x 8" 16 minutes, 25 minutes for 12" x 12"
Gasoline	3.5" diameter, 8" x 8", 12" x 12"	33 minutes, 46 minutes for 3.5" diameter 11 minutes, 16 minutes for 8" x 8" 8 minutes, 12 minutes for 12" x 12"

As mentioned earlier all the tests were repeated for smoke pattern study. After each test, gypsum wall was photographed in the presence of the gray scale and for the next test a new gypsum wall was used.

For all the fuels three different pan sizes were used to generate different fire sizes. 4"x 4", 8" x 8", 12" x 12" pans were used for each fuel. Each test was performed in two different categories; short test and long test. Test duration was changed by increasing the thickness of the fuel sample. The ABS samples for 8" x 8"and 12" x 12" were different than 4"x 4" samples. Since ABS generates more smoke than any other tested fuel, in order to decrease the smoke generation, different fuel set up was used. ABS was cut in to 2"x 2" squares. 2"x 2" ABS samples were placed on the 8" x 8" pan with a checkerboard arrangement with 1" gap between the samples as shown in Figure 3-36.

Figure 3-36: ABS samples set up for 8" x 8" wall tests.

The same sample set up was used for a 12" x 12" pan except 16 pieces of 2"x 2" ABS samples were used and the gap between the samples was 1.5". The ABS fuel set up for 12" x 12" wall test is shown in Figure 3-37. This fuel set up for ABS, makes the test duration shorter than burning a 12"x 12" piece of ABS.

54

Figure 3-37: ABS samples set up for 12" x 12 wall tests.

Gasoline was burned in a smaller round shape pan (3.5" diameter) and 8" x 8", 12" x 12" pans. 25 ml, 45 ml, 350 ml, 500 ml, 1000 ml, and 2000 ml of gasoline were burned to achieve different test durations. For PMMA and ABS, the propane torch was held on top of the sample for 1 minute for 4" x 4" samples, 2 minutes for 8" x 8" samples and 3 minutes for 12" x 12" samples. Propane torch was applied to 4" x 4" PP samples for 6 minutes, 8" x 8" samples for 9 minutes and 12" x 12" samples for 12 minutes. The PP samples were ignited separately and after ignition they were moved to their locations against the gypsum wall.

Data collection was continued until the fuel samples were completely burned and all the properties were back to ambient conditions.

3.2.2.4 Recovering Wall Filters

Wall filters were collected after each test. These filters needed to be handled carefully because gravimetric and optical measurements needed to be performed on them. The gravimetric and optical measurements were done on the wall filters with the same method as hood experiment filters. The filters were picked up when they were hot and since there was no noticeable amount of water in the sample so the mass gain is properly interpreted as smoke.

55

3.2.2.5 Gravimetric and Optical Measurements on the Filters

Smoke deposition on the wall filters were measured with two methods as explained in 3.1.2.5 for the wall filters from hood experiments. These methods are; gravimetric and optical measurements.

For gravimetric measurements, each filter's weight was measured by a high accuracy scale (0.1 mg) before and after each test. Total smoke deposition per unit area on each filter was determined after weighing the filters.

In addition to gravimetric measurement, filters were scanned next to a Kodak gray scale by using a Canon flat bed scanner. Kodak gray scale was used every time the filters were scanned in order to calibrate digital image based on the gray scale values. For calibration, Image J [2] software was used. The calibration method which was used for wall tests was exactly the same method which was applied for hood test filters and it has been discussed in details in 3.1.2.5. The calibration function suggested by Image J for optical density is "RodBard". The general form of this function is:

$$O.D. = d + \frac{(a-d)}{1+(\frac{x}{c})^b} \qquad \text{Equation 3-24}$$

a, b, and c are constants. O.D. is the optical density and G.S. is the gray scale value measured by Image J.

After calibration, optical density values were measured by Image J software. Figure 3-38 shows the calibration curve and the measured gray scale values. This is an exemplar representative of family of curves. The calibration parameters varied from sample to sample but the variation was within 5% of the presented values. All the digital images from the wall filters were calibrated with a Kodak gray scale using the same calibration method explained.

Table 3-5: Measured gray scale values vs. optical density values for a wall test

Step Number	Gray Scale Value	Optical Density Number
1	238.26	0.05
2	212.066	0.15
3	184.318	0.25
4	153.443	0.35
5	129.504	0.45
6	109.151	0.55
7	93.107	0.65
8	80.09	0.75
9	68.785	0.85
10	58.739	0.95
11	50.671	1.05
12	40.967	1.15
13	35.955	1.25
14	30.185	1.35
15	24.363	1.45
16	20.989	1.55
17	16.717	1.65
18	13.223	1.75
19	10.48	1.85
20	9.679	1.95

O.D.=d+(a-d)/(1+(G.S/c^b))
a=-2.35, b=-0.45
c=139.78, d=3.16

R^2=0.99
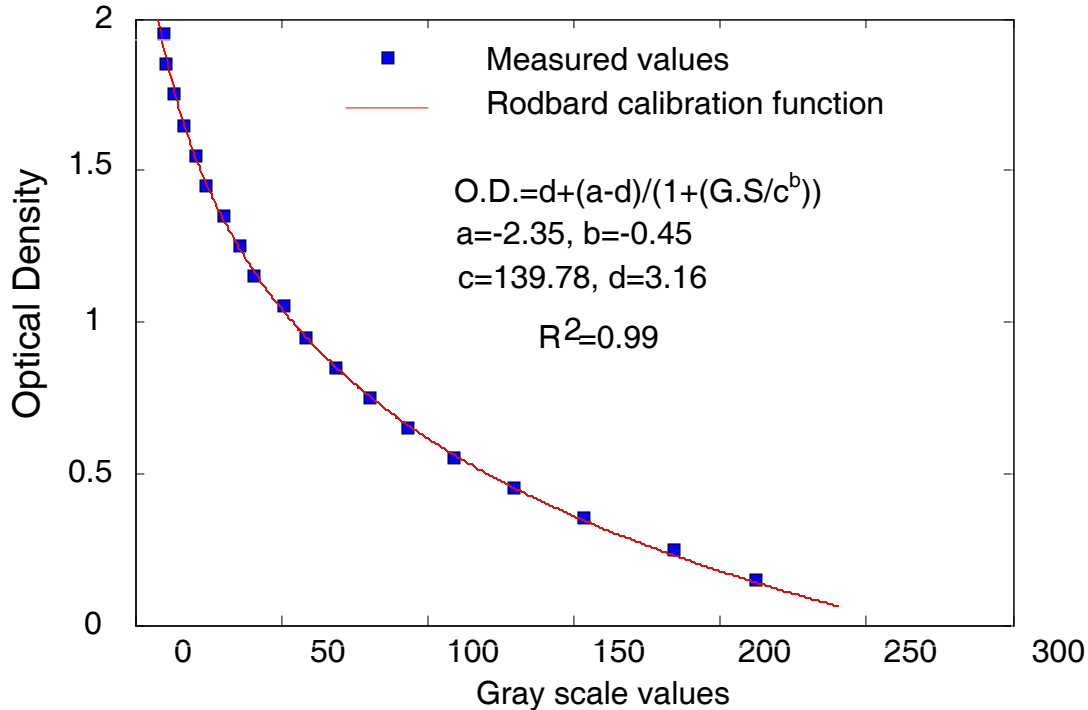
Figure 3-38: Rodbard calibration for the measured gray scale values for a wall test

3.2.2.6   Using a Digital Photography Method for Optical Measurements

Scanning filters after each test is a straightforward optical measurement and it is a point measurement. However, it is not a practical method for field investigation of a fire scene. As a part of developing of an optical measurement technique, wall filters were photographed using two different digital cameras in the presence of the gray scale. The distance between the camera and the filter was 1.5 m and the camera's flash was used in addition to the normal lighting in the laboratory. It needs to be mentioned that the person who is taking the pictures should not get too close (1 meter) to the filters because it will overexpose the filter and the gray scale to the light. The two cameras which were used in this work were; Kodak Easy Share Z7121S and Sony Cyber shot PSC-P722. Also the same wall filters were scanned with the flat bed scanner in the presence of the same gray scale. The optical properties of the filters were measured using the Image J software and the Rodbard calibration curve. Figure 3-39 shows the optical properties of

the wall filters from PMMA, gasoline, and PP tests. The digital pictures were taken with two different cameras (Kodak and Sony cameras). It shows that the change in the camera doesn't change the optical properties of the surface which was exposed to the smoke.
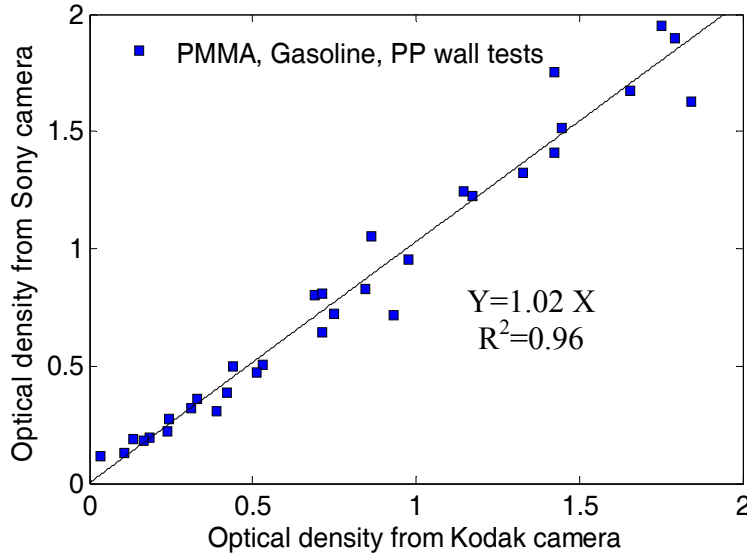
Figure 3-39: Optical measurements on the wall filters from two different digital cameras

One of the most important results from the Figure 3-39 is that the digital photography method for measuring the optical properties of the filters is not dependent on the digital camera which was used.
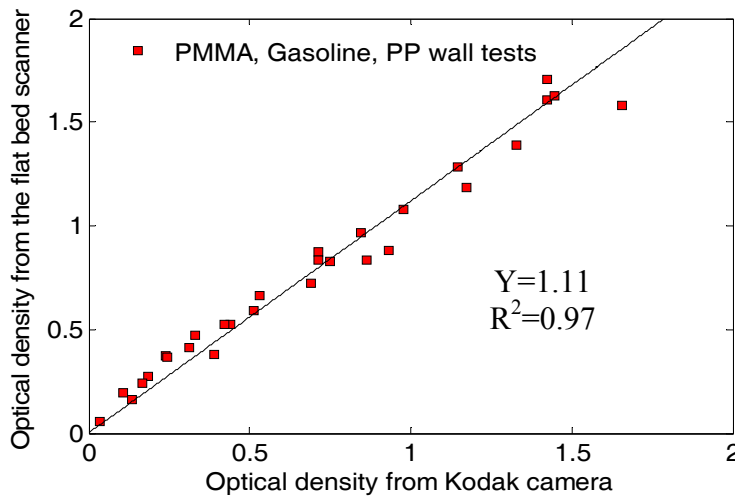
Figure 3-40: Comparison between optical properties of the filters scanned with flat bed scanner and the digital pictures taken by Kodak camera

Figure 3-40 shows that the optical properties on the wall filters which were determined based on digital pictures taken with Kodak camera are close to the optical properties of the filters determined from the flat bed scanner digital images. This means that taking a digital picture of a surface exposed to the smoke in the presence of a gray scale and processing the image with Image J software will be a practical field method to measure the optical properties of the surface. Also the same procedure was performed on the digital images from the Sony camera (Figure 3-41).
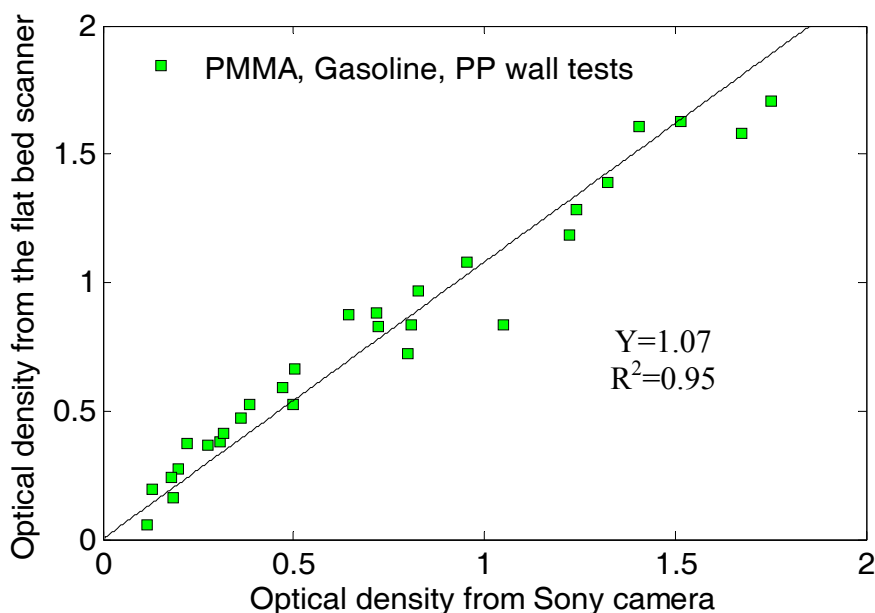
Figure 3-41: Comparison between optical properties of the filters scanned with flat bed scanner and the digital pictures taken by Sony camera

3.2.2.7 Using a Digital Photography Method for Optical Measurements for the Soot Pattern Tests

The optical measurement method explained in 3.2.2.6 was applied to the wall tests performed for smoke pattern study. The gypsum wall was exposed to smoke from a PMMA, PP, gasoline, and ABS fuels with different test durations. After each test was finished, the digital picture of the wall in the presence of a gray scale was taken. The gray scale which was used for the pattern

tests was the same as the one used for the filters from the wall tests except for its dimensions. The gray scale was 35 cm long. The one which was used for scanning the filters was 25 cm. Since the wall's dimensions are larger than the glass filter, there was a need for using a larger gray scale in order to have the necessary resolution on the pictures from the wall tests. The larger gray scale has the same number of steps as the smaller one. (20 steps) and the same procedure was used for the calibration and the same calibration curve (Rodbard calibration function) was used for the wall pattern tests. Figure 3-42 shows a soot pattern on the gypsum wall from a 12" x 12" PMMA test against the wall. The picture was taken in the gray scale's (35 cm long) presence.

Figure 3-42: Soot pattern on the gypsum wall from a 12" x 12" PMMA test against the wall

For all the wall tests the clean burn zone (the area which was in direct contact with the flame) was blown clean with compressed air and another picture was taken to compare the results between the clean burn zones. All the ash from burning the paper on the gypsum wall was removed by compressed air. The clean burn zone is supposed to be a white zone which it is not in Figure 3-42. Since the gypsum is made of gypsum material covered by layers of paper, first the paper on the wall burns and then soot deposits on the paper from the wall and leaves a residue on the clean burn zone which results in the gray color [30] on the clean burn zone. After cleaning the clean burn area with air all the residue and ash from the paper falls off and the clean burn zone will be white as shown in Figure 3-43 .

Figure 3-43: Smoke pattern on the gypsum wall from a 12" x 12" PMMA test against the wall after cleaning the clean burn zone.

All the digital pictures were processed using the Image J software. The only difference was to process the data for the wall tests automatically instead of measuring the optical properties of the surface using the Image J software manually.

First step for processing the digital image from the wall test is to scale the image using the scale function in the Image J software. It provides the number of pixels/cm. For example, for Figure 3-42 the scale factor is 18 pixels/cm. The next step is to discretize the image into 1 cm^2 squares, in which the optical properties will be measured. The results of analysis were combined to create a contour plot of the smoke deposition on the wall for comparison with the actual digital image. Since the process of measuring the optical properties of the 1 cm^2 squares on the wall is a tedious procedure, a Matlab program was written specifically for this purpose and linked to the macro feature in the Image J software. This makes the determination of the optical properties of the wall surface. The final step was to combine all the results and plot the optical density contours of the wall, and compare the contours to the digital photographic images.

The same procedure was performed on the digital images from the wall tests after cleaning the ash residue from the clean burn zone using compressed air to remove the ash. By comparing the contours from a cleaned wall and an uncleaned wall, the amount of ash deposited on the clean burn area can be determined. This explains why the clean burn zone was not initially white for the soot pattern tests against the gypsum wall. After cleaning the area becomes white.

Figure 3-44 shows the digital image from the 12" x 12" PMMA test against the wall after being discretized in to 1 cm^2 squares.

63
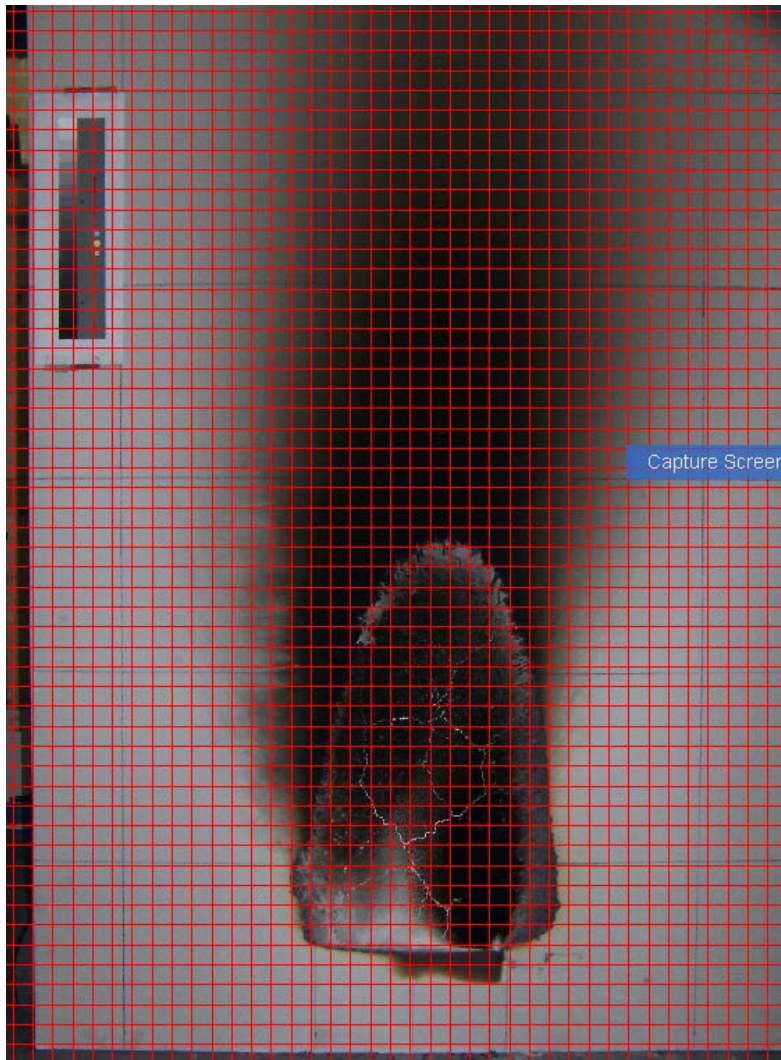
Figure 3-44: Digital image from the wall test after dicretizing into 1 cm^2 squares

Figure 3-45 shows the optical density contours for the 12" x 12" PMMA test against the wall before and after cleaning the clean burn zone. These optical density contours for this test are shown in Figure 3-42 (before cleaning) and Figure 3-43 (after cleaning). For all the wall tests, the same method was applied and the digital images were compared to the optical density contours derived from the smoke deposition analysis.
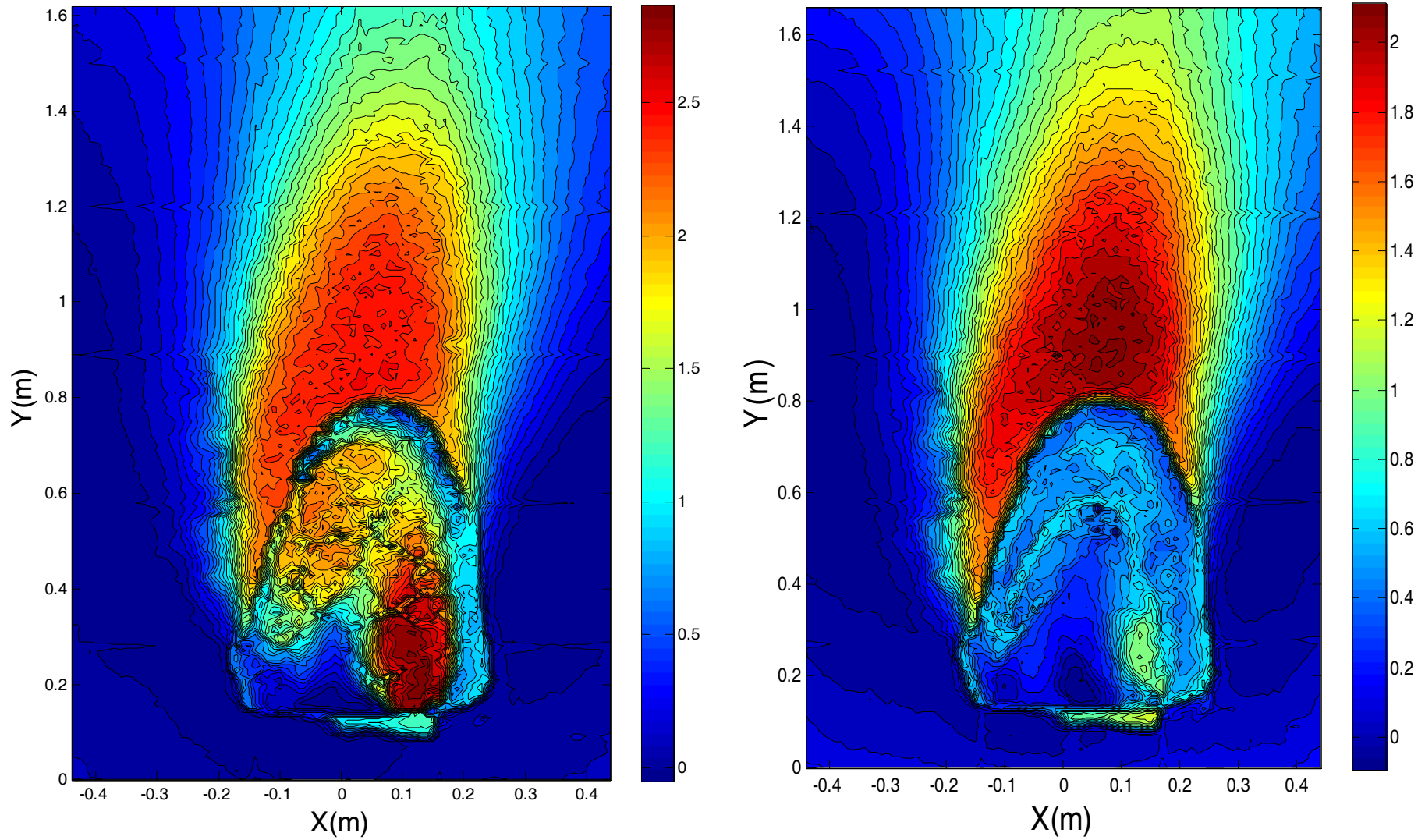
Figure 3-45: Optical density contours for the 12" x 12" PMMA test against the wall before and after cleaning the clean burn zone

3.2.3 Data Reduction

Data reduction for the wall tests was performed in Matlab code the same way it was done for the hood tests. The parameters which were determined for the wall tests are as follows:

- Thermophoretic velocity.

- Extinction optical density.

- Soot deposition on the filters based on the thermophoretic velocity.

3.2.3.1 Thermophoretic Velocity

Thermophoretic velocity was determined for the gypsum wall tests the same method it was determined for the hood tests. Thermophoretic velocity is calculated by Equation 3-3;

$$V_{th} = \frac{k_{th}\eta}{\rho T}\frac{\Delta T}{\Delta x} = \frac{k_{th}\eta}{\rho T}(\frac{dT}{dx}) \qquad \text{Equation 3-3}$$

Where η is the viscosity and ρ, T are the density and temperature at film temperature. Film temperature is the average between the wall and gas temperature at the location. $\dfrac{\Delta T}{\Delta x}$, is the temperature gradient at the surface. K_{th} is the thermophoretic velocity coefficient. (0.55)

As explained in Section 3.1.3.1, the temperature gradient was calculated by using the conservation of energy equation at the boundary layer. Temperature gradient was calculated by Equation 3–13;

$$\frac{\Delta T}{\Delta x} = \frac{dT}{dx} = \frac{(\dot{q}''_{total} - \dot{q}''_{rad})(T_{gas} - T_{wall})}{k_{air}(T_{gas} - T_{water})}$$

Thermophoretic velocity was calculated by Equation 3-14;

$$V_{th} = \frac{(0.55)\eta}{\rho T} \frac{(\dot{q}''_{total} - \dot{q}''_{rad})(T_{gas} - T_{wall})}{k_{air}(T_{gas} - T_{water})}$$

66

3.2.3.2   Extinction Optical Density

Smoke concentrations in the gas phase for the gypsum wall tests were determined using a different method than hood tests. Due to small path length, using a laser and detector was not possible for measuring the soot concentrations.

In order to measure the extinction optical density per meter at both sample points, an indirect method based on combustion product concentrations was developed. A sample line was installed at a location which was above the flame tip. The reason this location was selected for sampling the combustion products was to sample at the point which was outside the flame zone. If the sample point is in the flame zone (reaction zone) the combustion is not complete and that will cause inaccuracy for the further calculations. The necessary measurements for calculating the optical density per meter at low and high locations are; Gas temperature measurements at both, low and high locations, Gas temperature measurement at the sampling point, CO_2, and CO concentrations at the sampling point. Also the fuel properties (Soot yield, CO_2 yield, and Co yield) need to be determined.
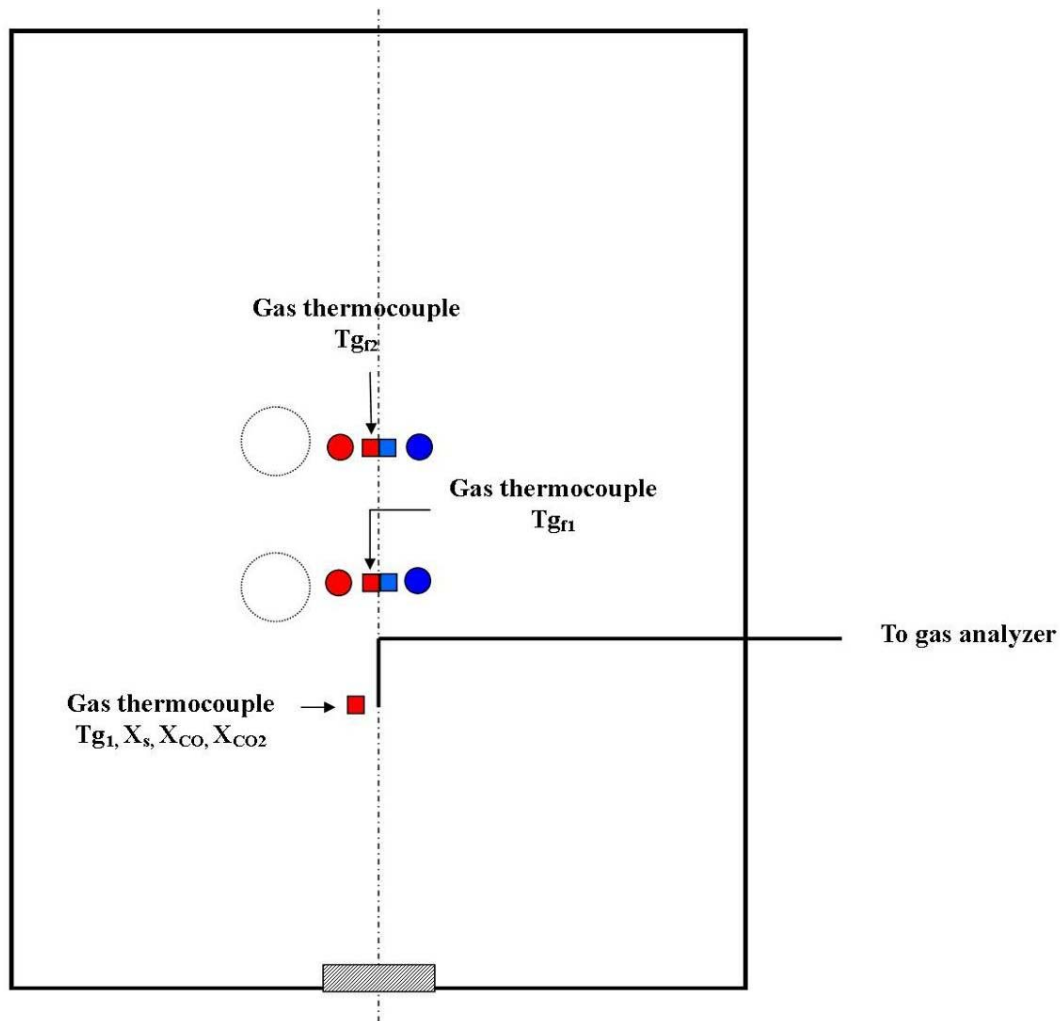
Figure 3-46: Wall test measurements for the extinction optical density calculation

The fuel properties for each set of tests (4 "x 4 ", 8" x 8 ", 12 "x 12 ") were determined for hood tests and cone calorimeter test results. By measuring the combustion product concentrations at the point above the flame tip and using the smoke yield and CO_2 yield measured for each fuel, smoke concentration can be calculated. The following procedure was conducted on the raw data for each test in order to calculate the soot concentration at low and high locations.

By using the conservation of energy equation between the sampling point and the low filter location. It has been assumed that the reduction in the smoke concentration is due to dilution and losses due to radiative and conductive losses are assumed to be negligible.
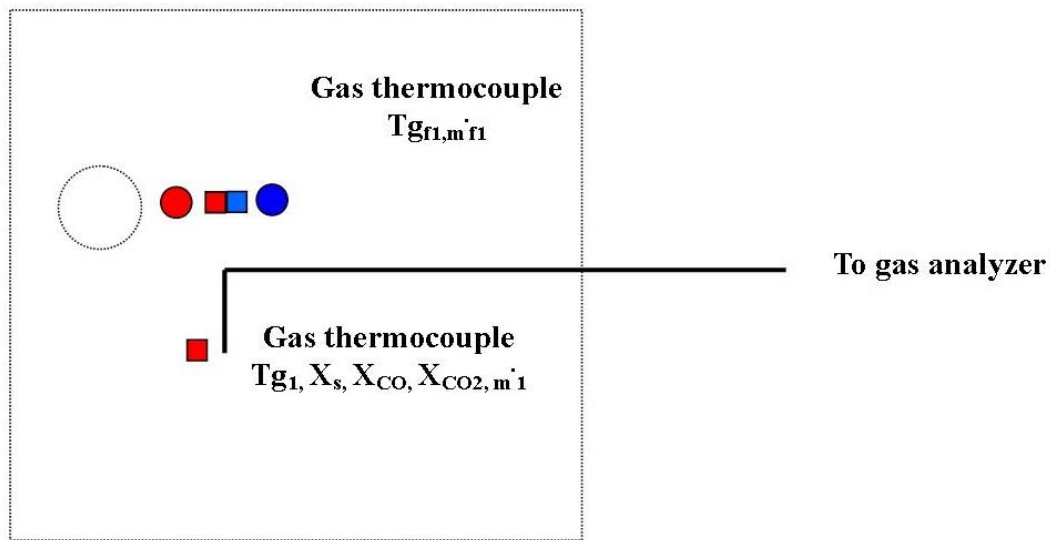
Figure 3-47: Control volume for the conservation of energy between the sampling point and the low filter location

$$\dot{m}_1 cp_1 T_{g_1} = \dot{m}_{f_1} cp_{f1} T_{g_{f1}} \qquad \text{Equation 3-25}$$

Also by using conservation of species between the sampling point and the low filter location;

$$\dot{m}_1 (Y_C)_1 = \dot{m}_{f_1} (Y_C)_{f1} \quad \text{Equation 3-26}$$

$\dot{m}_1, \dot{m}_{f_1}$, are the mass flow rate at the sampling point and at the low filter locations. $(Y_C)_1, (Y_{CO_2})_{f1}$, are the carbon (smoke) mass fractions at the sampling point and at the low filter locations.

$$(Y_C)_{f1} = (\frac{\dot{m}_1}{\dot{m}_{f_1}})(Y_C)_1 \qquad \text{Equation 3-27}$$

By rearranging Equation 3-26;

$$\frac{\dot{m}_1}{\dot{m}_{f_1}} = (\frac{cp_{f1}}{cp_1})(\frac{T_{g_{f1}}}{T_{g_1}}) \qquad \text{Equation 3-28}$$

By assuming that the specific heat doesn't vary too much by temperature variation, Equation 3-29 will be as follow;

69

$$\frac{\dot{m}_1}{\dot{m}_{f_1}} = \frac{T_{gf_1}}{T_{g_1}} \qquad\qquad \text{Equation 3-29}$$

By replacing Equation 3-29 in Equation 3-27;

$$(Y_c)_{f1} = (\frac{T_{gf1}}{T_{g1}})(Y_c)_1 \qquad\qquad \text{Equation 3-30}$$

This means by knowing the smoke concentration at the sampling point and measuring the gas temperatures at sampling point and both low and high filter locations; smoke concentrations will be calculated.

Smoke concentration cannot be measured directly from the gas analyzer but it can be determined based on other measurements from the gas analyzer.

$$(Yc) = (\frac{y_{soot}}{y_{CO_2}})_{Experiments}(X_{CO_2})_{Gas\ analyzer}(\frac{MW_{CO_2}}{X_{mixture}MW_{mixture}}) \qquad \text{Equation 3-31}$$

y_{soot} and y_{CO_2} are the smoke yield and CO_2 yield for each fuel which was used in the tests. These values were measured for each fuel and each fire size separately. Also, $(X_{CO_2})_{Gas\ analyzer}$ is the CO_2 mole fraction measured at the sampling point. MW_{CO_2} is the molecular weight for CO_2 and $X_{mixture}MW_{mixture}$ is assumed to be 29g.

$$(Yc)_{f1} = (\frac{T_{gf1}}{T_{g1}})(\frac{y_{soot}}{y_{CO_2}})_{Experiments}(X_{CO_2})_{Gas\ analyzer}(\frac{MW_{CO2}}{X_{mixture}MW_{mixture}}) \qquad \text{Equation 3-32}$$

Equation 3-33 calculates the smoke concentration at the low filter location. Using the same concept the smoke concentration at the high filter location will be:

$$(Yc)_{f2} = (\frac{T_{gf2}}{T_{g1}})(\frac{y_{soot}}{y_{CO2}})_{Experiments}(X_{CO2})_{Gas\ analyzer}(\frac{MW_{CO2}}{X_{mixture}MW_{mixture}}) \qquad \text{Equation 3-33}$$

3.2.3.3   Soot Deposition Based on Thermophoretic Velocity

Total soot deposition based on thermophoresis mechanism is dependent on thermophoretic

velocity and soot concentration.

$$m'' = \int_o^t V_{th}(t)C_{smoke}(t)dt \quad C_{smoke} = Y_c\rho$$

Where, ρ is the density of the air.

CHAPTER 4 FUEL CHARACTERISTICS

4.1   Fuel Characteristics for Hood Experiments

Fuel characteristics relate to both test series and need to be discussed before the results from hood and wall tests. These characteristics are; heat of combustion, smoke yield, CO_2 yield, and CO yield. These parameters were measured for PMMA, PP, gasoline, ABS, and fiber board.

PMMA

Details for calculating all the properties were discussed in Section 3.1.3, data reduction section. Heat of combustion was calculated based on heat release rate and fuel mass loss rate for each test. The heat of combustion was averaged over the test period and the average heat of combustion is presented for each test. The values for smoke yield, CO_2 yield, and CO yield were also averaged over the test period. Table 4-1 shows the properties for PMMA tests.

Table 4-1: PMMA properties for the hood tests

Test Number	ΔH_c (kJ/g)	Ys (g/g)	Y CO_2 (g/g)	Y CO (g/g)
050409-T2	23.63	0.0153	2.55	0.0085
050409-T1	26.46	0.0155	2.5	0.008
050609-T3	23.92	0.0151	2.6	0.0084
050609-T1	26.14	0.0148	2.45	0.0085
050609-T2	27.23	0.0155	2.65	0.0086
050709-T2	24.99	0.0151	2.5	0.008
050709-T3	24.23	0.0148	2.55	0.009
043009-T1	23.05	0.0152	2.45	0.0085
043009-T4	23.71	0.0151	2.75	0.0097
042909-T1	23.10	0.0153	2.65	0.0085
050109-T1	23.51	0.0155	2.68	0.0088
072109-T1-Low	23.67	0.0152	2.48	0.0088
072109-T1-High	23.67	0.015	2.51	0.009
072209-T1-Low	23.82	0.0152	2.45	0.0094
072209-T1-High	23.82	0.015	2.35	0.0085

Average heat of combustion values for PMMA are between 23.04 – 27.22 kJ/g. Average smoke yield values are between 0.0148 - 0.0155, Average CO_2 yield values are between 2.35 – 2.75, and average CO yield values are between 0.008 – 0.0097. Table 4-2 shows the average properties for PMMA. These values were averaged for all the tests presented in Table 4-1. These average values are very close to values presented by Tewarson [5], as shown in Table 4-3.

Table 4-2: PMMA average properties for the hood tests

	ΔH_c (kJ/g)	Y_S (g/g)	$Y\ CO_2$ (g/g)	$Y\ CO$ (g/g)
Range	23.04 - 27.22	0.0148 - 0.0155	2.35 – 2.75	0.008 - 0.0097
Average	24.33	0.015	2.54	0.008
Standard Deviation	1.28	0.0002	0.106	0.0046

Table 4-3: Average properties for PMMA from hood tests and values reported by Tewarson [5]

	ΔH_c (kJ/g)	Y_S (g/g)	$Y\ CO_2$ (g/g)	$Y\ CO$ (g/g)
Hood Experiments	24.33	0.015	2.54	0.008
Tewarson Values	25.2	0.022	2.12	0.01
Cone Tests Values	20.9	0.016	1.905	0.007
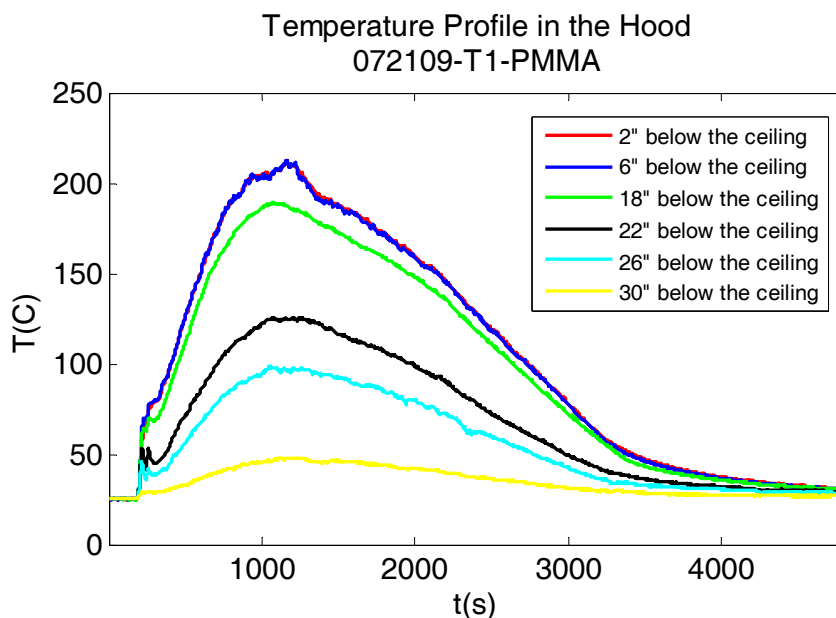
Figure 4-1: Temperature profile in the hood for PMMA test 072109-T1

73

Figure 4-1 shows the temperature profile in the hood for PMMA test, 072109-T1. Temperature profile was averaged over the test period for the first thermocouple in the thermocouple tree (2" below the ceiling) in order to have a temperature representative for the temperature in the hood for different PMMA tests.

Figure 4-2 shows the exhaust rate and fuel mass loss rate for the PMMA test, 072109-T1. Fuel mass loss rate and exhaust rate were used to find the heat release rate and determine the heat of combustion for each test. Exhaust rate and fuel mass loss rates were also used to determine the equivalence ratio for each test.
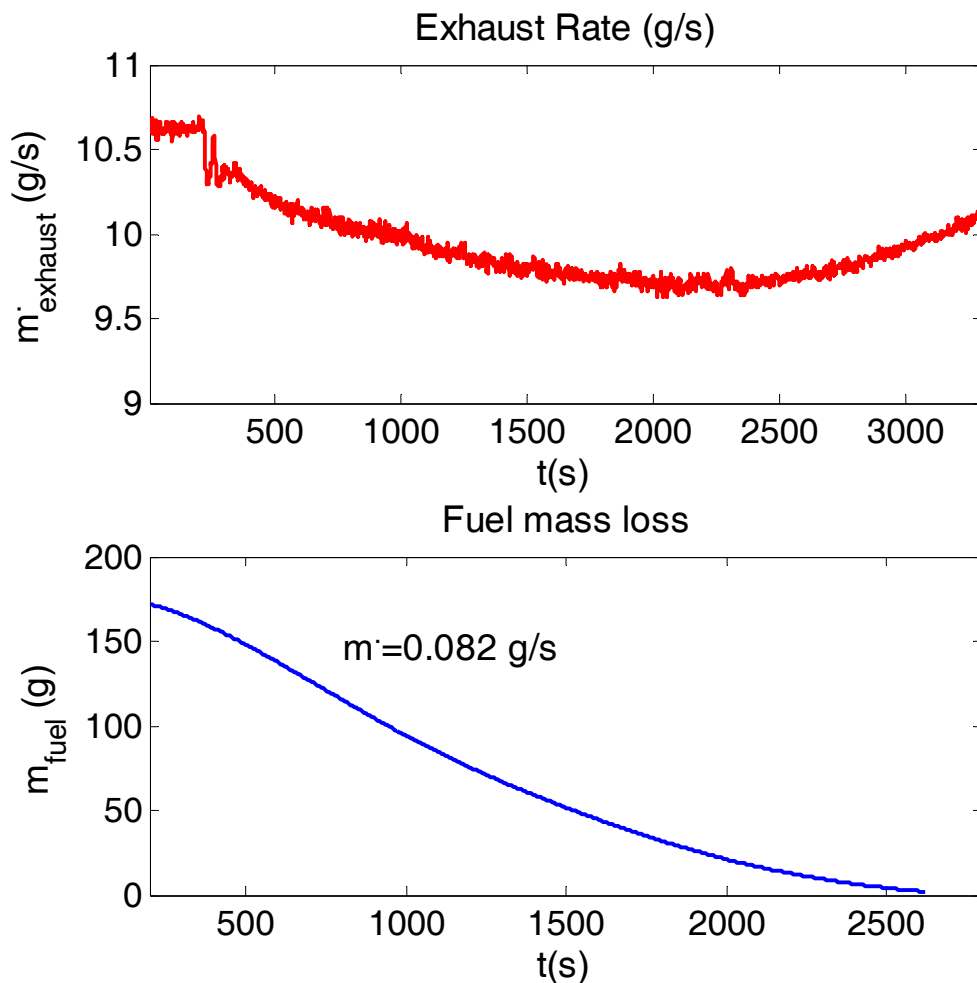
Figure 4-2: Exhaust rate and fuel mass loss rate for PMMA test 072109-T1

Figure 4-3 shows the O_2, CO_2, CO concentrations and heat release rate for the PMMA test, 072109-T1. The heat of combustion was calculated by using the heat release rate and the fuel mass loss rate as explained in Equation 3-24. The heat of combustion was averaged over the test period for all the values presented in Table 4-1.
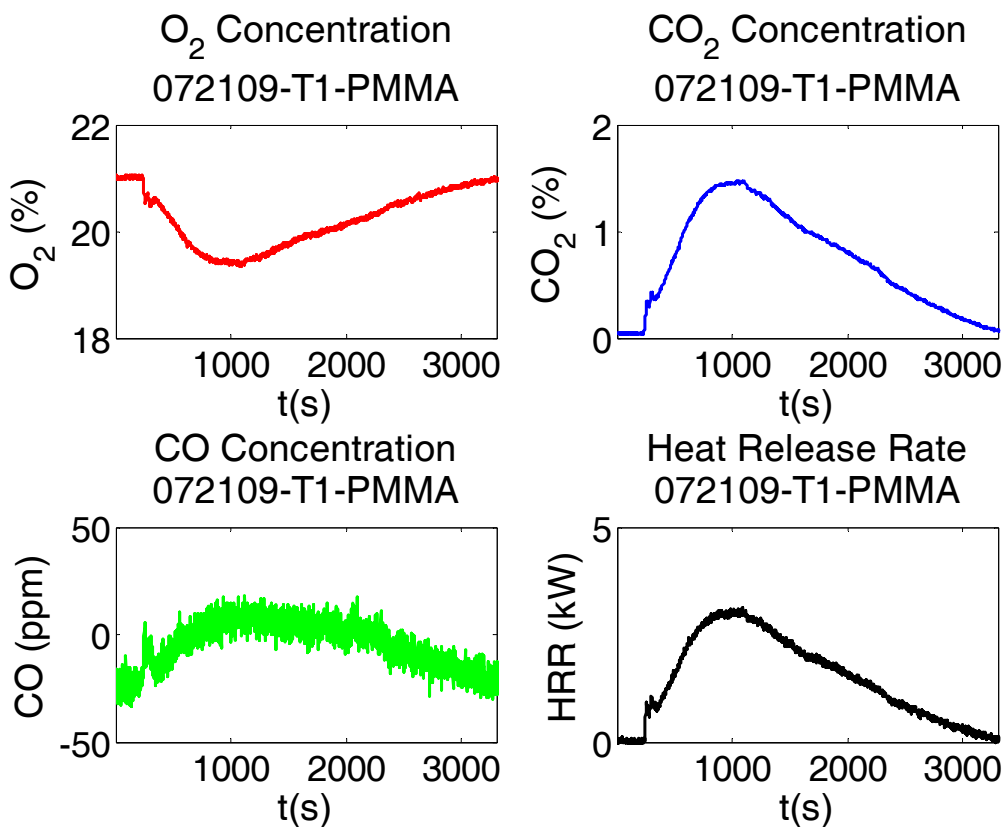
Figure 4-3: O_2, CO_2, CO concentrations and heat release rate for PMMA test 072109-T1

Table 4-4 shows average layer temperature, equivalence ratio, exhaust rate, fuel mass loss rate, and heat release rate for PMMA tests. All the values were averaged over the test period in order to have a representative of each value for each test.

Table 4-4: Average values for smoke layer properties for PMMA hood tests

Test Number	T_{layer} (°C)	ϕ	$\dot{m}_{exh}$ (g/s)	$\dot{m}_f$ (g/s)	$\dot{Q}$ (kW)
050409-T2	133.02	0.068	7.79	0.063	1.49
050409-T1	162.85	0.080	7.62	0.073	1.93
050609-T3	161.47	0.097	9.08	0.105	2.51
050609-T1	200.27	0.121	9.01	0.130	3.40
050609-T2	207.77	0.113	8.93	0.120	3.27
050709-T2	131.16	0.079	9.13	0.087	2.17
050709-T3	153.78	0.291	2.23	0.092	2.23
043009-T1	213.48	0.357	2.78	0.130	3.00
043009-T4	216.92	0.118	7.83	0.110	2.61
042909-T1	223.20	0.115	7.88	0.108	2.42
050109-T1	199.28	0.100	8.04	0.096	2.26
072109-T1-Low	161.95	0.069	9.91	0.082	1.94
072109-T1-High	161.95	0.069	9.91	0.082	1.94
072209-T1-Low	165.35	0.068	9.92	0.081	1.93
072209-T1-High	165.35	0.068	9.92	0.081	1.93

There is a significant difference between temperature at each elevation in the layer and it was studied by using different thermocouples in the thermocouple tree in order to have a good history of the temperatures at each elevation in the smoke layer. For smoke concentration laser and detectors were places at only two locations to measure the extinction optical density at both low and high locations. There was not a significant difference between low and high location extinction optical densities for each test. Average smoke layer temperatures in the hood are between 131 – 223 º C. equivalence ratio values are between 0.07 – 0.36, and heat release rates are between 1.49 – 3.6 kW. Low and high indicates the filter location in the hood apparatus.

Table 4-5: Smoke layer properties range for PMMA tests

	$T_{layer}(^{\circ}C)$	ϕ	$\dot{m}_{exh}$ (g/s)	$\dot{m}_f$ (g/s)	$\dot{Q}$ (kW)
Range	131.16 - 223.20	0.07- 0.36	2.23 -9.92	0.06 - 0.13	1.49 - 3.40
Average	177.19	0.12	8.00	0.10	2.34
Standard Deviation	30.22	0.09	2.39	0.02	0.54

Figure 4-4 shows the optical density per meter for a PMMA test, 072109-T1. The optical
density per meter for the high location is slightly higher than the low location but it is not
significant as discussed earlier.
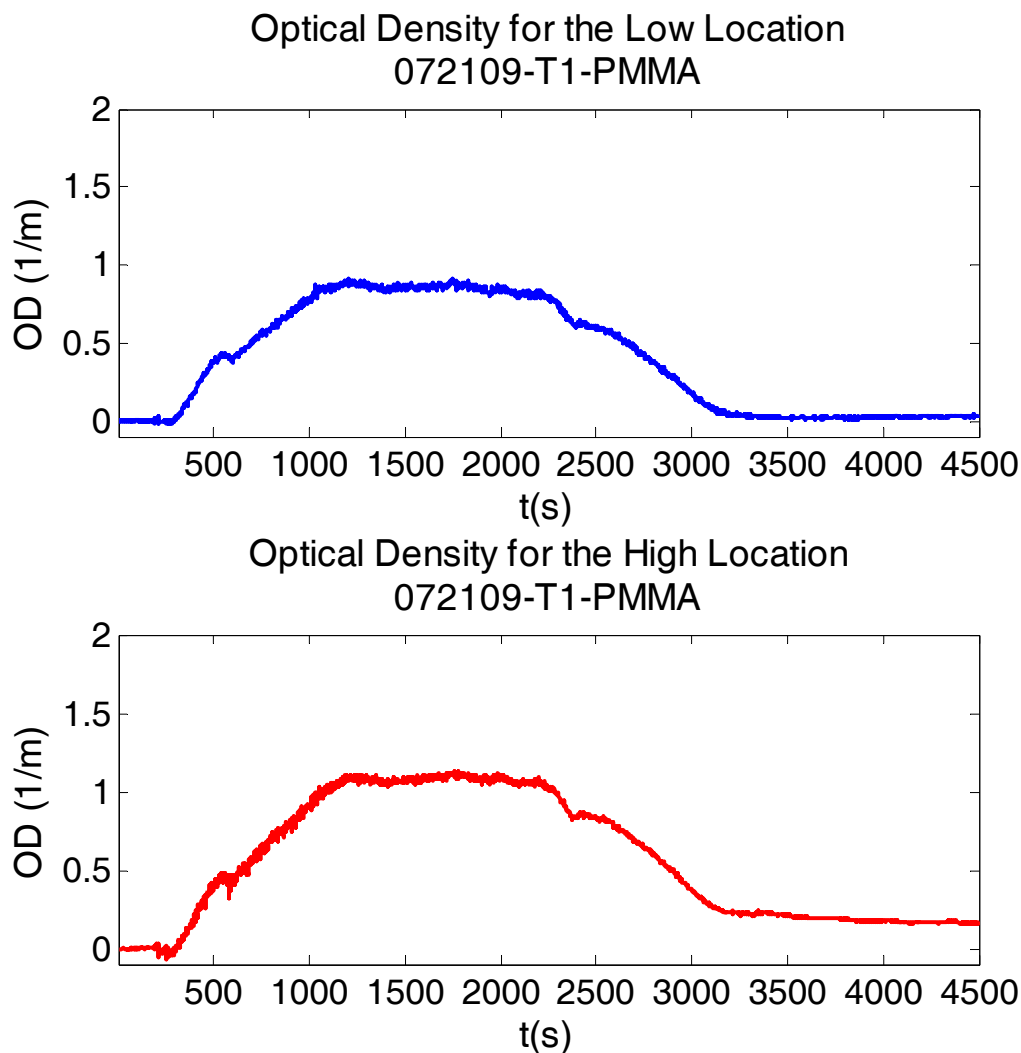
Figure 4-4: Optical density per meter for both low and high location for PMMA test, 072109-T1

Gasoline

Average heat of combustion values for gasoline are between 40.5 – 45.64 kJ/g. Average smoke yield values are between 0.068 – 0.09, average CO_2 yield values are between 1.8 – 2.5, and average CO yield values are between 0.009-0.0123.

Table 4-6: Gasoline properties for the hood tests

Test Number	ΔH_c (kJ/g)	Ys (g/g)	Y CO_2 (g/g)	Y CO (g/g)
042009-T3-Low	44.51	0.068	2.4	0.009
042009-T2-High	41.17	0.07	2.23	0.0095
060309-T2-High	42.83	0.069	2.3	0.011
060909-T1-Low	40.51	0.088	2.5	0.012
061009-T1-Low	45.64	0.09	2	0.0123
061009-T1-High	45.64	0.09	2	0.0123
061009-T2-Low	43.99	0.083	2.3	0.011
061009-T2-High	43.99	0.083	2.3	0.011

Table 4-7 shows the average properties for gasoline. These values were averaged for all the tests presented in Table 4-6. These average values are slightly different than values reported by Tewarson [5]. The values reported by Tewarson are for Octane and the gasoline properties are different from Octane but it is the closest fuel to gasoline. The aromatics in gasoline increase smoke yield.

Table 4-7: Gasoline average properties for hood tests

	ΔH_c (kJ/g)	Ys (g/g)	Y CO_2 (g/g)	Y CO (g/g)
Range	40.5 - 45.64	0.068 - 0.09	2.0 - 2.5	0.009-0.0123
Average	43.54	0.080	2.254	0.011
Standard Deviation	1.91	0.010	0.176	0.001

78

Table 4-8: Average properties for gasoline from hood tests and values reported by Tewarson [5]

	ΔH_c (kJ/g)	Ys (g/g)	Y CO_2 (g/g)	Y CO (g/g)
Hood Experiments	43.54	0.080	2.254	0.011
Tewarson Values for Octane	44.5	0.038	2.84	0.011
Cone Test Values	42.15	0.072	2.12	0.009

Figure 4-5 shows the temperature profile in the hood for gasoline test, 061009-T1.

Temperature profile was averaged over the test period for the first thermocouple in the

thermocouple tree (2 " below the ceiling) in order to have a temperature representative for the

temperature in the hood for different gasoline tests.
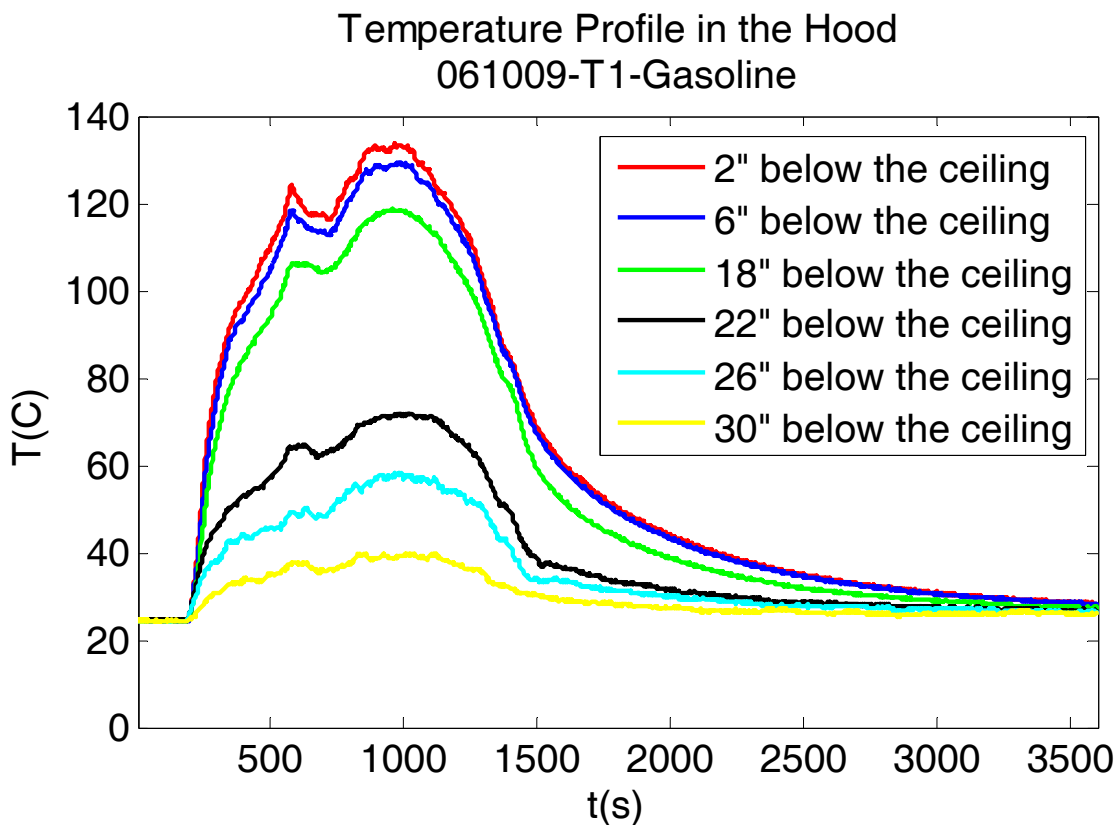
Figure 4-5: Temperature profile in the hood for gasoline test 061009-T1

Figure 4-6 shows the exhaust rate and fuel mass loss rate for the gasoline test, 061009-T1. Fuel mass loss rate and exhaust rate were used to find the heat release rate and determine the heat of combustion for each test. Exhaust rate and fuel mass loss rates were also used to determine the equivalence ratio for each test.
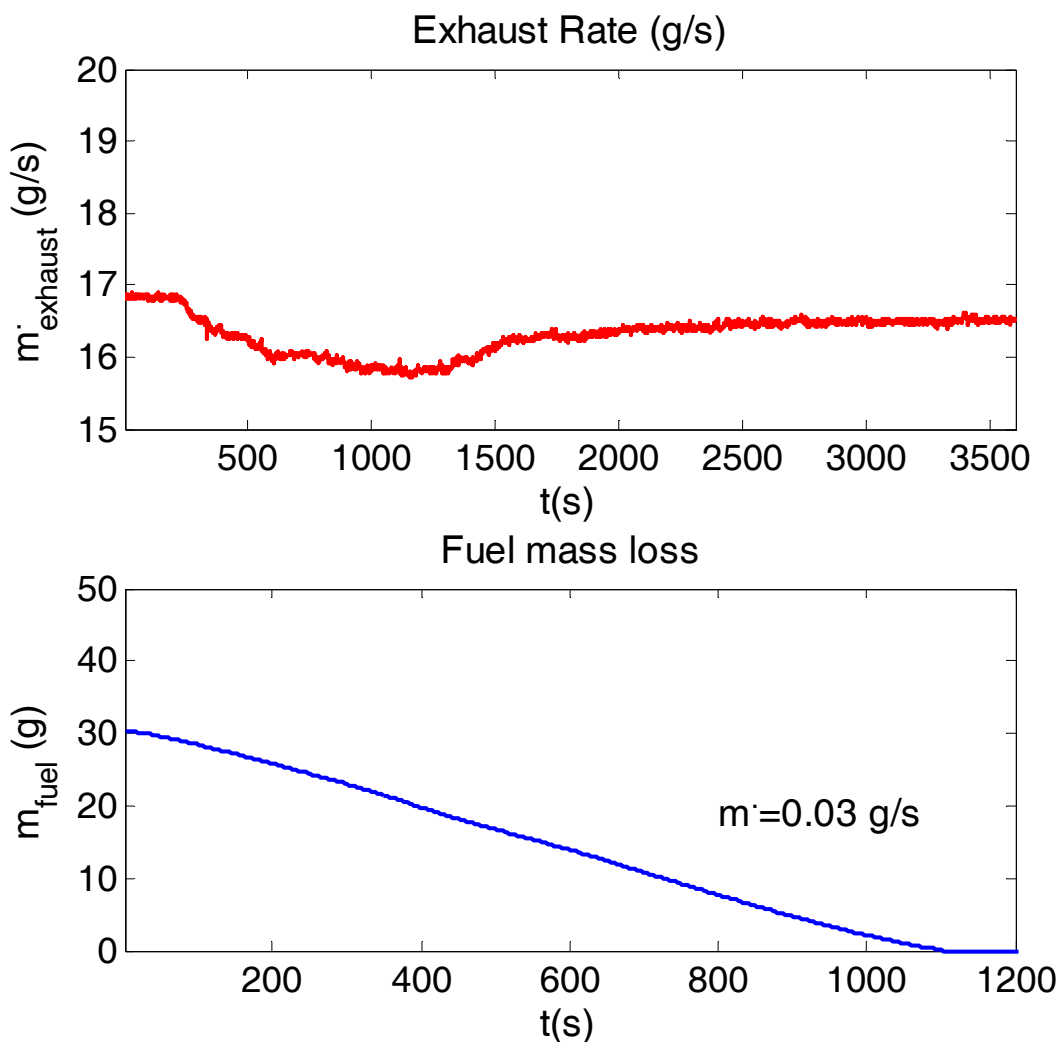
Figure 4-6: Exhaust rate and fuel mass loss rate for gasoline test 061009-T1

Figure 4-7 shows the O_2, CO_2, CO concentrations and heat release rate for the gasoline test, 061009-T1. The heat of combustion was calculated by using the heat release rate and the fuel mass loss rate as explained in Equation 3-24. The heat of combustion was averaged over the test period for all the values presented in Table 4-6.
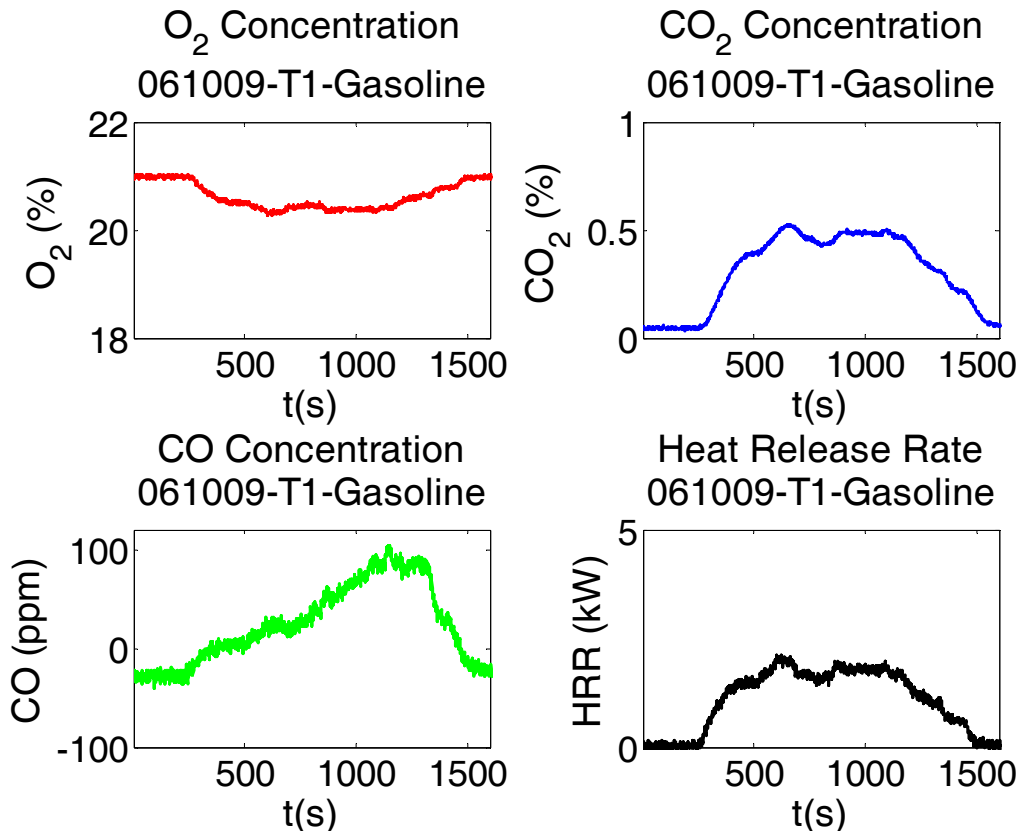
Figure 4-7: O_2, CO_2, CO concentrations and heat release rate for gasoline test 061009-T1

Table 4-9 shows average layer temperature, equivalence ratio, exhaust rate, fuel mass loss rate, and heat release rate for gasoline tests. All the values were averaged over the test period in order to have a representative of each value for each test.

Table 4-9: Average values for smoke layer properties for gasoline hood tests

Test Number	$T_{layer}(\,^\circ C)$	ϕ	$\dot{m}_{exh}$ (g/s)	$\dot{m}_f$ (g/s)	$\dot{Q}$ (kW)
042009-T3-low	141.54	0.045	15.26	0.045	2.02
042009-T2-high	126.49	0.040	15.40	0.041	1.68
060309-T2-high	65.19	0.004	30.86	0.008	0.09
060909-T1-low	40.12	0.021	9.22	0.013	0.50
061009-T1-low	108.94	0.028	16.06	0.030	1.37
061009-T1-high	108.94	0.028	16.06	0.030	1.37
061009-T2-low	118.77	0.034	15.84	0.034	1.50
061009-T2-high	118.77	0.034	15.84	0.034	1.50

Average smoke layer temperatures in the hood are between 40 – 141 º C. equivalence ratio values are between 0.004 – 0.045, and heat release rates are between 0.09 – 2.0 kW.

Table 4-10: Smoke layer properties range for gasoline tests

	T_{layer}(˚C)	ϕ	$\dot{m}_{exh}$ (g/s)	$\dot{m}_f$ (g/s)	$\dot{Q}$ (kW)
Range	40.12 - 141.54	0.004 - 0.045	9.22 - 30.86	0.01 - 0.05	0.09 - 2.02
Average	103.60	0.03	16.82	0.03	1.25
Standard Deviation	33.78	0.01	6.12	0.01	0.63

Figure 4-8 shows the optical density per meter for gasoline test, 061009-T1. Optical density per meter is higher for the high location. (76 cm from the hood base)
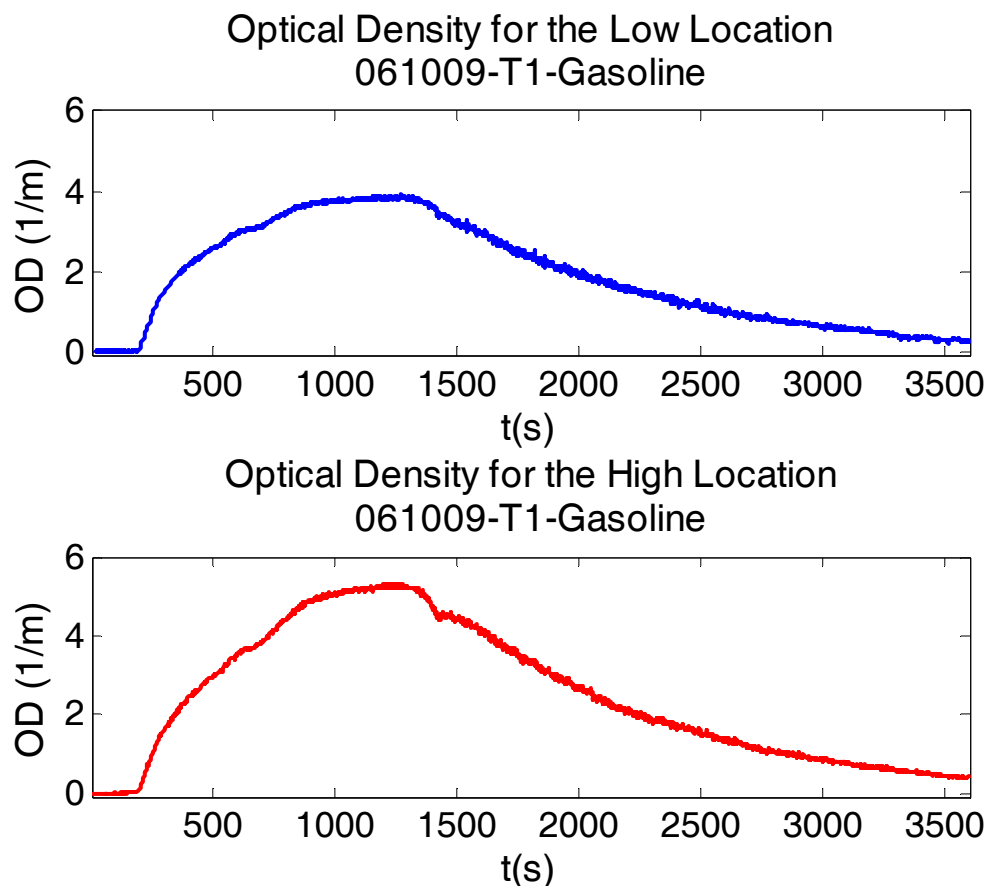
Figure 4-8: Optical density per meter for both low and high locations for gasoline test, 061009-T1

Polypropylene

Average heat of combustion values for PP are between 40.1 - 44.1 kJ/g. Average smoke yield values are between 0.04 - 0.055, Average CO_2 yield values are between $2.7 - 2.95$, and average CO yield values are between 0.04-0.055.

Table 4-11: Polypropylene properties for the hood tests

Test Number	ΔH_c (kJ/g)	Ys (g/g)	Y CO_2 (g/g)	Y CO (g/g)
063009-T1-Low	41.11	0.055	2.95	0.0204
063009-T1-High	41.11	0.05	2.85	0.022
070109-T1-Low	42.10	0.045	2.85	0.023
070109-T1-High	42.10	0.052	2.81	0.02
070609-T1-Low	44.17	0.04	2.8	0.026
070609-T1-High	44.17	0.042	2.95	0.027
070609-T2-Low	42.12	0.043	2.81	0.0276
070709-T1-low	41.43	0.041	2.7	0.02
070709-T1-High	41.43	0.045	2.8	0.025
070909-T1-Low	40.15	0.045	2.85	0.02
070909-T1-High	40.15	0.044	2.86	0.024

Table 4-12 shows the average properties for polypropylene. These values were averaged for all the tests presented in Table 4-11. These average values are slightly different than values reported by Tewarson [5].

Table 4-12: Polypropylene average properties for hood tests.

	ΔH_c (kJ/g)	Ys (g/g)	Y CO_2 (g/g)	Y CO (g/g)
Range	40.1 - 44.1	0.04 - 0.055	2.70- 2.95	0.04 - 0.055
Average	41.82	0.045	2.83	0.023
Standard Deviation	1.34	0.004	0.070	0.002

Table 4-13: Average properties for polypropylene from hood tests and values reported by Tewarson [5]

	ΔH_c (kJ/g)	Y_s (g/g)	Y CO_2 (g/g)	Y CO (g/g)
Hood Experiments	41.82	0.045	2.83	0.023
Tewarson Values	43.4	0.059	2.79	0.024
Cone Tests Values	38.5	0.041	2.84	0.020

Figure 4-9 shows the temperature profile in the hood for polypropylene test, 070609-T1. Temperature profile was averaged over the test period for the first thermocouple in the thermocouple tree (2 " below the ceiling) in order to have a temperature representative for the temperature in the hood for different polypropylene tests. There is an early peak in temperature in the polypropylene test. This is due to the period which torch was held on the fuel sample to melt it which was explained in fuel set up section in Chapter 3.
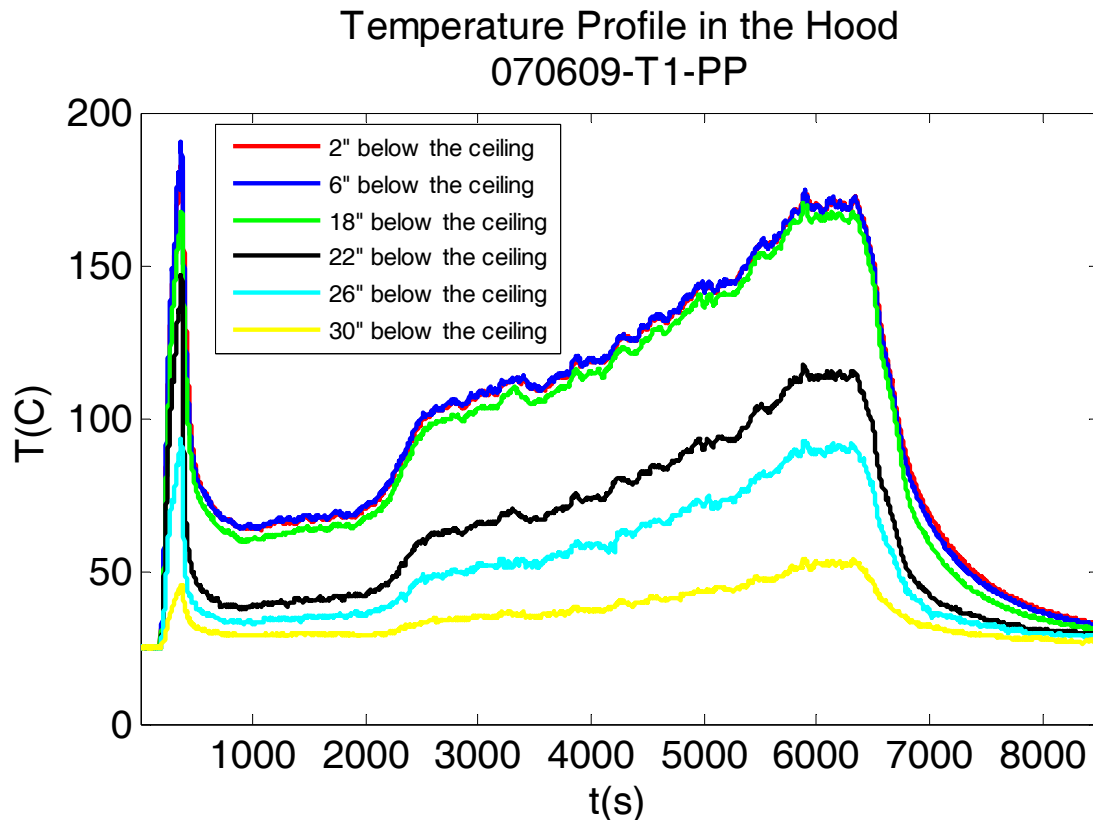
Figure 4-9: Temperature profile in the hood for polypropylene test 070609-T1

Figure 4-10 shows the exhaust rate and fuel mass loss rate for the polypropylene test, 070609-T1. Fuel mass loss rate and exhaust rate were used to find the heat release rate and determine the heat of combustion for each test. Exhaust rate and fuel mass loss rates were also used to determine the equivalence ratio for each test.
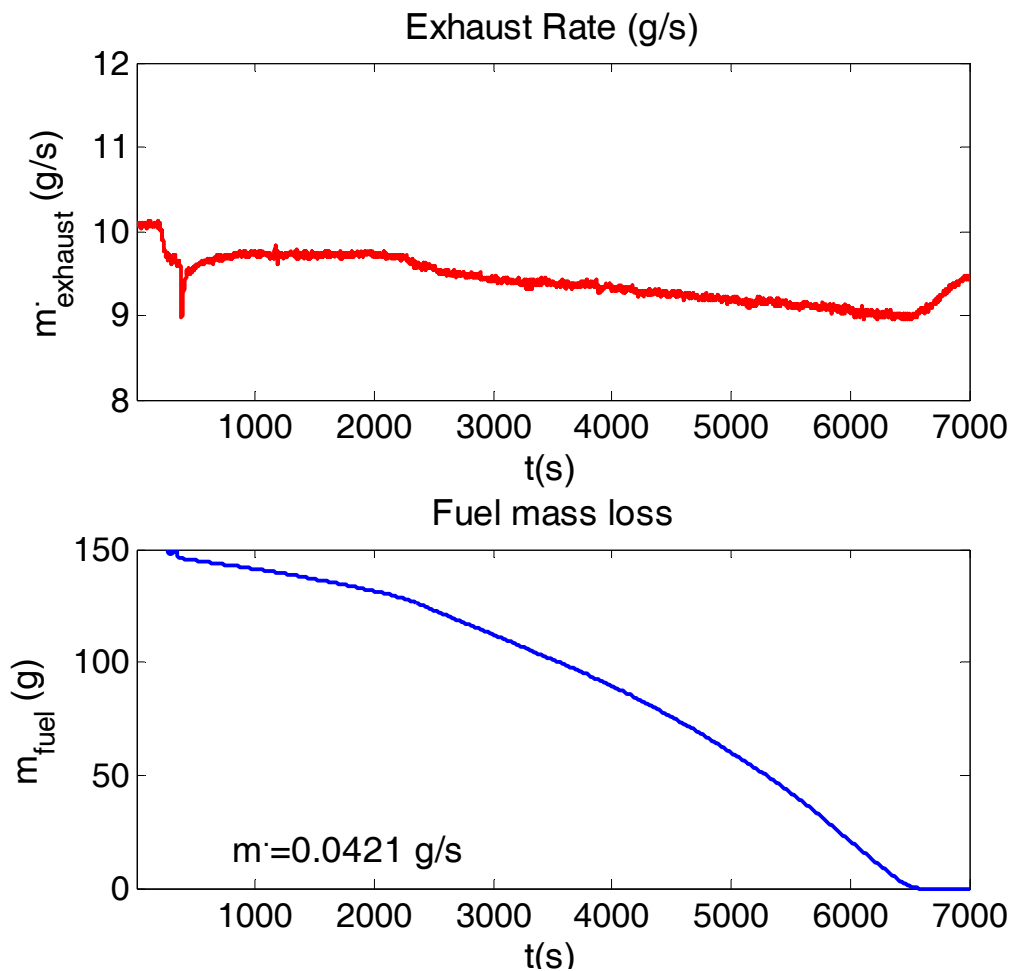
Figure 4-10: Exhaust rate and fuel mass loss rate for polypropylene test 070609-T1

Figure 4-11 shows the O_2, CO_2, CO concentrations and heat release rate for the polypropylene test, 070609-T1. The heat of combustion was calculated by using the heat release rate and the fuel mass loss rate as explained in Equation 3–24. The heat of combustion was averaged over the test period for all the values presented in Table 4-11. The sudden reduction in oxygen concentration is due to the propane torch which was used to ignite the polypropylene

sample. There is also a sudden increase in the heat release rate and carbon dioxide and carbon monoxide concentrations. These are all due to the ignition time with the propane torch.
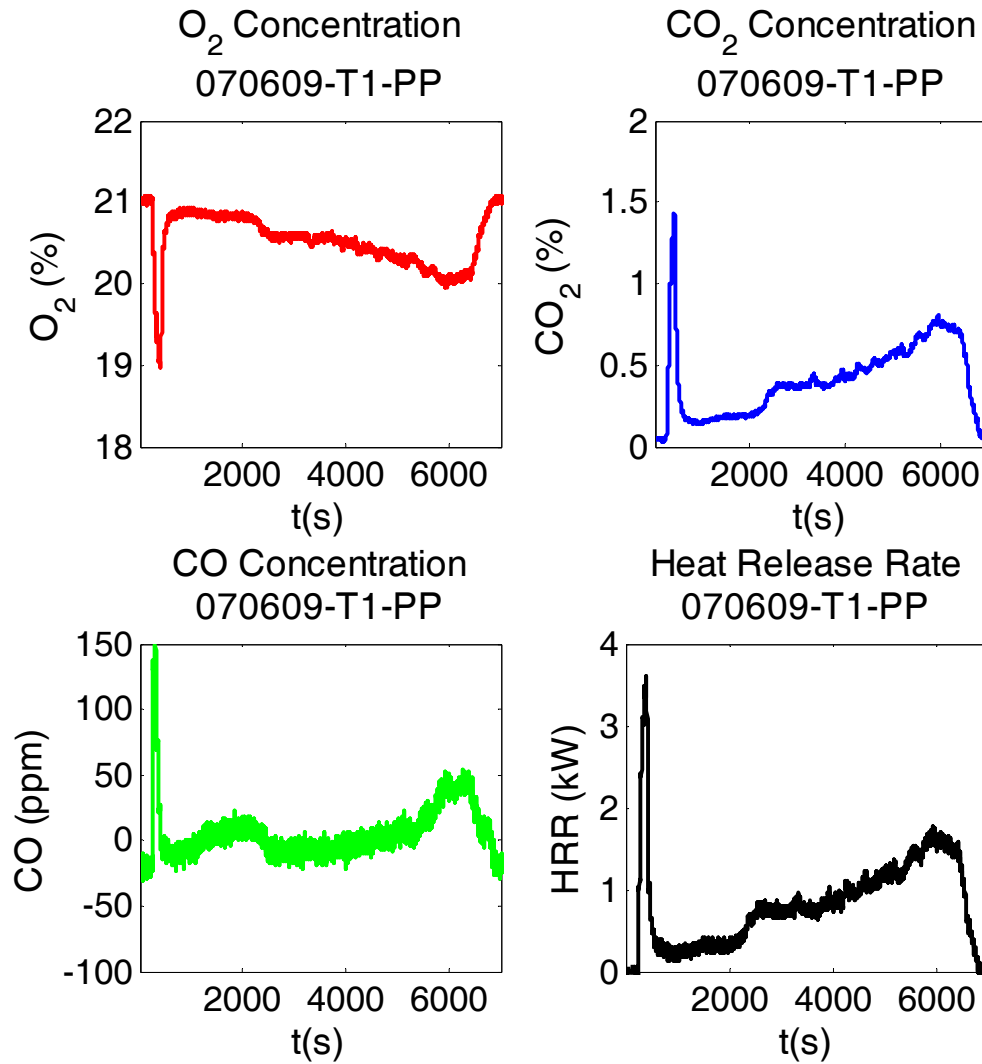
Figure 4-11: O_2, CO_2, CO concentrations and heat release rate for polypropylene test 070609-T1

Table 4-14 shows average layer temperature, equivalence ratio, exhaust rate, fuel mass loss rate, and heat release rate for polypropylene tests. All the values were averaged over the test period in order to have a representative of each value for each test.

Table 4-14: Average values for smoke layer properties for polypropylene hood tests

Test Number	T_{layer}(˚C)	ϕ	$\dot{m}_{exh}$ (g/s)	$\dot{m}_f$ (g/s)	$\dot{Q}$(kW)
063009-T1-Low	118.82	0.019	29.10	0.037	1.52
063009-T1-High	118.82	0.019	29.10	0.037	1.52
070109-T1-Low	124.05	0.014	29.05	0.028	1.20
070109-T1-High	124.05	0.014	29.05	0.028	1.20
070609-T1-Low	109.21	0.027	16.43	0.031	1.35
070609-T1-High	109.21	0.027	16.43	0.031	1.35
070609-T2-Low	150.50	0.067	9.27	0.042	1.77
070709-T1-Low	127.52	0.040	9.07	0.025	1.04
070709-T1-High	127.52	0.040	9.07	0.0251	1.04
070909-T1-Low	87.79	0.019	9.49	0.0125	0.50
070909-T1-High	87.79	0.019	9.49	0.0125	0.50

Average smoke layer temperatures in the hood are between 87 – 150 º C. equivalence ratio values are between 0.01 – 0.07, and heat release rates are between 0.5 – 1.77 kW.

Table 4-15: Smoke layer properties range for polypropylene tests

	T_{layer}(˚C)	ϕ	$\dot{m}_{exh}$ (g/s)	$\dot{m}_f$ (g/s)	$\dot{Q}$(kW)
Range	87.79 - 150.50	0.01- 0.07	9.07 - 29.10	0.01 - 0.04	0.5-1.77
Average	116.84	0.03	17.78	0.03	1.18
Standard Deviation	18.10	0.02	9.35	0.01	0.40

Figure 4-12 shows the optical density per meter for polypropylene test, 070609-T1. Optical density per meter history for both low and high locations for polypropylene test have the same pattern and smoke concentration is not significantly different between low and high locations.
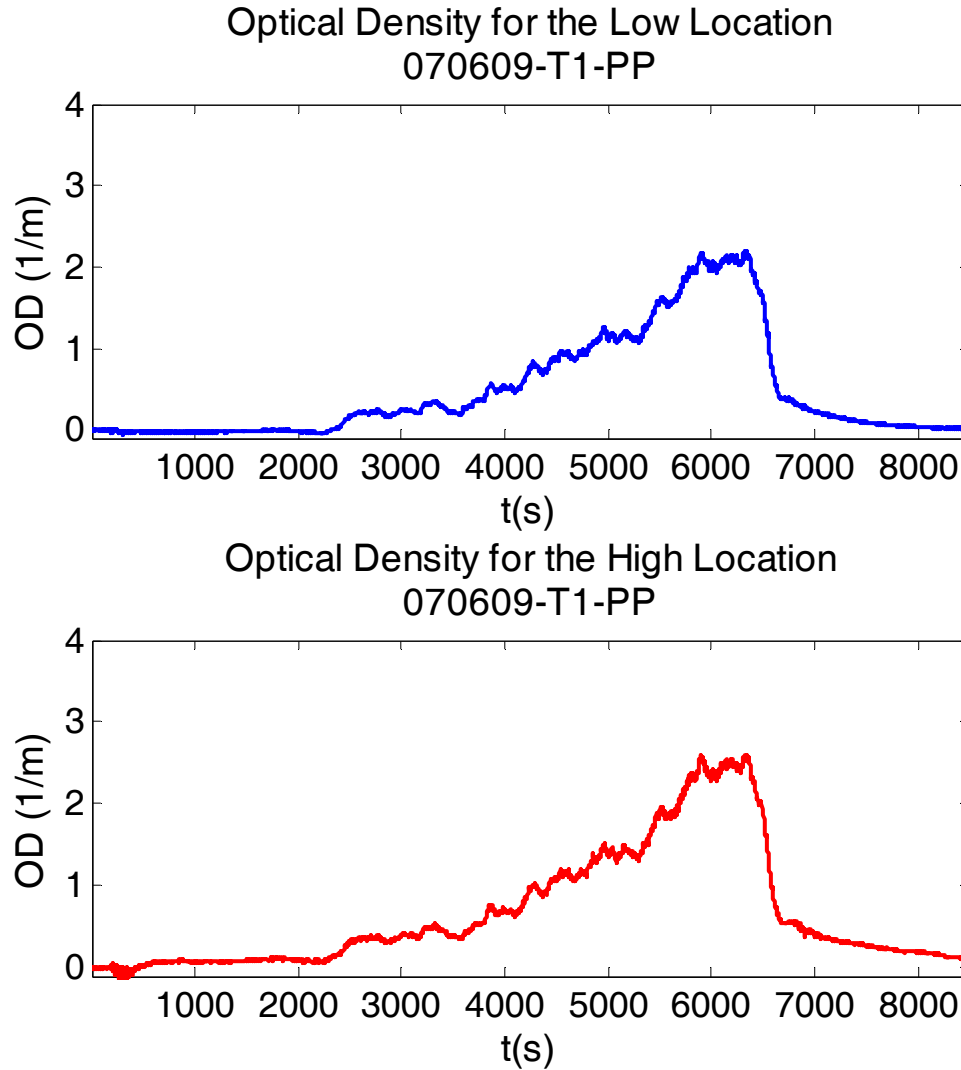
Figure 4-12: Optical density per meter for both low and high locations for polypropylene test 070609-T1

ABS

Average heat of combustion values for ABS are between $23.2 - 26.7$ kJ/g. Average CO_2 yield values are between $1.95 - 2.2$, and average CO yield values are between 0.06-0.075.

Table 4-16: ABS properties for the hood tests

Test Number	ΔH_c (kJ/g)	Y CO_2 (g/g)	Y CO (g/g)
061809-T1-High	24.12	2.2	0.067
061809-T2-High	26.56	2.12	0.065
062209-T1-Low	26.71	2	0.06
062209-T1-High	26.71	2	0.065
062209-T2-Low	26.17	2.2	0.07
062209-T2-High	26.17	2.1	0.075
062409-T1-Low	23.26	1.95	0.065
062409-T1-High	23.26	2.2	0.068
062409-T2-Low	25.95	2.1	0.07
062409-T2-High	25.95	2	0.07

Table 4-17 shows the average properties for polypropylene. These values were averaged for all the tests presented in Table 4-16.

Table 4-17: ABS average properties for the hood tests

	ΔH_c (kJ/g)	Y CO_2 (g/g)	Y CO (g/g)
Range	23.26 - 26.71	1.95 – 2.2	0.06-0.075
Average	25.49	2.087	0.0675
Standard Deviation	1.39	0.095	0.004

Smoke yield was not measured for ABS tests due to high smoke generation rate of ABS and the resulting lack of extinction optical density measurements.

Table 4-18: Average properties for ABS from hood tests and values reported by Tewarson [5]

	ΔH_c (kJ/g)	Y CO$_2$ (g/g)	Y CO (g/g)	Ys (g/g)
Hood Experiments	25.49	2.087	0.0675	-
Tewarson values	30	-	-	-
Cone test values	26.4	2.0746	0.0687	

The values for carbon dioxide yield and carbon monoxide yields were not reported by Tewarson. Figure 4-13 shows the temperature profile in the hood for ABS test, 062409-T2. Temperature profile was averaged over the test period for the first thermocouple in the thermocouple tree (2 " below the ceiling) in order to have a temperature representative for the temperature in the hood for different ABS tests.
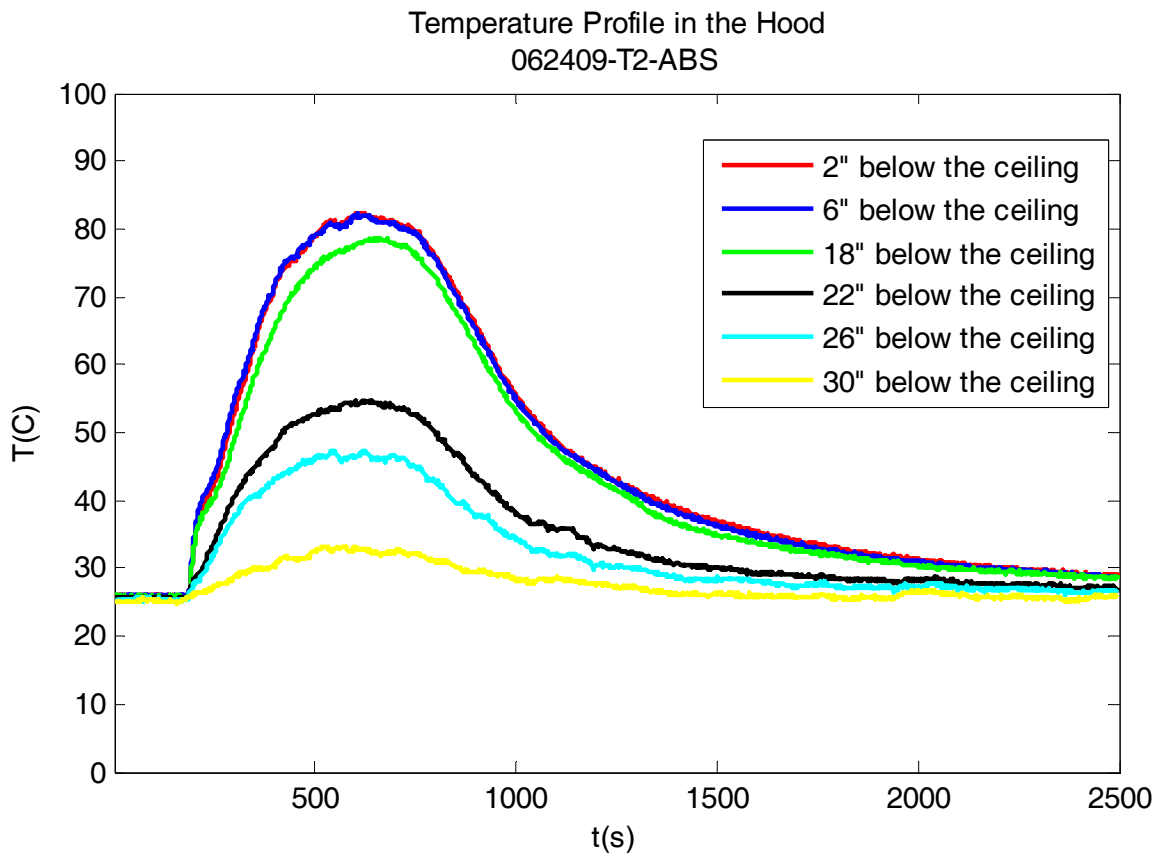
Figure 4-13: Temperature profile in the hood for ABS test 062409-T2

Figure 4-14 shows the exhaust rate and fuel mass loss rate for the ABS test, 062409-T2. Fuel mass loss rate and exhaust rate were used to find the heat release rate and determine the heat of combustion for each test. Exhaust rate and fuel mass loss rates were also used to determine the equivalence ratio for each test.
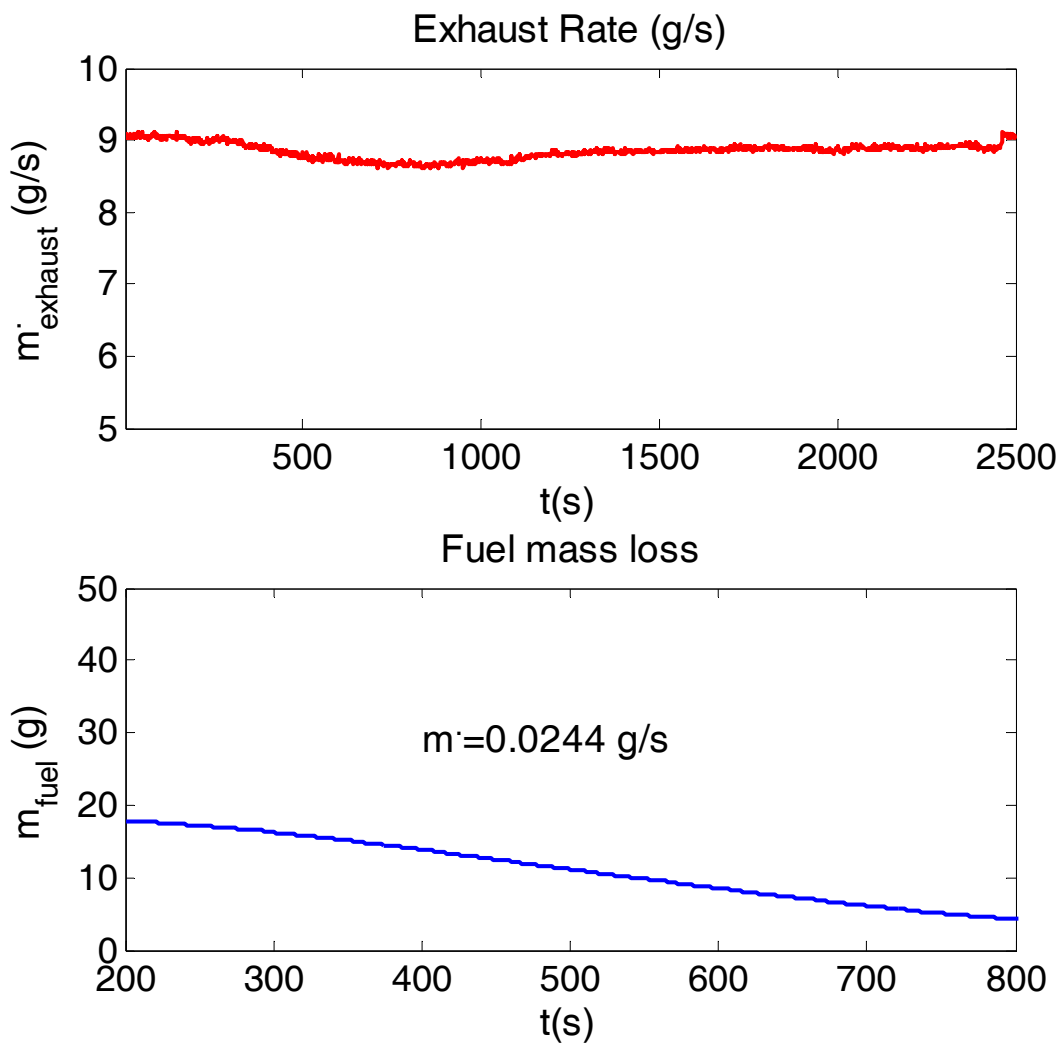
Figure 4-14: Exhaust rate and fuel mass loss rate for ABS test 062409-T2

Figure 4-15 shows the O_2, CO_2, CO concentrations and heat release rate for the ABS test, 062409-T2. The heat of combustion was calculated by using the heat release rate and the fuel mass loss rate as explained in Equation 3–24. The heat of combustion was averaged over the test period for all the values presented in Table 4-16.

91
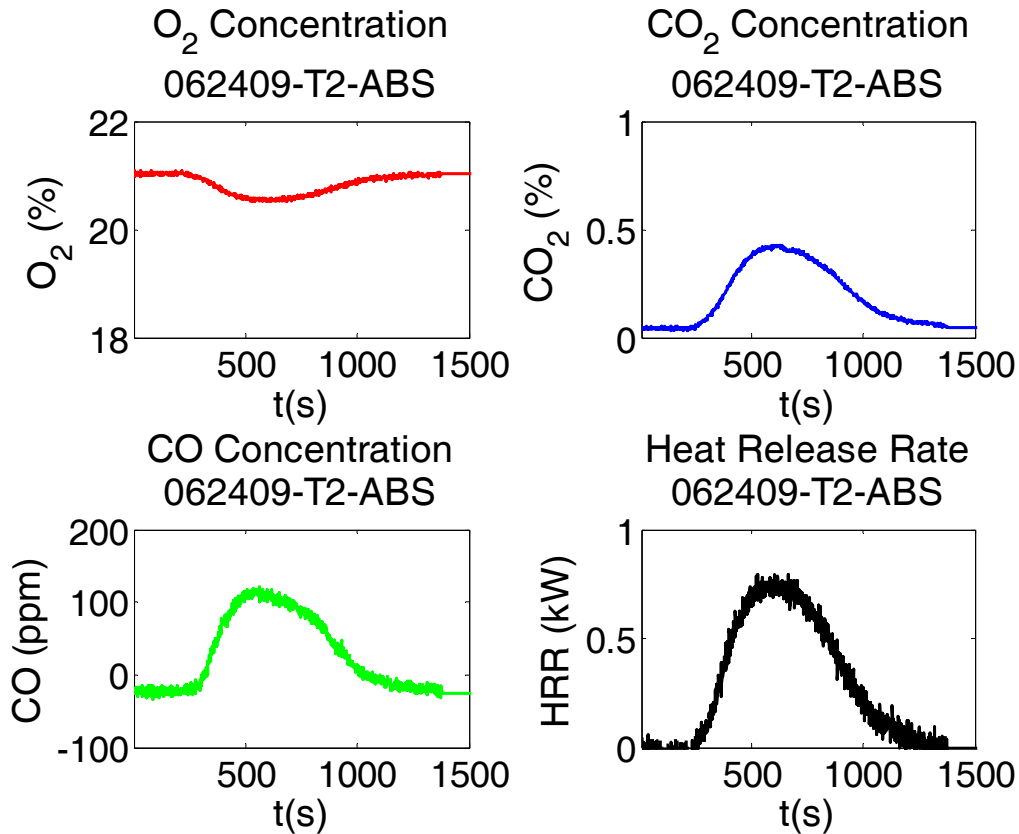
Figure 4-15: O_2, CO_2, CO concentrations and heat release rate for ABS test 062409-T2

Table 4-19 shows average layer temperature, equivalence ratio, exhaust rate, fuel mass loss rate, and heat release rate for polypropylene tests. All the values were averaged over the test period in order to have a representative of each value for each test.

Average smoke layer temperatures in the hood are between 60 – 103 º C. equivalence ratio values are between 0.01 – 0.06, and heat release rates are between 0.47 – 1.03 kW.

Table 4-19: Average values for smoke layer properties for ABS hood tests

Test Number	T_{layer}(˚C)	ϕ	$m_{exh}^{\cdot}$ (g/s)	$m_f^{\cdot}$ (g/s)	$Q^{\cdot}$(kW)
061809-T1-High	60.51	0.010	16.21	0.012	0.59
061809-T2-High	67.31	0.024	9.12	0.018	0.47
062209-T1-Low	103.23	0.055	8.77	0.038	1.03
062209-T1-High	103.23	0.055	8.77	0.038	1.03
062209-T2-Low	101.22	0.056	8.63	0.039	1.01
062209-T2-High	101.22	0.056	8.63	0.039	1.01
062409-T1-Low	95.26	0.063	8.65	0.044	1.01
062409-T1-High	95.26	0.063	8.65	0.044	1.01
062409-T2-Low	77.64	0.035	8.72	0.024	0.63
062409-T2- High	77.64	0.035	8.72	0.024	0.63

Table 4-20: Smoke layer properties range for ABS tests

	T_{layer}(˚C)	ϕ	$m_{exh}^{\cdot}$ (g/s)	$m_f^{\cdot}$ (g/s)	$Q^{\cdot}$(kW)
Range	60.51 - 103.23	0.01 - 0.06	8.63 - 16.21	0.01- 0.04	0.47 -1.03
Average	88.26	0.05	9.49	0.03	0.84
Standard Deviation	16.04	0.02	2.36	0.01	0.22

Fiber board

Heat of combustion value for fiber board is between 10.2-15.7kJ/g. CO_2 yield values are between 0.9-1.41 g/g, and CO yield values are between 0.018-0.024 g/g. Smoke yield was not measured for fiberboard since it doesn't generate enough smoke to be measured by laser extinction meter. Fiberboard properties are presented in Figure 4-21.

Table 4-21: Fiberboard properties for hood tests

Test Number	ΔH_c (kJ/g)	Y CO_2 (g/g)	Y CO (g/g)
072709-T1-High	15.28	1.1	0.019
073009-T1-High	14.27	0.9	0.02
073009-T2-High	10.28	1.21	0.022
080409-T1-High	14.94	1.32	0.018
080409-T2-High	13.44	1.41	0.023
080409-T3-High	15.28	1	0.024
080609-T1-High	15.77	0.99	0.02
081009-T1-High	14.79	1.3	0.018

Table 4-22 shows the average properties for fiberboard. These values were averaged for all the tests.

Table 4-22: Fiberboard average properties for hood tests

	ΔH_c (kJ/g)	Y CO_2 (g/g)	Y CO (g/g)
Range	10.27 - 15.76	0.9 - 1.41	0.018 - 0.024
Average	14.25	1.154	0.021
Standard Deviation	1.76	0.183	0.002

Table 4-23 shows the comparison between the average hood test values and the values that were reported from the cone calorimeter tests. The values are very close and it shows a good agreement.

94

Table 4-23: Average properties for fiberboard from hood tests and values reported from the cone tests

	ΔH_c (kJ/g)	Y CO_2 (g/g)	Y CO (g/g)
Hood Experiments	14.25	1.154	0.021
Cone test values	14	1.373	0.0213

Figure 4-16 shows the temperature profile in the hood for fiberboard test, 081009-T1. Temperature profile was averaged over the test period for the first thermocouple in the thermocouple tree (2 " below the ceiling) in order to have a temperature representative for the temperature in the hood for different fiberboard tests.
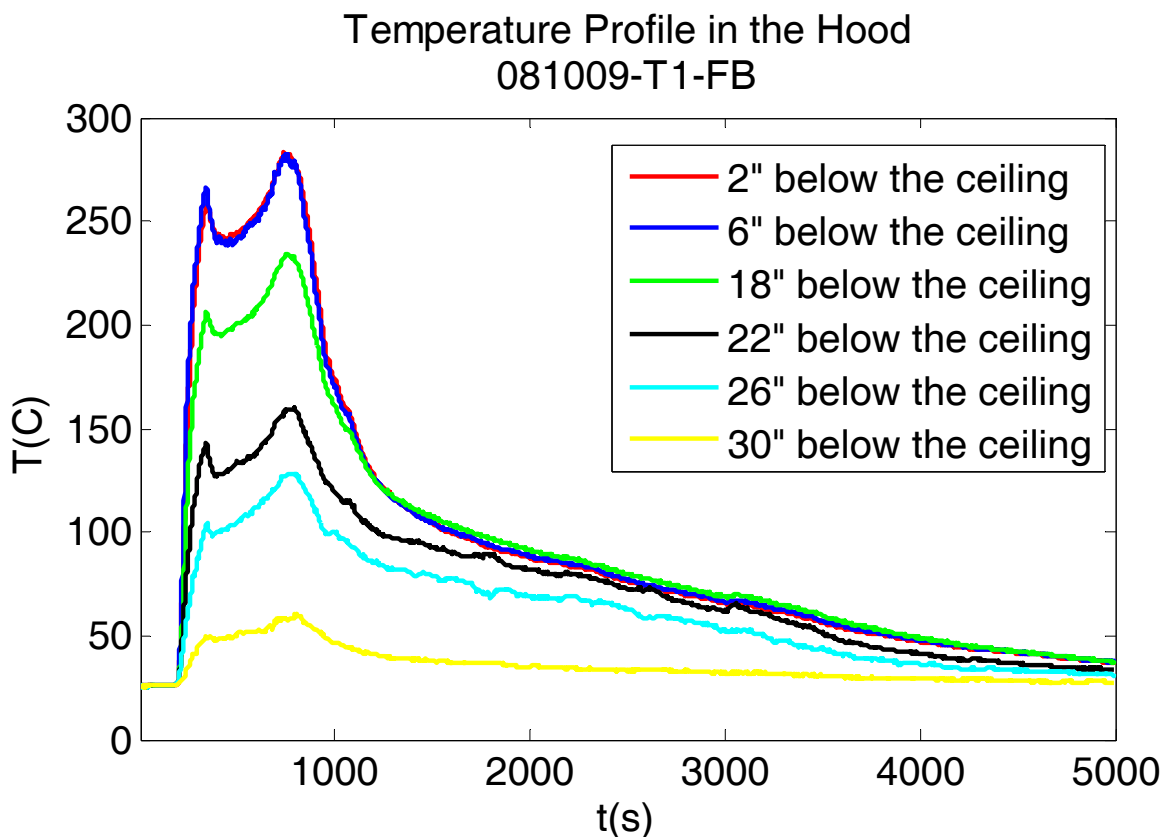
Figure 4-16: Temperature profile in the hood for fiberboard test 081009-T1

Figure 4-17 shows the exhaust rate and fuel mass loss rate for the fiberboard test, 081009-T1. Fuel mass loss rate and exhaust rate were used to find the heat release rate and determine the heat

of combustion for each test. Exhaust rate and fuel mass loss rates were also used to determine the equivalence ratio for each test.
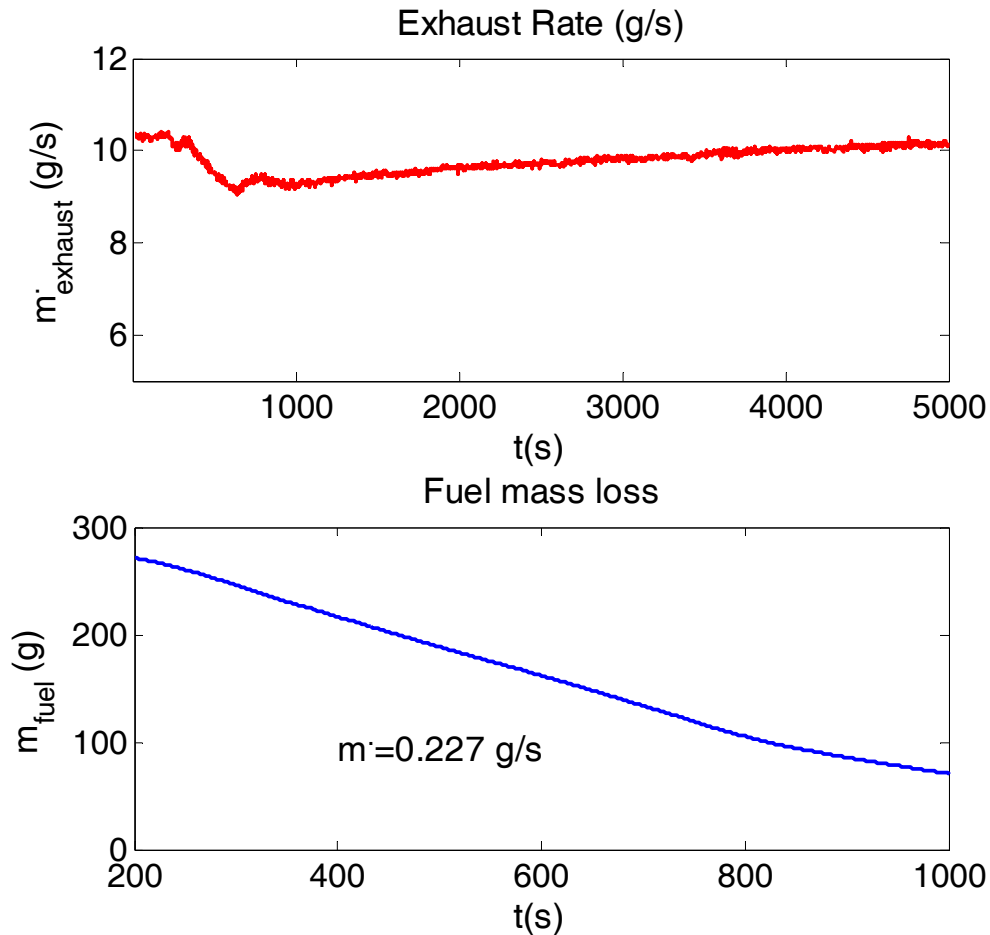
Figure 4-17: Exhaust rate and fuel mass loss rate for fiberboard test 081009-T1

Figure 4-18 shows the O_2, CO_2, CO concentrations and heat release rate for the fiberboard test, 081009-T1. The heat of combustion was calculated by using the heat release rate and the fuel mass loss rate as explained in Equation 3-24. The heat of combustion was averaged over the test period for all the tests.
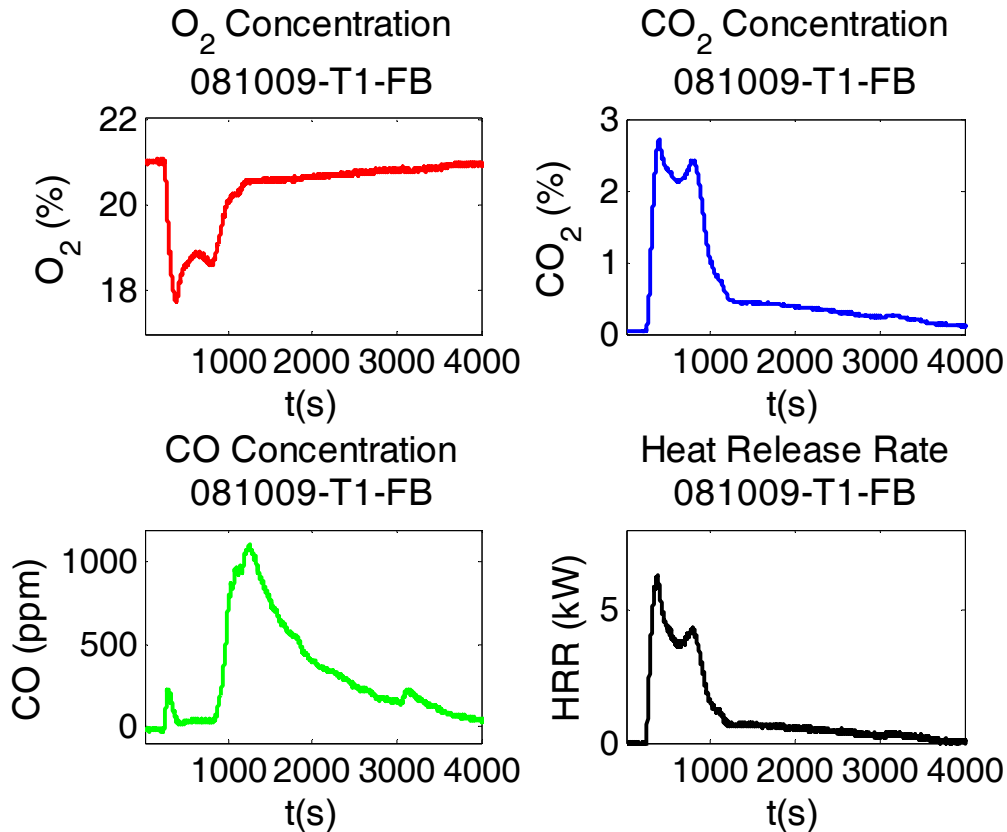
Figure 4-18: O_2, CO_2, CO concentrations and heat release rate for fiberboard test 081009-T1

Figure 5-6 shows average layer temperature, exhaust rate, fuel mass loss rate, and heat release rate for fiberboard tests. All the values were averaged over the test period in order to have a representative of each value for each test.

Average smoke layer temperatures in the hood are between 125 – 227 º C, and heat release rates are between 1–3.44 kW.

Table 4-24: Average values for smoke layer properties for fiberboard hood tests.

Test Number	$T_{layer}(^\circ C)$	$\dot{m}_{exh}$ (g/s)	$\dot{m}_f$ (g/s)	$\dot{Q}$ (kW)
072709-T1-High	124.96	16.42	0.065	1.00
073009-T1-High	171.40	16.16	0.140	2.00
073009-T2-High	166.04	16.25	0.127	1.31
080409-T1-High	170.96	16.23	0.230	3.44
080409-T2-High	176.67	9.39	0.160	2.15
080409-T3-High	226.93	9.44	0.225	3.44
080609-T1-High	189.15	9.46	0.147	2.32
081009-T1-High	129.99	9.43	0.227	3.36

Table 4-25: Smoke layer properties range for fiberboard tests

	$T_{layer}(^\circ C)$	$\dot{m}_{exh}$ (g/s)	$\dot{m}_f$ (g/s)	$\dot{Q}$ (kW)
Range	124.96 - 226.96	9.39 - 16.42	0.07 - 0.23	1 - 3.44
Average	169.51	12.85	0.17	2.37
Standard Deviation	32.29	3.65	0.06	0.96

4.2   Fuel Characteristics for Wall Experiments

Fuel characteristics needed to be measured separately for the wall test experiments. As explained in Section 3.2, wall tests were performed in three different categories. 4"x4" pan size, 8"x8" pan size, and 12"x12" pan size. Fuel characteristics such as smoke yield, CO_2 yield, and CO yield vary with the fire size. The fuel characteristics for 4"x4" pan size were determined in Section 4.1. Since there are no values reported for the larger fire sizes in the literature, these values were measured independently in a different apparatus. This apparatus works with the same concept as the hood apparatus except it is capable of measurements for large scale fires. The exhaust rate range for the apparatus is 1400 CFM. Also running fire sizes up to 100 kW is

possible with this apparatus. Figure 4-19 shows the apparatus used. Table 4-26 and Table 4-27 show the average values for the 8" x 8" pan size and 12" x 12" pan size tests for PMMA.

Figure 4-19: Test apparatus for measuring the fuel properties for 8" x 8" pan size and 12" x 12" tests

Table 4-26: PMMA average properties for the 8" x 8" pan size tests

	ΔH_c (kJ/g)	Ys (g/g)	YCO_2 (g/g)	YCO (g/g)
Range	23.5-25.2	0.02-0.026	1.9-2.02	0.01-0.012
Average	24.20	0.024	1.98	0.011
Standard Deviation	1.10	0.003	0.044	0.005

Table 4-27: PMMA average properties for the 12" x 12" pan size tests

	ΔH_c (kJ/g)	Ys (g/g)	YCO_2 (g/g)	YCO (g/g)
Range	24.2-26.1	0.029-0.032	1.7-1.69	0.014-0.018
Average	25.1	0.031	1.650	0.013
Standard Deviation	1.2	0.004	0.05	0.006

Table 4-28 and Table 4-29 show the average values for the 8" x 8" pan size and 12" x 12" pan size tests for gasoline.

Table 4-28: Gasoline average properties for the 12" x 12" pan size tests

	ΔH_c (kJ/g)	Ys (g/g)	YCO_2 (g/g)	YCO (g/g)
Range	40.2-44.5	0.089-0.10	1.70-1.90	0.018-0.022
Average	43.2	0.095	1.75	0.0175
Standard Deviation	1.95	0.02	0.15	0.002

Table 4-29: Gasoline average properties for the 8" x 8" pan size tests

	ΔH_c (kJ/g)	Ys (g/g)	YCO_2 (g/g)	YCO (g/g)
Range	41.0-45.0	0.082-0.091	1.9-2.3	0.015-0.019
Average	42.5	0.086	2.0	0.012
Standard Deviation	2.1	0.018	0.2	0.003

Table 4-30 and Table 4-31 show the average values for the 8" x 8" pan size and 12" x 12" pan size tests for polypropylene.

Table 4-30: Polypropylene average properties for the 8" x 8" pan size tests

	ΔH_c (kJ/g)	Ys (g/g)	YCO_2 (g/g)	YCO (g/g)
Range	39.8-43.2	0.06-0.07	2.8-3.1	0.045-0.055
Average	42.1	0.063	2.92	0.048
Standard Deviation	1.52	0.003	0.08	0.003

Table 4-31: Polypropylene average properties for the 12" x 12" pan size tests

	ΔH_c (kJ/g)	Ys (g/g)	YCO_2 (g/g)	YCO (g/g)
Range	40.2-44.1	0.07-0.08	1.95-2.1	0.05-0.065
Average	43.2	0.074	2.08	0.059
Standard Deviation	1.35	0.002	0.07	0.004

Table 4-32 and Table 4-33 show the average values for the 8" x 8" pan size and 12" x 12" pan size tests for ABS.

Table 4-32: ABS average properties for the 8" x 8" pan size tests

	ΔH_c (kJ/g)	Ys (g/g)	YCO_2 (g/g)	YCO (g/g)
Range	24.0-27.2	0.22-0.28	1.3-1.7	0.07-0.082
Average	25.2	0.26	1.5	0.075
Standard Deviation	1.85	0.08	0.09	0.005

Table 4-33: ABS average properties for the 12" x 12" pan size tests

	ΔH_c (kJ/g)	Ys (g/g)	YCO_2 (g/g)	YCO (g/g)
Range	25.2-28.1	0.24-0.29	1.4-1.8	0.075-0.088
Average	26.1	0.27	1.61	0.079
Standard Deviation	2.0	0.06	0.1	0.006

Figure 4-20 shows that as the pan size diameter increases the smoke yield values increase for all the fuels. However, the smoke yield does not increase when the pan size increase from 8"x 8" to 12"x 12". The ratio between the CO yield and the smoke yield is very close for all the fuels except for the gasoline as shown in Figure 4-21.
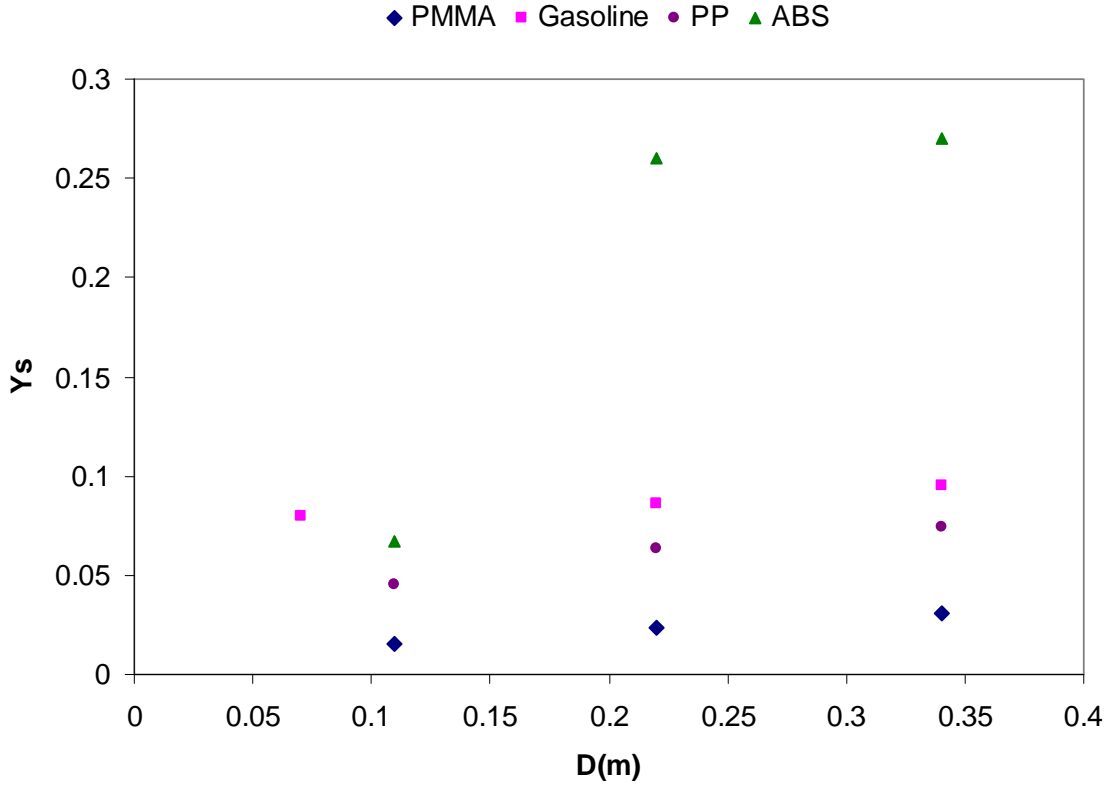
Figure 4-20 : Smoke yield variation with the pan size diameter for the different fuels
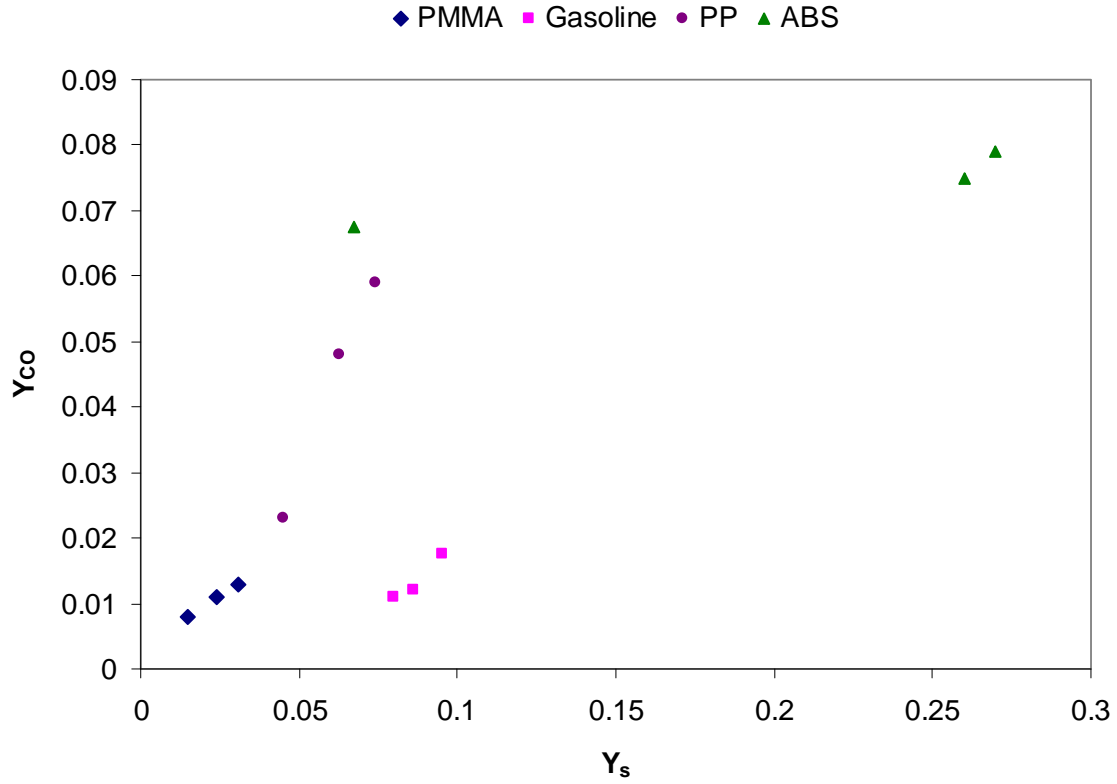
Figure 4-21: CO yield variation vs. smoke yield variation for different fuels and different pan sizes

CHAPTER 5 RESULTS FOR HOOD EXPERIMENTS

Experiments were performed on each test set to determine the fuel characteristics which were presented in Section 4.1, gas phase and solid phase properties of the smoke. Also, a new method was developed to measure the optical properties of the smoke deposited on the surface. Some of the developed methods for the hood tests were applied to the wall tests and these methods were used to determine the optical properties of the smoke on the wall as well. In addition to determination of the mentioned values, an analytical smoke deposition model based on thermophoresis mechanism was used. The analytical thermophoresis smoke deposition model was validated with the hood experiment data.

5.1   Gas Phase Mass Specific Extinction Coefficient $(\sigma_{s,g})$

Gas phase mass specific extinction coefficient was determined for PMMA, PP, and gasoline (Section 3.1.1, data reduction). It was not measured for ABS and fiber board due to high and low smoke generation rates and the resulting lack of optical extinction measurements. The following sections will present the values for gas phase mass specific extinction for each fuel and the average values that were used for validating the thermophoresis analytical model. Table 5-1 through Table 5-6 show the gas phase mass specific extinction coefficient for PMMA, polypropylene, and gasoline for the hood tests.

Table 5-1: Gas phase mass specific extinction coefficient values for PMMA tests

Test Number	$\sigma_{s,g}$ (m²/g)
050409-T2	8.2
050409-T1	7.8
050609-T3	7.7
050609-T1	8.3
050609-T2	8.4
050709-T2	7.9
050709-T3	8.3
043009-T1	8.4
043009-T4	7.9
042909-T1	7.5
050109-T1	8.1
072109-T1-Low	8.2
072109-T1-High	8.4
072209-T1-Low	8.5
072209-T1-High	8.2

Table 5-2: Gas phase mass specific extinction coefficient range, average, and standard deviation for PMMA tests

	$\sigma_{s,g}$ (m²/g) - PMMA Tests
Range	7.5 - 8.5
Average	8.12
Standard Deviation	0.29

Table 5-3: Gas phase mass specific extinction coefficient values gasoline tests

Test Number	$\sigma_{s,g}$ (m²/g)
042009-T3-low	7.8
042009-T2-high	7.9
060209-T2-high	7.5
060309-T2-high	7.4
060909-T1-low	7.9
061009-T1-low	8
061009-T1-high	8.1
061009-T2-low	8.2
061009-T2-high	8.4

Table 5-4 : Gas phase mass specific extinction coefficient range, average, and standard deviation for gasoline tests

	$\sigma_{s,g}$ (m^2/g) - gasoline tests
Range	7.4 - 8.4
Average	7.91
Standard Deviation	0.31

Table 5-5: Gas phase mass specific extinction coefficient values for polypropylene tests

Test Number	$\sigma_{s,g}$ (m^2/g)
063009-T1-Low	7.5
063009-T1-High	7.4
070109-T1-Low	7.9
070109-T1-High	8.1
070609-T1-Low	8.2
070609-T1-High	8.4
070609-T2-Low	7.9
070709-T1-Low	8
070709-T1-High	7.8
070909-T1-Low	7.7
070909-T1-High	8

Table 5-6 : Gas phase mass specific extinction coefficient range, average, and standard deviation for polypropylene tests

	$\sigma_{s,g}$ (m^2/g) - polypropylene tests
Range	7.4 - 8.4
Average	7.90
Standard Deviation	0.29

The average values for gas phase mass specific extinction coefficient are as follows:

$$\overline{\sigma}_{s,g} = 8.1 \text{ (m}^2\text{/g), PMMA} \quad \overline{\sigma}_{s,g} = 7.9 \text{ (m}^2\text{/g), PP} \quad \overline{\sigma}_{s,g} = 7.7 \text{ (m}^2\text{/g), Gasoline}$$

The average values and standard deviations values for all three fuels are presented in Table 5-2, Table 5-4 and Table 5-6. These values are within the range reported by Mulholland, 8.7 ± 1.1 m^2/g [28].

5.2   Solid Phase Mass Specific Extinction Coefficient $(\sigma_{s,s})$

A new parameter is introduced and used in this work. Surface optical density is determined by using the gray scale values. The glass filters were scanned next to a gray scale and by using the proper calibration curve the gray scale values were calibrated and the optical density values were determined. Solid phase mass specific extinction coefficient which correlates the optical density values for the filter and the gravimetric measurements on them. Wall filters were collected and data were processed by using the Matlab code. For each fuel, surface optical density values were plotted vs. the measured smoke deposited on the filter. The slope for this plot has the units of the gas phase mass specific extinction coefficient (m^2/g).

PMMA Tests

Figure 5-1 shows the linear least square fit for the PMMA data with an intercept (0.071). When the linear least square fit is forced to go through the origin and the change in r-squared value is from 0.92931 to 0.92017 (not significant). This means that forcing the least square fit to go through the origin is an acceptable assumption and the intercept is due to the measurement errors from the high accuracy scale and also image processing errors when the wall filters were scanned next to gray scale for each test. The linear least square fit was selected for these results because the solid phase mass specific extinction coefficient has the same units as gas phase mass specific extinction coefficient. Also the fit was forced to gothrough origin because when the smoke deposition is zero the optical density on the filter is supposed to be zero. The intercept in the fit is due to errors.

106
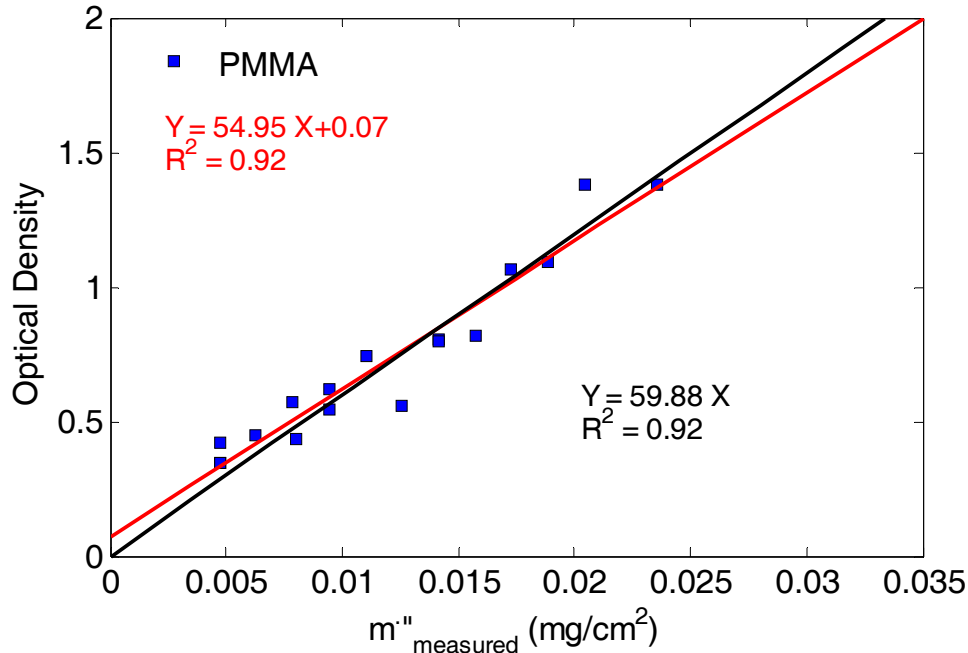
Figure 5-1: Surface optical density of smoke deposition vs. the measured deposition for PMMA

The maximum optical density on the filters that can be measured is 1.95. Beyond 1.95 the surface is black and optical density value which has been calibrated based on gray scale values is not a proper method for smoke deposition measurements. The gravimetric smoke deposition values change from 0 to 0.035 (mg/cm^2). The slope of the plot shown in Figure 5-1 has the same units as gas phase mass specific extinction coefficient and it will be called solid phase mass specific extinction coefficient $(\sigma_{s,s})$. The units for the solid phase mass specific extinction coefficient in Figure 5-2 are cm^2/mg. Figure 5-2 shows the surface optical density values vs. measured smoke deposited on the filters for PMMA tests. The linear least square fit is forced to go through origin and the units for solid phase mass specific extinction coefficient are changed to m^2/g to be consisted with the gas phase mass specific extinction coefficient units. $\sigma_{s,s}$ for PMMA hood test is 6.0 (m^2/g) as shown in Figure 5-2.
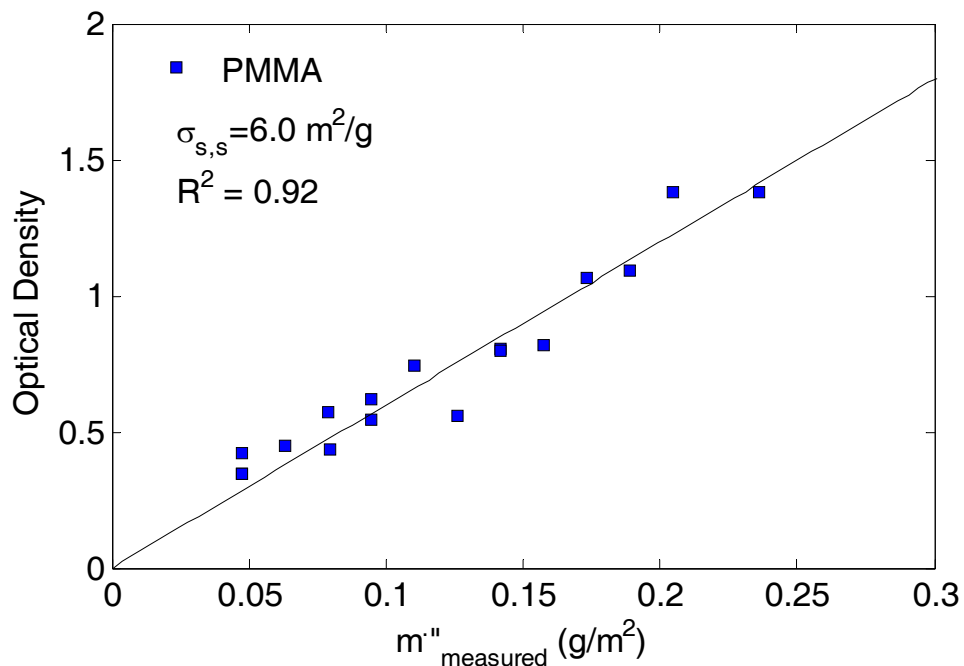
Figure 5-2: Solid phase mass specific extinction coefficient value for PMMA hood tests

Table 5-7 shows the gravimetric deposition values and optical density values for PMMA tests. Test conditions for these tests were presented in Table 4-1 – Table 4-4.

Table 5-7: Deposition and optical density values for PMMA tests

Test Number	m" (mg/cm^2)	OD
050409-T2	0.0047	0.423
050409-T1	0.0094	0.62
050609-T3	0.0063	0.452
050609-T1	0.0189	1.091
050609-T2	0.0236	1.382
050709-T2	0.0079	0.569
050709-T3	0.0110	0.74
043009-T1	0.0142	0.805
042909-T1	0.0173	1.064
050109-T1	0.0142	0.798
072109-T1-Low	0.0047	0.347
072109-T1-High	0.0094	0.547
072209-T1-Low	0.0047	0.348
072209-T1-High	0.0126	0.558

Polypropylene (PP) Tests

Figure 5-3 shows the linear least square fit for the PP data. The intercept of the linear least square fit is 0.14. The change in R-squared value when the plot is forced to go through origin is from 0.86 to 0.90. Solid phase mass specific extinction coefficient value for polypropylene tests is 6.5 (m^2/g) and it is shown in Figure 5-4.

The solid phase mass specific extinction coefficient for polypropylene is slightly higher than the solid phase mass specific extinction coefficient for PMMA tests 5.9 (m^2/g).
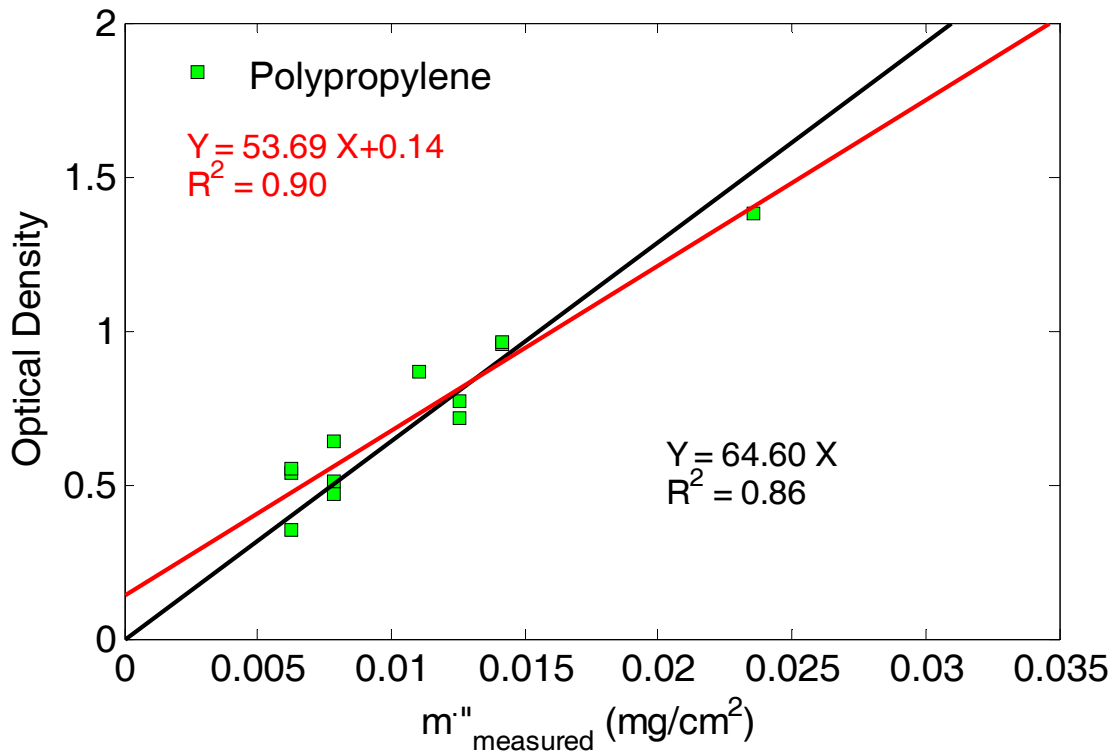
Figure 5-3: Surface optical density of smoke deposition vs. the measured deposition for PP
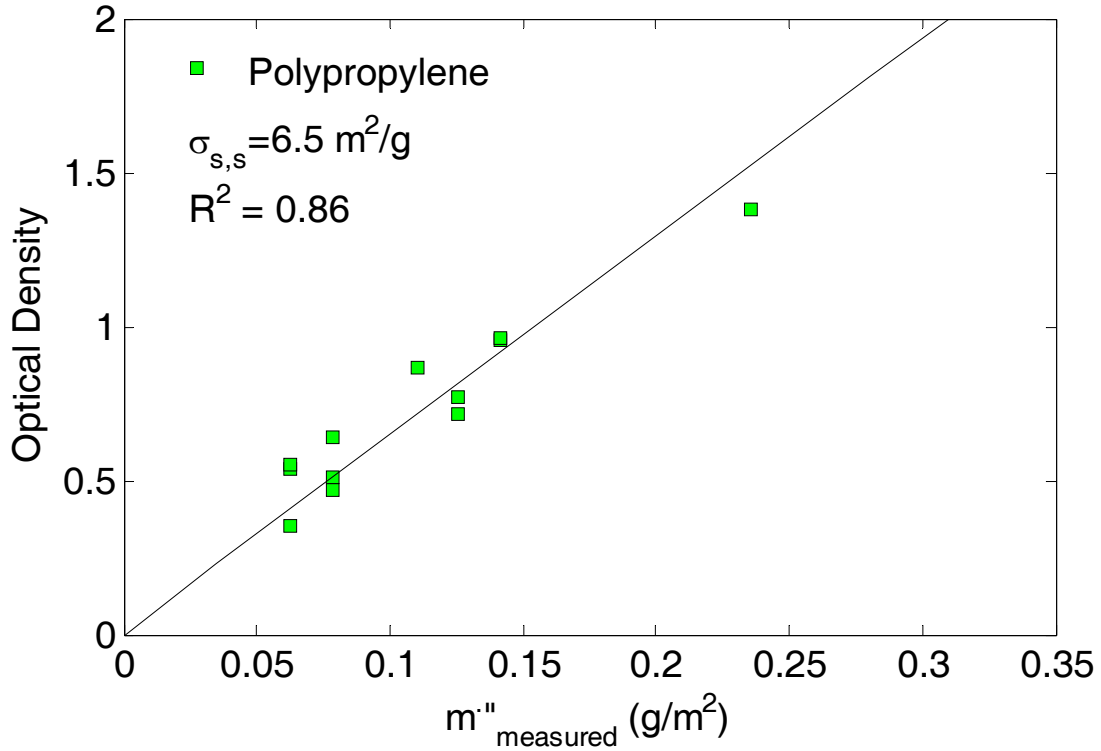
Figure 5-4: Solid phase mass specific extinction coefficient value for PP hood tests

Table 5-8 shows the gravimetric deposition values and optical density values for polypropylene tests. Test conditions for these tests were presented in Table 4-11 – Table 4-14.

Table 5-8: Deposition and optical density values for polypropylene tests

Test Number	m" (mg/cm^2)	OD
063009-T1-low	0.0063	0.352
063009-T1-high	0.0126	0.713
070109-T1-low	0.0079	0.509
070109-T1-high	0.0142	0.954
070609-T1-low	0.0079	0.641
070609-T1-high	0.0142	0.963
070609-T2-low	0.0063	0.541
070709-T1-low	0.0063	0.549
070709-T1-high	0.0110	0.868
070909-T1-low	0.0126	0.772
070909-T1-high	0.0236	1.382

Gasoline Tests

Figure 5-5 shows the linear least square fit for the gasoline data. The intercept of the linear least square fit is 0.07. The change in R-squared value when the plot is forced to go through origin is from 0.91 to 0.90. Solid phase mass specific extinction coefficient value for gasoline tests is 5.7 (m^2/g). This value is close to PMMA value (5.9 m^2/g) and slightly lower than PP value (6.4 m^2/g).
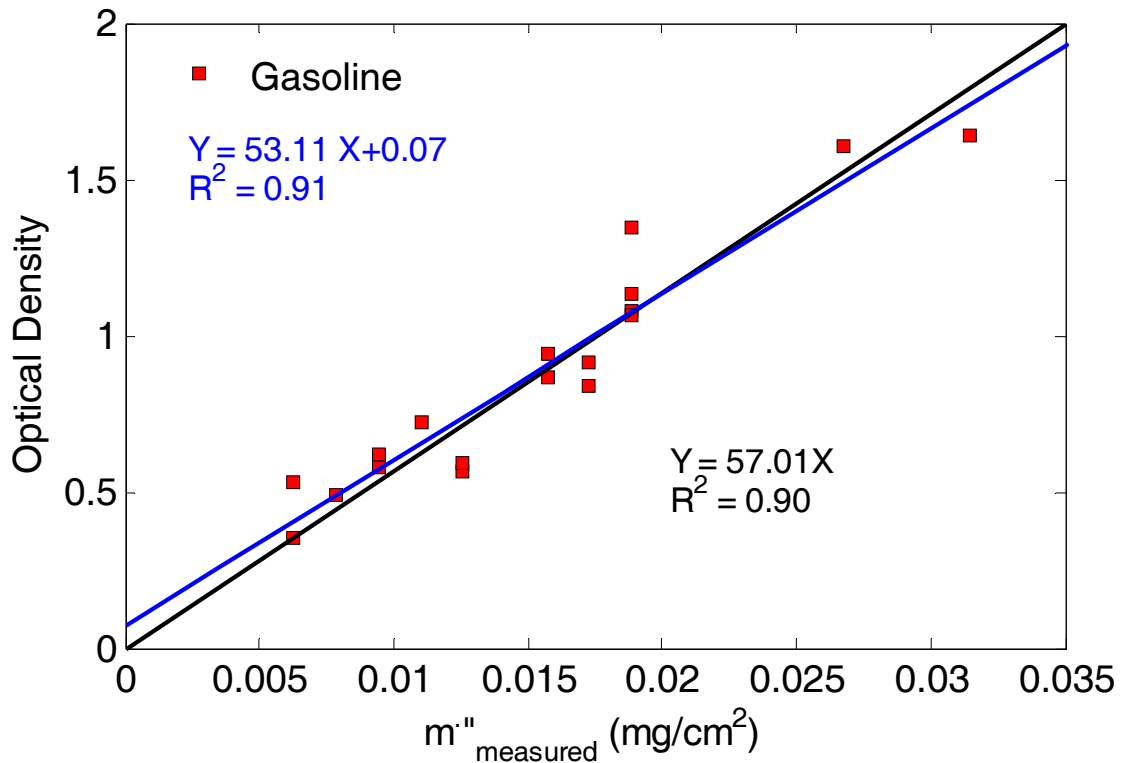
Figure 5-5: Surface optical density of smoke deposition vs. the measured deposition for gasoline
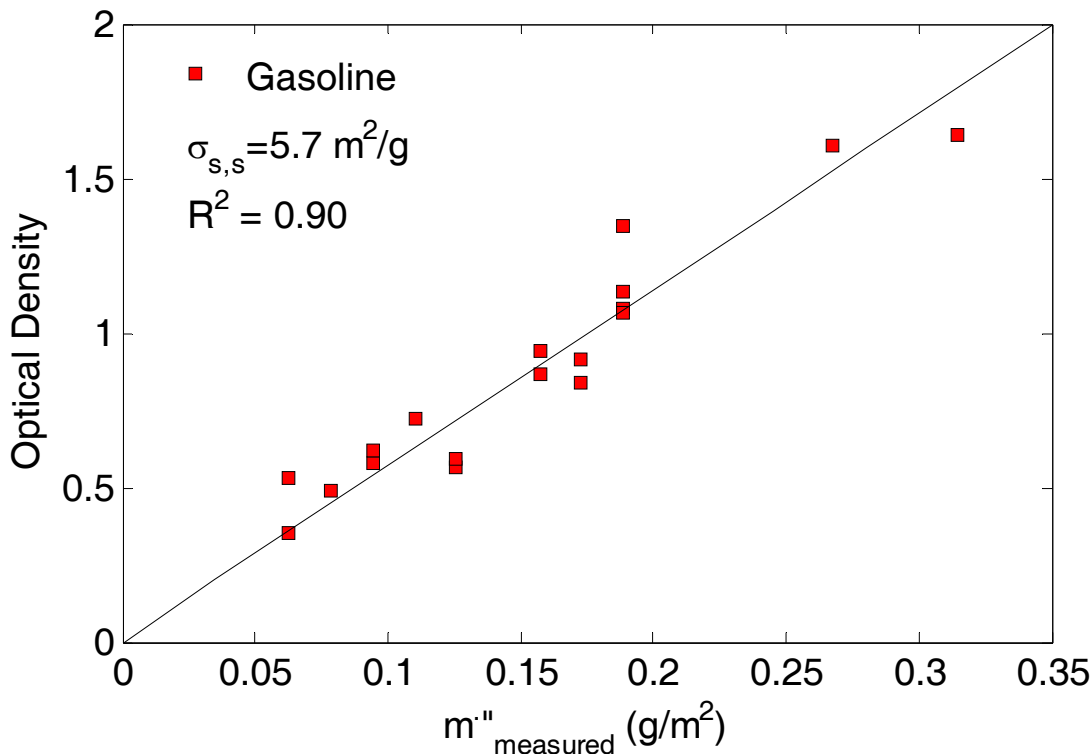
Figure 5-6: Solid phase mass specific extinction coefficient value for gasoline hood tests

Table 5-9 shows the gravimetric deposition values and optical density values for gasoline tests. Test conditions for these tests were presented in Table 4-6 – Table 4-10.

Table 5-9: Deposition and optical density values for gasoline tests

Test Number	m" (mg/cm^2)	OD
042009-T3-low	0.0189	1.079
042009-T2-high	0.0315	1.642
060209-T2-high	0.0157	0.945
060309-T2-high	0.0126	0.564
060909-T1-low	0.0189	1.132
061009-T1-low	0.0189	0.35
061009-T1-high	0.0063	0.868
061009-T2-low	0.0157	0.593
061009-T2-high	0.0126	1.349

ABS Tests

Figure 5-7 shows the linear least square fit for the ABS data. The intercept of the linear least square fit is 0.014. The change in R-squared value when the plot is forced to go through origin is from 0.887 to 0.886. Solid phase mass specific extinction coefficient value for ABS tests is 3.4 (m^2/g) and it has been shown in Figure 5-8.
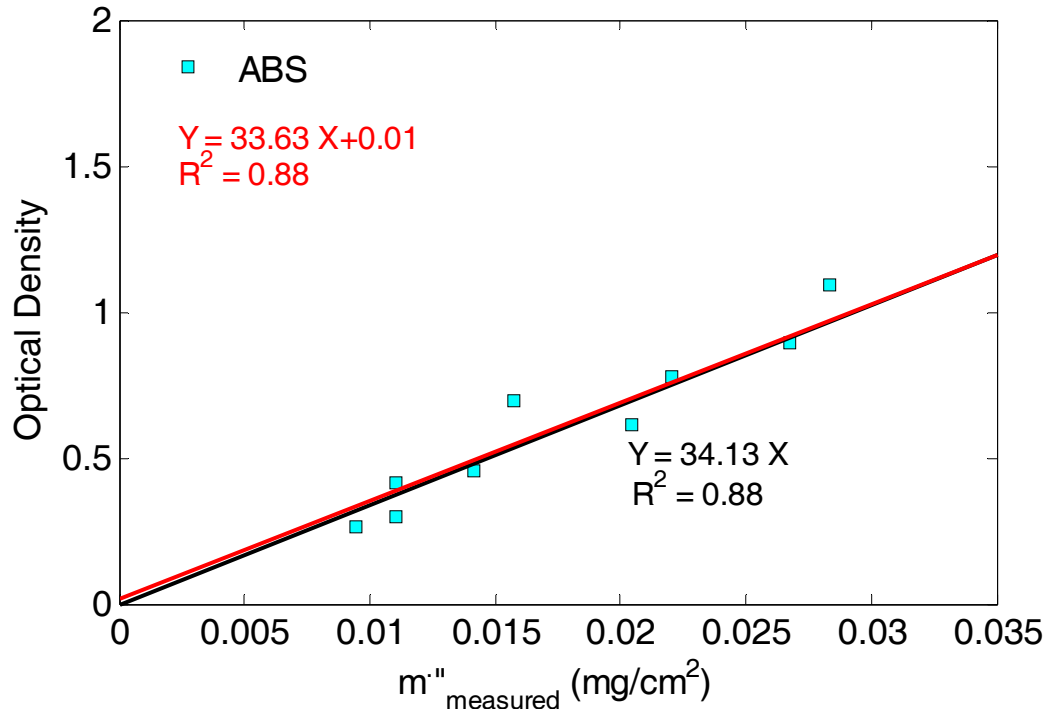
Figure 5-7: Surface optical density of smoke deposition vs. the measured deposition for ABS

Solid phase mass specific extinction coefficient for ABS is almost 50% of $\sigma_{s,s}$ for PMMA, PP, and gasoline. After processing the scanned images of wall filters, it was evident that ABS wall filters have large agglomerates on them which can be easily identified. For PMMA, PP, and gasoline these agglomerates cannot be identified. Since these agglomerates from ABS tests are not spread on the filter's surface, they are not optically as efficient as other fuels. They increase the mass on the filters; however, the optical properties of the filter do not change as much as gravimetric properties. This is the reason for lower solid phase mass specific coefficient on the wall filters

from the ABS tests. More detailed quantitative analysis will be performed on the data for these

tests on agglomerate size in the next section.
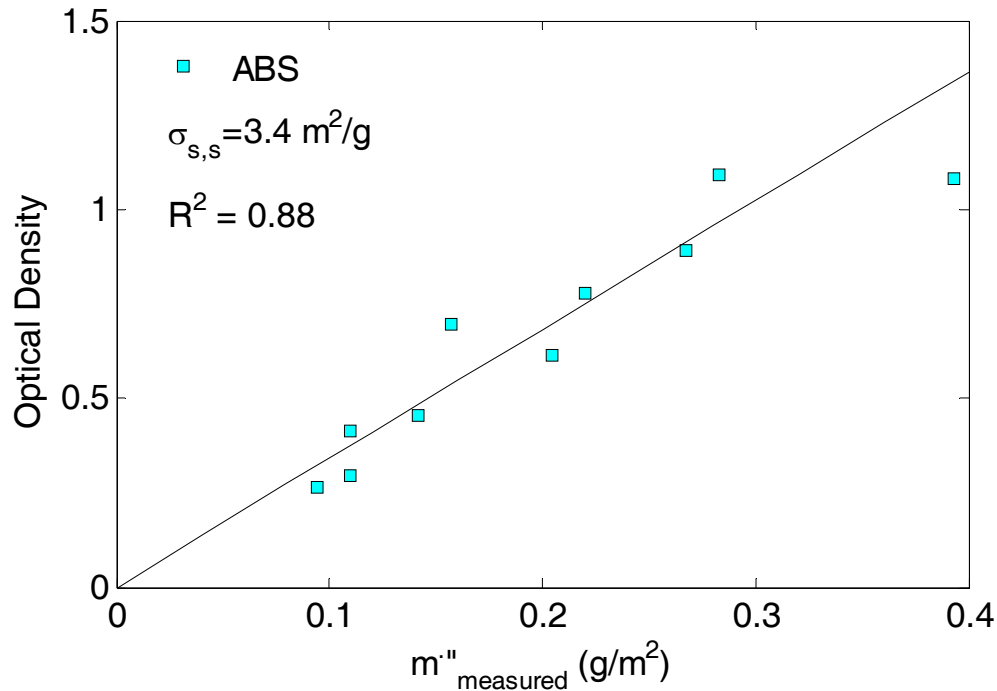
Figure 5-8: Solid phase mass specific extinction coefficient value for ABS hood tests

Table 5-10 shows the gravimetric deposition values and optical density values for ABS tests.

Test conditions for these tests were presented in Tables 4-16 – 4-20.

Table 5-10: Deposition and optical density values for ABS tests

Test Number	m" (mg/cm2)	OD
061809-T1-High	0.0157	0.698
061809-T2-High	0.0204	0.615
062209-T1-low	0.0393	1.079
062209-T1-high	0.0377	1.599
062209-T2-low	0.0267	0.892
062209-T2-high	0.0456	1.459
062409-T1-low	0.0220	0.778
062409-T1-high	0.0283	1.094
062409-T2-low	0.0110	0.297
062409-T2-high	0.0110	0.414

Fiber Board Tests

Figure 5-9 shows the linear least square fit for the fiber board data. The intercept of the linear least square fit is -0.0130. The change in R-squared value when the plot is forced to go through origin is from 0.91 to 0.90. Solid phase mass specific extinction coefficient value for ABS tests is 0.89 (m^2/g) and it has been shown in Figure 5-10.
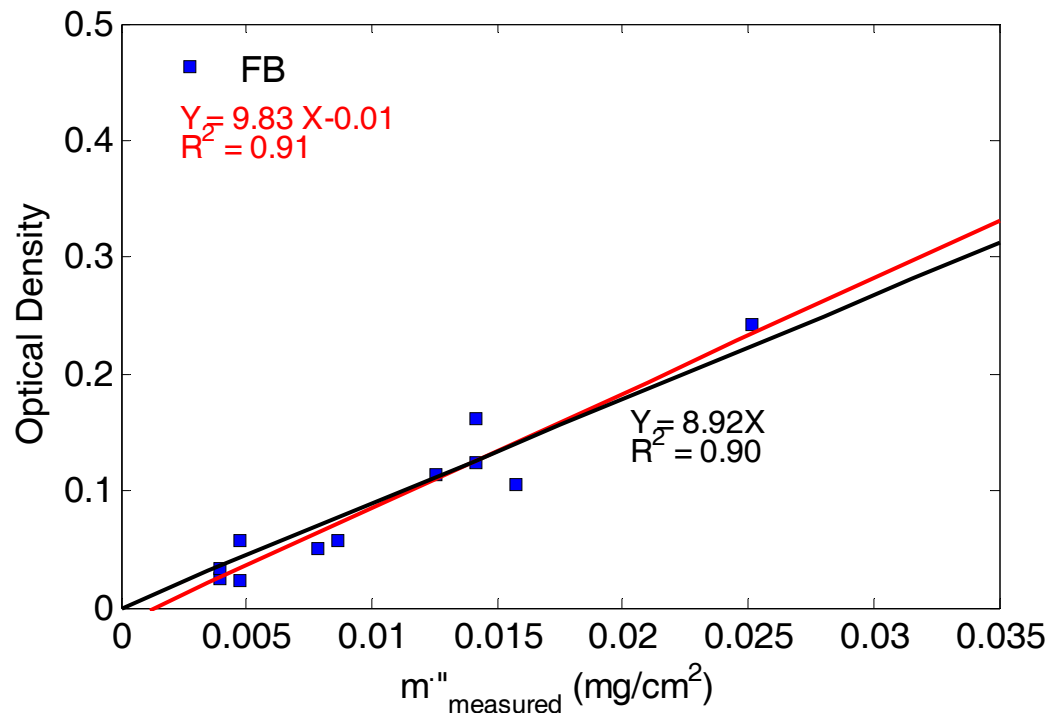
Figure 5-9: Surface optical density of smoke deposition vs. the measured deposition for fiber board

Solid phase mass specific extinction coefficient for fiber board is 15% of $\sigma_{s,s}$ for PMMA, PP, and gasoline. After processing the wall filters from fiber board tests, it was noted that wall filter's color changes to yellow which is different from other filters from PMMA, PP, ABS, and gasoline test. It was also noticed that fiber board generates liquid aerosols which leaves a yellow residue on the glass piece which was used for the air purge system for both laser and detector. In the next section more quantitative analysis will be presented for identifying the filter color from fiber board tests.
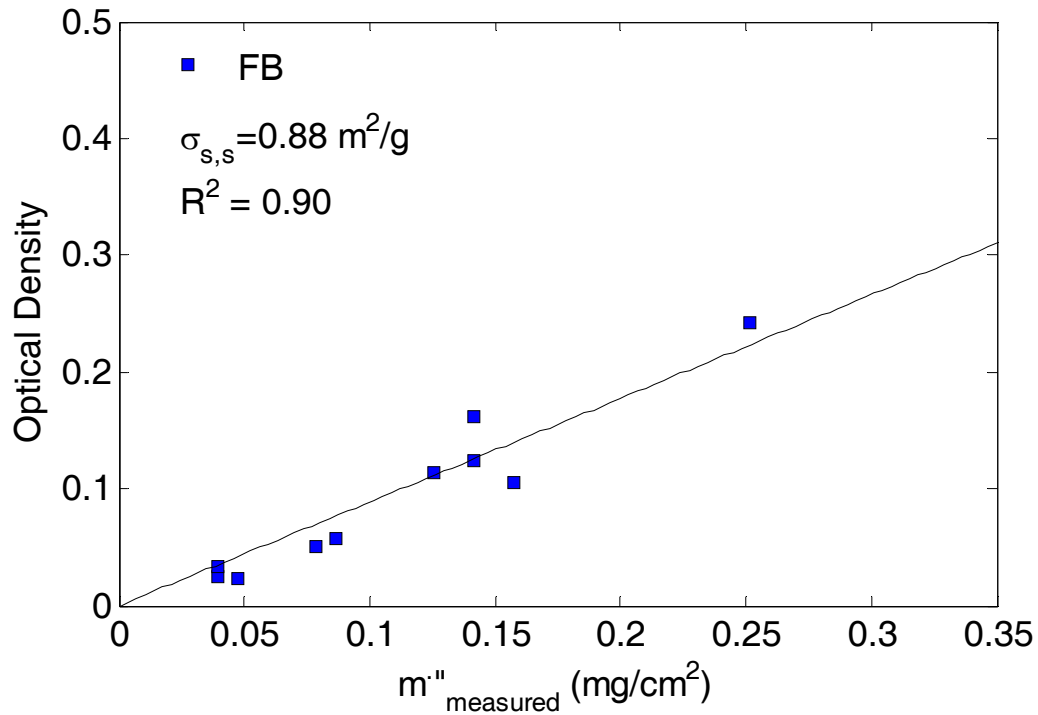
Figure 5-10: Solid phase mass specific extinction coefficient value for fiber board hood tests

Table 5-11 shows the gravimetric deposition values and optical density values for gasoline tests. Test conditions for these tests were presented in Table 4-21 through Table 4-24.

Table 5-11: Deposition and optical density values for fiber board tests

Test Number	m" (mg/cm^2)	OD
072709-T1-High	0.0047	0.023
073009-T1-High	0.0252	0.242
073009-T2-High	0.0142	0.162
080409-T1-High	0.0086	0.057
080409-T2-High	0.0039	0.024
080409-T3-High	0.0039	0.033
080609-T1-High	0.0157	0.106
081009-T1-High	0.0079	0.05

116

PMMA, PP, and Gasoline Tests

Figure 5-11 shows the linear least square fit for PMMA, polypropylene, and gasoline data. The intercept of the linear least square fit is 0.10. The change in R-squared value when the plot is forced to go through origin is from 0.91 to 0.89. Solid phase mass specific extinction coefficient for these fuels is 5.9 (m^2/g) as shown in Figure 5-12.
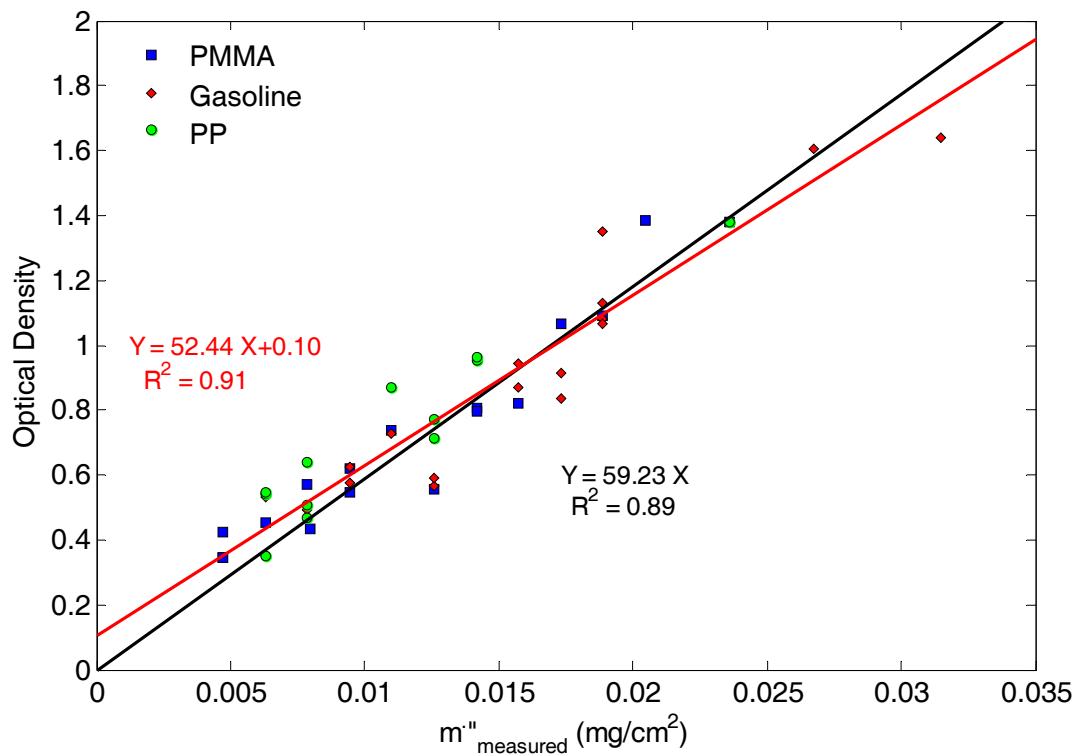
Figure 5-11: Surface optical density of smoke deposition vs. the measured deposition for PMMA, PP, and gasoline

The average value proposed in Figure 5-12 is only for PMMA, polypropylene, and gasoline. Solid phase mass specific extinction coefficient for these fuels were close to each other and for ABS and fiber board as presented earlier in this chapter values are different. The difference in the solid phase mass specific extinction coefficient for ABS and fiber board is due different reasons which will be discussed in the next section.
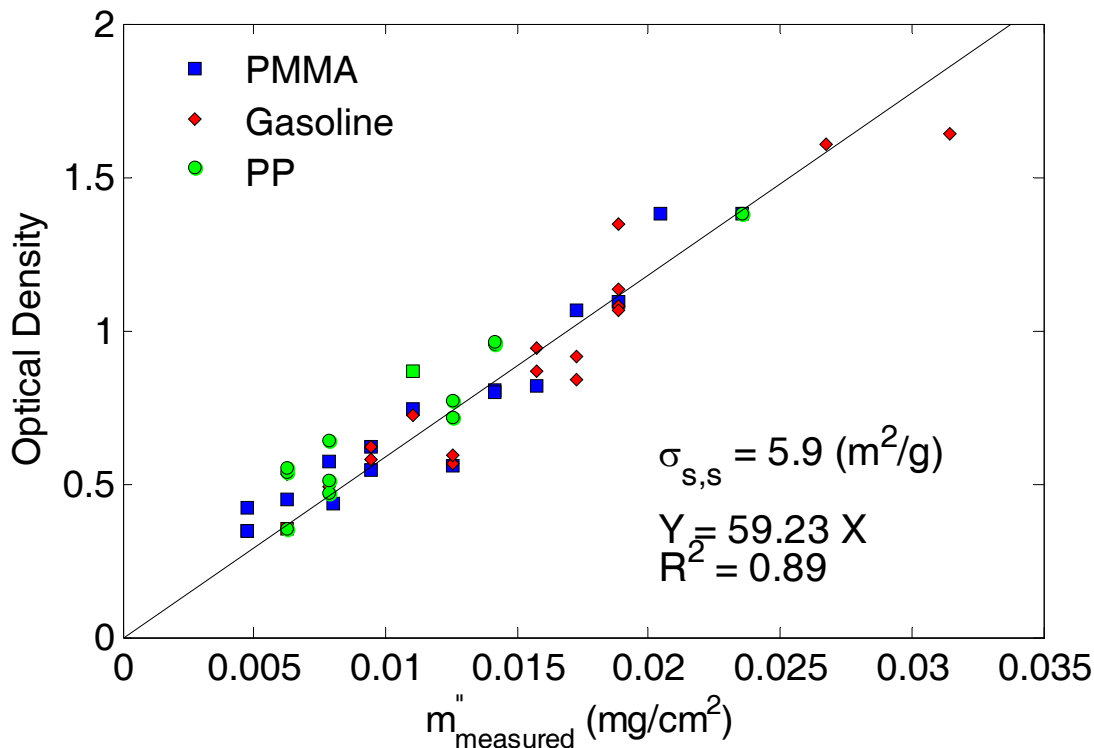
Figure 5-12: Solid phase mass specific extinction coefficient value for PMMA, PP, and gasoline hood tests

Table 5-12: Gas phase and solid phase mass specific extinction coefficient values for

PMMA, PP, ABS, gasoline, and fiber board

Fuel	$\sigma_{s,g} \, (m^2/g)$	$\sigma_{s,s} \, (m^2/g)$
PMMA	8.1	5.9
PP	7.9	6.4
Gasoline	7.7	5.7
ABS	NA	3.4
Fiber board	NA	0.88

Table 5-12 is a summary of all the findings for both gas phase and solid phase mass specific extinction coefficients. As discussed before, solid phase mass specific extinction coefficient values for PMMA, PP, and gasoline are very close and Figure 5-12 shows the average value that can be used for these fuels is 5.9 (m^2/g).

5.3 Agglomerate Size Analysis for PMMA, PP, Gasoline and ABS Tests

Figure 5-14 shows the scanned images from PMMA, PP, gasoline, ABS, and fiber board tests. By looking at the ABS filter (061809-T2-High), larger agglomerates can be identified than PMMA filter (072109-T1-High-PMMA). The polypropylene filter is very similar to PMMA filter in the lack of large agglomerates. Gasoline is intermediate between the PMMA and ABS filters. These filters were selected because their optical density values are very close to each other. Table 5-13 shows the optical density and amount of smoke deposited on each filter.

Table 5-13: Smoke deposition and optical density values for PMMA, polypropylene, gasoline, and ABS tests

Test	m" (mg/cm^2)	OD
072109-T1-High, PMMA	0.0047	0.547
071009-T1-Low, PP	0.0079	0.509
061009-T2-Low, Gasoline	0.0126	0.593
061809-T2-High, ABS	0.0204	0.615

Data analysis was performed on the wall filters with the Image J software. Number of agglomerates was plotted vs. agglomerate diameter for each filter. Table 5-14 shows the agglomerate size distribution for polypropylene, PMMA, gasoline, and ABS wall filters. The agglomerate diameter size was calculated based on the pixel concept. Image J software identifies agglomerates within the size which can be specified in the software. Agglomerate diameter size was changed from low to high. One of the outcomes of this analysis is the number of agglomerates within the same diameter is higher for ABS than PMMA, polypropylene, and gasoline.

119

Table 5-14: Smoke agglomerate size distribution for PMMA, gasoline, ABS, and polypropylene

Agglomerate Diameter Size	Number of Agglomerates			
d (mm)	PP	PMMA	Gasoline	ABS
0.0042	1625	2326	3299	5758
0.0075	1383	1976	2956	5211
0.0098	1236	1796	2727	4836
0.0116	1123	1679	2532	4548
0.0132	1067	1567	2434	4403
0.0237	572	888	1442	2903
0.0309	374	630	991	2190
0.0366	274	466	748	1685
0.0416	220	359	600	1376
0.0750	49	95	170	407
0.0976	19	44	101	209

Figure 5-13 shows that ABS wall filter has more agglomerates within each diameter. For example if we select a certain agglomerate size and count number of agglomerates on the wall filter from PMMA, gasoline, PP, and ABS tests; number of agglomerates will be higher for the ABS filter than for the PMMA and PP filters. This means that these agglomerates are more effective gravimetrically on ABS filters. Another significant outcome from the agglomerate analysis is the relationship between the number of agglomerates for each fuel and the solid phase mass specific extinction coefficient ($\sigma_{s,s}$) for that fuel. By comparing the results from Table 5-12 for the solid phase mass specific extinction coefficient values for each fuel with the number of the agglomerates, it is obvious that solid phase mass specific extinction values are higher for the fuels that have fewer agglomerates. This means that if the number of agglomerates is lower for a

fuel, the solid phase mass specific extinction coefficient will be higher for that fuel since the agglomerates are more effective optically for that fuel than the others.

Table 5-15 shows that for a given diameter size (0.0098 mm) as the number of agglomerates increases, the solid phase mass specific extinction coefficient decreases. Polypropylene has the highest solid phase mass specific extinction coefficient and ABS has the lowest solid phase mass specific extinction coefficient.

Table 5-15: Number of agglomerates vs. solid phase mass specific extinction coefficient

Agglomerate Diameter Size	Number of Agglomerates			
d (mm)	PP	PMMA	Gasoline	ABS
0.0098	1236	1796	2727	4836
$\sigma_{s,s}$ (m^2/g)	6.4	5.9	5.7	3.4
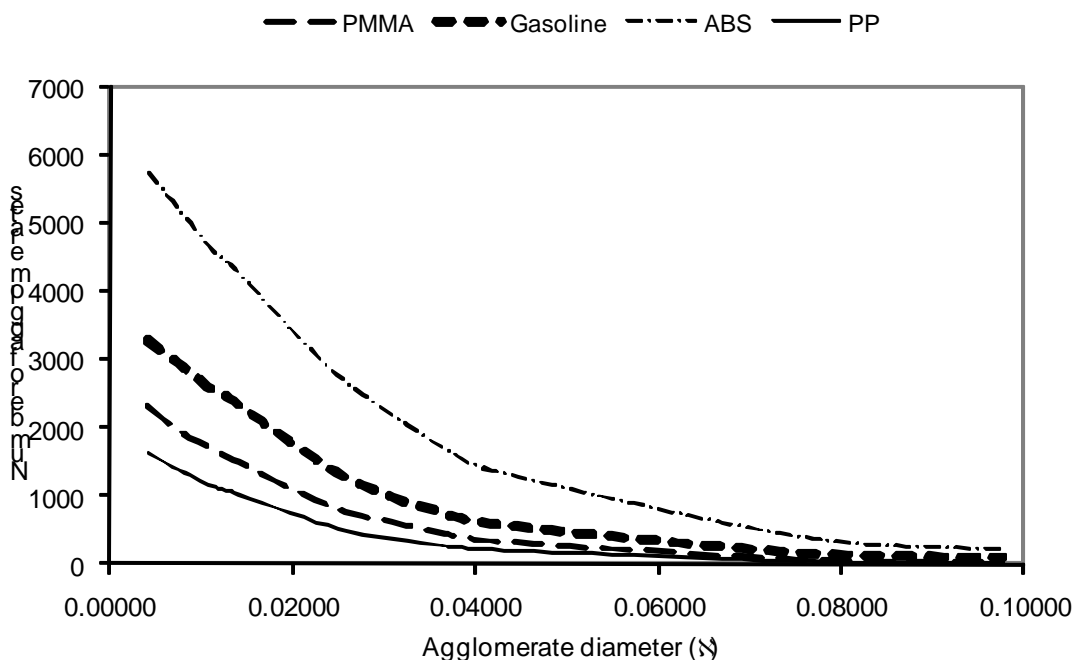
Figure 5-13: Agglomerate size distribution for wall filter
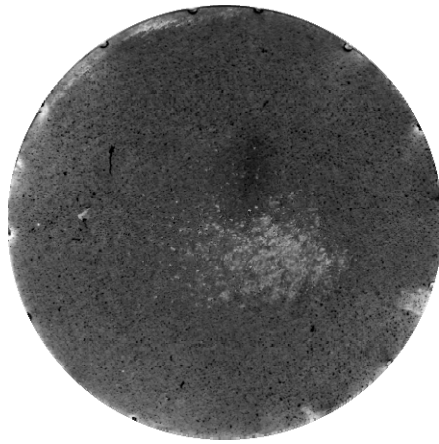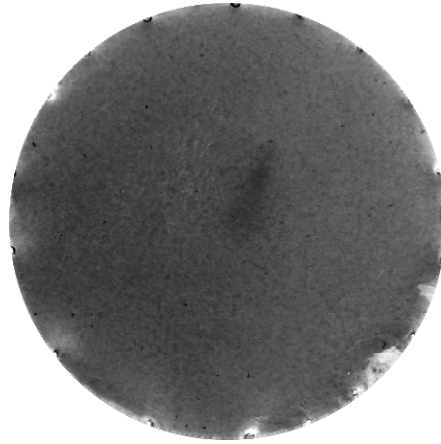
072109-T1-High-PMMA   071009-T1-Low-PP   061009-T2-Low-Gasoline
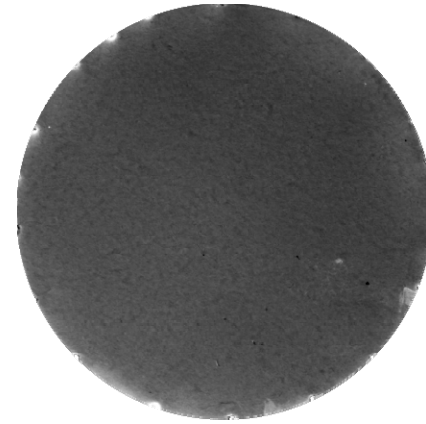
061809-T2-High-ABS   072709-T1-High-Fiber board

Figure 5-14: Scanned images for PMMA, PP, gasoline, ABS, and fiber board wall filters

Table 5-16 : Solid phase mass specific extinction coefficient vs. smoke yield for the fuels

	PP	PMMA	Gasoline	ABS	Fiber Board
$\sigma_{s,s}$ (m^2/g)	6.8 ± 1.56	6.3 ± 1.07	5.8 ± 0.937	3.4 ± 0.574	0.820 ± 0.198
Smoke yield (g/g)	0.069	0.018	0.080	0.15	0.01

Table 5-16 shows the fuels and the solid phase mass specific extinction coefficient for the fuels as well as smoke yields for those fuels. These results suggest that increased smoke yield increases agglomeration and lowers solid phase mass specific extinction coefficient.

Figure 5-15 shows the $\sigma_{s,s}$ vs. smoke yield for the fuels used in the experiments. Except for fiber board, as the smoke yield increases the solid phase mass specific extinction coefficient decreases.
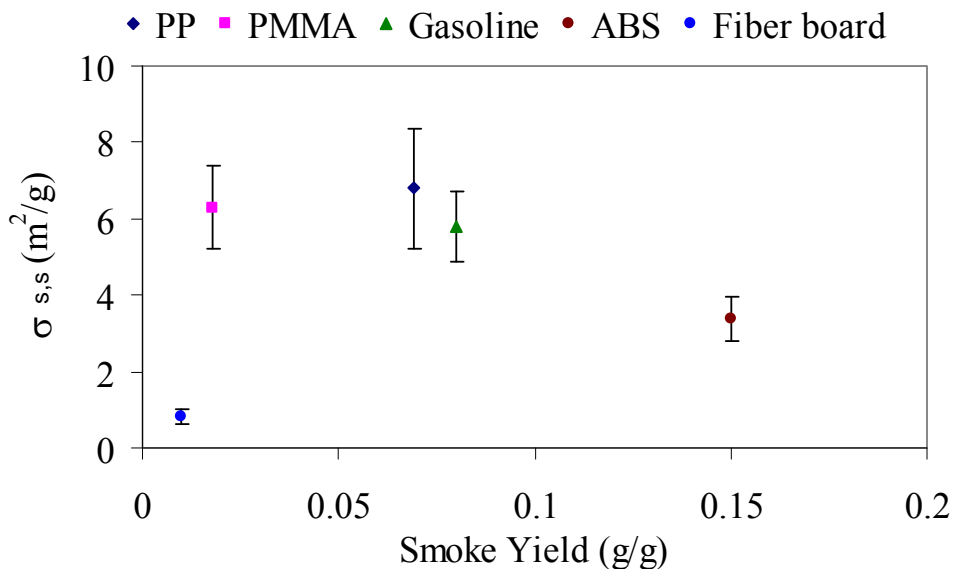
Figure 5-15: Solid phase mass specific extinction coefficient vs. Smoke yield for different fuels

Figure 5-16 shows three filters from fiber board tests. Previously, it was shown that the solid phase mass specific extinction coefficient for fiber board tests is lower than polymers. Filters from fiber board tests have a yellow shade resulting from the liquid aerosols from fiber board combustion. This differs from the rest of the fuels. Since the filters have a yellow/ brown color,

their optical density values are low and that reduces the solid phase mass specific extinction coefficient significantly. Table 5-17 shows the RGB values for the scanned filters from fiber board tests. By using color tables and compare these values with the numbers reported in the tables, it will be noticed these values represent colors that are very close to yellow, brown, beige.

072709-T1-High-Fiber board

073009-T1-High-Fiber board

073009-T2-High-Fiber board

Figure 5-16: Scanned images for fiber board wall filters

Table 5-17: Red, Green, Blue values for scanned filters from fiber board tests

	R	G	B
072709-T1-High	241	232	210
073009-T1-High	156	125	107
073009-T2-High	182	154	135

RGB values for the fiberboard filters were used as an input in Microsoft paint software to generate the colors and are shown in Figure 5-17. These colors are similar to the colors on the fiber board filters and are very close to yellow, brown and beige.

R=241; G=232; B=210   R=156; G=125; B=107

R=182; G=154; B=135

Figure 5-17: Colors created by MS paint based on RGB values for the fiber board filters

5.4 Thermophoretic Analytical Smoke Deposition Model Validation

Thermophoretic analytical smoke deposition model which was discussed in Section 3.1.3 was validated with the experimental data from the hood tests. Thermophoretic smoke deposition on the filters was determined by using Equation 3–21.

$$m'' = \int_{0}^{t} V_{th}(t)C_{s}(t)dt$$

125

Thermophoretic velocity and smoke concentration were determined in Section 3.1.3 and smoke deposition per unit area based on thermophoresis mechanism was determined by using Equation 3–23.

$$m'' = \int_0^t \left(\frac{(0.55)\eta}{\rho T} \frac{(\dot{q}''_{total} - \dot{q}''_{rad})(T_{gas} - T_{wall})}{k_{air}(T_{gas} - T_{water})} \right) \left(\frac{OD/meter}{\sigma_{s,g}} \right) dt$$

PMMA Tests

Smoke deposition based on thermophoretic velocity was calculated for each test as explained in 3.1.3. The following sections will compare the experimental data for smoke deposition on wall filters with analytical smoke deposition model.

Table 5-18 shows the experimental data for the PMMA tests which were used to validate the analytical smoke deposition model. Temperature gradient and optical density per meter were averaged over the test period for each test in order to give a representative for test conditions. Since smoke deposition analytical model needs three important factors; thermophoretic velocity, optical density per meter, and test duration, all these three factors were used for the analytical smoke deposition model and integrated over the test period for validation. Average temperature gradients for PMMA tests change between 3008 (deg/m) and 9386 (deg/m). Optical density per meter values for PMMA tests change between 1.0 (1/m) and 3.0 (1/m). All the test conditions for the tests presented in Table 5-18 were presented in Table 4-1 through Table 4-5.

Table 5-18: Test duration, average temperature gradient, and average optical density per meter for PMMA tests.

Test Number	Test Duration (s)	dT/dx (deg/m)	OD (1/m)
050409-T2	2300	6312	0.94
050409-T1	2400	7010	1.34
050609-T3	1400	9129	1.61
050609-T1	2000	9386	2.68
050609-T2	3000	8202	2.62

Test Number	Test Duration (s)	dT/dx (deg/m)	OD (1/m)
050709-T2	1200	8195	1.10
050709-T3	1400	4243	2.03
043009-T1	1900	7347	2.57
043009-T4	3600	8332	1.85
042909-T1	3000	7107	1.72
050109-T1	2800	8404	1.27
072109-T1-Low	2500	6397	0.67
072109-T1-High	2500	5428	0.83
072209-T1-Low	2600	5977	0.65
072209-T1-High	2600	3008	0.88

Figure 5-18 shows the history of gas and wall temperatures for both low and high locations for the PMMA tests 072109-T1. Gas and wall temperature were used to calculate the thermophoretic velocity. Optical density history for the PMMA test was presented in Figure 4-4. Figure 5-19 shows the smoke deposition history calculated based analytical model for both low and high locations for the PMMA test 072109-T1. These data were integrated over the test period for each test and compared to the gravimetric measurements on the filters.
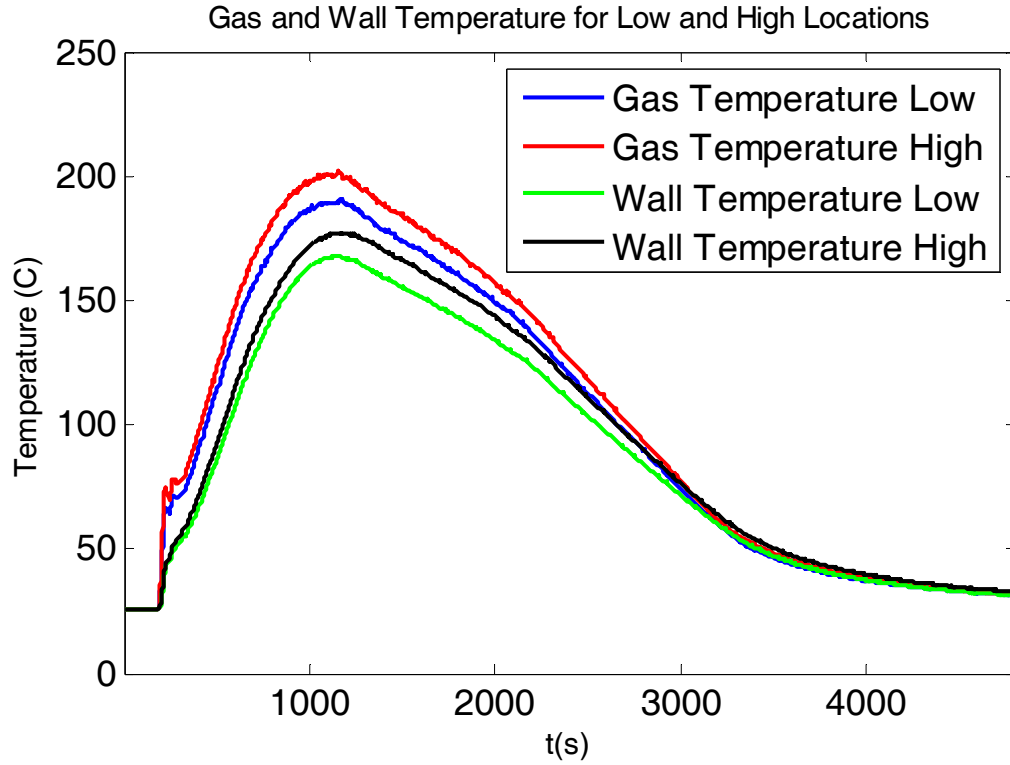
Figure 5-18: Gas and wall temperature for low and high locations for PMMA test 072109-T1
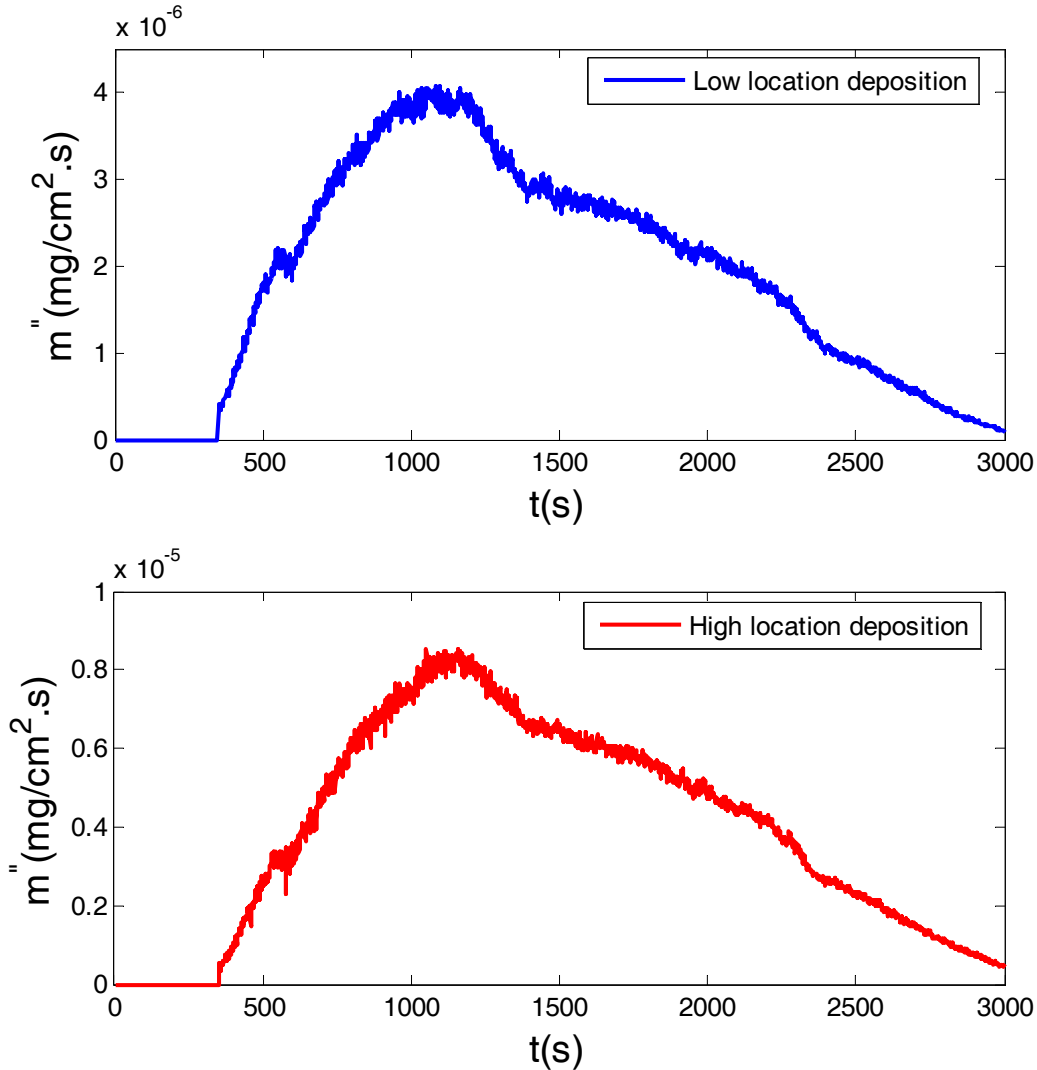
Figure 5-19: Smoke deposition rate calculated based on thermophoretic analytical model for both low and high locations for PMMA test 072109-T1

Figure 5-20 shows the predicted thermophoretic deposition vs. measured (gravimetric) deposition for PMMA. The slope on the plot (0.98) shows a very close agreement between analytical smoke deposition model and experimental data. The slope on the linear least square fit was forced to one and the change in R-squared value is not significant.
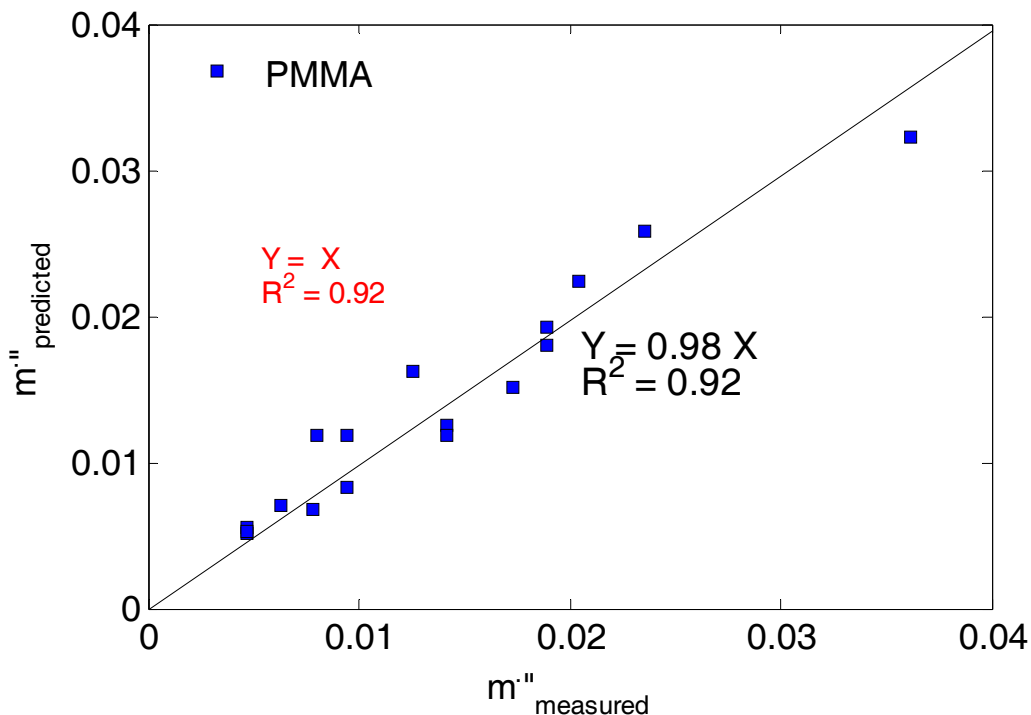
Figure 5-20: Predicted thermophoretic deposition vs. measured deposition for PMMA hood tests

Same procedure was performed on PP and gasoline. The analytical smoke deposition model based on thermophoretic velocity was not validated for ABS and fiber board due to lack of optical density per meter measurements which was discussed before.

Gasoline Tests

Table 5-19 shows the experimental data for the gasoline tests which were used to validate the analytical smoke deposition model. Temperature gradient and optical density per meter were averaged over the test period for each test in order to give a representative for test conditions. Average temperature gradients for gasoline tests change between 2497 (deg/m) and 9938 (deg/m). Optical density per meter values for gasoline tests, change between 2.1 (1/m) and 4.1 (1/m). All the test conditions for the tests presented in Table 5-19 were presented in Table 4-6 – Table 4-10.

Table 5-19: Test duration, average temperature gradient, and average optical density per meter for gasoline tests

Test Number	Test Duration (s)	dT/dx (deg/m)	OD (1/m)
042009-T3-Low	2000	9938	3.51
042009-T2-High	1600	11035	4.29
060309-T2-High	3900	2497	2.13
060909-T1-Low	3500	2796	3.18
061009-T1-Low	1450	4901	3.07
061009-T1-High	1450	6500	3.95
061009-T2-Low	2000	4252	3.14
061009-T2-High	2000	6327	4.11

Figure 5-21 shows the history of gas and wall temperatures for both low and high locations for the gasoline test 061009-T1. Gas and wall temperature were used to calculate the thermophoretic velocity. Optical density history for the gasoline test was presented in Figure 5-22 shows the smoke deposition history calculated based analytical model for both low and high locations for the gasoline test 061009-T1. These data were integrated over the test period for each test and compared to the gravimetric measurements on the filters.
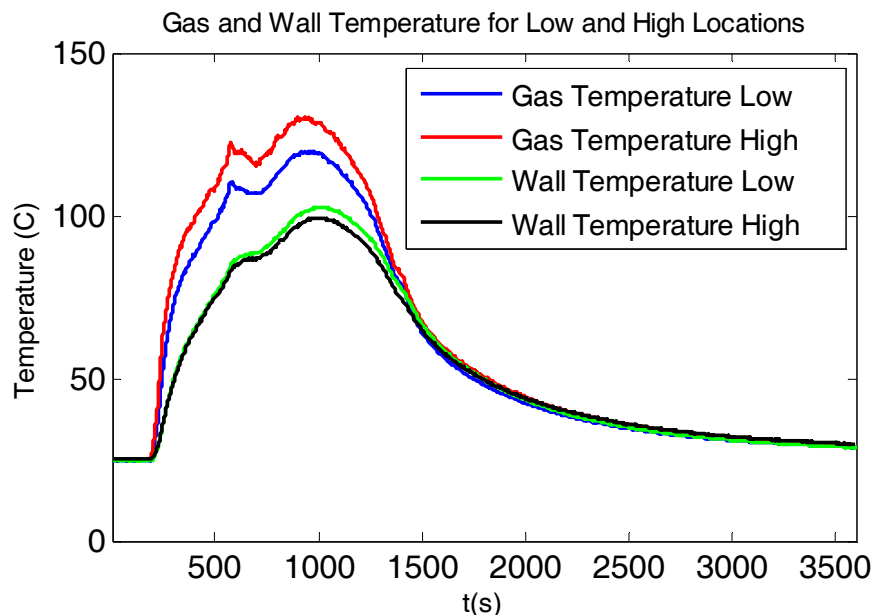
Figure 5-21: Gas and wall temperature for low and high locations for PMMA test 072109-T1
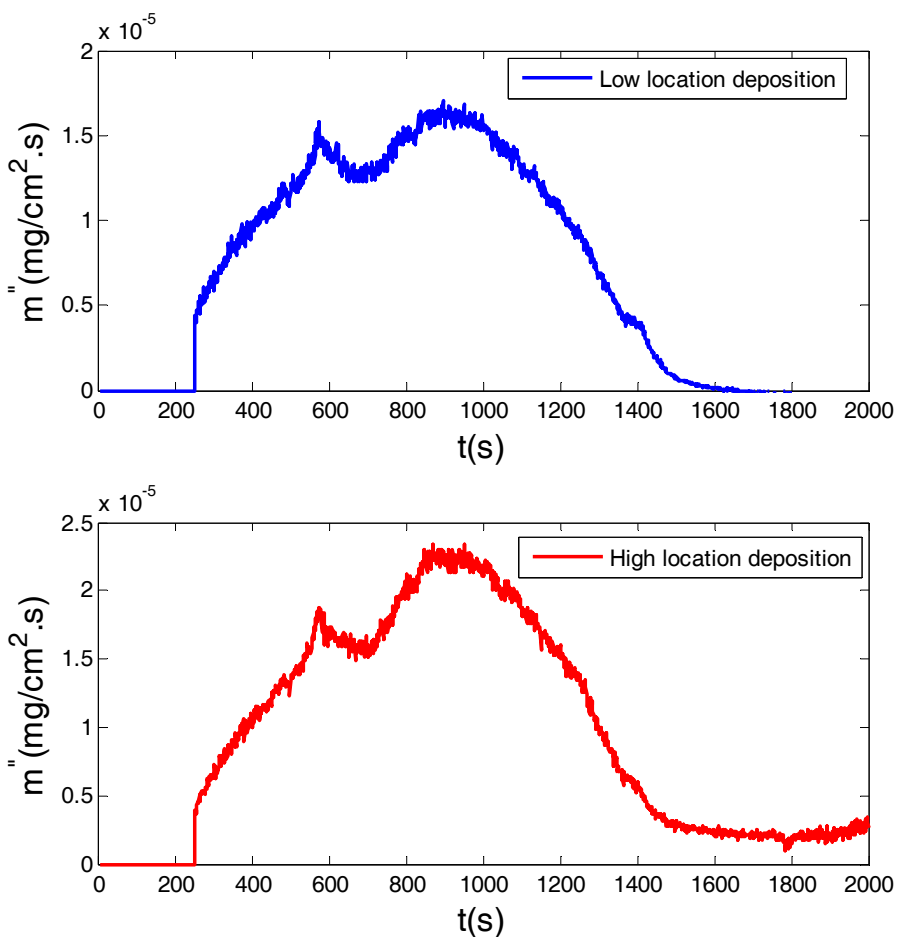
Figure 5-22: Smoke deposition rate calculated based on thermophoretic analytical model for both low and high locations for gasoline test 061009-T1

132

Figure 5-23 shows the predicted thermophoretic deposition vs. measured (gravimetric) deposition for gasoline. The slope on the plot (0.97) shows a very close agreement between analytical smoke deposition model and experimental data. The slope on the linear least square fit was forced to one and the change in R-squared value is not significant.
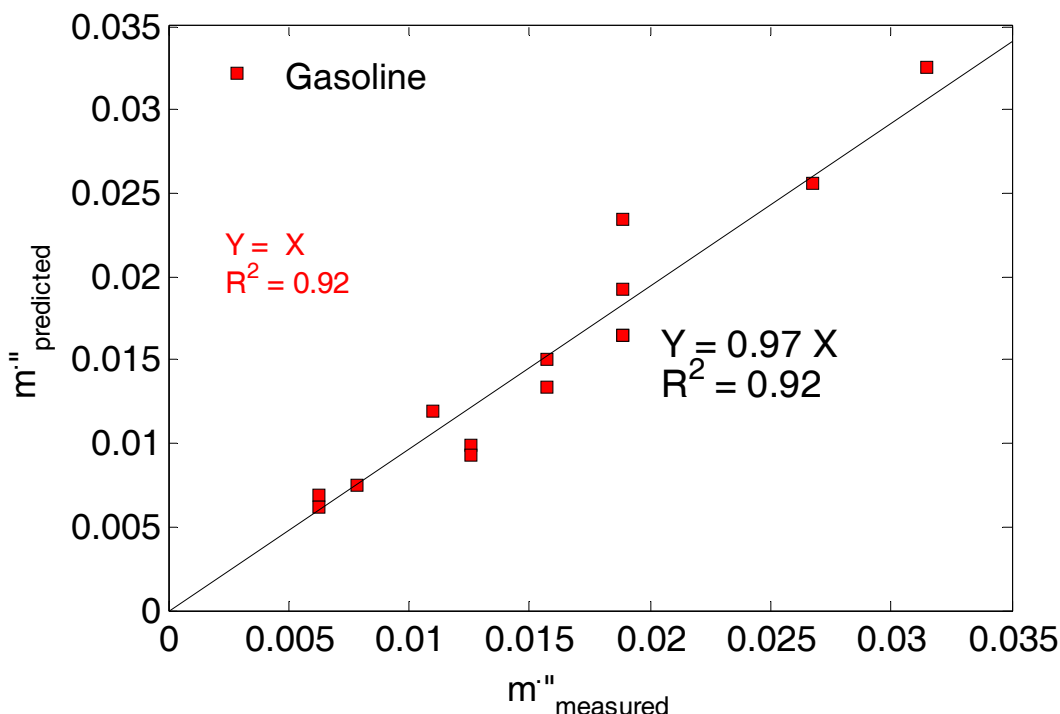
Figure 5-23 : Predicted thermophoretic deposition vs. measured deposition for gasoline hood tests

Polypropylene Tests

Figure 5-24 shows the experimental data for the polypropylene tests which were used to validate the analytical smoke deposition model. Temperature gradient and optical density per meter were averaged over the test period for each test in order to give a representative for test conditions. Average temperature gradients for gasoline tests change between 3647 (deg/m) and 6196 (deg/m). Optical density per meter values for polypropylene tests, change between 0.28 (1/m) and 1.34 (1/m). All the test conditions for the tests presented in were presented in Table 4-11 – Table 4-15.

Figure 5-24 : Test duration, average temperature gradient, and average optical density per meter for polypropylene tests

Test Number	Test Duration (s)	dT/dx (deg/m)	OD (1/m)
063009-T1-Low	2500	4582	0.81
063009-T1-High	2500	6185	0.99
070109-T1-Low	4500	4602	0.62
070109-T1-High	4500	5881	0.88
070609-T1-Low	2500	4071	0.28
070609-T1-High	2500	5207	0.45
070609-T2-Low	1100	6196	1.34
070709-T1-Low	3500	3647	0.65
070709-T1-High	3500	5568	0.84
070909-T1-Low	13500	3056	0.01
070909-T1-High	13500	4366	0.14

Figure 5-25 shows the history of gas and wall temperatures for both low and high locations for the polypropylene test 070609-T1. Gas and wall temperature were used to calculate the thermophoretic velocity. Optical density history for the gasoline test was presented in Figure 4-12. The incident jump in the wall and gas temperatures is due to the propane torch which was used to ignite the polypropylene sample.

Figure 5-26 shows the smoke deposition history calculated based analytical model for both low and high locations for the polypropylene test 070609-T1. These data were integrated over the test period for each test and compared to the gravimetric measurements on the filters.
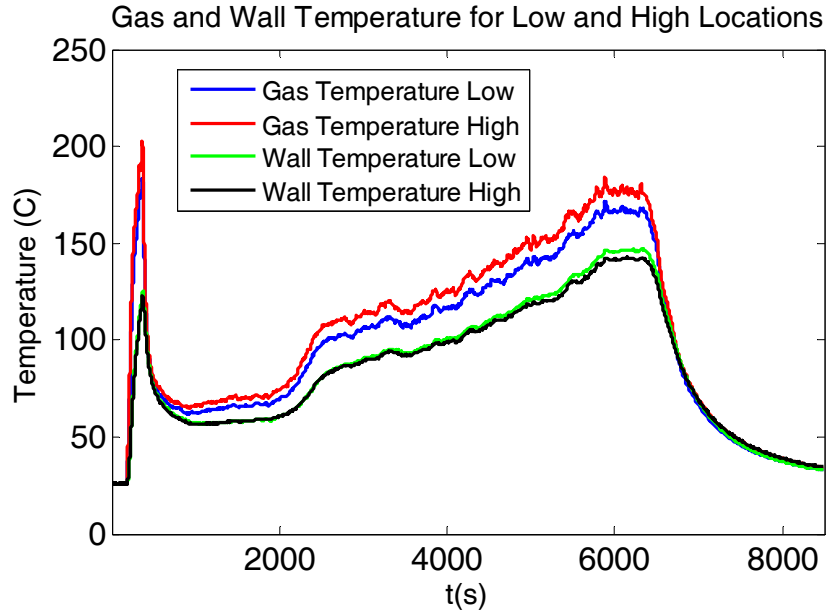
Figure 5-25: Gas and wall temperature for low and high locations for polypropylene test 070609-T1
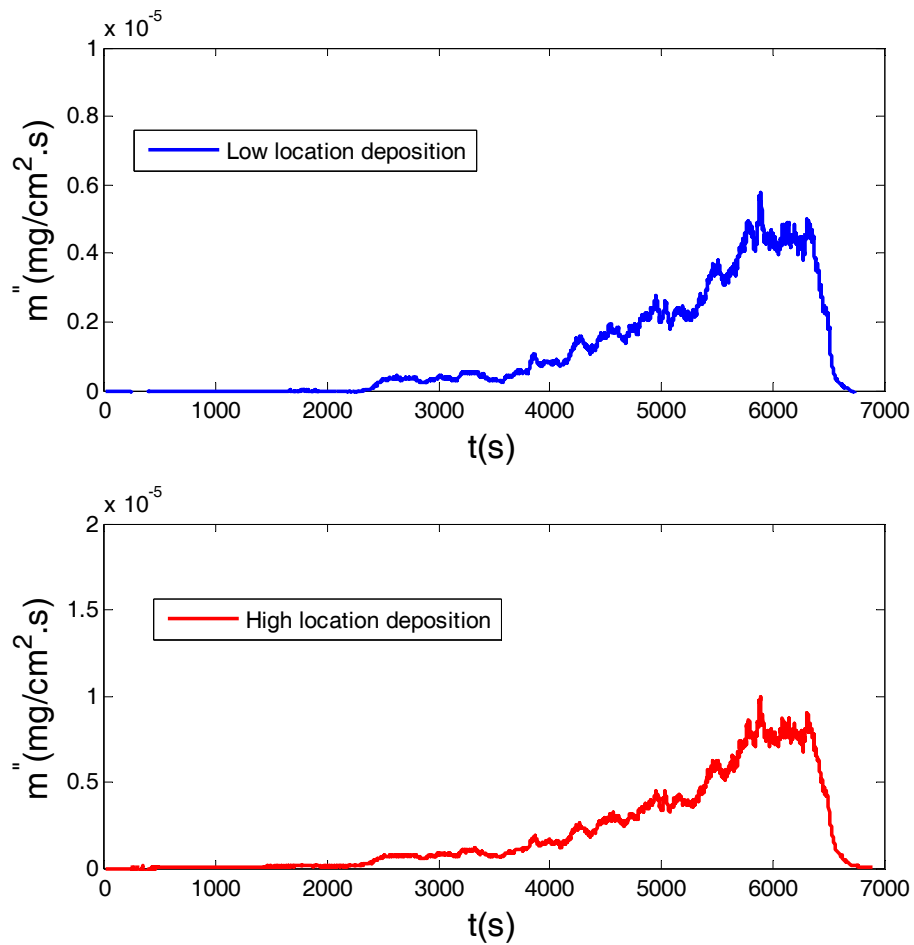
Figure 5-26: Smoke deposition rate calculated based on thermophoretic analytical model for both low and high
locations for polypropylene test 071069-T1

Variability in Deposition with Time

Test duration was changed for each fuel in order to study its effect on the smoke deposition on the walls. Test duration was increased by stacking fuel samples on top of each other. Figure 5-27 shows the smoke deposition history for the PMMA test, 050609-T3. In this test one sample of PMMA (4" x 4") was burned for 1400 seconds and the total smoke deposition per unit area on the low filter was 0.0063 mg/cm^2.
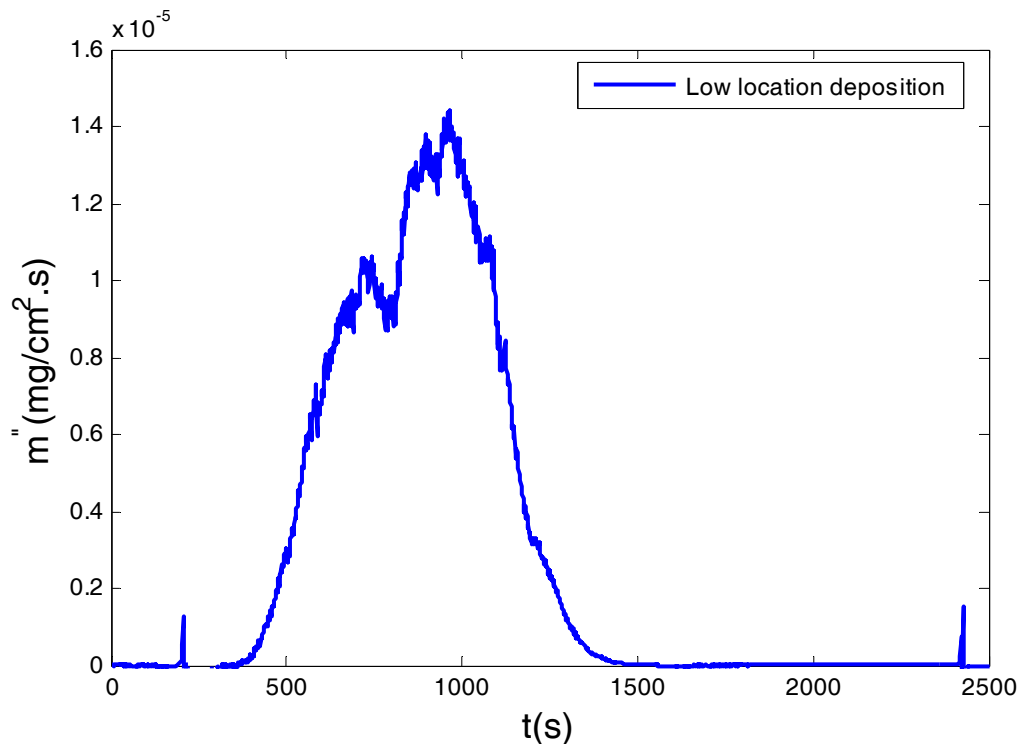
Figure 5-27: Smoke deposition rate for the PMMA test 050609-T3, 1 sample of PMMA, 4" x 4"

Figure 5-28 shows the smoke deposition history for the PMMA test, 050609-T2. In this test three samples of PMMA (4" x 4") was burned for 3000 seconds and the total smoke deposition per unit area on the low filter was 0.0236 mg/cm^2. The maximum smoke deposition per unit area for the shorter test is slightly higher than the longer test; however, the total amount of smoke deposition on the filter is more on the filter from the longer test (050609-T2). The total amount of smoke deposited on the low filter for the longer test is 3.7 times more than the smoke

deposited on the filter for the shorter test. This shows the significant effect of the time which the surface is exposed to smoke on smoke deposition.
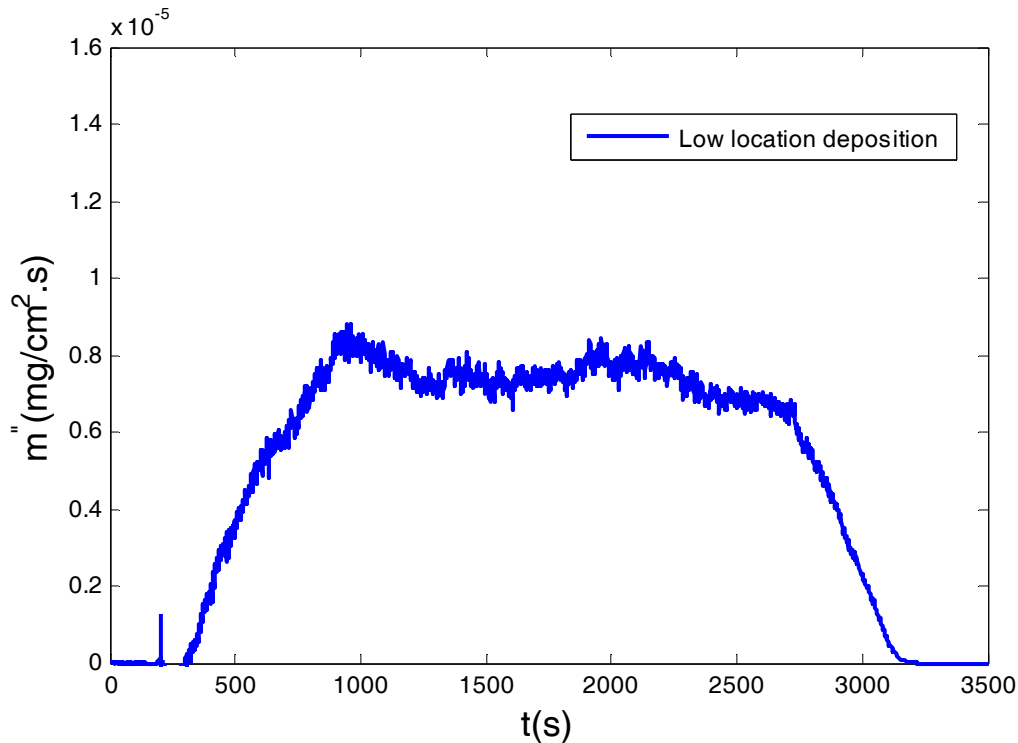
Figure 5-28: Smoke deposition rate for the PMMA test 050609-T2, 3 samples of PMMA, 4" x 4"

PMMA, PP, and Gasoline Tests

Figure 5-29 shows the predicted thermophoretic deposition vs. measured (gravimetric) deposition for PMMA, PP, and gasoline all together. It shows that thermophoretic model is predicting the smoke deposition for PMMA, PP, and gasoline very well. Thus, the thermophoretic model can be an accurate model to predict smoke deposition in fires. The thermophoretic model has not been validated for ABS and fiber board due to high and low extinction optical density for these fuels.
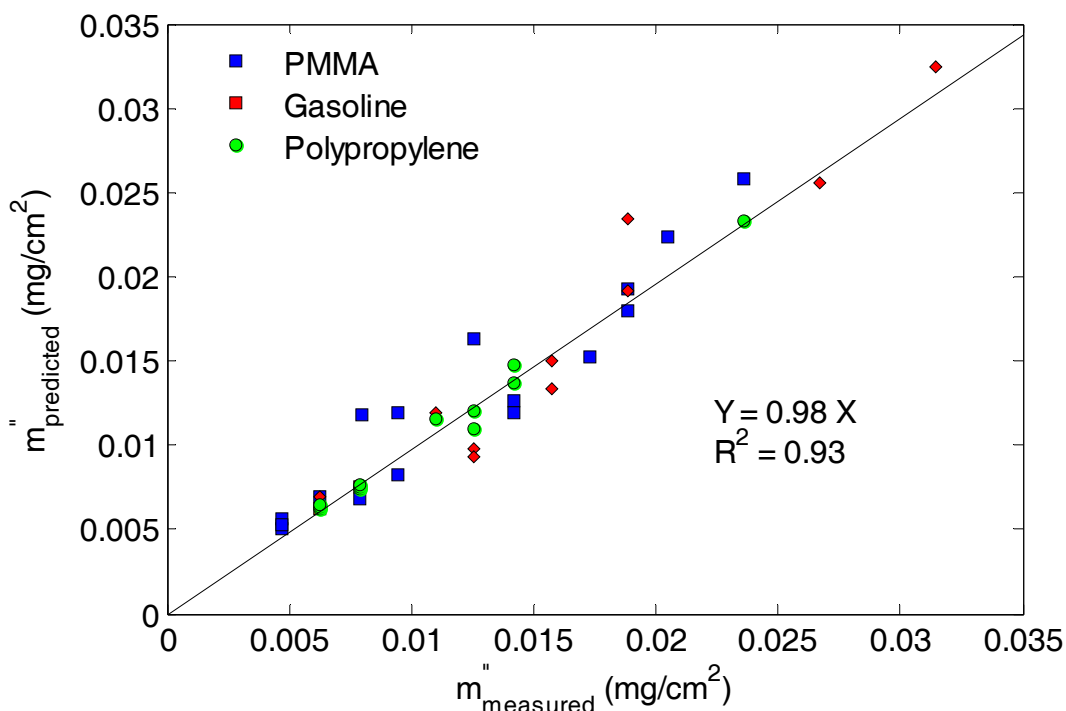
Figure 5-29: Predicted thermophoretic deposition vs. measured deposition for PMMA, PP, and gasoline hood tests

5.5   Discussion of Hood Test Results

The optical method which was developed for this research is an accurate method to
determine the optical properties of the surface which has been exposed to smoke. Gravimetric
measurement is a very straightforward method for laboratory measurements; however, it is not a
feasible method for field measurements. The optical method was initially developed based on the
point measurements from glass filters. By scanning the filters next to a gray scale and the
calibration function the optical density values on the glass filters were determined. In addition to
the point measurements, the filters were photographed next to a gray scale and the digital images
were processed using the Image J software. The pictures were taken with two different cameras
as explained in Section 3.2.2.6. Results show a very good agreement between the results from
scanned images and the digital photographs. By using a digital camera the optical properties of a
surface which has been exposed to smoke can be determined. The developed optical

measurement method is a practical and nondestructive method that can be used at the fire scenes for smoke deposition measurements.

Another developed measurement from the hood tests was the solid phase mass specific extinction coefficient. By plotting the optical properties of the glass filters after exposure to the smoke vs. the gravimetric values on those, the solid phase mass specific extinction coefficient will be determined. Solid phase mass specific extinction coefficient can be used to determine the amount of the smoke which is deposited on the surface. As discussed in Section 5.2, the solid phase mass specific extinction coefficient values for PMMA, gasoline, and PP are close to each other and the average value of 5.9 (m^2/g) is suggested for the aforementioned fuels. However, the solid phase mass specific extinction coefficient value for ABS is 3.4 (m^2/g) (58% of the suggested value for PMMA, gasoline, and PP). The value for ABS is different due to the difference in the agglomerate size distribution between ABS and other fuels. Due to the aromatic nature of ABS, it generates larger agglomerates which deposit on the filters; these agglomerates increase the weight on the filters. However, they do not affect the solid optical properties of the filters, therefore the solid phase mass specific extinction coefficient decreases for the ABS tests. The solid phase mass specific extinction coefficient value for fiber board is 0.89 (m^2/g) (15% of the value for PMMA, gasoline, and PP). The particles from the combustion of the fiber board are liquid aerosols that deposit on the filters and unlike the smoke particles, they change the filter's color to brown/yellow and solid optical density values for the filter's from the fiber board tests is significantly lower than the rest of the fuels. Table 5-20 compares the solid phase mass specific extinction values for the different fuels.

Table 5-20: Solid phase mass specific extinction coefficients for different fuels for the hood experiments

Fuel	$\sigma_{\sigma,s}$ (m²/g)
PMMA	5.9
PP	6.4
Gasoline	5.7
ABS	3.4
Fiber board	0.88

For the similar solid optical density values on the filter from PMMA, gasoline, PP, and ABS tests, the smoke particles can identified on the ABS filters and as mentioned the solid phase mass specific extinction coefficient value is lower for the ABS filters. Agglomerate size analysis was performed on the filters to achieve more quantitative analysis. Within each agglomerate diameter size, the number of the agglomerates increases as the smoke yield increases. This analysis confirms that, if there is a fuel which generates more smoke, larger agglomerates will deposit on the surface and the solid phase mass specific extinction coefficient will decrease. This is a very useful tool to predict the smoke yield for the fuel which was used based on the optical properties of the deposited smoke on the surface.

Analytical smoke deposition model base on thermophoresis was validated with the experimental data from the hood tests. Several different test scenarios were created for the hood tests to study and validate the analytical model. Smoke concentration was varied by changing the fuels and it is one of the most important parameters in the smoke deposition model based on thermophoresis. In addition to smoke concentration, Smoke layer temperature was changes by using different fuels as well as change in the exhaust rate. Smoke layer temperature variation has an impact on the temperature gradient and will change the thermophoretic velocity. Moreover, the test duration for each fuel was changes by stacking the fuel samples on top of each other. By increasing the test duration total amount of smoke deposition will increase. Figure 5-26 shows a

shorter PMMA test in the hood and Figure 5-28 shows the longer PMMA test. From the figures it is evident that the longer test will result in higher amount of smoke depositions. However, the smoke deposition rate for the longer test is lower than the shorter test. This is due to the fact that the exhaust rate on the longer test was higher than the shorter test and it reduces the smoke deposition rate but since it has been integrated over the longer time the smoke deposition amount is higher for this test. Also, different fuels have different burning rates. For example PP melts first and then starts flaming which is different than gasoline. The model was not validated for ABS and fiber board in the hood test due to high and low rate of smoke generation and the resulting lack of optical extinction measurements. By comparing the results from the model and experimental data, it is evident that the model predicts the experimental smoke deposition.

CHAPTER 6 RESULTS FOR WALL EXPERIMENTS

Wall tests were performed against the gypsum wall. Unlike hood tests which were one size pan size, three different pan sizes were used for the wall tests to study the effect of fire size on the optical properties of the smoke deposited on the surface. Fire size has a significant effect on the optical properties of the smoke deposited on the surface. Also the agglomerate size distribution is affected by the pan size. The optical properties were determined by two methods; point measurements which were similar to the method used for the hood tests. Glass filters were placed in locations and optical measurements and gravimetric measurements were performed on the filters. Moreover, a field method based on digital photography was developed and used for the fire tests against the wall. Based on the digital photography method, smoke patterns were determined on the wall. From the smoke optical properties some information such as; flame height, clean burn height, and fire size can be determined. Also by using the agglomerate size analysis and optical properties of the surface, the solid phase mass specific extinction coefficient range can be evaluated for the surface which has been exposed to smoke. The analytical smoke deposition model based on thermophoresis was validated with the experimental data for the wall experiments. Although several different test scenarios were created, the model predicts the smoke deposition for all three pan sizes.

6.1   Solid Phase Mass Specific Extinction Coefficient $(\sigma_{s,s})$

For all the wall tests, filters were collected from both locations and data were processed using the Matlab code. For each fuel, surface optical density values were plotted vs. the measured smoke mass deposited on the filter. Solid phase mass specific extinction coefficient $(\sigma_{s,s})$ was determined for PMMA, polypropylene, gasoline, and ABS. For each fuel three different set of tests were conducted; 4" x 4" pan size, 8" x 8" pan size, 12" x 12" pan size. Each test was

performed twice; the first test was shorter than the second test. Also these tests were repeated in order to study the smoke pattern on the gypsum walls.

6.1.1   4" x 4" Pan Size Tests

PMMA Tests

For the 4" x 4" pan size tests the glass filters were located at 3 ft and 4 ft above the pan. All the details for the filter installation on the wall were discussed in Section 3.2.1. Figure 6-1 shows the linear least square fit for the PMMA data with an intercept (0.071). The linear least square fit should go through origin and the change in r-squared value is not significant (0.9354 to 0.925).
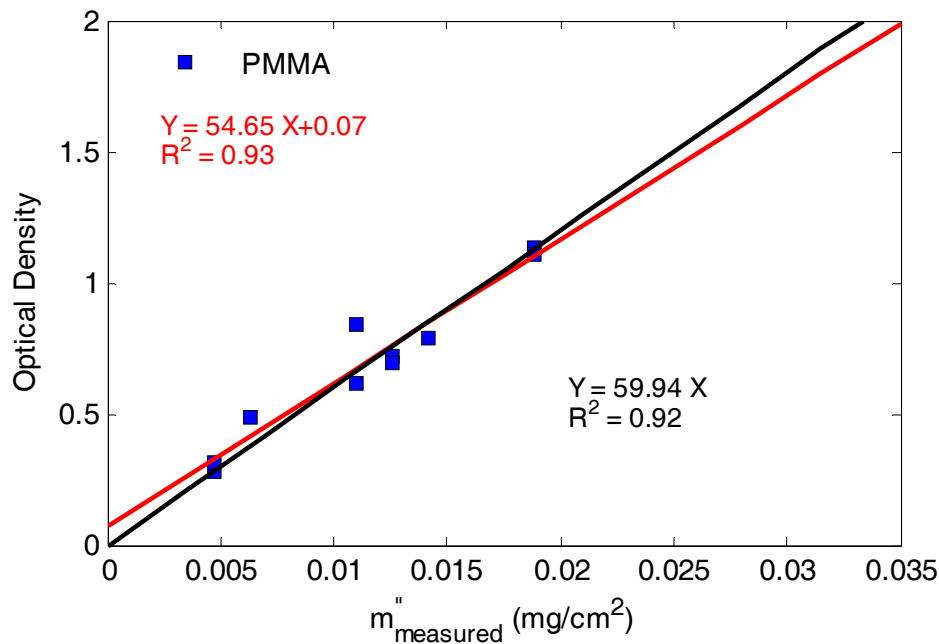
Figure 6-1: Surface optical density of smoke deposition vs. the measured deposition for PMMA

The slope of the plot shown in Figure 6-1 has the same units as gas phase mass specific extinction coefficient and it will be called solid phase mass specific extinction coefficient $(\sigma_{s,s})$. The units for the solid phase mass specific extinction coefficient in Figure 6-1 are cm^2/mg. Figure 6-2 shows the surface optical density values vs. measured smoke deposited on the filters for PMMA tests. The linear least square fit is forced to go through origin and the units for solid

phase mass specific extinction coefficient are changed to m^2/g to be consistent with the gas phase mass specific extinction coefficient units. $\sigma_{s,s}$ for PMMA hood test is 6.0 (m^2/g) as shown in Figure 6-2.
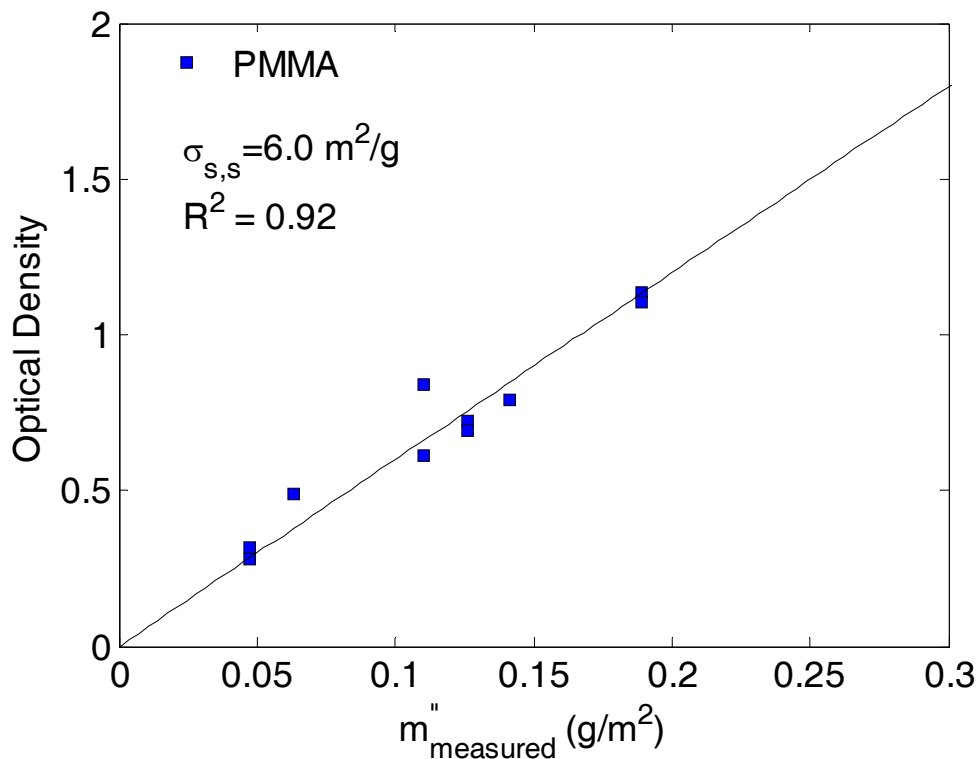
Figure 6-2: Solid phase mass specific extinction coefficient value for PMMA hood tests

Table 6-1 shows the gravimetric deposition values and optical density values for PMMA tests.

Table 6-1: Deposition and optical density values for PMMA tests

Test number	m" (mg/cm²)	OD
091109-T3-2ft	0.012582	0.722
091409-T1-2ft	0.011009	0.839
091409-T1-3ft	0.011009	0.613
091409-T1-4ft	0.006291	0.491
091409-T2-2ft	0.018872	1.137
091409-T2-3ft	0.014154	0.792

Test number	m" (mg/cm^2)	OD
091409-T2-4ft	0.004718	0.315
091409-T3-2ft	0.018872	1.107
091409-T3-3ft	0.012582	0.693
091509-T1-2ft	0.025163	1.389
091509-T1-3ft	0.012582	0.743

Polypropylene Tests

Figure 6-3 shows the linear least square fit for the PP data. The intercept of the linear least

square fit is 0.12. The change in R-squared value when the plot is forced to go through origin is

from 0.97 to 0.95. Solid phase mass specific extinction coefficient value for polypropylene tests

is 5.0 (m^2/g) and it is shown in Figure 6-4.
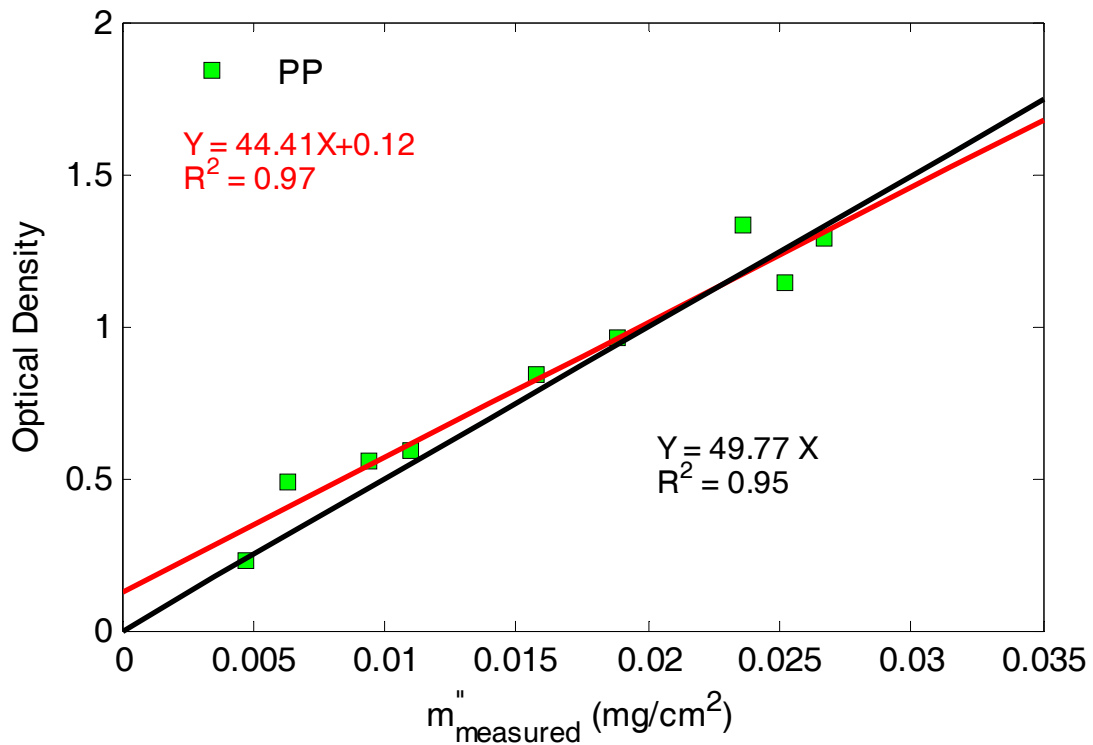
Figure 6-3 : Surface optical density of smoke deposition vs. the measured deposition for PP
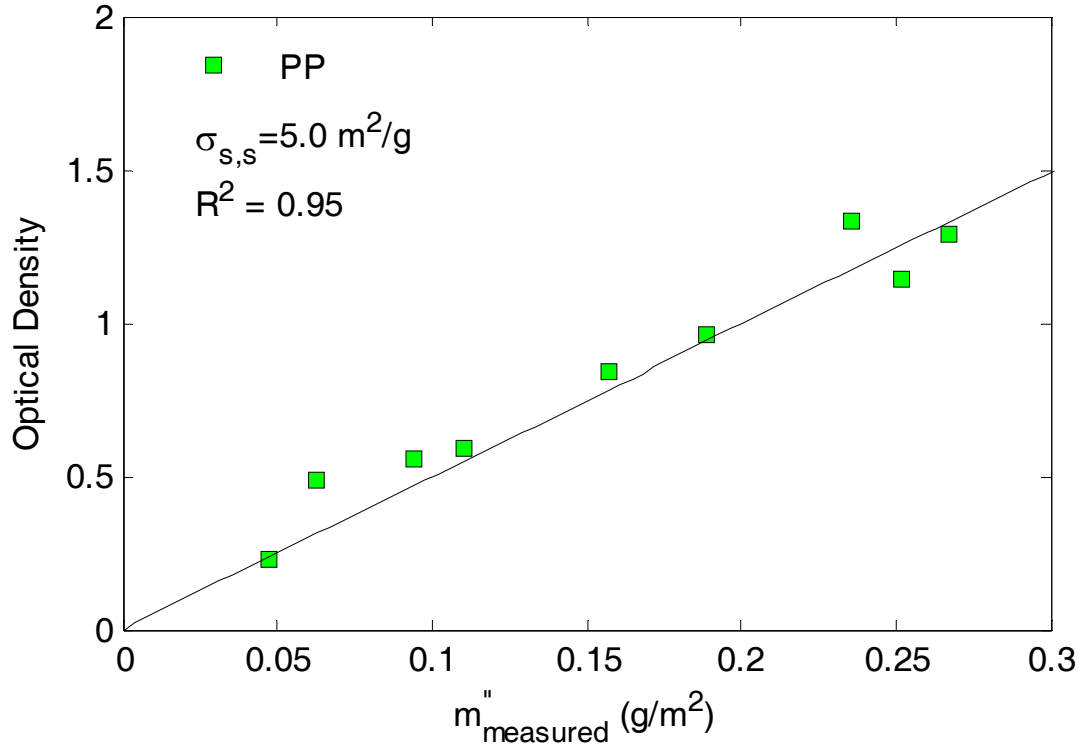
Figure 6-4: Solid phase mass specific extinction coefficient value for PP wall tests

Table 6-2 shows the gravimetric deposition values and optical density values for PP tests.

Table 6-2: Deposition and optical density values for PP tests

Test Number	m" (mg/cm²)	OD
091609-T1-2ft	0.037745	1.786
091609-T1-3ft	0.025163	1.144
091609-T1-4ft	0.009436	0.554
091709-T1-2ft	0.02359	1.33
091709-T1-3ft	0.015727	0.842
091709-T1-4ft	0.006291	0.49
091709-T2-2ft	0.004718	0.232
091709-T3-2ft	0.026736	1.285
091709-T3-3ft	0.018872	0.962
091709-T3-4ft	0.011009	0.594

Gasoline Tests

Figure 6-5 shows the linear least square fit for the gasoline data. The intercept of the linear least square fit is 0.044. The change in R-squared value when the plot is forced to go through origin is from 0.937 to 0.934. Solid phase mass specific extinction coefficient value for polypropylene tests is 5.4 (m^2/g) and it is shown in Figure 6-6.
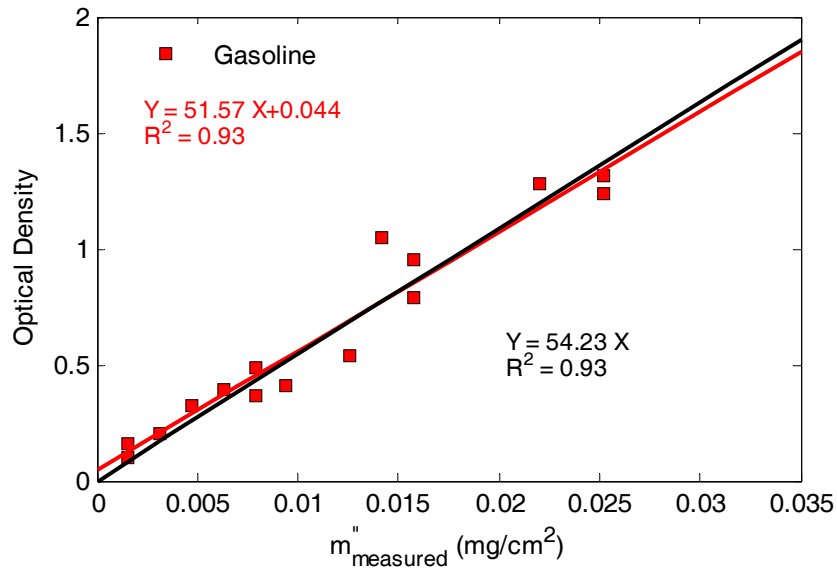
Figure 6-5: Surface optical density of smoke deposition vs. the measured deposition for gasoline
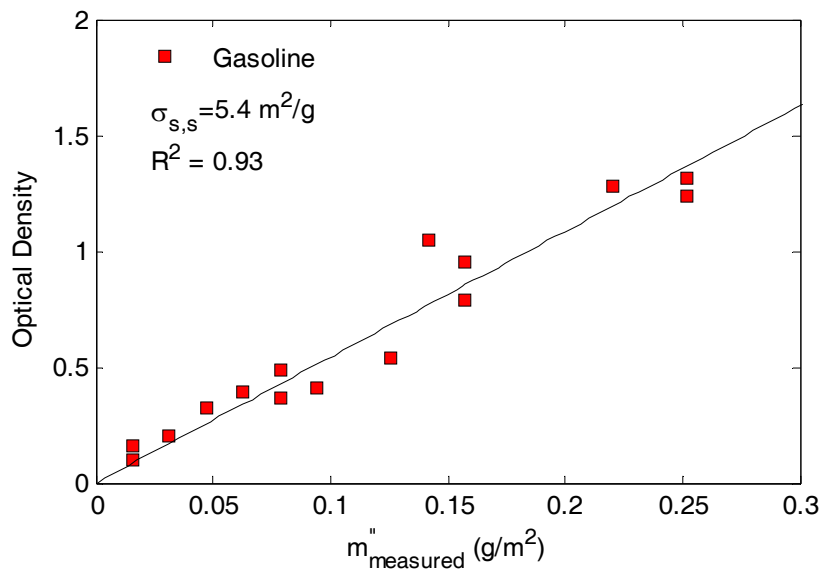
Figure 6-6: Solid phase mass specific extinction coefficient value for gasoline wall tests

147

Figure 6-6 shows the gravimetric deposition values and optical density values for gasoline tests.

Table 6-3: Deposition and optical density values for gasoline tests

Test Number	m" (mg/cm^2)	OD
090809-T1-2ft	0.015727	0.955
090809-T1-3ft	0.004718	0.32
090809-T2-2ft	0.025163	1.312
090809-T2-3ft	0.009436	0.411
090909-T1-2ft	0.006291	0.389
090909-T1-3ft	0.015727	0.787
090909-T1-4ft	0.001573	0.162
090909-T2-2ft	0.022018	1.282
090909-T2-3ft	0.007863	0.483
090909-T3-2ft	0.014154	1.044
090909-T3-3ft	0.007863	0.363
091109-T1-2ft	0.003145	0.2
091109-T1-3ft	0.001573	0.102
091109-T2-2ft	0.025163	1.241
091109-T2-3ft	0.012582	0.539

ABS Tests

Figure 6-7 shows the linear least square fit for the ABS data. The intercept of the linear least square fit is -0.021. The change in R-squared value when the plot is forced to go through origin is from 0.997 to 0.9952. Solid phase mass specific extinction coefficient value for polypropylene tests is 3.3 (m^2/g) and it is shown in Figure 6-8.

148
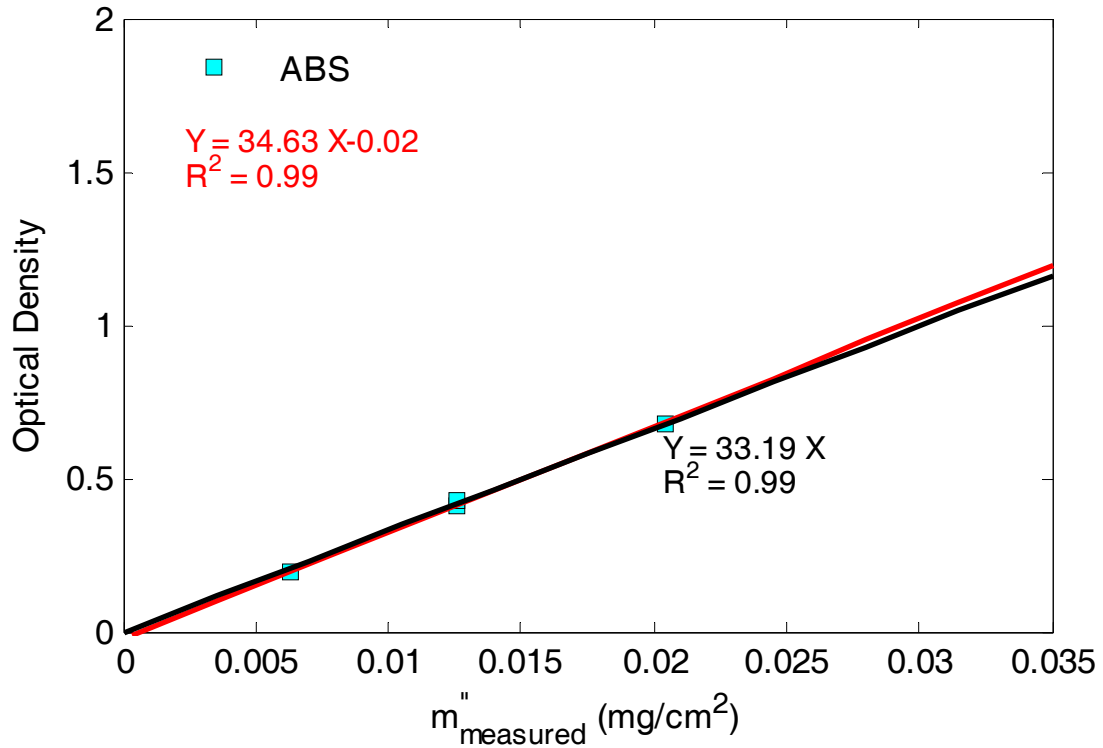
Figure 6-7: Surface optical density of smoke deposition vs. the measured deposition for ABS
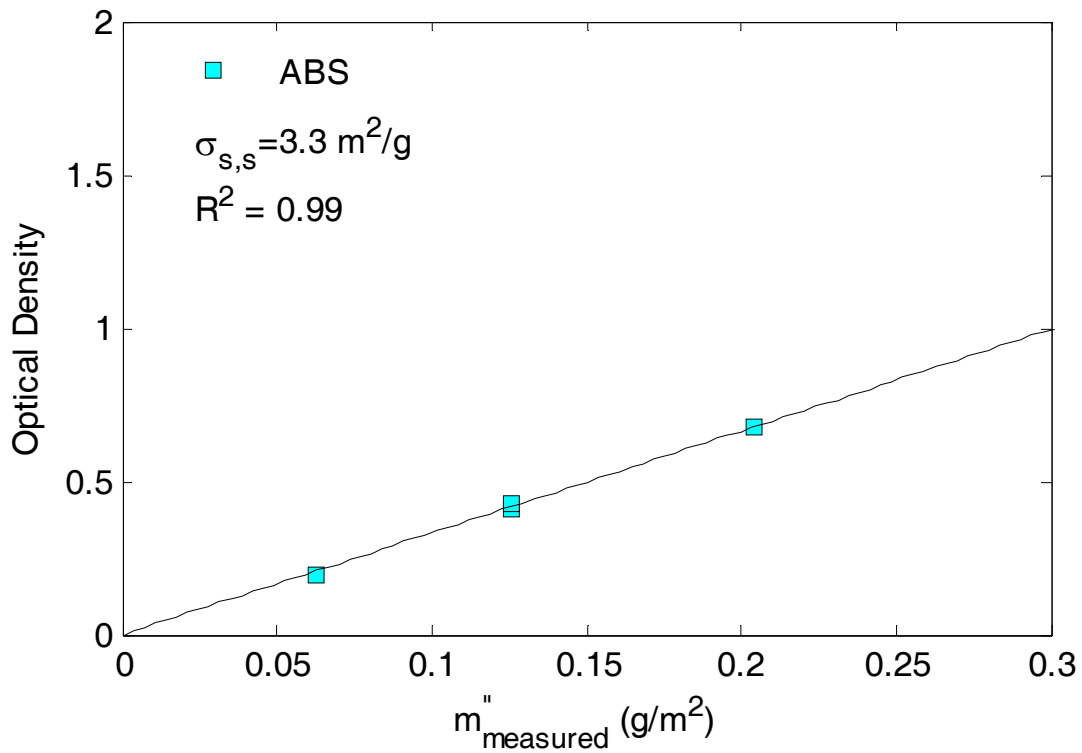
Figure 6-8: Solid phase mass specific extinction coefficient value for ABS wall tests

Table 6-4 shows the gravimetric deposition values and optical density values for ABS tests.

Table 6-4: Deposition and optical density values for ABS tests

Test Number	m" (mg/cm^2)	OD
031010-T1-Low	0.01258	0.41
031010-T1-High	0.00629	0.19
031010-T2-Low	0.0204	0.68
031010-T2-High	0.01258	0.43

PMMA, PP, and Gasoline Tests

Figure 6-9 shows the linear least square fit for PMMA, polypropylene, and gasoline data. The intercept of the linear least square fit is 0.10. The change in r-squared value when the plot is forced to go through origin is from 0.94 to 0.92. Solid phase mass specific extinction coefficient for these fuels is 5.3 (m^2/g) as shown in Figure 6-10.
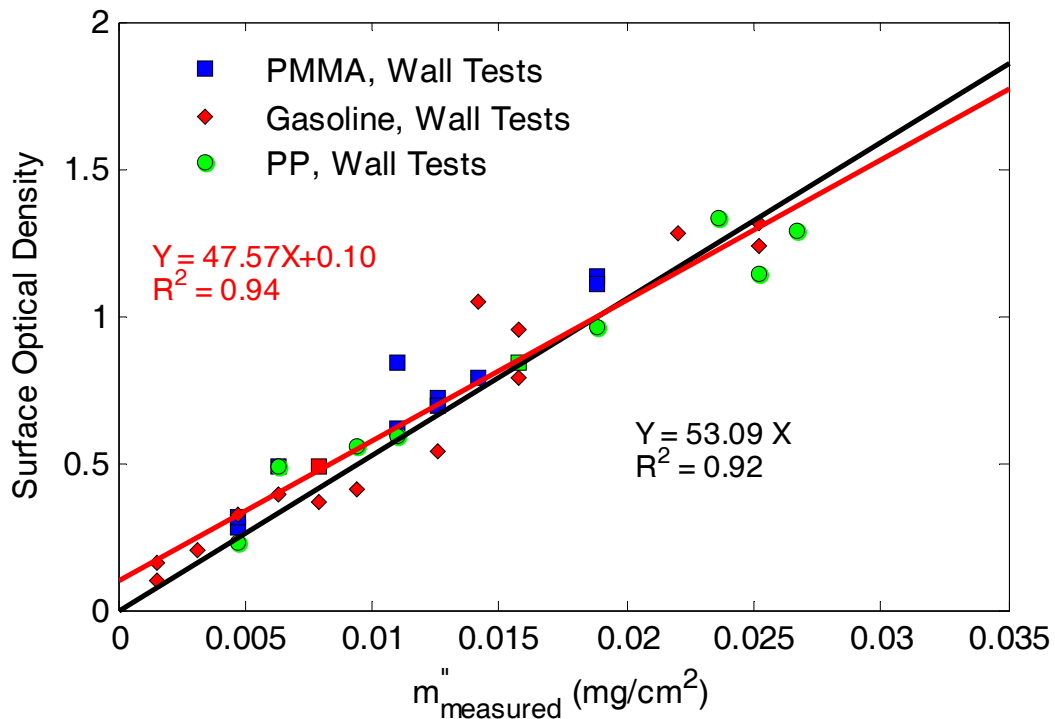
Figure 6-9: Surface optical density of smoke deposition vs. the measured deposition for PMMA, PP, and gasoline for wall tests

150
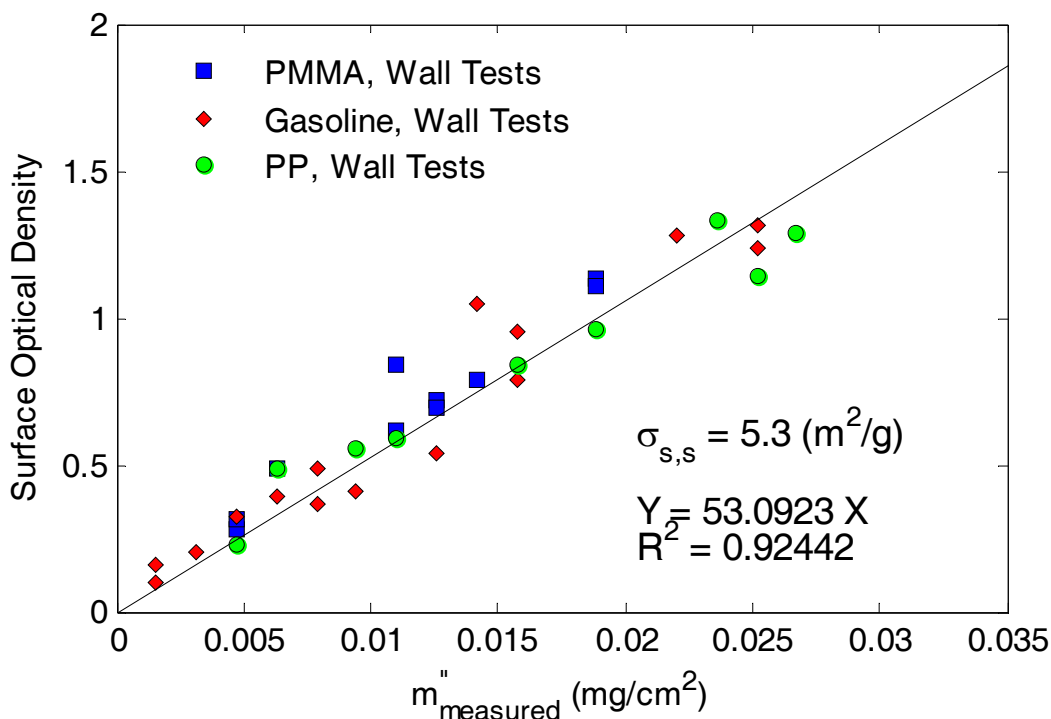
Figure 6-10: Solid phase mass specific extinction coefficient value for PMMA, PP, and gasoline wall tests

6.1.2   8" x 8" Pan Size Tests

PMMA, PP, and Gasoline Tests

For the 8" x 8" pan size tests the glass filters were located at 4 ft and 5 ft above the pan. All the details for the filter installation on the wall were discussed in Section 3.2.1. Figure 6-11 shows the linear least square fit for the PMMA, PP, and gasoline data for both 8" x 8" pan size tests with an intercept (-0.023). The linear least square fit goes through origin and the change in r-squared value is not significant (0.928 to 0.927).
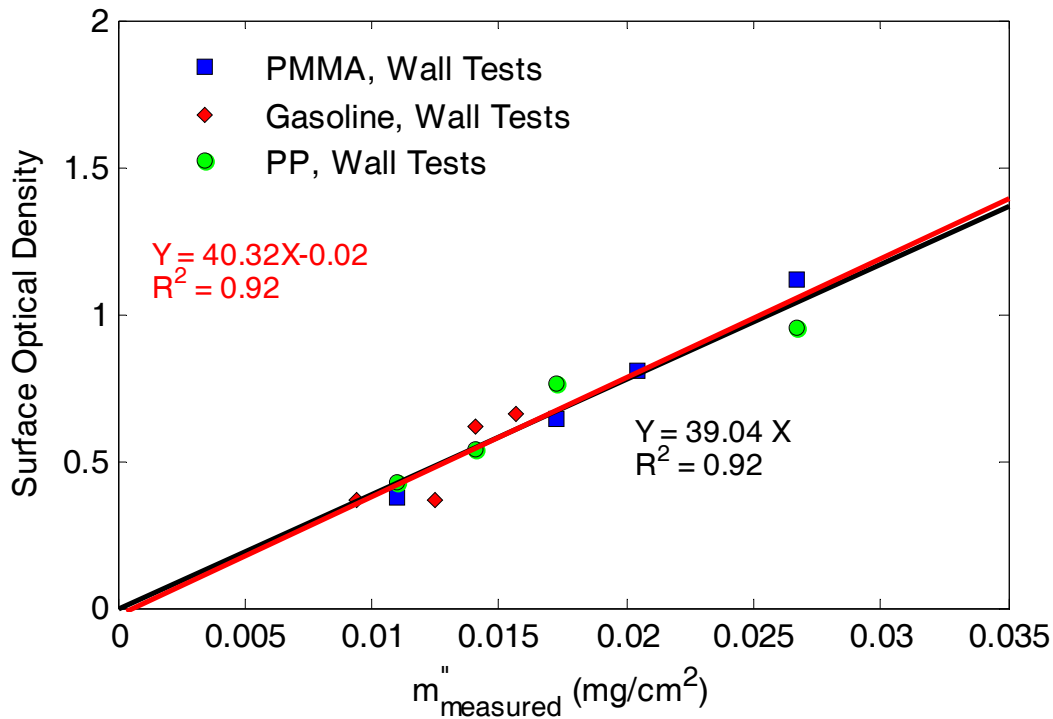
Figure 6-11: Surface optical density of smoke deposition vs. the measured deposition for PMMA, PP, and gasoline for the 8" x 8" pan size tests

The slope of the plot shown in Figure 6-11 has the same units as gas phase mass specific extinction coefficient and it will be called solid phase mass specific extinction coefficient $(\sigma_{s,s})$.

The units for the solid phase mass specific extinction coefficient in Figure 6-11 are cm^2/mg. shows the surface optical density values vs. measured smoke deposited on the filters for PMMA tests. The linear least square fit is forced to go through origin and the units for solid phase mass specific extinction coefficient are changed to m^2/g to be consistent with the gas phase mass specific extinction coefficient units. $\sigma_{s,s}$ for PMMA hood test is 3.9 (m^2/g) as shown in Figure 6-12. $\sigma_{s,s}$ for the 8" x 8" pan size tests (3.9) is lower than the $\sigma_{s,s}$ for the 4" x 4" pan size tests (5.3).
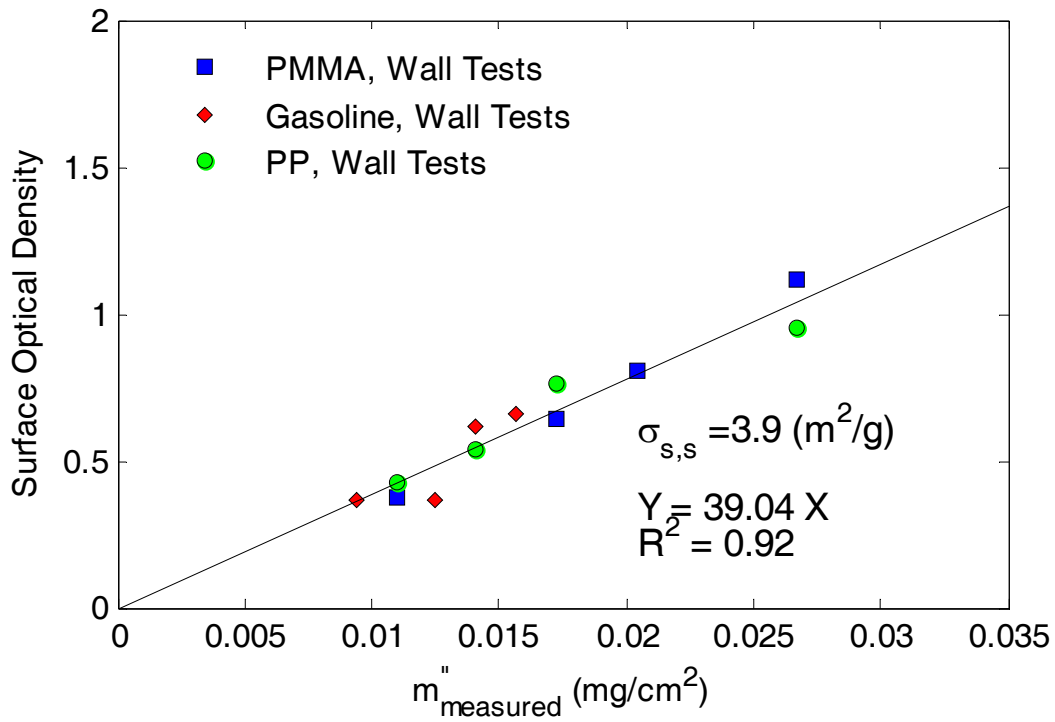
Figure 6-12: Solid phase mass specific extinction coefficient value for PMMA, PP, and gasoline 8" x 8"
pan size tests

Table 6-5: Deposition and optical density values for PMMA tests

Test Number- PMMA	m'' (mg/cm^2)	OD
021510-T1-Low	0.020445	0.803
021510-T1-High	0.011009	0.377
021510-T2-Low	0.026736	1.119
021510-T2-High	0.0173	0.646

Table 6-6: Deposition and optical density values for PP tests

Test Number- PP	m'' (mg/cm^2)	OD
021510-T3-Low	0.01729	0.761
021510-T3-High	0.011	0.431
021710-T1-Low	0.0267	0.949
021710-T1-High	0.0141	0.54

153

Table 6-7: Deposition and optical density values for gasoline tests

Test Number- Gasoline	m" (mg/cm^2)	OD
021710-T2-low	0.0141	0.616
021710-T2-high	0.0125	0.367
021710-T3-low	0.0157	0.658
021710-T3-high	0.00943	0.369

Table 6-5, Table 6-6, and Table 6-7 show the gravimetric deposition values and optical density values for PMMA, PP, and gasoline tests for the 8" x 8" pan size tests.

ABS Test

Figure 6-13 shows the linear least square fit for the ABS data. The intercept of the linear least square fit is 0.392. The change in R-squared value when the plot is forced to go through origin is from 0.97 to 0.84. Solid phase mass specific extinction coefficient value for polypropylene tests is 1.7 (m^2/g) and it is shown in Figure 6-14.
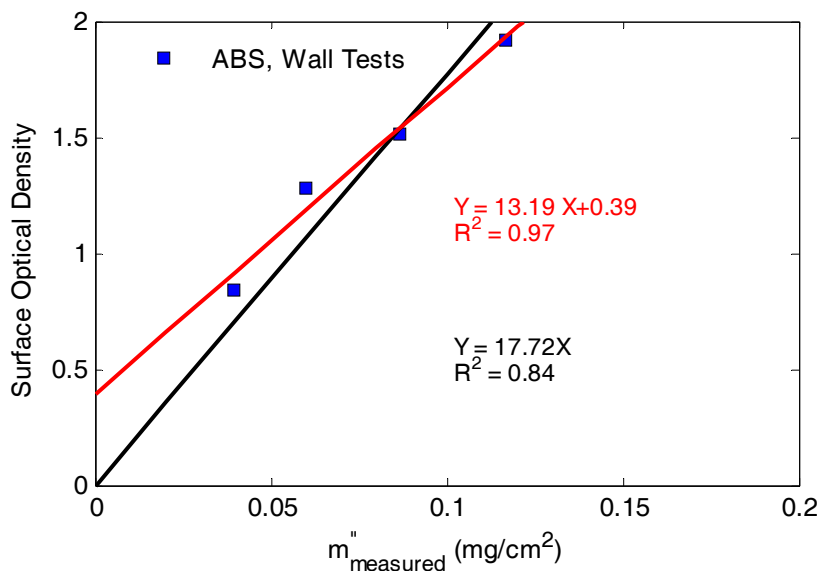
Figure 6-13 : Surface optical density of smoke deposition vs. the measured deposition for ABS for the 8"x 8" pan size tests
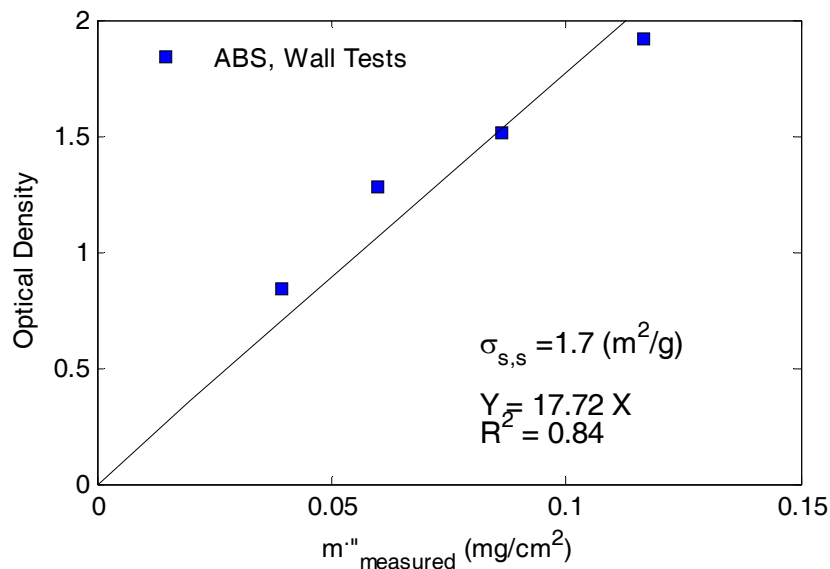
Figure 6-14: Solid phase mass specific extinction coefficient value for ABS, 8" x 8" pan size tests

Table 6-8: Deposition and optical density values for ABS tests

Test Number - Gasoline	m" (mg/cm²)	OD
031510-T1-Low	0.1166	1.917
031510-T1-High	0.0864	1.512
031510-T2-Low	0.0597	1.283
031510-T2-High	0.0393	0.844

Table 6-8 shows the gravimetric deposition values and optical density values for ABS test for the 8" x 8" pan size tests.

6.1.3   12" x 12" Pan Size Tests

PMMA, PP, and Gasoline Tests

For the 12" x 12" pan size tests the glass filters were located at 5 ft and 6 ft above the pan. All the details for the filter installation on the wall were discussed in Section 3.2.1. Figure 6-15 shows the linear least square fit for the PMMA, PP, and gasoline data for 12" x 12" pan size tests

with an intercept (-0.00559). The linear least square goes through origin and the change in r-squared value is not significant (0.9723 to 0.9270).
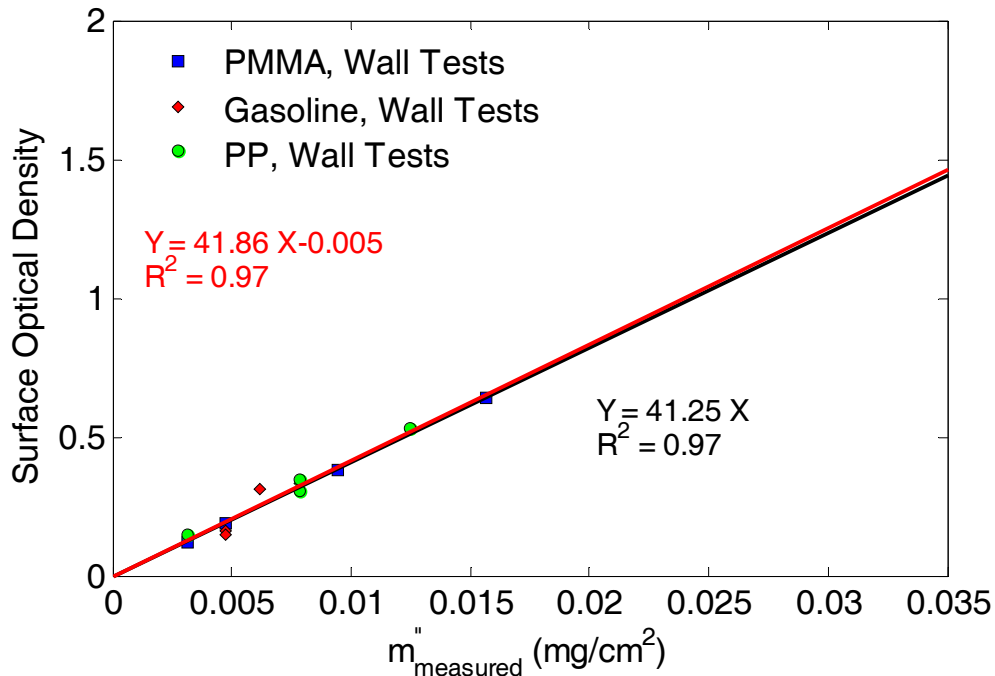
Figure 6-15: Surface optical density of smoke deposition vs. the measured deposition for PMMA, PP, and gasoline for the 12" x 12" pan size tests

The slope of the plot shown in Figure 6-15 has the same units as gas phase mass specific extinction coefficient and it will be called solid phase mass specific extinction coefficient $(\sigma_{s,s})$. The units for the solid phase mass specific extinction coefficient in Figure 6-15 are cm^2/mg. shows the surface optical density values vs. measured smoke deposited on the filters. The linear least square fit is forced to go through origin and the units for solid phase mass specific extinction coefficient are changed to m^2/g to be consistent with the gas phase mass specific extinction coefficient units. $\sigma_{s,s}$ for the wall tests is 4.1 (m^2/g) as shown in Figure 6-16. $\sigma_{s,s}$ for the 12" x 12" pan size tests (4.1) is close to the $\sigma_{s,s}$ for the 8" x 8" pan size tests (3.9).
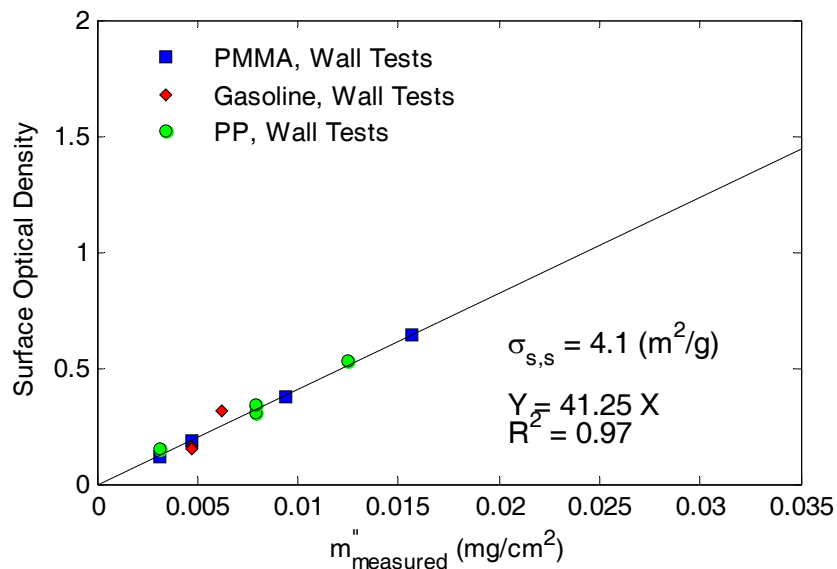
Figure 6-16: Solid phase mass specific extinction coefficient value for PMMA, PP, and gasoline 12" x 12" pan size tests

Table 6-9: Deposition and optical density values for PMMA tests

Test Number - PMMA	m" (mg/cm²)	OD
022210-T1-Low	0.0157	0.64
022210-T1-High	0.00943	0.377
022510-T1-Low	0.00471	0.188
022510-T1-High	0.00314	0.12

Table 6-10: Deposition and optical density values for PP tests

Test Number - PP	m" (mg/cm²)	OD
030110-T2-Low	0.00786	0.308
030110-T2-High	0.003145	0.149
030110-T3-Low	0.0125	0.528
030110-T3-High	0.00786	0.344

157

Table 6-11: Deposition and optical density values for gasoline tests

Test Number - Gasoline	m" (mg/cm^2)	OD
022510-T2-Low	0.0062	0.313
022510-T2-High	0.00471	0.16
030110-T1-Low	0.00786	0.333
030110-T1-High	0.00471	0.15

Table 6-9, Table 6-10, and Table 6-11show the gravimetric deposition values and optical density values for PMMA, PP, and gasoline tests for the 12" x 12" pan size tests.

ABS Tests

Figure 6-17 shows the linear least square fit for the ABS data. The intercept of the linear least square fit is 0.143. The change in R-squared value when the plot is forced to go through origin is from 0.97 to 0.88. Solid phase mass specific extinction coefficient value for polypropylene tests is 1.9 (m^2/g) and it is shown in Figure 6-18.
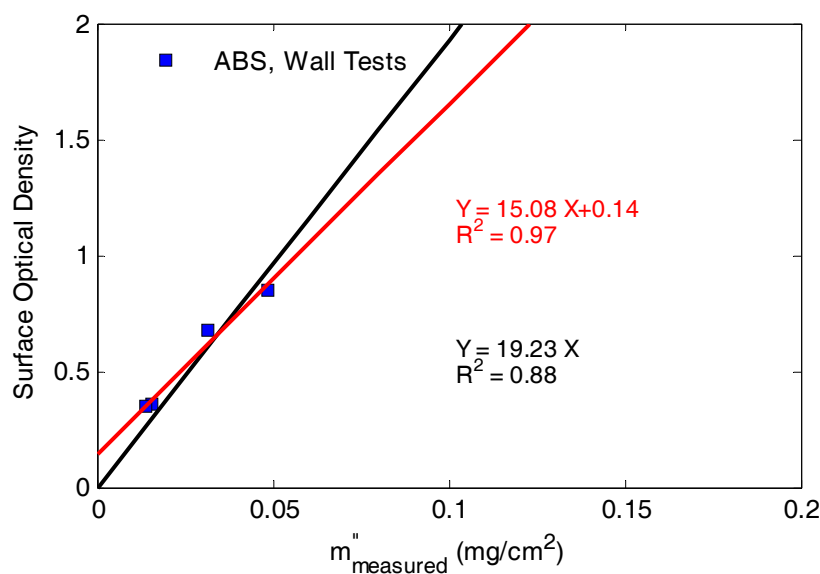
Figure 6-17: Surface optical density of smoke deposition vs. the measured deposition for ABS for the 12" x 12" pan size tests
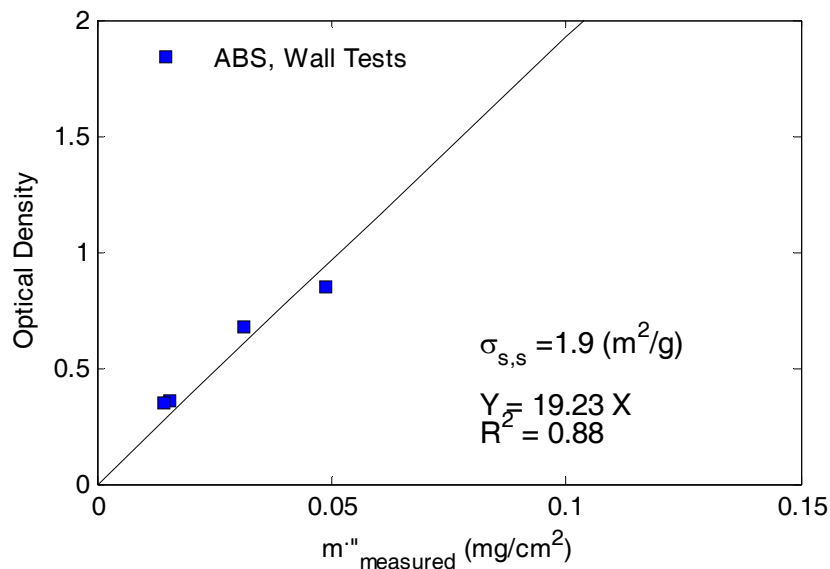
Figure 6-18: Solid phase mass specific extinction coefficient value for ABS, 12" x 12" pan size tests

Table 6-12: Deposition and optical density values for ABS tests

Test Number - Gasoline	m" (mg/cm²)	OD
031510-T3-Low	0.04875	0.853
031510-T3-High	0.03145	0.673
031610-T2-Low	0.01572	0.36
031610-T2-High	0.01415	0.35

Table 6-12 shows the gravimetric deposition values and optical density values for ABS tests for the 12" x 12" pan size tests.

6.2 Agglomerate Size Analysis for PMMA, PP, Gasoline and ABS Tests 4" X 4" Pan Size Tests

These filters were selected because their optical density values are very close to each other.

Table 6-13 shows the optical density and amount of smoke deposited on each filter.

159

Table 6-13: Smoke deposition and optical density values for PMMA, polypropylene, gasoline, and ABS tests for
4" x 4" pan size

Test	m" (mg/cm^2)	OD
091009-T3-PMMA	0.0125	0.693
091709-T1-PP	0.0157	0.842
090909-T1-Gasoline	0.0157	0.787
031010-T2-ABS	0.0204	0.68

Data analysis was performed on the wall filters with the Image J software. Number of
agglomerates was plotted vs. agglomerate diameter for each filter. Table 6-14 shows the
agglomerate size distribution for polypropylene, PMMA, gasoline, and ABS wall filters. The
agglomerate diameter size was calculated based on the pixel concept. Image J software identifies
agglomerates within the size which can be specified in the software. Agglomerate diameter size
was changed from low to high. One of the outcomes of this analysis is the number of
agglomerates within the same diameter is higher for ABS than PMMA, polypropylene, and
gasoline. Also, the number of the agglomerates for the 4" x 4" pan size wall tests is very close to
the values from the hood tests.

Table 6-14: Smoke agglomerate size distribution for PMMA, gasoline, ABS, and polypropylene for wall tests
(4" x 4" pan size)

Agglomerate Diameter Size	Number of agglomerates			
d (mm)	PP	PMMA	Gasoline	ABS
0.0042	3159	2213	4761	5533
0.0075	2904	1983	4150	4958
0.0098	2745	1849	3653	4623
0.0116	2623	1795	3147	4488
0.0132	2395	1700	2963	4250
0.0237	1595	977	2059	2443
0.0309	1183	686	1658	1985
0.0366	898	514	1365	1650
0.0416	730	394	1164	1523
0.0750	210	74	552	522
0.0976	116	36	156	215

160

Figure 6-19 shows that ABS wall filter has more agglomerates within each diameter. For example if we select a certain agglomerate size and count number of agglomerates on the wall filter from PMMA, gasoline, PP, and ABS tests; number of agglomerates will be higher and ABS filter than PMMA and PP filters. This means that these agglomerates are more effective gravimetrically on ABS filters.
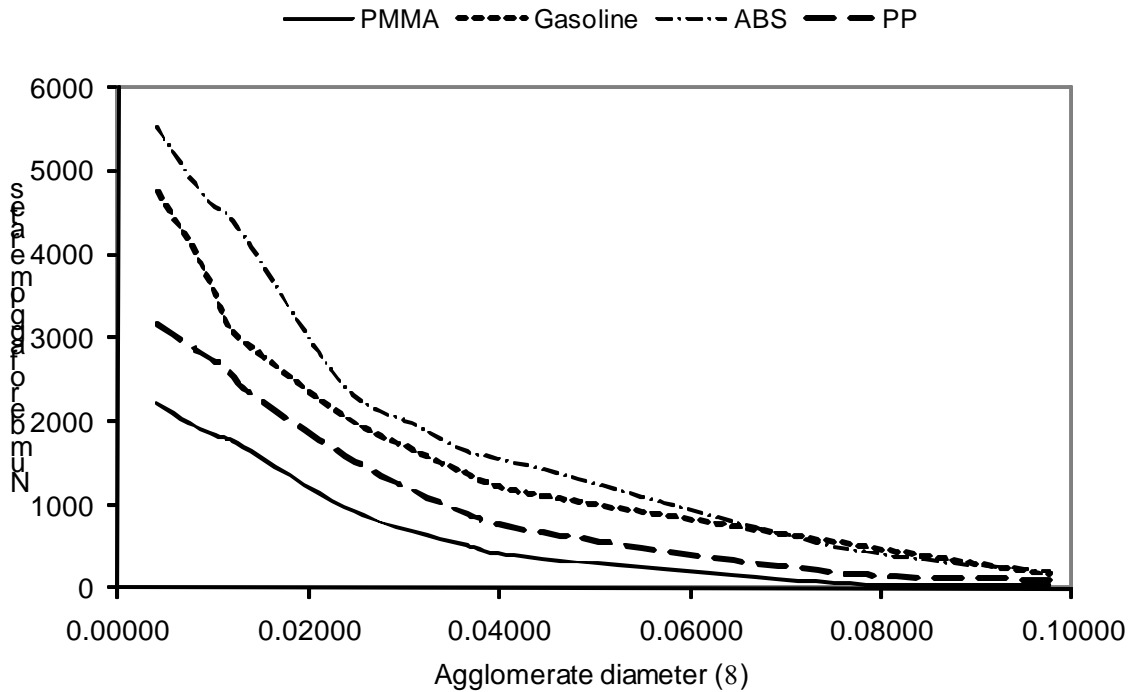
Figure 6-19: Agglomerate size distribution for wall filter, 4" x 4" pan size

Table 6-15: Solid phase mass specific extinction coefficient vs. smoke yield for the fuels, 4" x 4" pan size

	PP	PMMA	Gasoline	ABS
$\sigma_{s,s}$ (m^2/g)	5.4 ± 0.93	6.1 ± 0.79	5.9 ± 1.5	3.2 ± 0.17
Smoke yield (g/g)	0.069	0.018	0.080	0.15

Table 6-15 shows the fuels and the solid phase mass specific extinction coefficient for the fuels as well as smoke yields for those fuels. These results suggest that increased smoke yield

161

increases agglomeration and lowers solid phase mass specific extinction coefficient. Figure 6-20 shows the $\sigma_{s,s}$ vs. smoke yield for the fuels used in the experiments.
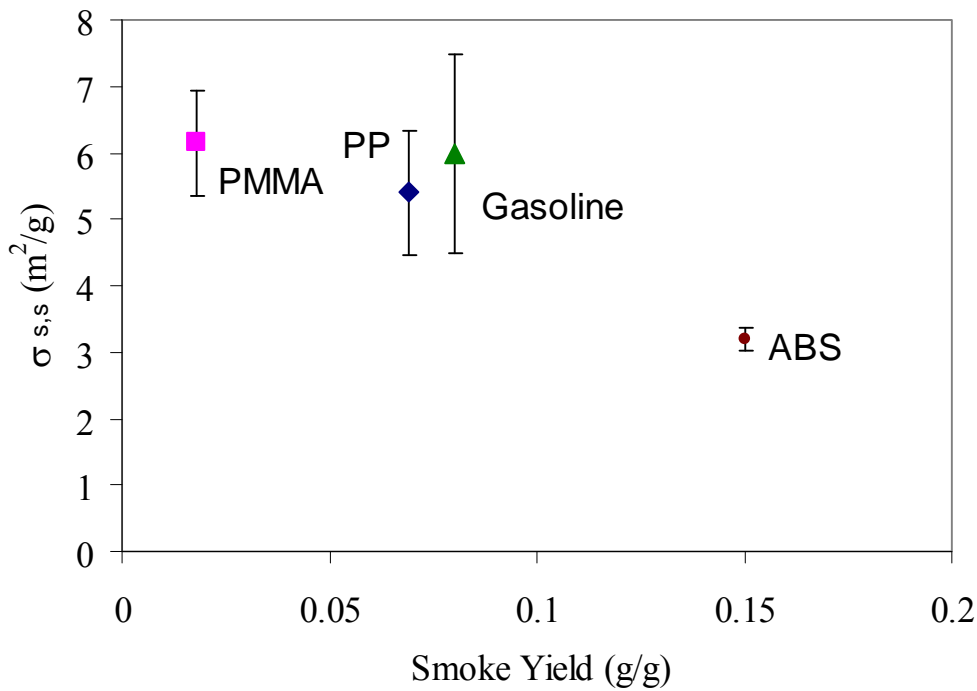
Figure 6-20: Solid phase mass specific extinction coefficient vs. Smoke yield for different fuels, 4" x 4" pan size

8" x 8" Pan Size Tests

These filters were selected because their optical density values are very close to each other. Table 6-16 shows the optical density and amount of smoke deposited on each filter.

Table 6-16: Smoke deposition and optical density values for PMMA, polypropylene, gasoline, and ABS tests for 8" x 8" pan size

Test	m" (mg/cm^2)	OD
021510-T1-PMMA	0.02044	0.803
021510-T3-PP	0.01729	0.761
021710-T3-Gasoline	0.0157	0.658
031510-T2-ABS	0.0393	0.844

Number of agglomerates was plotted vs. agglomerate diameter for each filter. Table 6-17 shows the agglomerate size distribution for polypropylene, PMMA, gasoline, and ABS wall

162

filters. The agglomerate diameter size was calculated based on the pixel concept. Agglomerate

diameter size was changed from low to high. One of the outcomes of this analysis is the number

of agglomerates within the same diameter is higher for ABS than PMMA, polypropylene, and

gasoline. Also, the number of the agglomerates for the 8" x 8" pan size wall tests is higher than

the values for the 4" x 4" pan size wall tests.

Table 6-17: Smoke agglomerate size distribution for PMMA, gasoline, ABS, and polypropylene for wall tests
(8" x 8" pan size)

Agglomerate Diameter Size	Number of Agglomerates			
d (mm)	PP	PMMA	Gasoline	ABS
0.0042	4315	3258	4962	5955
0.0075	4036	2980	4641	5570
0.0098	3700	2808	4255	5106
0.0116	3426	2673	3940	4728
0.0132	3244	2454	3731	4477
0.0237	2568	1810	2953	3544
0.0309	2043	1472	2349	2819
0.0366	1623	1247	1866	2240
0.0416	1271	1068	1462	1754
0.0750	425	375	489	587
0.0976	265	202	305	366

Figure 6-21 shows that ABS wall filter has more agglomerates within each diameter. Also by

comparing the number of the number of the agglomerates between the 4" x 4" pan size and

8" x 8" pan size, it will be noticed that the particles from the smaller tests are more effective

optically than the particles from the larger tests.

163
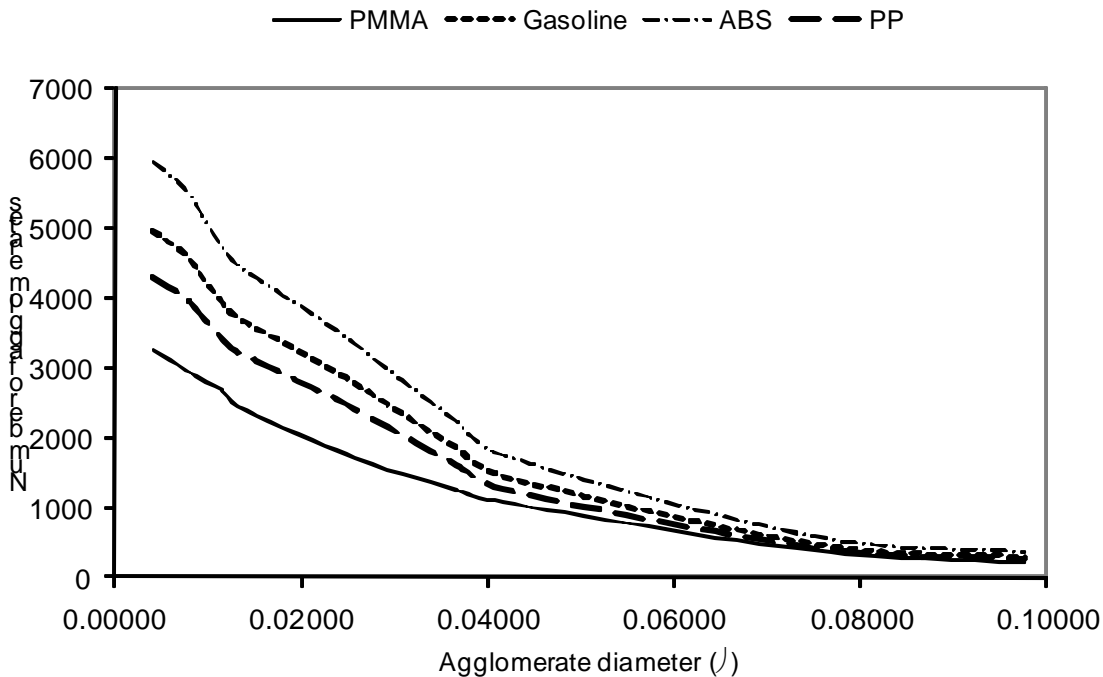
Figure 6-21: Agglomerate size distribution for wall filter, 8" x 8" pan size

Table 6-18 shows the fuels and the solid phase mass specific extinction coefficient for the fuels as well as smoke yields for those fuels. These results suggest that increased smoke yield increases agglomeration and lowers solid phase mass specific extinction coefficient. Figure 6-22 shows the $\sigma_{s,s}$ vs. smoke yield for the fuels used in the experiments. Figure 6-23 shows the scanned filters. Smoke particles can be identified from PMMA, PP, and gasoline tests. Also larger agglomerates can be identified on ABS filters.

Table 6-18: Solid phase mass specific extinction coefficient vs. smoke yield for the fuels, 8" x 8" pan size

	PP	PMMA	Gasoline	ABS
$\sigma_{s,s}$ (m²/g)	3.9 ± 0.35	3.8 ± 0.32	3.8 ± 0.63	1.9 ± 0.26
Smoke yield (g/g)	0.063	0.024	0.086	0.26
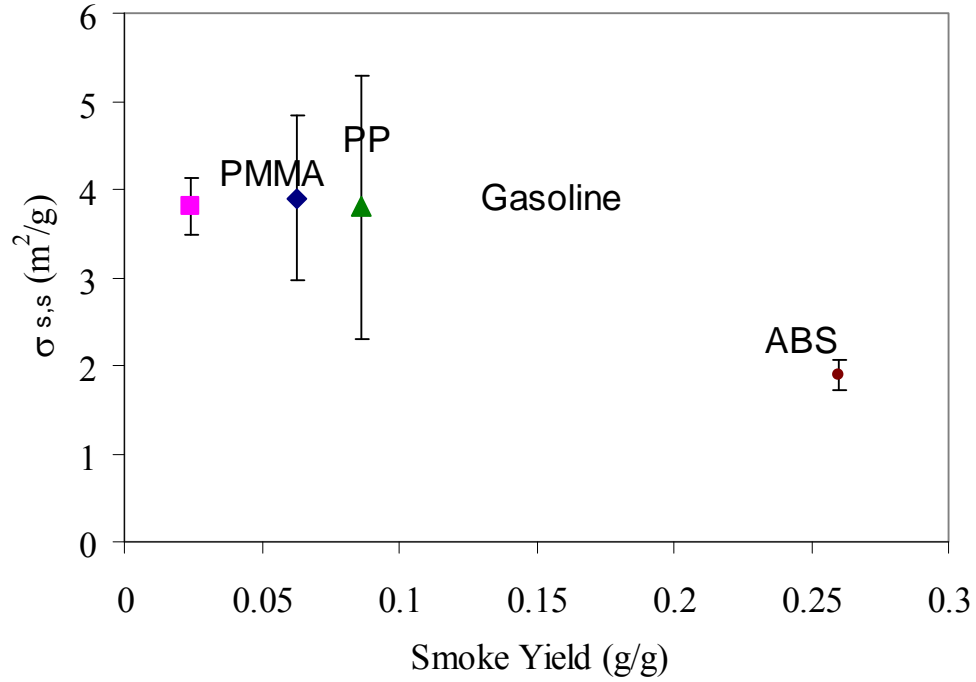
Figure 6-22: Solid phase mass specific extinction coefficient vs. Smoke yield for different fuels, 8" x 8" pan size

021510-T1-PMMA   021510-T3-PP   021710-T3-gasoline

031510-T2-ABS
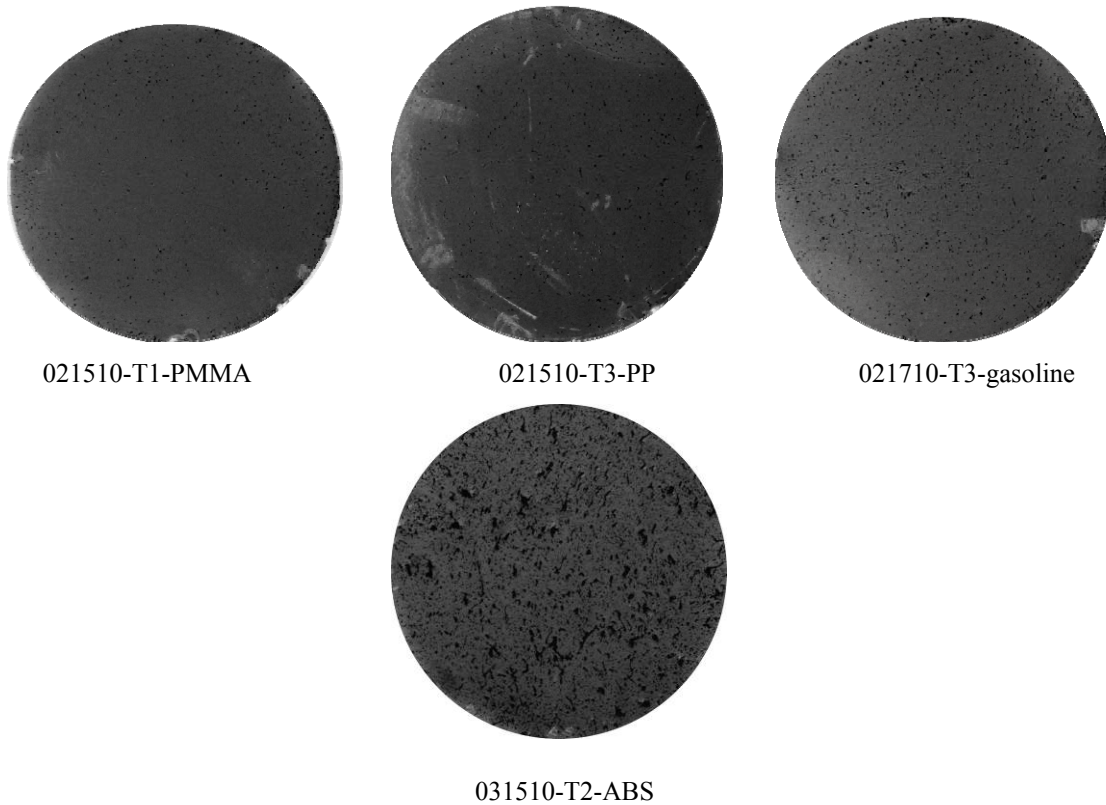
Figure 6-23: Scanned filter from wall tests (8"x 8" pan)

12" x 12" Pan Size Tests

These filters were selected because their optical density values are very close to each other.

Table 6-19 shows the optical density and amount of smoke deposited on each filter.

Table 6-19: Smoke deposition and optical density values for PMMA, polypropylene, gasoline, and ABS tests for 12" x 12" pan size

Test	m" (mg/cm^2)	OD
022210-T1-PMMA	0.00943	0.377
030110-T2-PP	0.00786	0.308
030110-T1-Gasoline	0.00786	0.333
031610-T2-ABS	0.01415	0.35

Number of agglomerates was plotted vs. agglomerate diameter for each filter. Table 6-17 shows the agglomerate size distribution for polypropylene, PMMA, gasoline, and ABS wall filters. The agglomerate diameter size was calculated based on the pixel concept. Agglomerate diameter size was changed from low to high. One of the outcomes of this analysis is the number of agglomerates within the same diameter is higher for ABS than PMMA, polypropylene, and gasoline. Also, the number of the agglomerates for the 12" x 12" pan size wall tests is close to the values for the 8" x 8" pan size wall tests.

Table 6-20: Smoke agglomerate size distribution for PMMA, gasoline, ABS, and polypropylene for wall tests (12" x 12" pan size)

Agglomerate Diameter Size	Number of Agglomerates			
d (mm)	PP	PMMA	Gasoline	ABS
0.0042	4229	3193	4888	5865
0.0075	3955	2920	4572	5486
0.0098	3626	2752	4191	5029
0.0116	3357	2620	3881	4657
0.0132	3179	2405	3675	4410
0.0237	2517	1774	2909	3491
0.0309	2002	1443	2314	2777
0.0366	1591	1222	1838	2206
0.0416	1246	1047	1440	1728

Agglomerate Diameter Size	Number of Agglomerates			
0.0750	417	368	481	578
0.0976	260	198	300	360

Figure 6-24 shows that ABS wall filter has more agglomerates within each diameter. Also by comparing the number of the number of the agglomerates between the 8" x 8" pan size and 12" x 12" pan size, it will be noticed that the number of the particles for both set of tests are very similar.
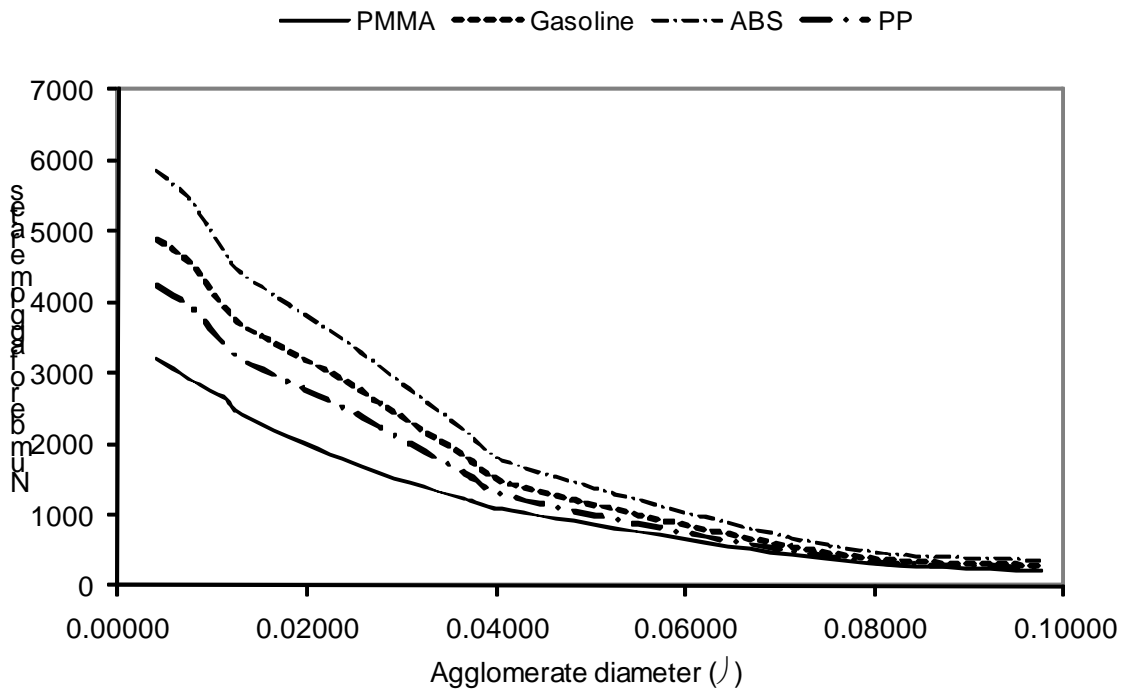
Figure 6-24: Agglomerate size distribution for wall filter, 12" x 12" pan size

Table 6-21 shows the fuels and the solid phase mass specific extinction coefficient for the fuels as well as smoke yields for those fuels. These results suggest that increased smoke yield increases agglomeration and lowers solid phase mass specific extinction coefficient. Figure 6-25 shows the $\sigma_{s,s}$ vs. smoke yield for the fuels used in the experiments.

Table 6-21: Solid phase mass specific extinction coefficient vs. smoke yield for the fuels, 12" x 12" pan size

	PP	PMMA	Gasoline	ABS
$\sigma_{s,s}$ (m^2/g)	3.9±0.35	3.8±0.32	3.8±0.63	1.9±0.26
Smoke yield (g/g)	0.074	0.031	0.095	0.27
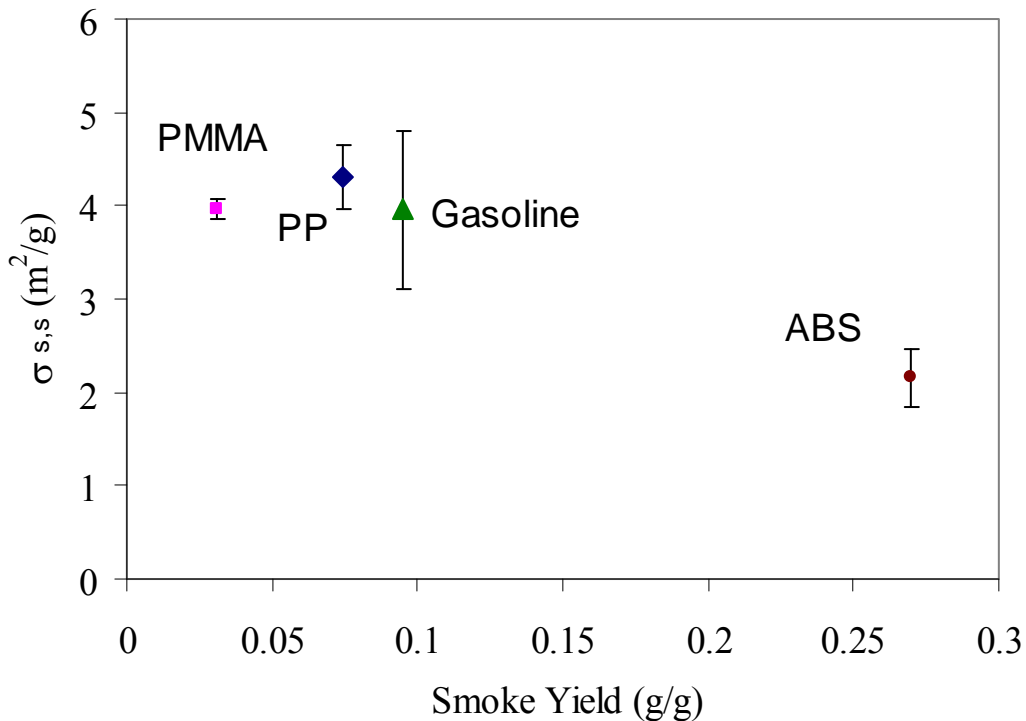
Figure 6-25: Solid phase mass specific extinction coefficient vs. Smoke yield for different fuels, 12" x 12" pan size

6.3   Thermophoretic Analytical Smoke Deposition Model Validation

Thermophoretic analytical smoke deposition model which was discussed in Section 3.2.3.3 was validated with the experimental data from the wall tests. Thermophoretic smoke deposition on the filters was determined by using Equation 3–21.

168

$$m'' = \int_{o}^{t} V_{th}(t)C_{s}(t)dt$$

Thermophoretic velocity and smoke concentration were determined in Section 3.2.3.

4" x 4" Pan Size Tests

Smoke deposition based on thermophoresis was calculated for each test as explained in Section 3.2.3. The following sections will compare the experimental data for the smoke deposition on the wall filters with analytical smoke deposition model.

Table 6-22, Table 6-23, Table 6-24, and Table 6-25 show the experimental data for the PMMA, gasoline, PP, and ABS tests (4" x 4" pan size). Temperature gradient and smoke concentration were averaged over the test period for each test in order to give a representative for these factors and test conditions. Since smoke deposition analytical model needs three important parameters; thermophoretic velocity, smoke concentration, and test duration, all three of these parameters were used for the analytical smoke deposition model and integrated over the test duration for validation.

Table 6-22: Test duration, average temperature gradient, and average smoke concentration for PMMA tests
(4" x 4" pan size)

Test Number	Test Duration (s)	dT/dx (deg/m)	Cs (g/m³)
011110-T1-Low	4500	8839.67	0.052
011110-T1-High	4500	3581.10	0.061
011110-T1-Low	5700	600.68	0.032

Table 6-23: Test duration, average temperature gradient, and average smoke concentration for gasoline tests
(2.5" diameter pan size)

Test Number	Test Duration (s)	dT/dx (deg/m)	Cs (g/m³)
121109-T2-Low	2400	7259.98	0.267
121109-T2-High	2400	3395.99	0.267
121109-T3-Low	2800	10655.38	0.188
121109-T3-High	2800	1929.04	0.188

169

Table 6-24: Test duration, average temperature gradient, and average smoke concentration for PP tests
(4" x 4" pan size)

Test Number	Test Duration (s)	dT/dx (deg/m)	Cs (g/m³)
121709-T3-Low	1800	7782.44	0.225
121709-T4-Low	1700	7608.48	0.126
121709-T4-High	1700	2758.90	0.126
122109-T4-High	2600	19540.04	0.142

Table 6-25: Test duration, average temperature gradient, and average smoke concentration for ABS tests
(4" x 4" pan size)

Test Number	Test Duration (s)	dT/dx (deg/m)	Cs (g/m³)
031010-T1-Low	1500	6702.73	0.729
031010-T1-High	1500	2177.69	0.729
031010-T2-Low	1900	2500.28	0.450
031010-T2-High	1900	1595.68	0.450

Average temperature gradient for all the fuels changes between 600 (deg/m) and 19000
(deg/m). Smoke concentration values for all the fuels changes between 0.03 (g/m³) and
0.72 (g/m³).
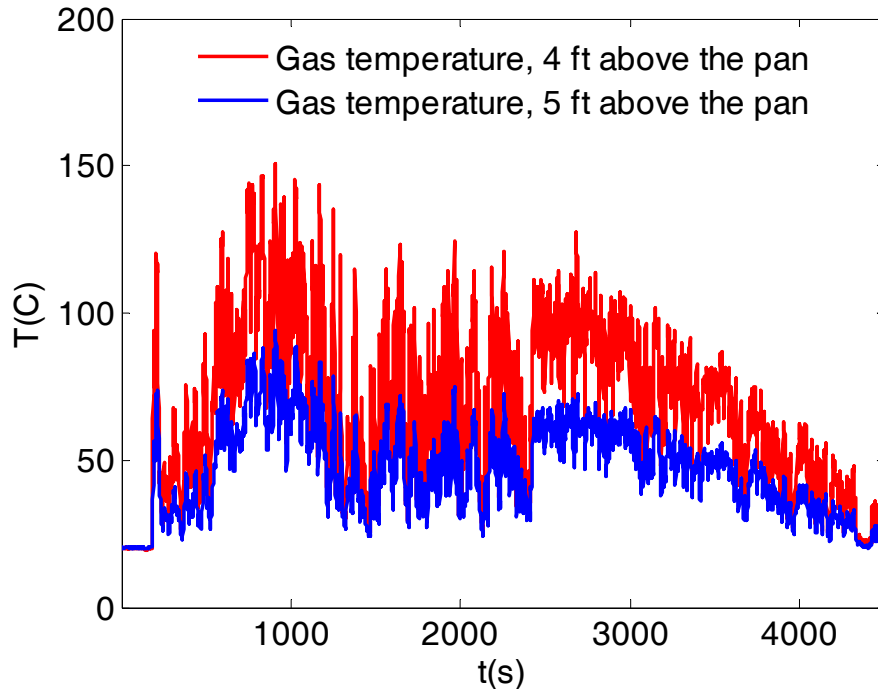
Figure 6-26: Gas temperature for low and high locations for PMMA test 011110-T1
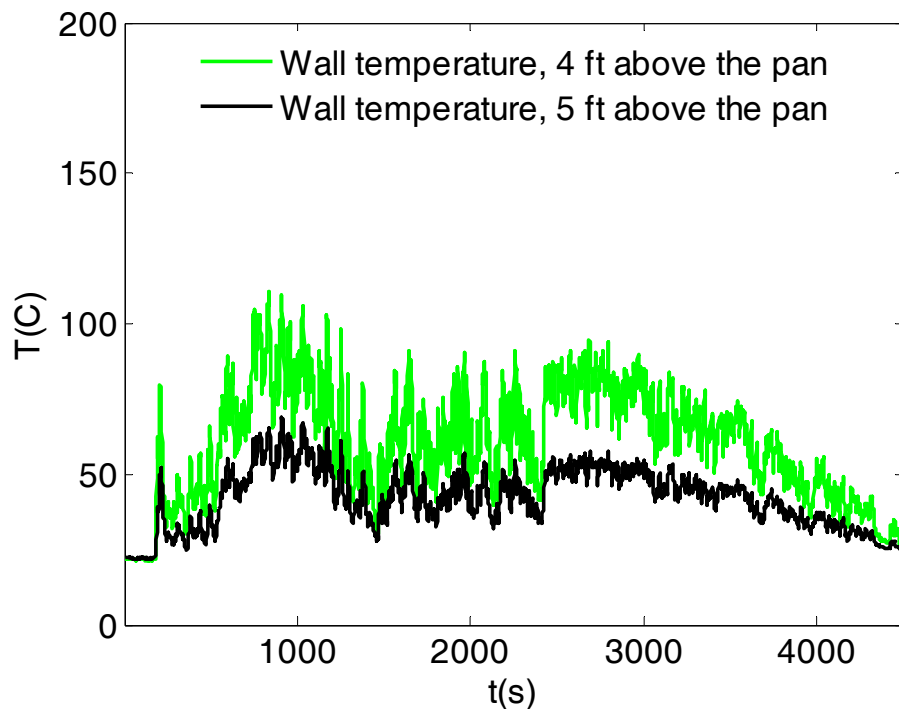
Figure 6-27: Wall temperature for low and high locations for PMMA test 011110-T1

Figure 6-26 and Figure 6-27 show the history of gas and wall temperature for both low and high locations for the PMMA test, 011110-T1. Gas and wall temperatures were used to calculate the thermophoretic velocity. Figure 6-28 shows the predicted thermophoretic deposition vs. measured (gravimetric) deposition for the wall tests (4" x 4" pan size). The slope on the plot (0.98) shows a very close agreement between the analytical smoke deposition model and the experimental data. The slope on the linear least square fit was forced to one and the change in the R- squared value is not significant.
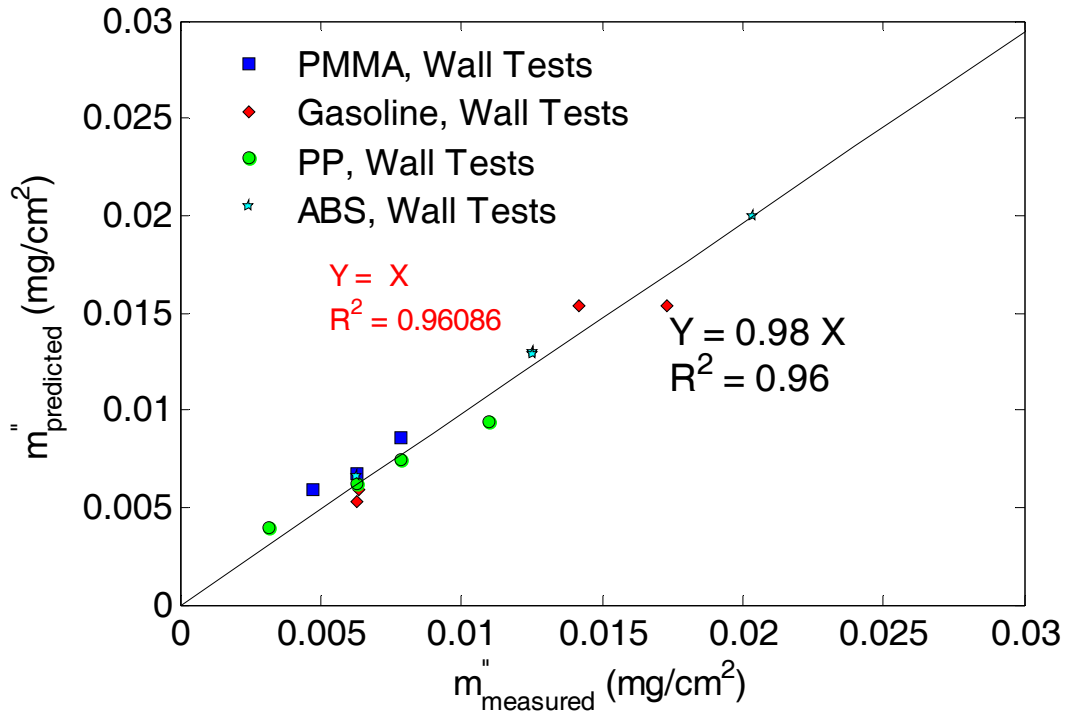
Figure 6-28: Predicted thermophoretic deposition vs. measured deposition for the wall tests (4" x 4" pan size)

The same procedure was performed on the 8" x 8" and 12" x 12" pan size fires. The analytical smoke deposition model based on thermophoretic velocity was validated for all three pan sizes.

8" x 8" Pan Size Tests

Table 6-26, Table 6-27, Table 6-28, and Table 6-29 show the experimental data for the PMMA, gasoline, PP, and ABS tests (8" x 8" pan size). Temperature gradient and smoke concentration were averaged over the test period for each test in order to give a representative for these factors and test conditions.

Table 6-26: Test duration, average temperature gradient, and average smoke concentration for PMMA tests (8" x 8" pan size)

Test number	Test duration (s)	dT/dx (deg/m)	Cs (g/m^3)
021510-T1-low	2900	8658.63	0.158
021510-T1-high	2900	5935.23	0.158
021510-T2-low	4400	10642.79	0.165
021510-T2-high	4400	7766.08	0.194

172

Table 6-27: Test duration, average temperature gradient, and average smoke concentration for gasoline tests
(8" x 8" pan size)

Test Number	Test Duration (s)	dT/dx (deg/m)	Cs (g/m³)
021710-T2-low	700	12710.11	0.517
021710-T2-high	700	11827.52	0.517
021710-T3-low	900	21098.61	0.449
021710-T3-high	900	8742.36	0.450

Table 6-28: Test duration, average temperature gradient, and average smoke concentration for PP tests
(8" x 8" pan size)

Test Number	Test Duration (s)	dT/dx (deg/m)	Cs (g/m³)
021510-T3-low	1700	8976.38	0.297
021510-T3-high	1700	9139.41	0.237
021710-T1-low	2400	10929.86	0.262
021710-T1-high	2400	5960.54	0.339

Table 6-29: Test duration, average temperature gradient, and average smoke concentration for ABS tests
(8" x 8" pan size)

Test Number	Test Duration (s)	dT/dx (deg/m)	Cs (g/m³)
031510-T1-low	1200	11708.81	3.643
031510-T1-high	1200	9075.99	3.644
031510-T2-low	900	13419.90	3.293
031510-T2-high	900	7622.25	3.294

Average temperature gradient for all the fuels changes between 5935 (deg/m) and 21098 (deg/m). Smoke concentration values for all the fuels changes between 0.158 (g/m³) and 0.517 (g/m³). Figure 6-29 and Figure 6-30 shows the history of gas and wall temperature for both low and high locations for the PP test, 021510-T3. Gas and wall temperatures were used to calculate the thermophoretic velocity.

173
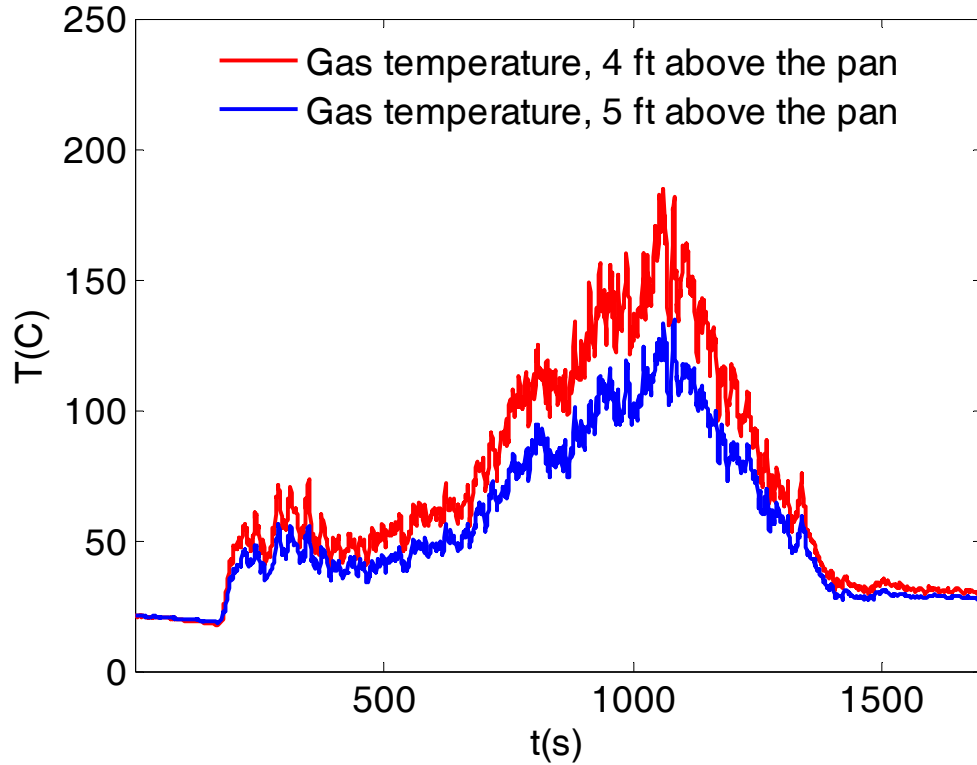
Figure 6-29: Gas temperature for low and high locations for PP test 021510-T3
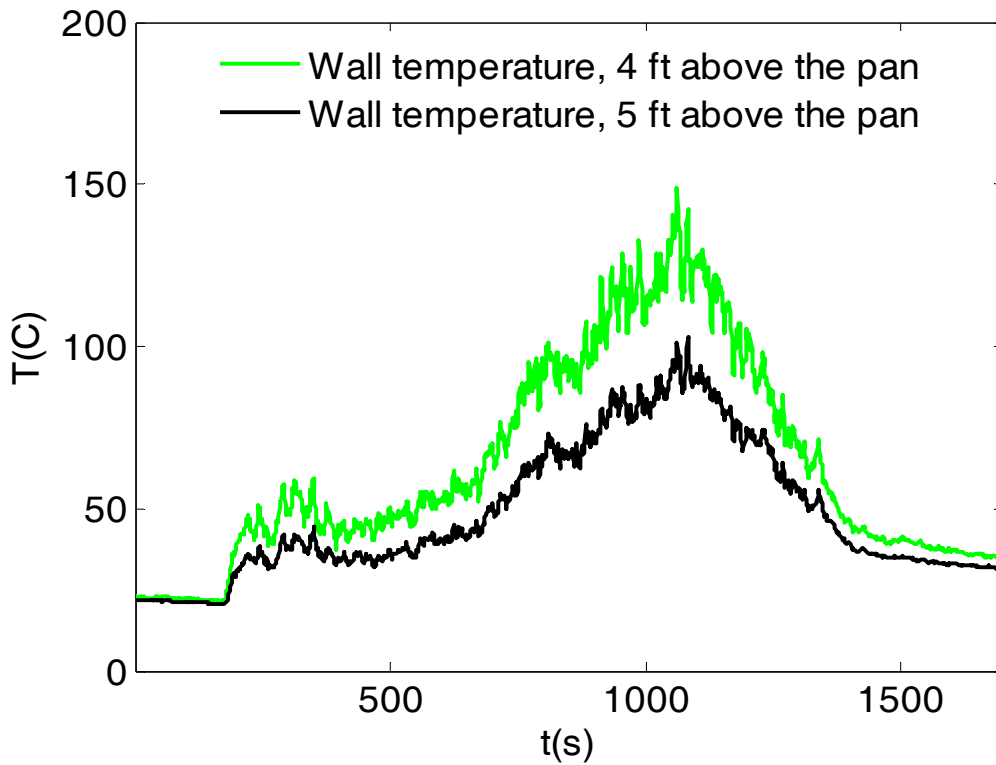
Figure 6-30: Wall temperature for low and high locations for PP test 021510-T3

174

Figure 6-31 shows the predicted thermophoretic deposition vs. measured (gravimetric) deposition for the wall tests (8" x 8" pan size). The slope on the plot (0.99) shows a very close agreement between the analytical smoke deposition model and the experimental data. The slope on the linear least square fit was forced to one and the change in the R- squared value is not significant.
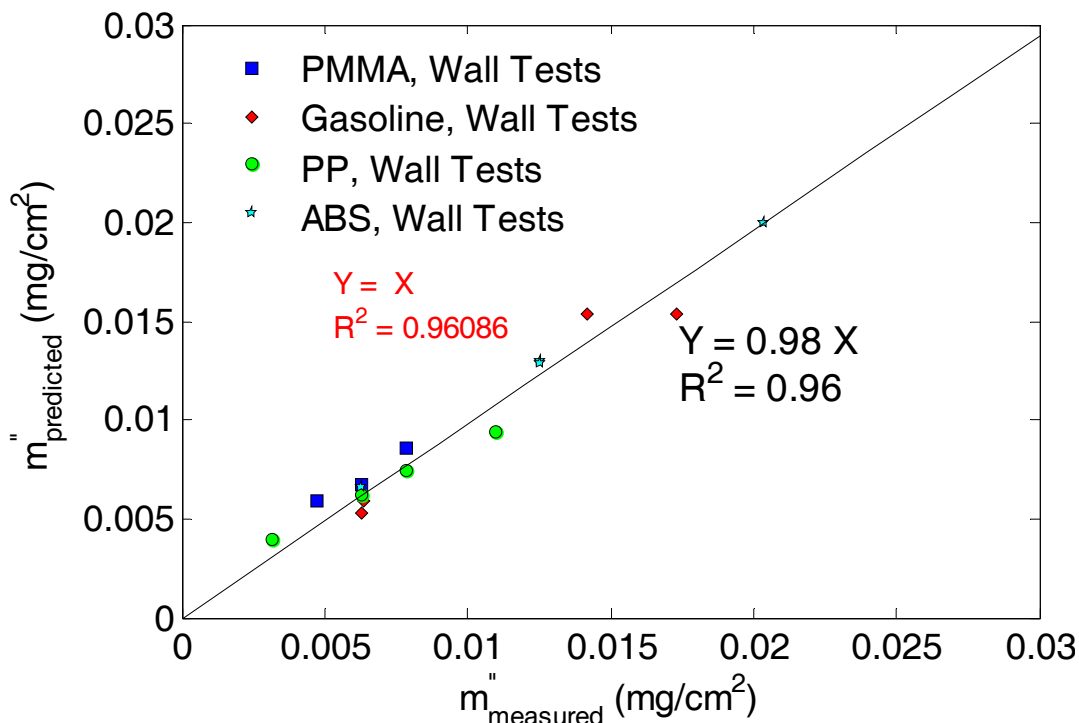
Figure 6-31: Predicted thermophoretic deposition vs. measured deposition for the wall tests (8" x 8" pan size)

12" x 12" Pan Size Tests

Table 6-30, Table 6-31, Table 6-32, and Table 6-33 show the experimental data for the PMMA, gasoline, PP, and ABS tests (12" x 12" pan size). Temperature gradient and smoke concentration were averaged over the test period for each test in order to give a representative for these factors and test conditions.

175

Table 6-30: Test duration, average temperature gradient, and average smoke concentration for PMMA tests (12" x 12" pan size)

Test Number	Test Duration (s)	dT/dx (deg/m)	Cs (g/m^3)
022210-T1-low	2700	9935.61	0.816
022210-T1-high	2700	7128.19	0.817
022510-T1-low	4400	6101.48	0.269
022510-T1-high	4400	5103.37	0.269

Table 6-31: Test duration, average temperature gradient, and average smoke concentration for gasoline tests (12" x 12" pan size)

Test Number	Test Duration (s)	dT/dx (deg/m)	Cs (g/m^3)
022510-T2-low	400	14124.04	0.790
022510-T2-high	400	11147.62	0.789
030110-T1-low	700	16214.12	0.820
030110-T1-high	700	10253.12	0.780

Table 6-32: Test duration, average temperature gradient, and average smoke concentration for PP tests (12" x 12" pan size)

Test Number	Test Duration (s)	dT/dx (deg/m)	Cs (g/m^3)
030110-T2-low	2500	1982.80	0.930
030110-T2-high	2500	693.35	0.820
030110-T3-low	2500	2114.91	0.880
030110-T3-high	2500	1120.10	0.780

Table 6-33: Test duration, average temperature gradient, and average smoke concentration for ABS tests (8" x 8" pan size)

Test Number	Test Duration (s)	dT/dx (deg/m)	Cs (g/m^3)
031510-T3-low	1000	5034.31	3.859
031510-T3-high	1000	4488.39	3.860
031610-T2-low	1200	2983.98	3.096
031610-T2-high	1200	840.61	3.097

Average temperature gradient for all the fuels changes between 840 (deg/m) and 16214 (deg/m). Smoke concentration values for all the fuels changes between 0.269 (g/m^3) and 3.86 (g/m^3). Figure 6-32 and Figure 6-33 show the history of gas and wall temperature for both

low and high locations for the ABS test, 031510-T3. Gas and wall temperatures were used to calculate the thermophoretic velocity.
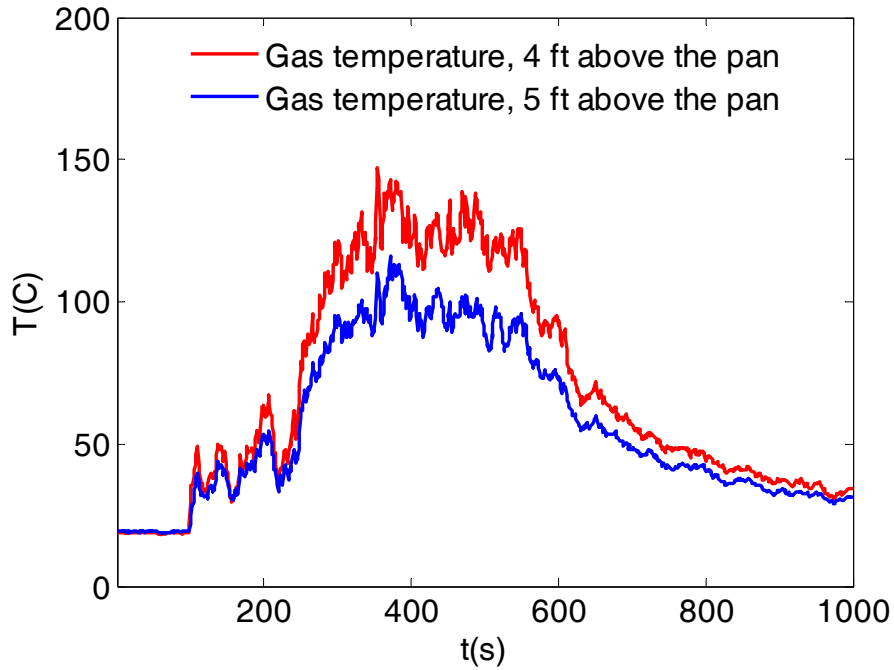
Figure 6-32: Gas temperature for low and high locations for ABS test 031510-T3
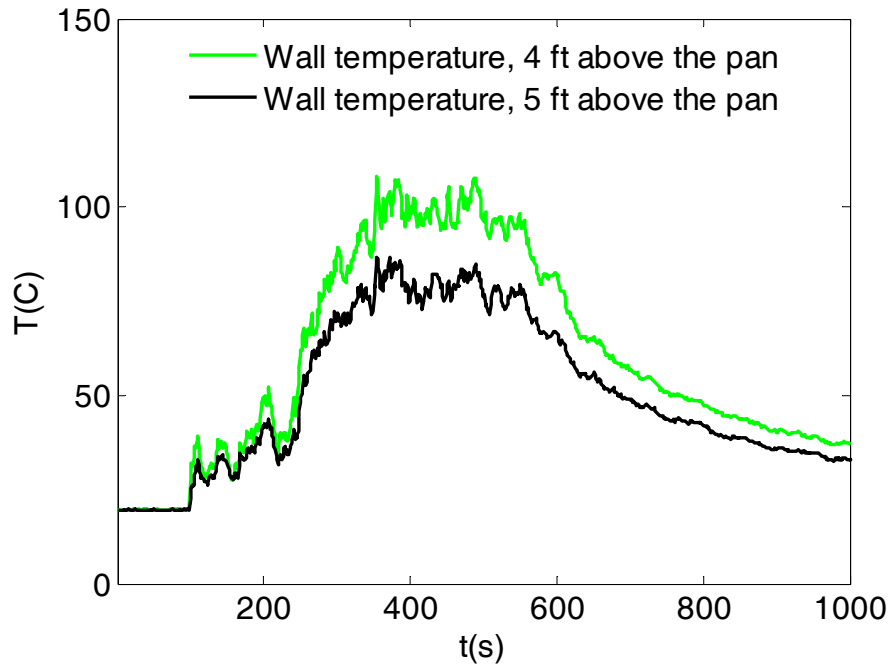
Figure 6-33: Wall temperature for low and high locations for ABS test 031510-T3

Figure 6-34 shows the predicted thermophoretic deposition vs. measured (gravimetric) deposition for the wall tests (12" x 12" pan size). The slope on the plot (1.07) shows a very close agreement between the analytical smoke deposition model and the experimental data. The slope on the linear least square fit was forced to one and the change in the R- squared value is not significant.
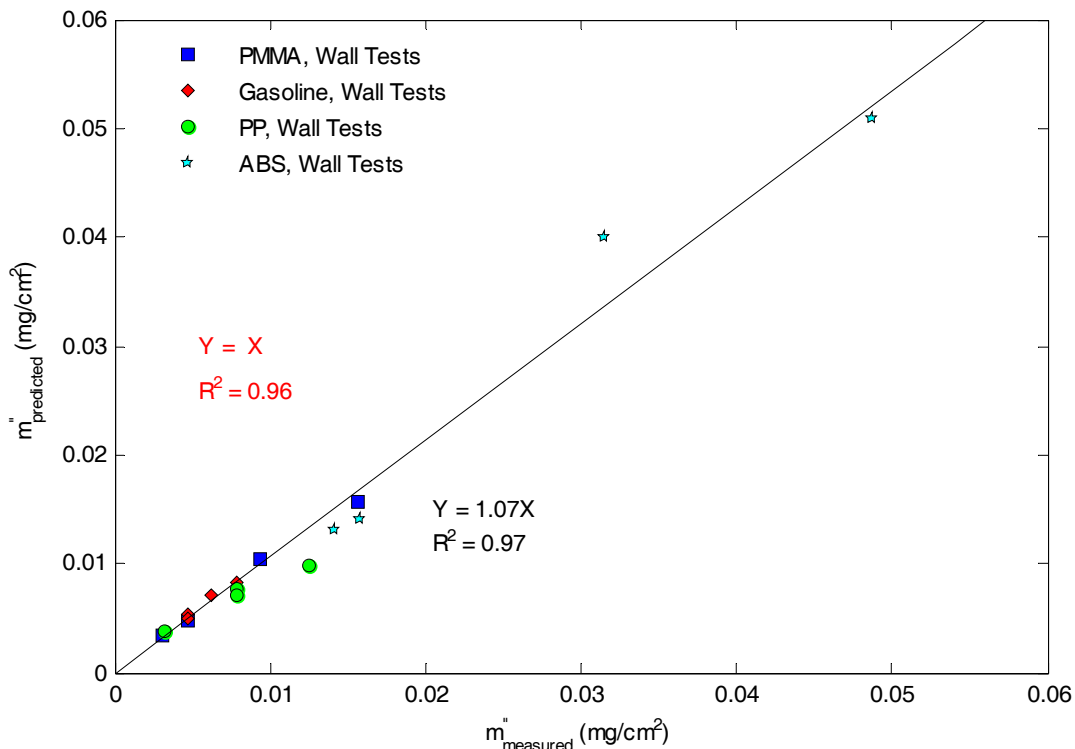
Figure 6-34: Predicted thermophoretic deposition vs. measured deposition for the wall tests (12" x 12" pan size)

4" x 4", 8" x 8", and 12" x 12"Pan Size Tests

Figure 6-35 shows the predicted thermophoretic deposition vs. measured (gravimetric) deposition for the wall tests (4" x 4" pan size, 8" x 8" pan size, and 12" x 12" pan size). The slope on the plot (1.003) shows a very close agreement between the analytical smoke deposition model and the experimental data. The slope on the linear least square fit was forced to one and the change in the R- squared value is not significant.
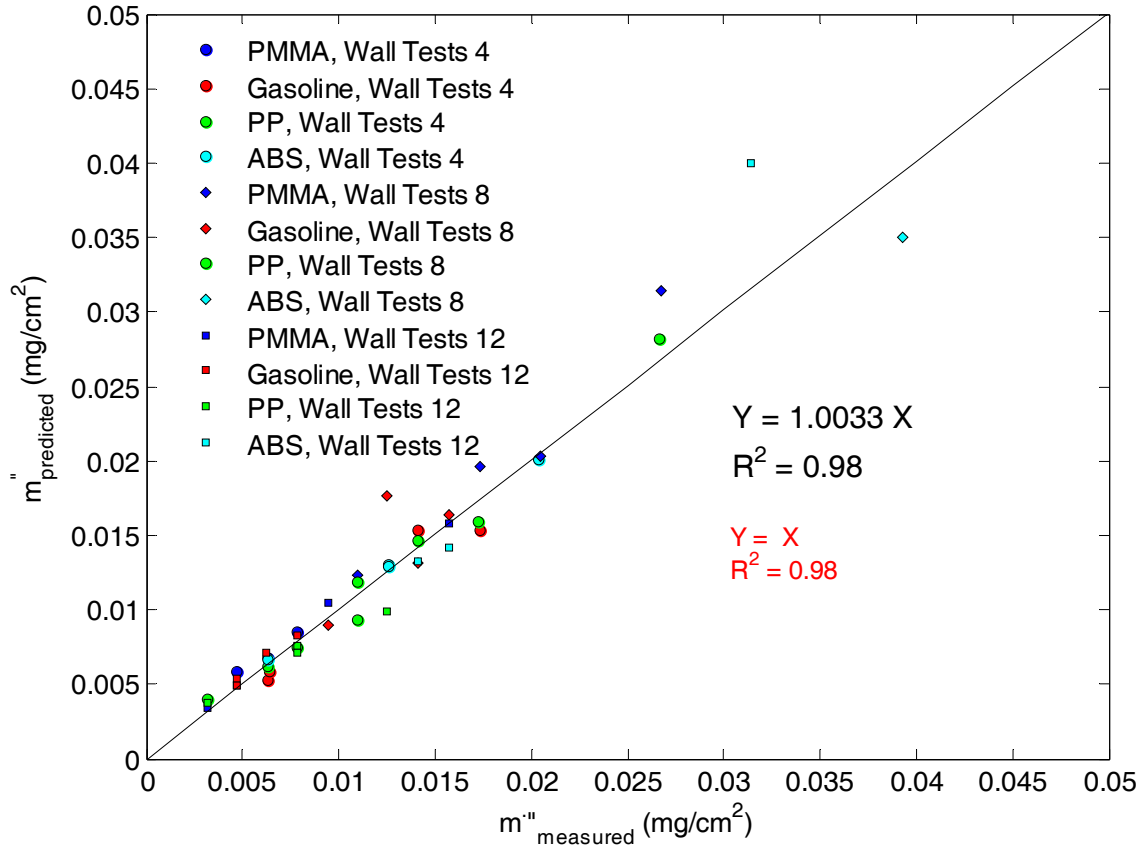
Figure 6-35: Predicted thermophoretic deposition vs. measured deposition for the wall tests (4" x 4" pan size, 8" x 8" pan size, and 12" x 12" pan size)

6.4 Study of Smoke Pattern on the Gypsum Walls

All the gypsum wall tests were performed separately in order to study the some deposition patterns for the 4"x4", 8"x8", and 12"x12" pan sizes. Test duration was changed for each test by stacking the fuel samples on top of each other. The smoke deposition pattern was studied by changing the fuel, pan size, and test duration. Table 6-34, Table 6-35, Table 6-35, Table 6-36, and Table 6-37 show the test matrix for the PMMA, gasoline, PP, and ABS tests. Gasoline tests for the 2.5 inch diameter were not performed since the smoke deposition pattern is not significant for those tests.

179

Table 6-34: PMMA test matrix for the smoke pattern tests

Material	Test number	Test duration (s)
PMMA	031210-T1	4400
4" x 4"	031210-T2	5400
Material	Test number	Test duration (s)
PMMA	012710-T1	3000
8" x 8"	021110-T1	4500
Material	Test number	Test duration (s)
PMMA	030510-T1	2700
12" x 12"	030510-T2	4400

Table 6-35: Gasoline test matrix for the smoke pattern tests

Material	Test number	Test duration (s)
Gasoline	021810-T1	713
8" x 8"	021810-T2	950
Material	Test number	Test duration (s)
Gasoline	030310-T1	440
12" x 12"	030310-T2	700

Table 6-36: PP test matrix for the smoke pattern tests

Material	Test number	Test duration (s)
PP	031210-T3	1600
4" x 4"	012610-T1	2400
Material	Test number	Test duration (s)
PP	012710-T2	1700
8" x 8"	012810-T1	2400
Material	Test number	Test duration (s)
PP	030310-T3	2100
12" x 12"	020210-T1	2500

Table 6-37: ABS test matrix for the smoke pattern tests

.Material	Test number	Test duration (s)
ABS	030810-T1	1500
4" x 4"	030810-T4	2000
Material	**Test number**	**Test duration (s)**
ABS	030810-T2	1200
8" x 8"	031010-T3	900
Material	**Test number**	**Test duration (s)**
ABS	031610-T2	1000
12" x 12"	031610-T3	700

In the following sections different effects on the test conditions will be compared between smoke deposition patterns. The effect of the pan size (fire size), effect of the fuel within the same fire size, and effect of test duration have been compared and presented.

Fire Size Effect

Figure 6-38, Figure 6-39, and Figure 6-40 show the smoke pattern on the gypsum wall for the PMMA tests. For a larger fire size the smoke yield will increase and this will increase the smoke concentration. Increase in all the mentioned parameters will increase the smoke deposition based on the thermophoresis on the wall. By looking at the smoke contours on the gypsum wall for different fire sizes it will be noticed that as the fire size increases the smoke pattern changes and the optical properties of the deposited smoke changes. Different parameters are involved in the smoke pattern. The gas and wall temperatures have effect on the temperature gradient which changes the thermophoretic velocity. The following are the smoke pattern for three fire sizes for PMMA. The fire size for the 4"x 4" pan size for PMMA is 3.0 kW and the pan equivalent diameter is 0.114 m. The calculated flame height [31] for this fire is 0.24 m which is shown on Figure 6-38 with a red color ($L = 0.23\dot{Q}_c^{2/5} - 1.02D$). The pan location is shown with green color on the smoke pattern contours. Same calculation was performed on the 8"x 8" pan size for PMMA, the fire size is 12 kW, the equivalent pan diameter is 0.229 m and the flame height is

0.38 m. for the 12"x 12" pan size the fire size is 30.0 kW, the equivalent pan diameter is 0.344 m and the flame height is 0.54 m. As explained earlier the optical density values change between 0-1.95 and for the larger tests some of the locations on the wall have optical density values higher than 1.95 which has been extrapolated with the calibration function. It needs to be mentioned that the optical density method is valid for the values that are below 1.95.

For all the fire sizes for the PMMA tests, the optical density values on the center line were plotted vs. the non dimensional value (z/L). Where z is the height for the location and l is the flame height.
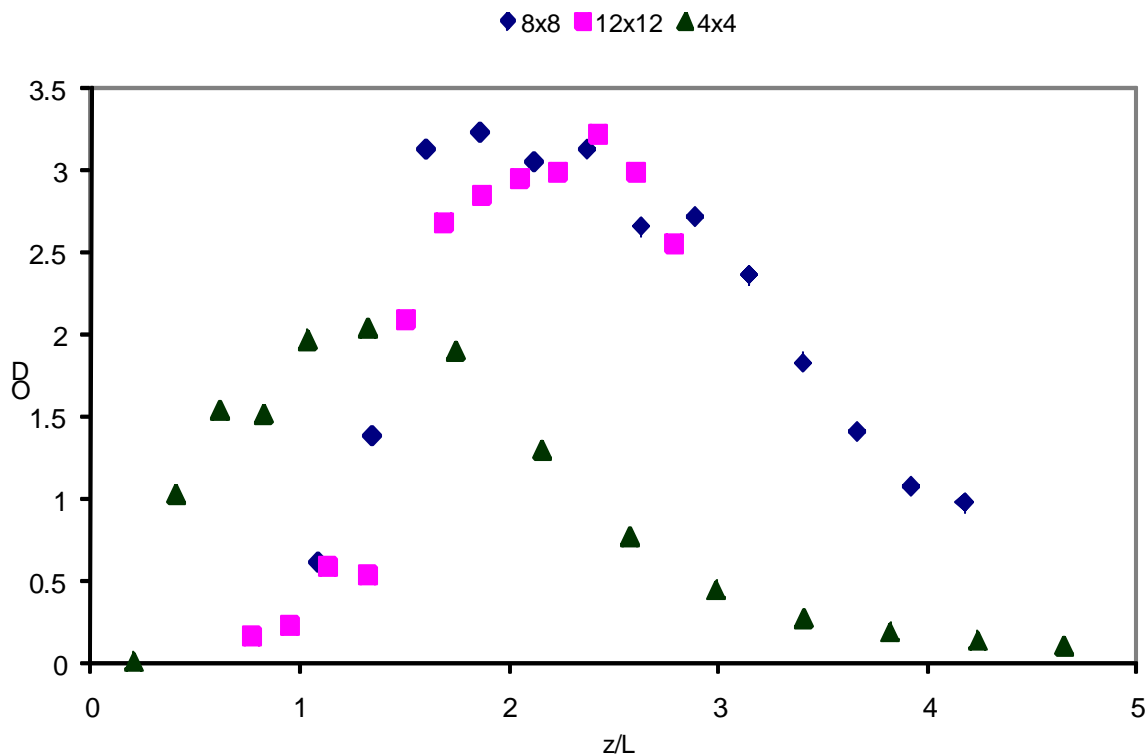
Figure 6-36: Optical density variation for different fire sizes at different locations on the flame center line

Figure 6-36 shows the optical density variation on the center line for three fire sizes for the PMMA test against the gypsum wall. Results show that for larger fires the smoke patterns are similar and more important by determining the optical density value for a surface, the fire size can be calculated. The smaller fire size which is for 4"x 4" pan size is different. The flame height

182

is lower for this test and also the optical density values are lower for a laminar wall tests. Figure

6-37 shows the smoke pattern variation for three different fire sizes for the PMMA test along the

wall width. The smaller fires have lower surface optical properties as explained before. Also in

Figure 6-37 the optical properties for 8"x 8" and 12"x 12" pan size fires are higher on the left

side of the y axis which is evident in the contour plots that the flame was leaning to the left.

Also, the clean burn zone for larger fire is bigger than then clean zone burn area for the smaller

fire. The clean burn zone is correlated with flame height.
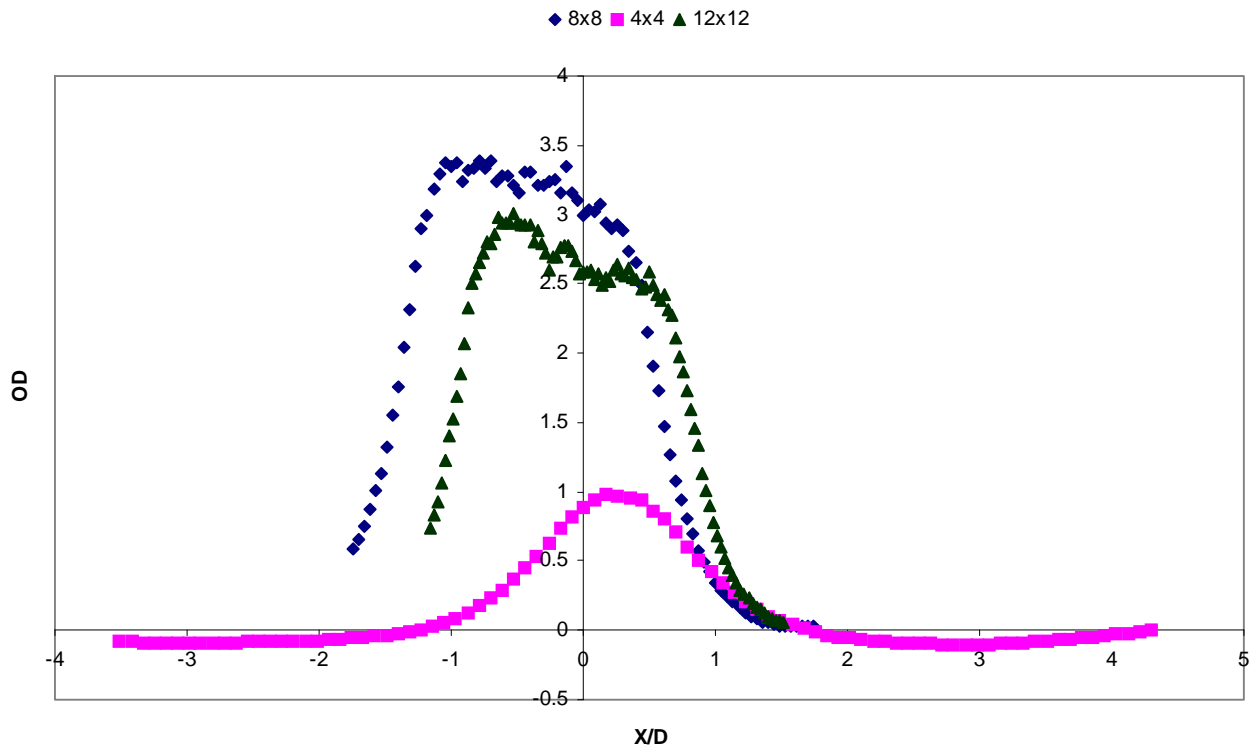
Figure 6-37: Optical density variation for different fire sizes along the wall width

183
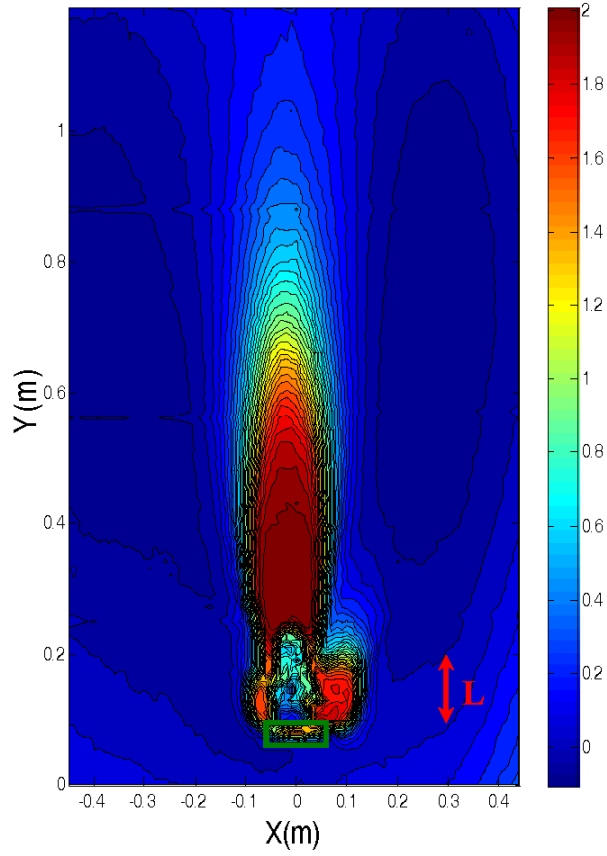
Figure 6-38: Smoke pattern for PMMA test,
031210-T1 (4" x 4" pan)
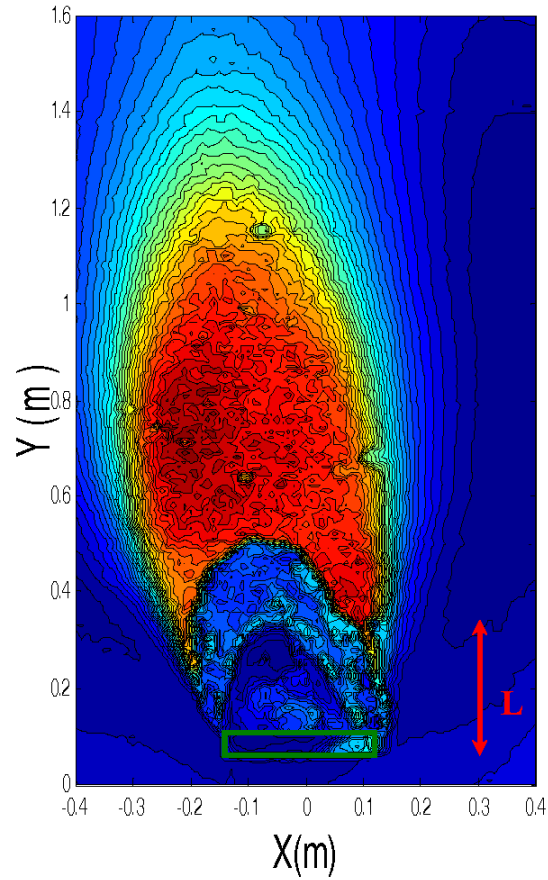
Figure 6-39: Smoke pattern for PMMA test,
021110-T1 (8" x 8" pan)
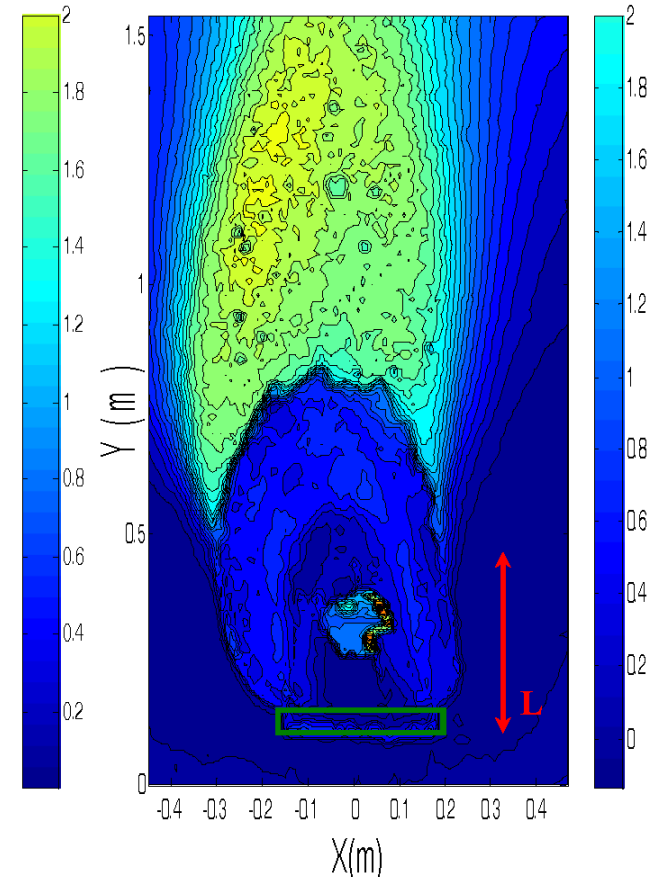
Figure 6-40: Smoke pattern for PMMA test,
030510-T2 (12" x 12" pan)

Fuel Effect

Figure 6-41, Figure 6-42, Figure 6-43, and Figure 6-44 show the smoke pattern for 8" x 8" pan and the only difference between those four tests is the fuel. The smoke deposition on the surface based on thermophoresis smoke deposition mechanism is dependent on the smoke concentration. As discussed in Chapter 4 fuel characteristics were measured and compared for different fuels and different pan sizes. ABS due to the high smoke yield deposits more on the surface for the same test duration. PMMA due to lower smoke yield has a lower amount of smoke deposition on the gypsum wall. It can be noticed that the clean zone area is also different for these tests. Gasoline has a higher heat of combustion compare to the other fuels and due to higher mass loss rate, the heat release rate for gasoline test is higher than the other fuels and it generates larger fire which results in larger clean burn area for gasoline test as shown in Figure 6-42. As shown in Figure 6-44, the smoke pattern size is slightly larger than rest of the fuels. This is due to the fact that ABS has a larger smoke yield and the smoke deposition due to ABS for the same test conditions will be more than rest of the fuels. Based on the fire size effect and fuel effect, it can be said that higher smoke deposition rates are due to a material which generates more smoke or a larger fire which results in increase of the smoke yield and temperature gradient. Also the test duration increase the smoke deposition which will be discussed in the next section. All the smoke pattern contours and digital photographs from the wall tests are presented in the Appendix A.
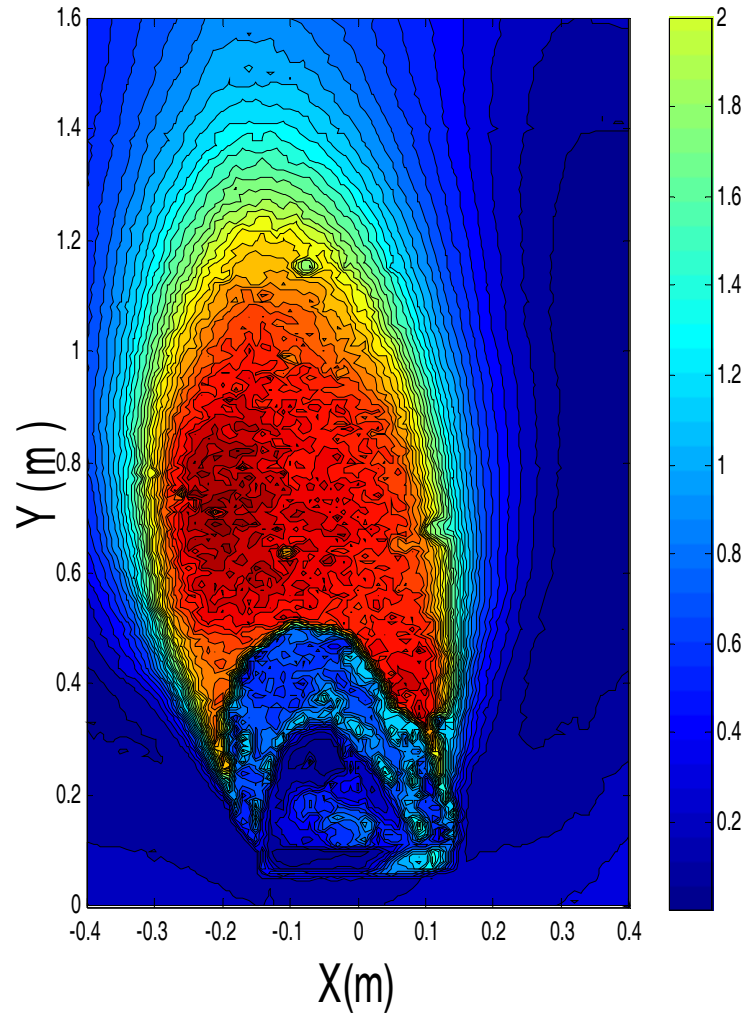
Figure 6-41: Smoke pattern for PMMA test, 021110-T1, (8" x 8" pan)
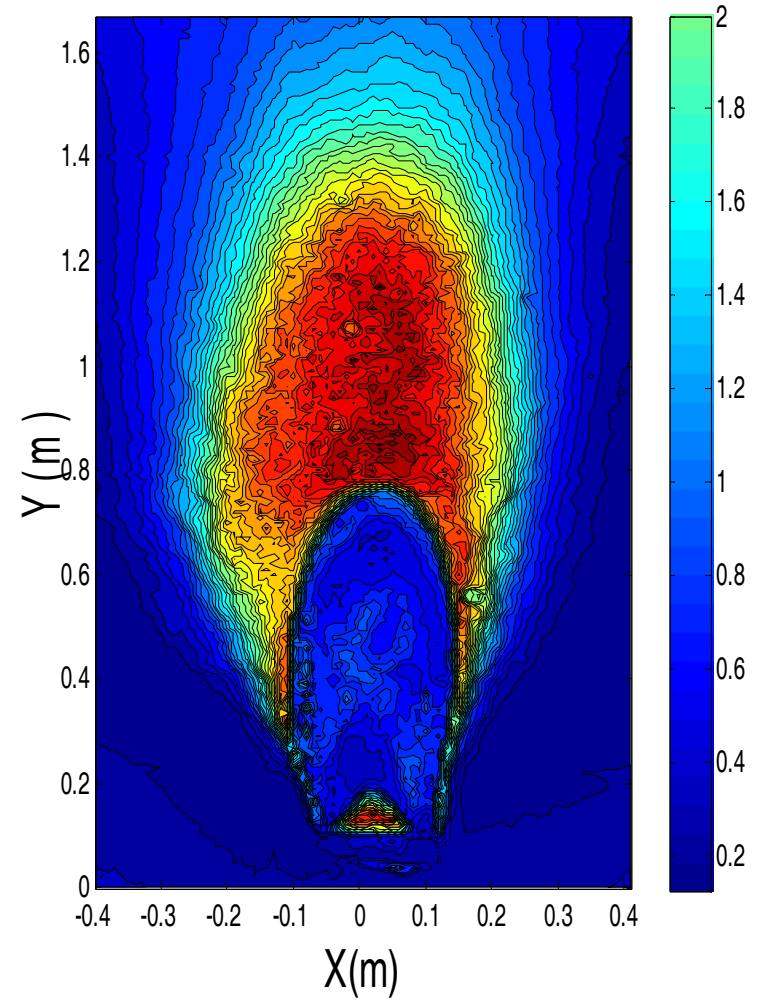
Figure 6-42: Smoke pattern for gasoline test, 021810-T2, (8" x 8" pan)

186
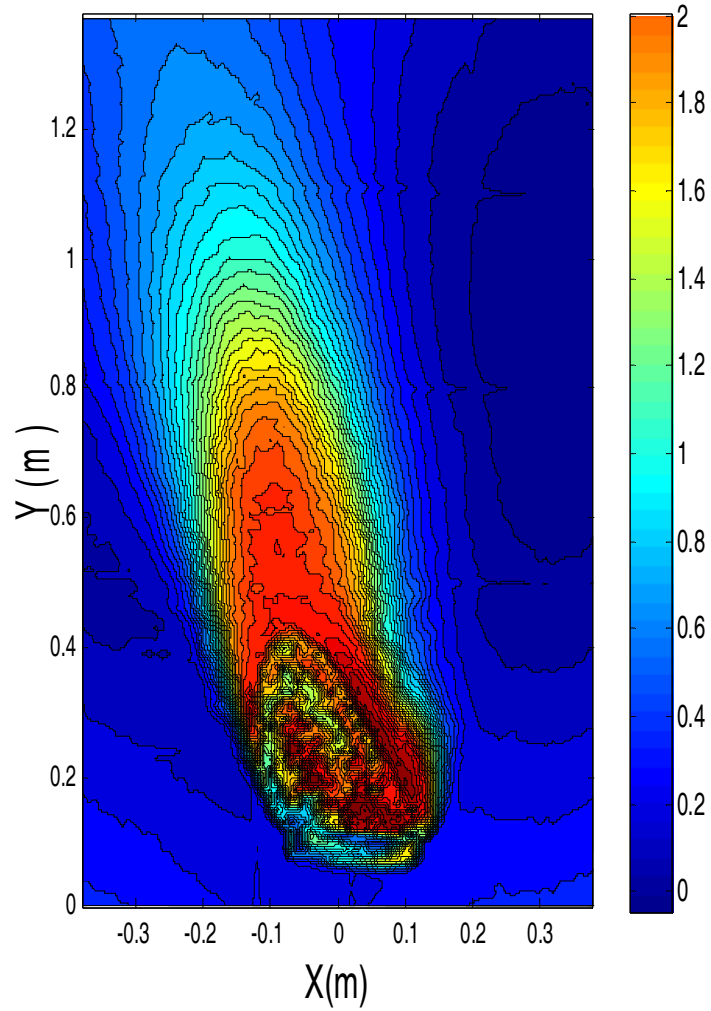
Figure 6-43: Smoke pattern for PP test, 012710-T2, (8" x 8" pan)
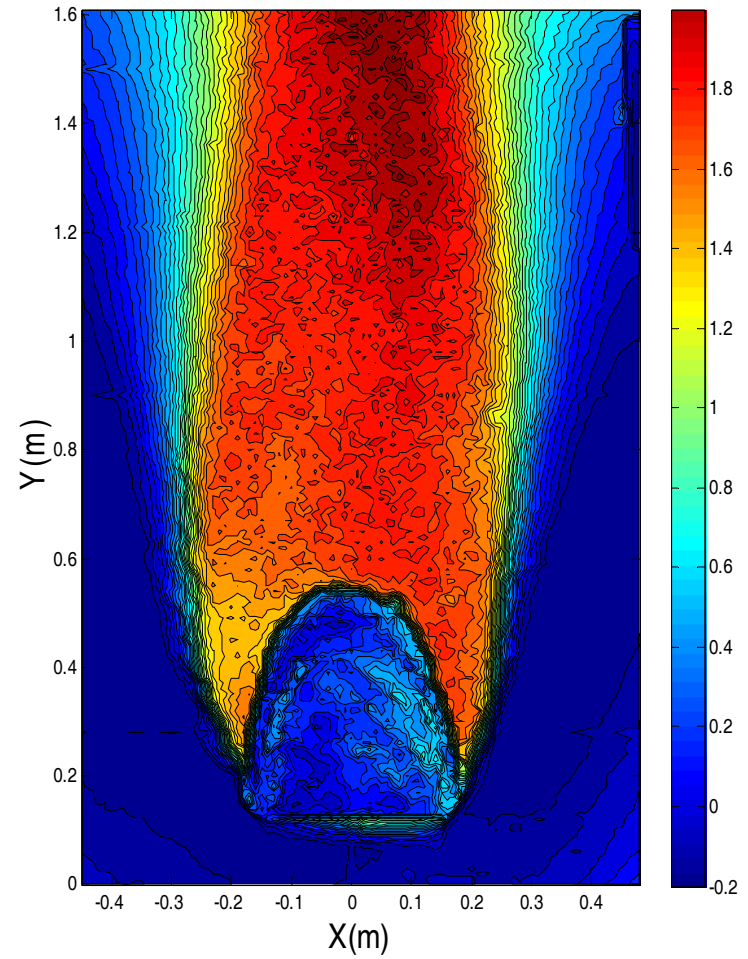
Figure 6-44: Smoke pattern for ABS test, 030810-T2, (8" x 8" pan)

187

Test Duration

Figure 6-45 and Figure 6-46 show the effect of the test duration for the gasoline test, 030310-T1, 030310-T2 (12"x 12" pan). The time scale for the conduction heat transfer is a very important factor in smoke deposition. Time scale is defined as, $t = \dfrac{L^2}{\alpha}$, where L is the thickness for the gypsum wall and α is the thermal diffusivity for the gypsum wall. The calculated time scale for the gypsum wall is 400 seconds and based on the difference between the test duration and time scale the smoke deposition will change for different tests. The smoke deposition increases as the test duration increases due to increase in the time which the surface has been exposed to the smoke.
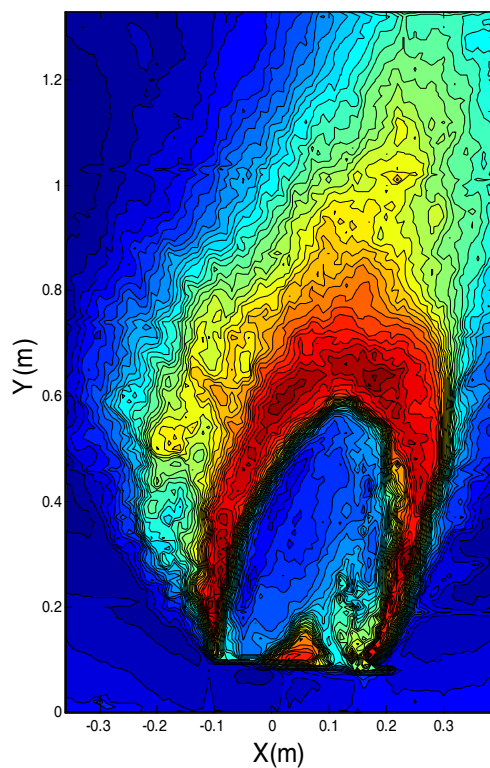
Figure 6-45: Smoke pattern for gasoline test (12" x 12" pan), 440 seconds
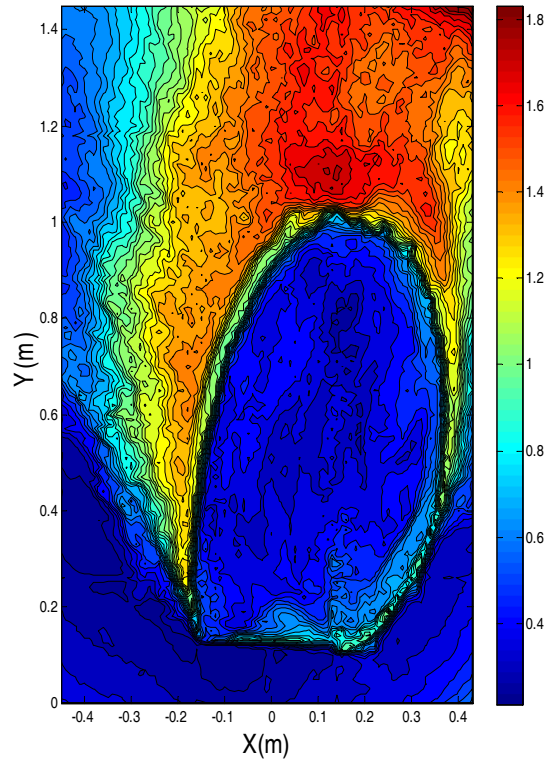
Figure 6-46: Smoke pattern for gasoline test (12" x 12" pan), 700 seconds

6.5   Discussion of Wall Test Results

The developed optical method which was described 3.2.2.5 was used for the wall tests. In the wall tests, the glass filters were used as a point measurement and also a digital photography method was developed. The digital images can be used to determine the optical properties of the surface which was exposed to the smoke. Also digital images can be processed and the agglomerate size distribution will be determined from the images. By using the developed optical method both optical properties of the surface and the particle analysis can be determined.

In the wall tests, both fuel and the pan size have been changed and both effects have been studied on the smoke deposition from a fire to the wall. As discussed in Chapter 4 the fuel characteristics change for different pan sizes. As the pan size changes from 4" x 4" to 8" x 8" and 12" x 12" the fuel characteristics such as smoke yield and CO yield change. Smoke yield for the larger fires are higher than the smaller fires. There is significant increase in the smoke yield between the 4" x 4" and 8" x 8" pan sizes and as pan size increases to 12" x 12" the smoke yield does not change significantly. The smoke yield increase will change the smoke deposition as discussed in the smoke pattern against the wall.

Solid phase mass specific extinction coefficient was determined for all four fuels and all three different pan sizes for the wall tests. Solid phase mass specific extinction coefficient is also dependent on the pan size. As the plume regime changes from laminar to turbulent, the agglomerate size distribution changes and the solid phase mass specific extinction coefficient decreases. The solid phase mass specific extinction coefficient values for the laminar wall tests and hood experiments are very similar as shown in Table 6-38. Both sets of tests are considered small scale tests and the wall tests are laminar tests. In the hood tests, the deposition to the surface occurs in the presence of the hot smoke layer but for the wall tests, there is no smoke

189

layer. The only solid phase mass specific extinction values which is different than the others, is ABS. ABS generates larger agglomerates due to its higher smoke yield and these particles increase the mass gravimetrically but they are not effective optically.

Table 6-38: Solid phase mass specific extinction coefficients for different fuels for the hood experiments and wall tests (4" x 4" pan)

Fuel	$\sigma_{s,s}$ (m^2/g) – hood tests	$\sigma_{s,s}$ (m^2/g) – wall tests (4" x 4" pan)
PMMA	5.9	6.0
PP	6.4	5.0
Gasoline	5.7	5.4
ABS	3.4	3.3

The solid phase mass specific values for the 8" x 8" and 12" x 12" pan sizes are very close for PMMA, PP, and gasoline tests as shown in Table 6-39. These values are 73% of the suggested values for the 4" x 4" tests. This difference is due to the physics of the tests. These tests were turbulent unlike the previous set of wall tests that were laminar. It is believed that turbulence increase the agglomerate size effect and increase the mass gravimetrically and decreases the solid phase mass specific extinction coefficient. The solid phase mass specific extinction coefficient value for ABS is 43% of the value for PMMA, gasoline, and PP. These values are different due to the difference in the agglomerate size from PMMA, gasoline, PP tests vs. ABS test. Due to the aromatic nature of the ABS, and turbulence the solid phase mass specific extinction coefficient drops for ABS tests.

Table 6-39: Solid phase mass specific extinction coefficients for different pan sizes

Fuel	$\sigma_{s,s}$ (m^2/g) wall tests (8" x 8" pan)	$\sigma_{s,s}$ (m^2/g) wall tests (12" x 12" pan)
PMMA, PP, gasoline	3.9	4.1
ABS	1.7	1.9

190

The smoke pattern was determined by using the digital image and optical measurement methods. The smoke pattern analysis showed that the smoke deposition is dependent on different factors such as; fire size, fuel type, and test duration. Moreover different test scenarios were conducted and the optical method was used for all the experiments and there was good agreement between the optical measurement method and the smoke pattern images.

The smoke deposition analytical method based on thermophoresis was also validated for the wall tests. For all three pan sizes and four fuels the model was validated with the experimental test data. Different parameters were changed in each test. By changing the fuel, the smoke concentration was either increased or decreased and the model predicted the test results accurately. In addition to the change in the fuel, the increase in the pan size will increase the smoke yield and the model was also validated for these tests. Another parameter was test duration which changes the exposure time for the smoke. It shows that the analytical model in such robust model which predicts the smoke deposition accurately and can be used a very power full tool for predicting the smoke deposition against the surface as well as in the presence of the hot layer.

CHAPTER 7 CONCLUSIONS

Two separate set of tests were conducted for this research. First set of tests were the hood tests and the smoke deposition was studied in the presence of the smoke hot layer. An optical measurement method was developed for these tests and used to determine optical properties of the smoke deposited on the glass filters. Also this optical measurement method was correlated with the gravimetric measurements and a newly defined parameter (solid phase mass specific extinction coefficient) was introduced to be used in addition to smoke yield and agglomerate size distribution to determine the smoke deposition characteristics.

All the results show that PMMA, PP, and gasoline follow the same pattern for the solid phase mass specific extinction coefficient and have similar values. On the other hand, ABS has a lower solid phase mass specific extinction coefficient value due to higher smoke yield value and the aromatic nature of the fuel. ABS generates larger agglomerates and when the smoke deposition occurs, the larger agglomerates increase the weight on the filter; however they are not optically as effective as other agglomerates.

By using the optical method, the optical properties of the surface were determined; also the agglomerate size distribution was measured. Moreover, the solid phase mass specific extinction coefficient can be determined by knowing the smoke yield level for the fuel. Gravimetric measurements are very straightforward methods for the laboratory measurements but they cannot be used as a field method. The optical measurement method can be used as a field method.

The smoke deposition analytical model based on thermophoresis was developed and validated with the experimental data from the hood experiments. Different test scenarios were generated and the model predicts the smoke deposition accurately.

192

Fuel characteristics were measured for the larger size fire wall tests. As explained, the fuel characteristics such as; smoke yield, CO yield, and CO_2 yield change with the fire size and these properties change the smoke deposition on the surfaces.

For the wall tests, the optical measurement method was improved and digital photography was implemented in the method. The digital image of the surface which was exposed to the smoke was taken in the presence of the gray scale. Also, the agglomerate size analysis was performed on the digital images. The processed data showed that the optical properties of the surface and agglomerate size analysis are not dependent on the camera type. The only important factor in taking the digital pictures is to avoid the over exposure of the surface to the light. The distance from the surface needs to be close to 3 ft and higher resolution image is better for the agglomerate size analysis.

Solid phase mass specific extinction coefficient values were determined for the wall tests. For the 4"x 4" size pan the values are similar to the hood experiment values. For the 8"x 8" and 12"x 12" the values are lower for PMMA, PP, and gasoline. This is due the fact that these tests are turbulent and turbulence changes the agglomerate size distribution on the surface. The solid phase mass specific extinction coefficient values are significantly lower for ABS. ABS is aromatic and generates larger agglomerates and these larger particles decrease the solid phase mass specific extinction coefficient values. Figure 7-1 shows the smoke yield and solid phase mass specific extinction coefficient variation for the wall tests. The solid phase mass specific extinction coefficient values are lower for the turbulent fires and as the smoke yield increases for a fuel the solid phase mass specific extinction value decreases.
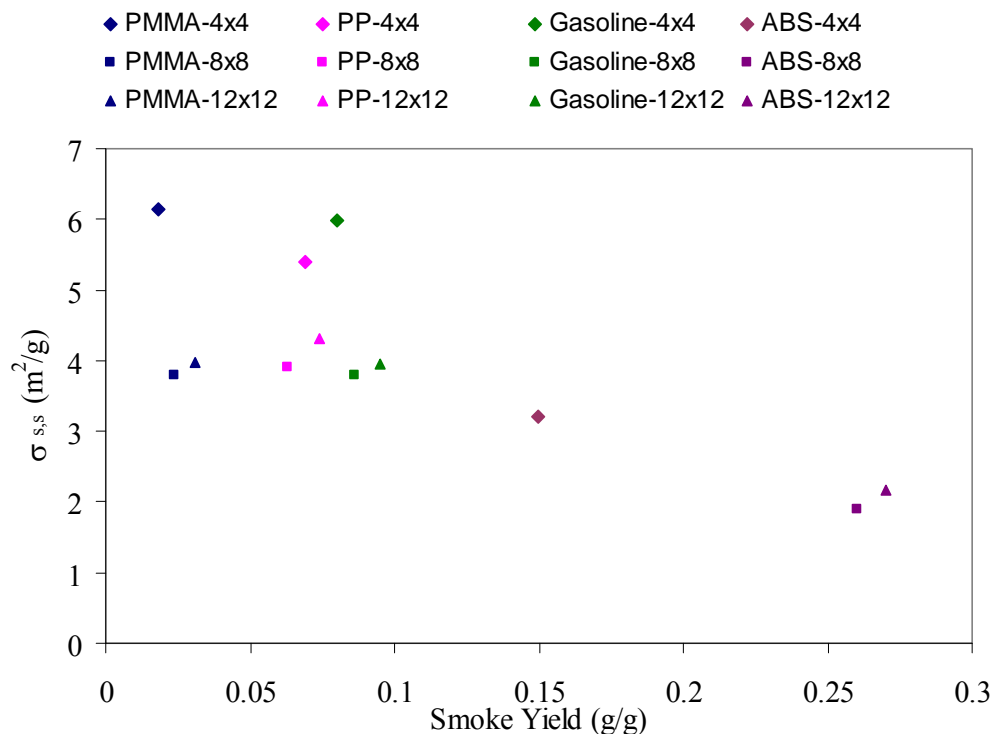
Figure 7-1: Smoke yield and solid phase mass specific extinction coefficient variation for the wall tests

By using the optical measurement method the smoke pattern was determined for the wall tests. Smoke pattern results, showed a difference between different test conditions for the wall tests and very good agreement for the method for all test conditions. By using the smoke pattern analysis, the smoke deposition optical properties can be determined. Also, based on the clean zone area, the flame height and the fire size can be calculated. Moreover, by agglomerate size analysis and optical density measurements the solid phase mass specific extinction coefficient can be determined and the actual amount of smoke deposited on the surface can be calculated. Table 7-1 shows the solid phase mass specific extinction coefficient values for turbulent wall tests. This table basically suggests two set of values for the solid phase mass specific extinction coefficient values. For the fuels that generate less smoke and the smoke yield values are lower the suggested values is 4.0 (m^2/g) and for the fuels that generate more smoke and have higher values of smoke yield the suggested value is 2.0 (m^2/g).

194

Table 7-1: Solid phase mass specific extinction coefficient for the turbulent wall tests

Fuel	$\sigma_{s,s}$ (m^2/g) wall tests (8" x 8" pan)	$\sigma_{s,s}$ (m^2/g) wall tests (12" x 12" pan)
PMMA, PP, gasoline	3.9	4.1
ABS	1.7	1.9

The analytical smoke deposition model based on thermophoresis is validated for the wall tests. The model predicts the smoke deposition for all test conditions and this is and evidence for the high level of robustness of the model. The model can be used as an accurate tool to predict the smoke deposition based on thermophoresis on the surfaces.

7.1   Contributions

A new measurement method based on optical density is developed for smoke deposition in the fire research. Gravimetric measurement is a straightforward method for the laboratory tests; however, it is not a feasible method for the field measurements.

For the first time in the fire research a new parameter is introduced, solid phase mass specific extinction coefficient ($\sigma_{s,s}$). This new parameter defines a relationship between the optical properties of the surface that is exposed to the smoke and the gravimetric measurements on the surface.

The optical method is developed for the digital imaging and calibrated. The digital optical method is used for the wall tests to analyze the smoke patterns, agglomerate size analysis, fire size, and fuel source.

The analytical smoke deposition model is developed based on thermophoresis. The model is validated with the experimental data for both hood and wall tests. Results show agreement between the experimental data and the smoke deposition model.

7.2 Future Work

The optical properties of the smoke deposited on the glass filters have been studied in this work and it needs to be completed for the variety of the fuels and fire sizes. Similar tests as hood tests need to be performed for the room fires and the solid phase mass specific extinction coefficient needs to be determined for other fuels. Moreover, combination of different fuels should be studied and different effects due to each fuel on the smoke deposition.

The most important mechanism for the smoke deposition is thermophoresis and was studied in this work. Studying other smoke deposition mechanisms and their contribution to the room fire will be interesting topic for the future work.

The digital optical method developed for smoke pattern can be applied for all the room fire tests and based on the results from the analysis, different fire properties can be determined for each test.

CHAPTER 8 REFERENCES

[1]   G.W. Mulholland, "Smoke Production and Properties," in *SFPE Handbook of Fire Protection Engineering*, Quincy, MA, 2002, pp. 2-258–2-268.

[2]   C.L. Tien, Lee, K.Y., Stretton, A.J., "Radiation Heat Transfer," in *SFPE Handbook of Fire Protection Engineering*, Quincy, MA, 2002.

[3]   D. Weinert, et al., "Light Scattering Characteristics and Size Distribution of Smoke and Nuisance Aerosols," in *Fire Safety Science – Proceedings of the Seventh International Symposium*, International Association for Fire Safety Science, 2002, pp. 209-220.

[4]   K.M. Butler and G.W. Mulholland, "Generation and transport of smoke components," *Fire Technology*, vol. 40, 2004, pp. 149-176.

[5]   A. Tewarson, "Generation of heat and chemical compounds in fires," in *SFPE Handbook of Fire protection Engineering*, 2002, pp. 3-82, 3-161.

[6]   T. Tanaka, "Effects of Smoke on Functional Circuits," Sandia National Laboratory1997.

[7]   B. T. Reagor, "Smoke corrosivity. Generation, impact, detection, and protection," *Journal of Fire Sciences*, vol. 10, pp. 169-169, 1992.

[8]   W.D. Ciro, et al., "Experimental and numerical investigation of transient soot buildup on a cylindrical container immersed in a jet fuel pool fire," *Combustion Science and Technology*, vol. 178, 2006, pp. 2199-2218.

[9]   M.R. Sippola and W. W. Nazaroff, "Particle deposition in ventilation ducts: Connectors, bends and developing turbulent flow," *Aerosol Science and Technology*, vol. 39, 2005, pp. 139-150.

[10]   A. Guha, "A unified Eulerian theory of turbulent deposition to smooth and rough surfaces," *Journal of Aerosol Science*, vol. 28, 1997, pp. 1517-1537.

[11]   D. Gottuk, C. Mealy, and J. Floyd, "Smoke Transport and FDS Validation," in *Proceedings of the Ninth International Symposium*, Fire Safety Science, Germany, 2008, pp. 12.

[12]   M.A. Hamins, R. Johnson, M. Donnelly, J. Yang, G. Mulholland, R. Anleitner, "Report of Experimental Results for the International model Benchmarking and Validation Exercise #3," November 2003.

[13]   N.C. Dunston and S.M. Spivak, "Preliminary investigation of the effects of ozone on post-fire volatile organic compounds," *Journal of Educational Computing Research*, vol. 6, 1996, pp. 231-242.

[14]   Y. Tsuchiya, "Air quality problems inside a house following a fire," *Journal of Fire Sciences*, vol. 10, 1992, pp. 58-58.

[15]   M.M. Hirschler, "Soot from Fires: II. Mechanisms of Soot Formation," *Journal of Fire Sciences*, vol. 3, 1985, pp. 380-414.

[16]   M. Pinorini, et al., "Soot as an indicator in Fire Investigations: Physical and Chemical Analyses," *Journal of Forensic Science*, vol. 39, 1994, pp. 933-973.

[17]   B. De Vos, et al., "Organic Vapors Emitted from the plumes of Pool Fires on Carpet Material," *Journal of Fire Sciences*, vol. 17, 1999, pp. 383-420.

[18]   L. Talbot, et al., "Thermophoresis of Particles in a Heated Bondary Layer," *Journal of Fluid Mechanics*, vol. 101, 1980, pp. 737-758.

[19]   L. Waldmann and K. Schmitt, *Aerosol Science*, New York: Academic Press, 1966.

[20]   Derjaguin, et al., "Theory of thermophoresis of large aerosol particles," *Journal Colloid Science*, vol. 20, 1965, pp. 555-570.

[21]   B.V. Derjaguin, et al., "Experimental verification of theory of thermophoresis of aerosol particles," *Journal of Colloid and Interface Science*, vol. 21, 1966, pp. 35-58.

[22]   B.V. Derjaguin, et al., "Diffusiophoresis of large aerosol particles," *Journal of Colloid and Interface Science*, vol. 22, 1966, pp. 117-125.

[23]   S. Friedlander, *Smoke, Dust, and Haze: Fundamentals of Aerosol Dynamics*, 2nd ed. New York: Oxford University Press, 2000.

[24]   Y. Nomura, "Turbulent particle deposition in a rectangular chamber: The study of effect of particle size and ventilation regimes," M.S., Department of chemistry, Clarckson University, Potsdam, 1996.

[25]   S. Johnson, Stephen Johnson on digital photography. Italy: O'Reilly, 2006.

[26]   *Manual for Image J*, National Institute of Health.

[27]   J.P. Holman, *Heat Transfer*, 8th ed. New York: McGraw-Hill, 1997.

[28]   G.W. Mulholland and C. Croarkin, "Specific extinction coefficient of flame generated smoke," *Fire and Materials*, vol. 24, 2000, pp. 227-230.

[29]   M. Janseens, "Calorimetry," in *SFPE Handbook of Fire protection Engineering*, Quincy, MA, 2002, pp. 3-38, 3-62.

[30]   M.Y. Choi, et al., "Comparisons of the soot volume fraction using gravimetric and light extinction techniques," *Combustion and Flame*, vol. 102, 1995, pp. 161-169.

[31]   D. Drysdale, *An Introduction to Fire Dynamics*, 2nd ed, Chichester: John Wiley & Sons, 1998.

APPENDIX A
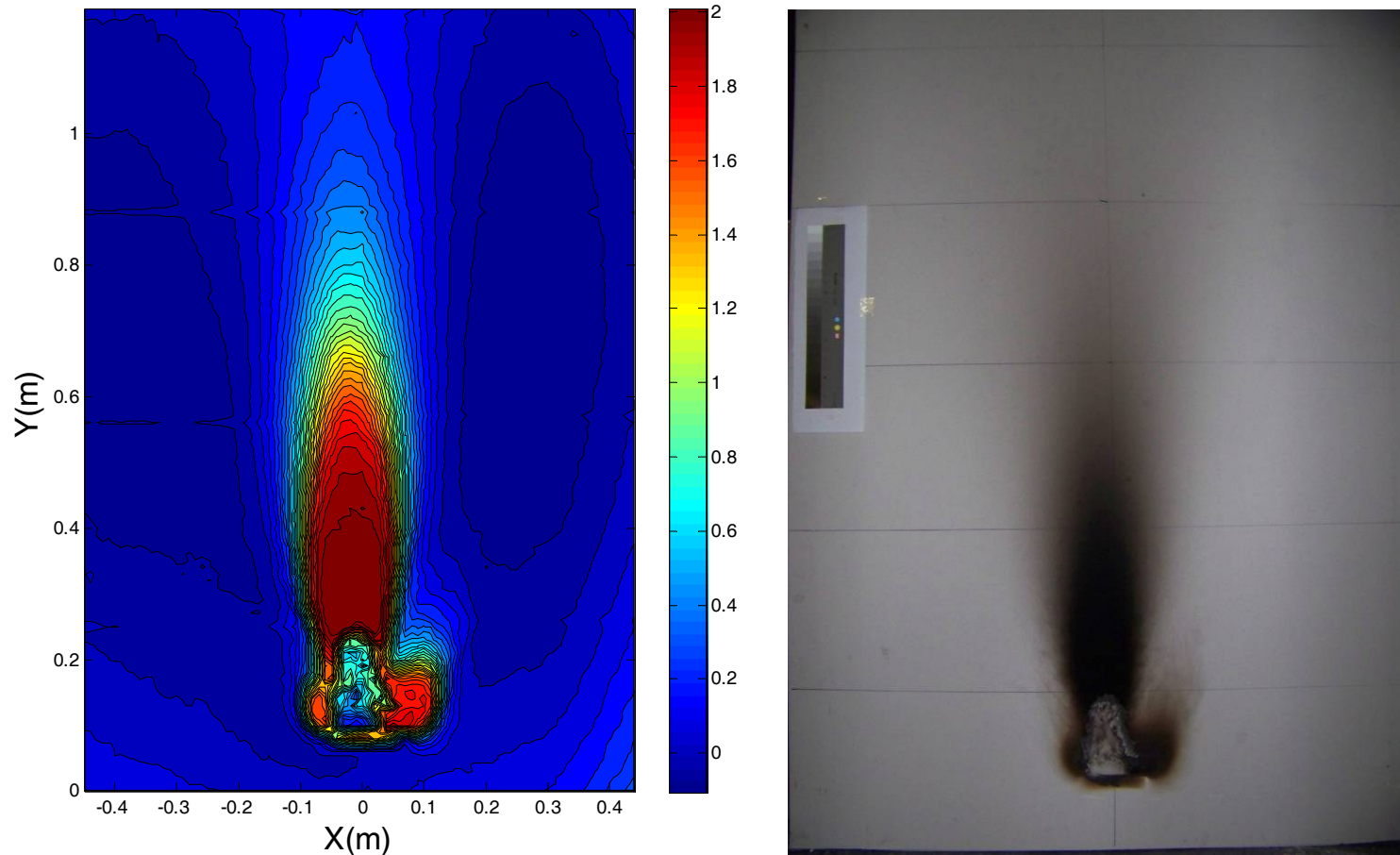
Figure A-1: 031210-T1, 4 x 4 PMMA (4400 seconds)
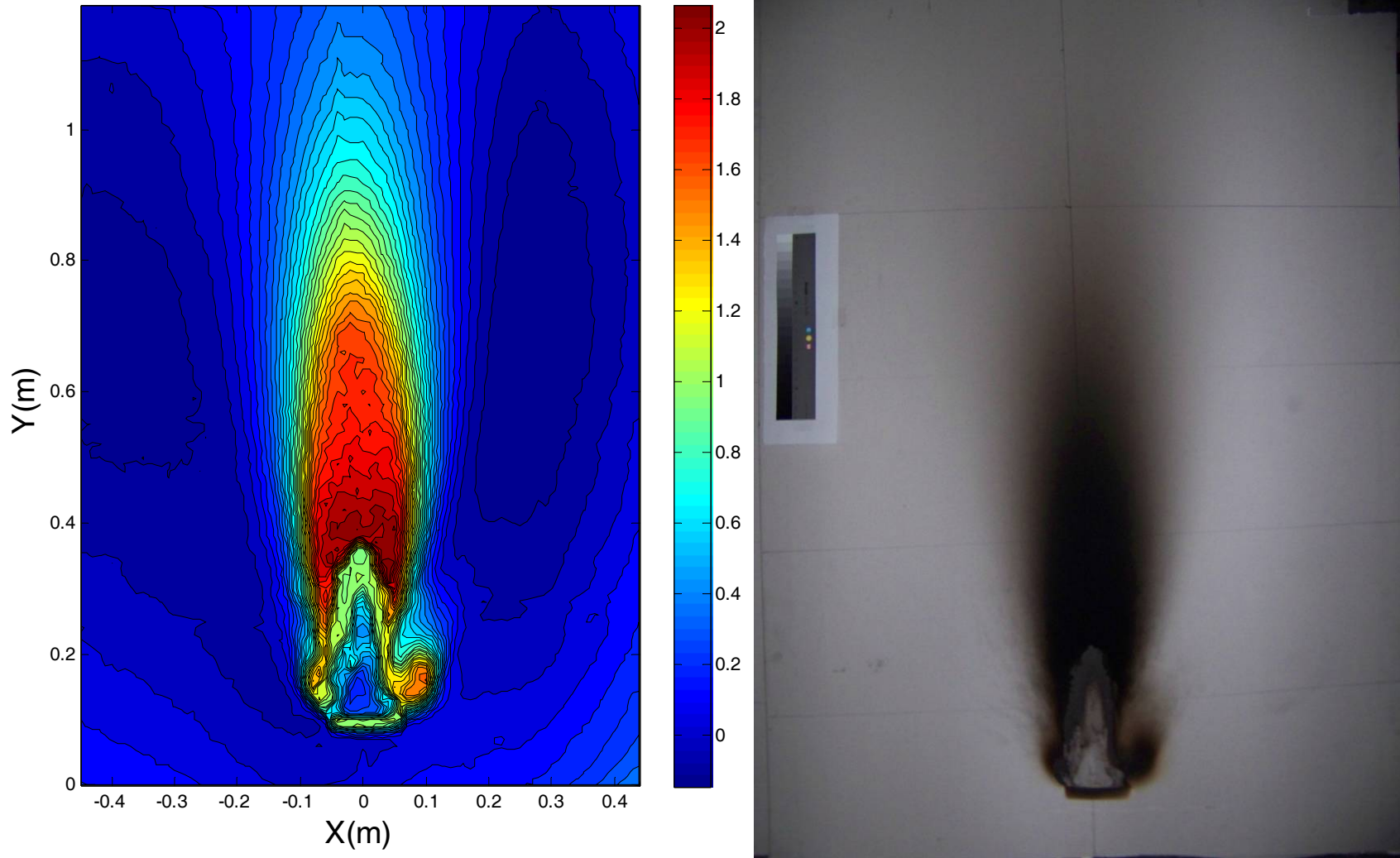
Figure A-2: 031210-T2, 4 x 4 PMMA (5400 seconds)
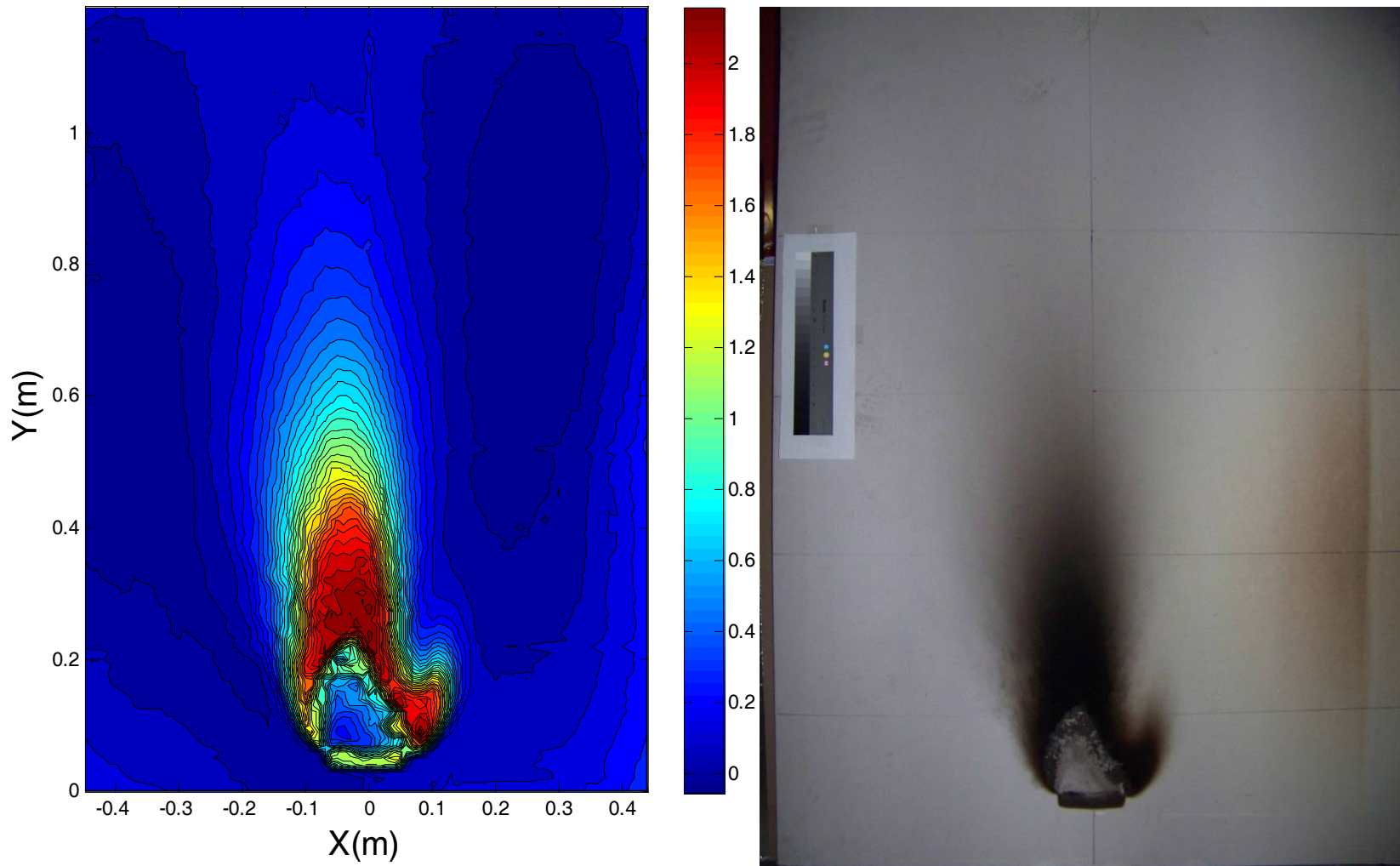
Figure A-3: 031210-T3, 4 x 4 PP (1600 seconds)
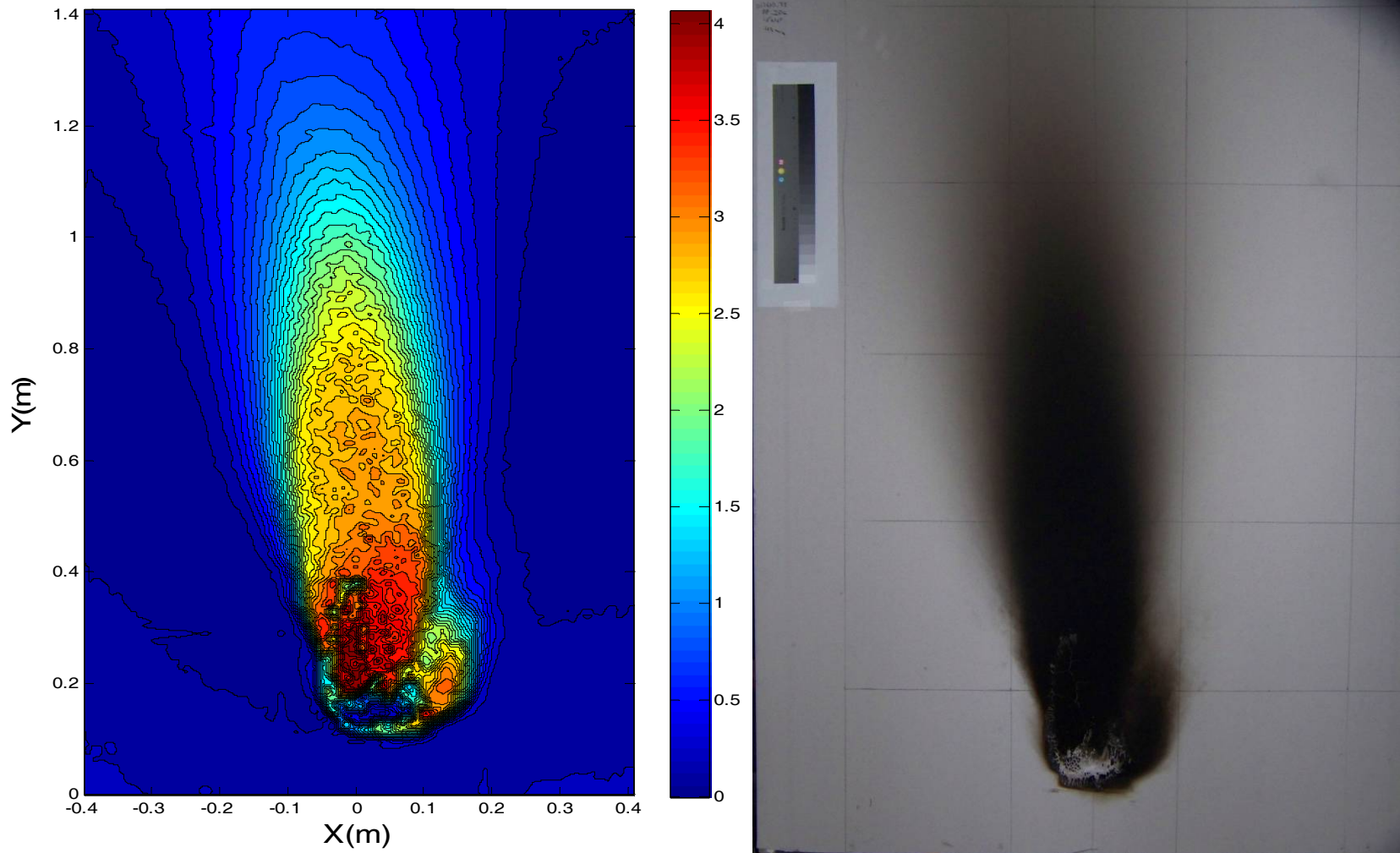
Figure A-4: 012610-T1, 4 x 4 PP (2400 seconds)
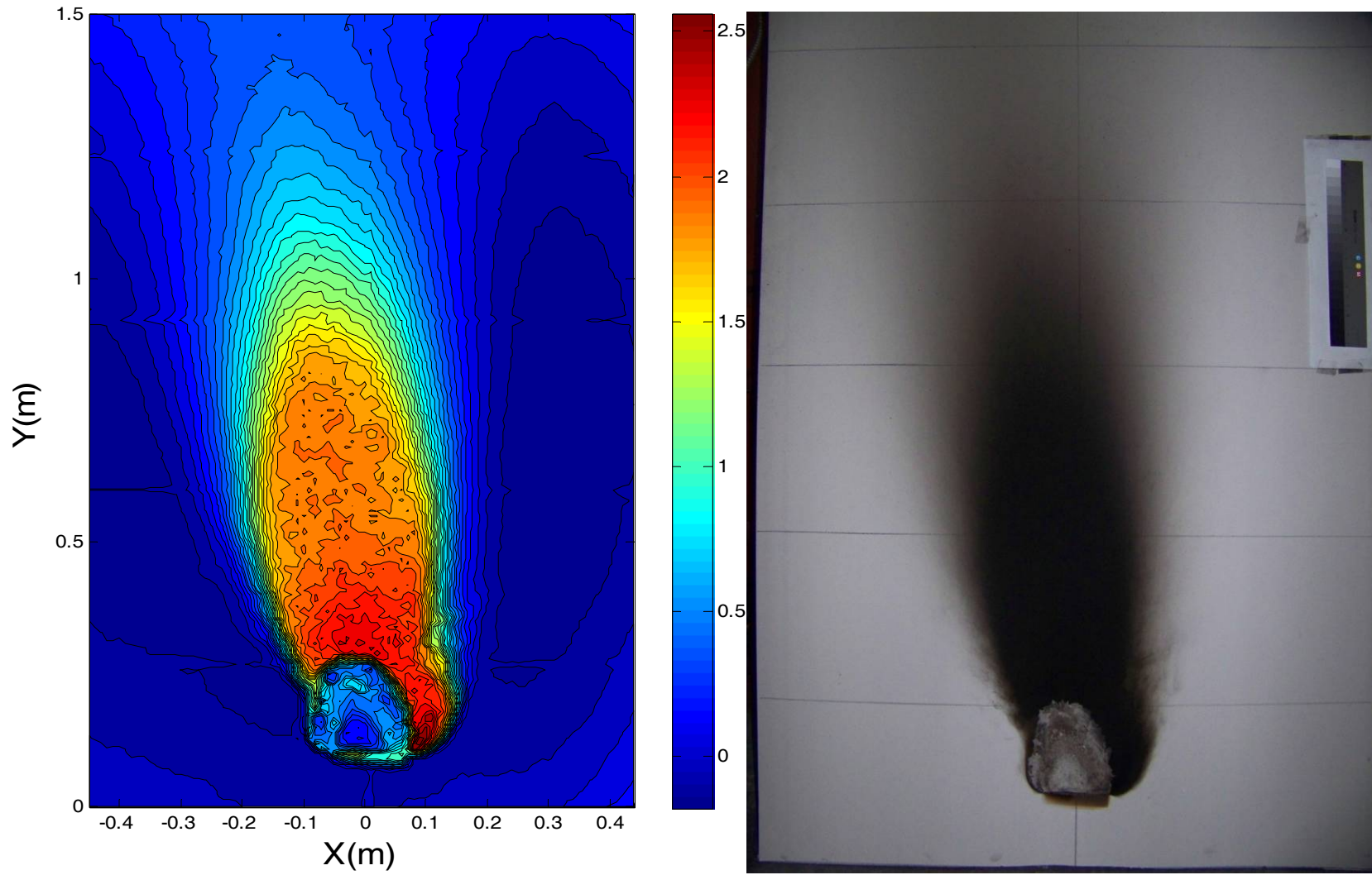
Figure A-5: 030810-T1, 4 x 4 ABS (1500 seconds)
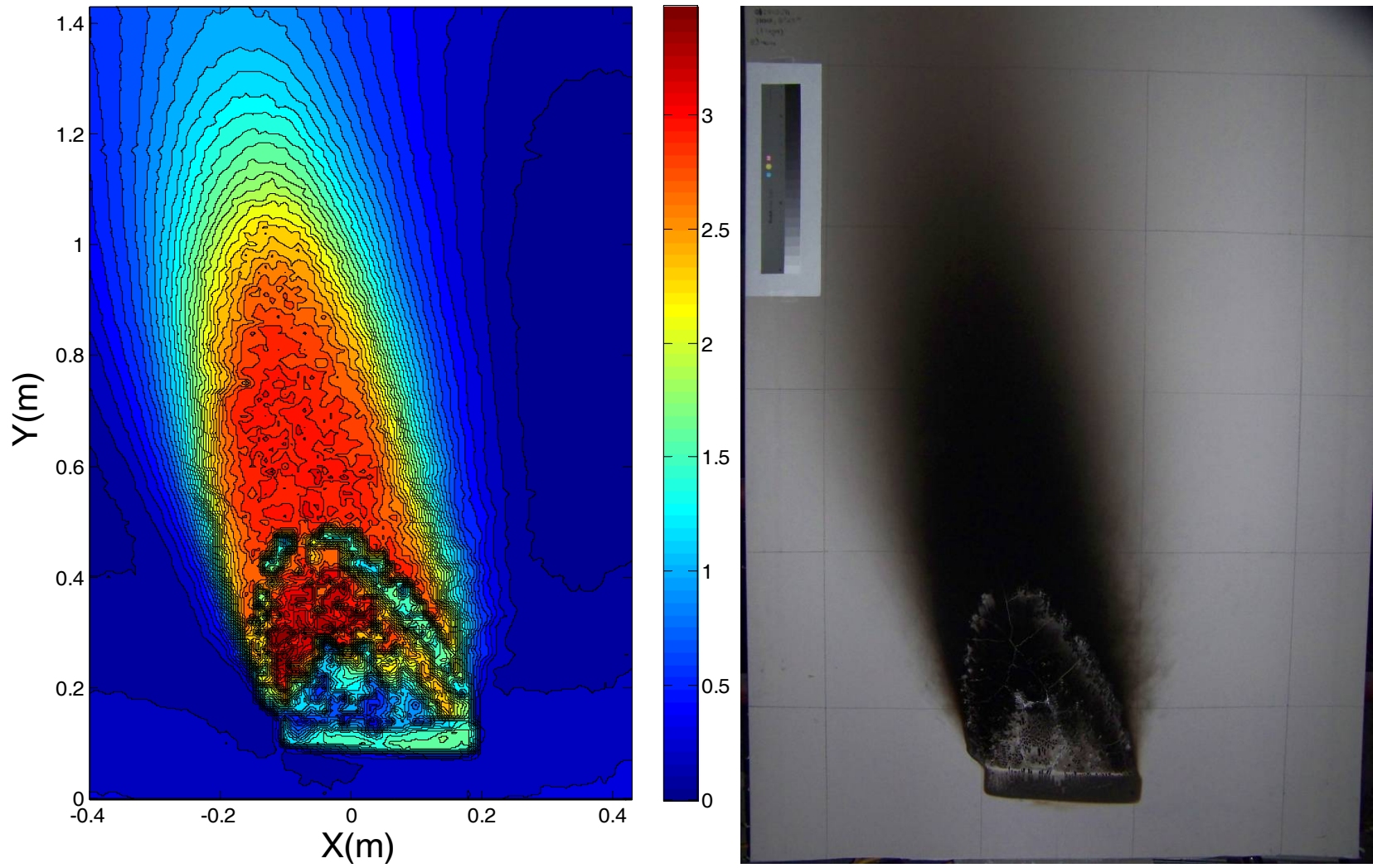
Figure A-6: 012710-T1, 8 x 8 PMMA (3000 seconds)
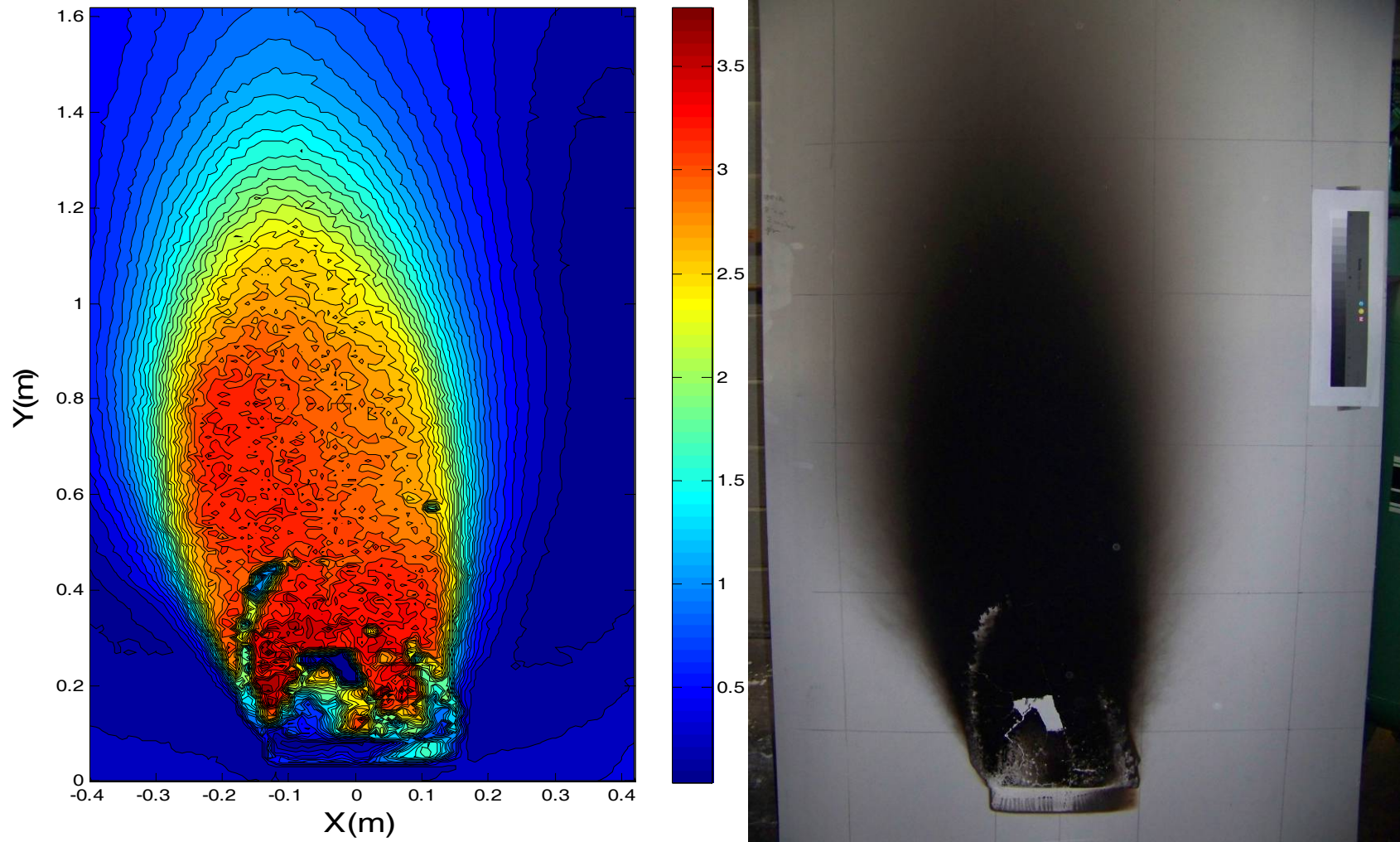
Figure A-7: 021110-T1, 8 x 8 PMMA (4500 seconds)
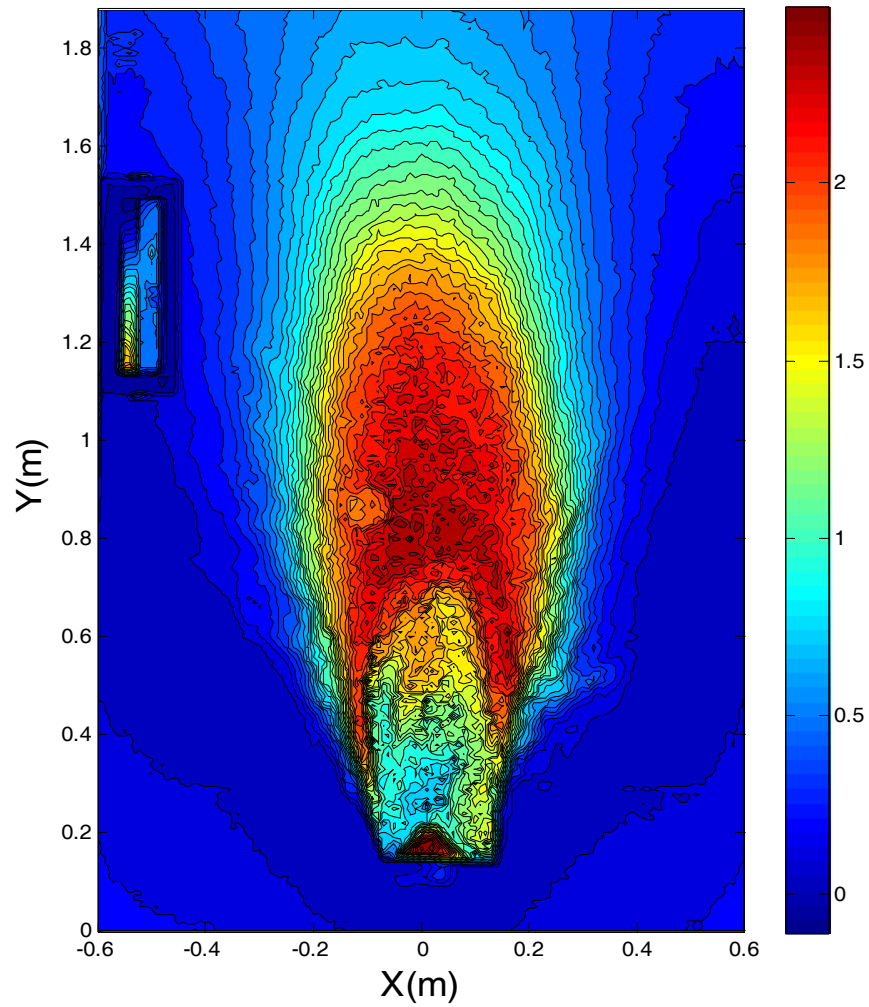
Figure A-8: 021810-T1, 8 x 8 gasoline (713 seconds)
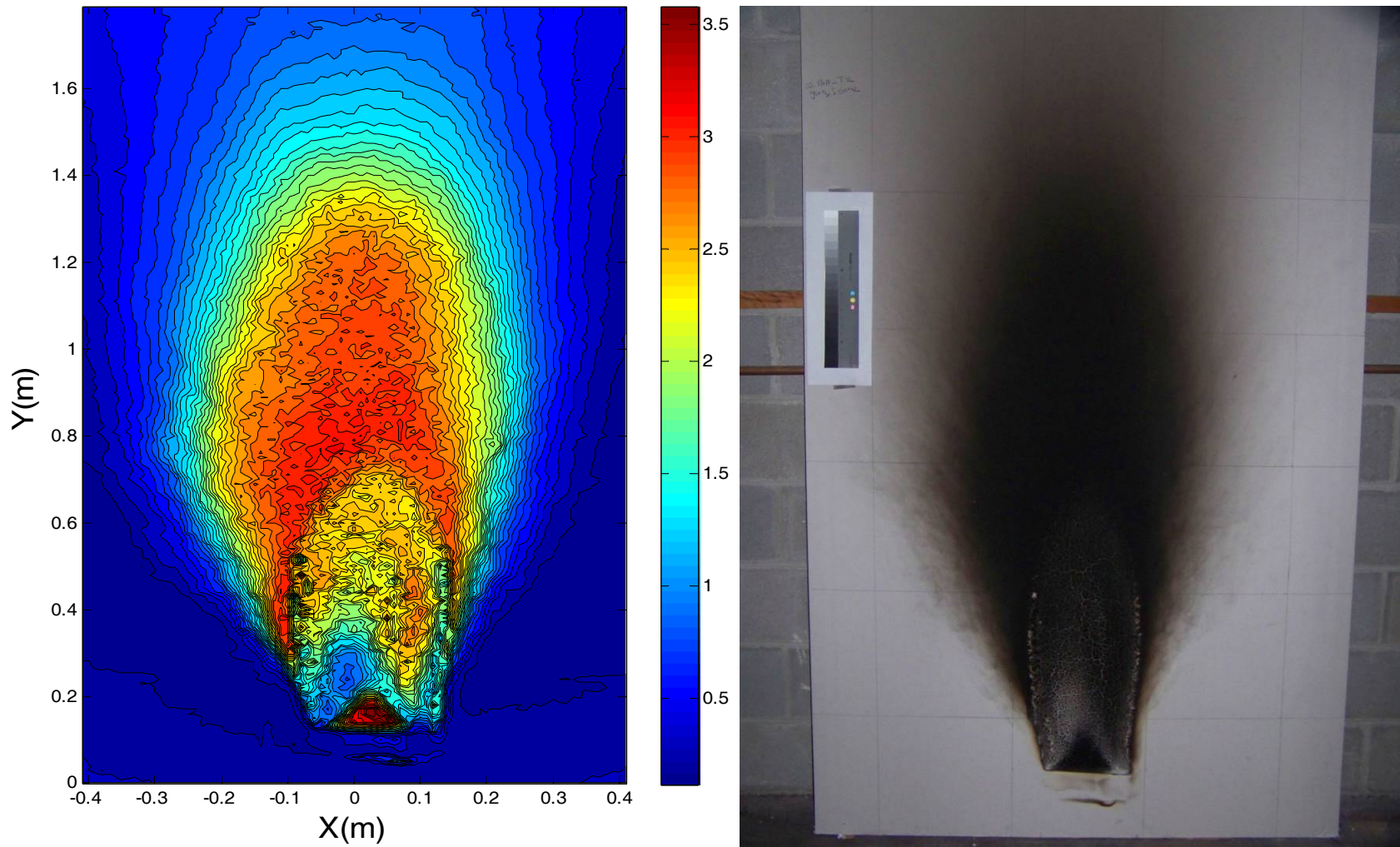
Figure A-9: 021810-T2, 8 x 8 gasoline (950 seconds)
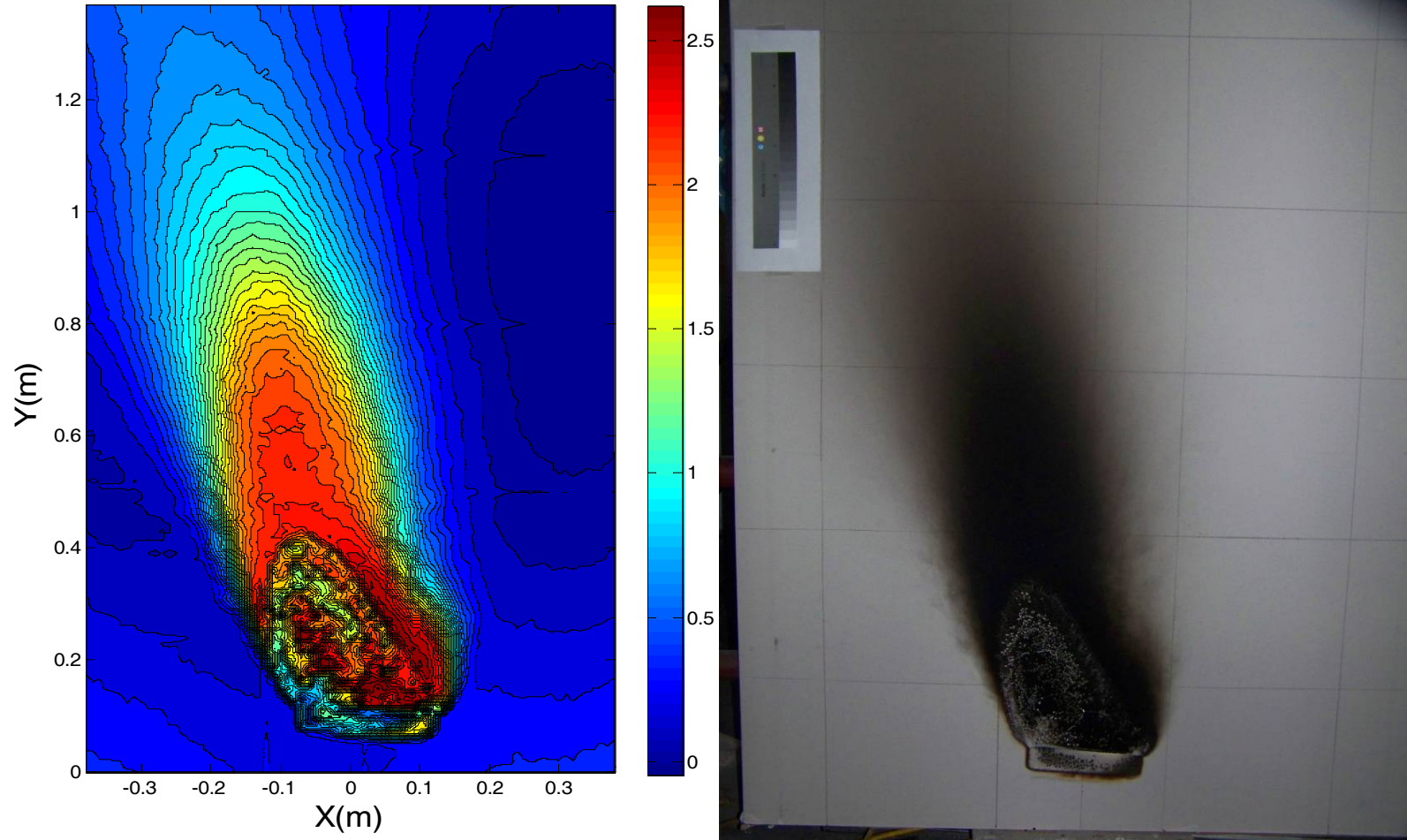
Figure A-10: 012710-T2, 8 x 8 PP (1700 seconds)
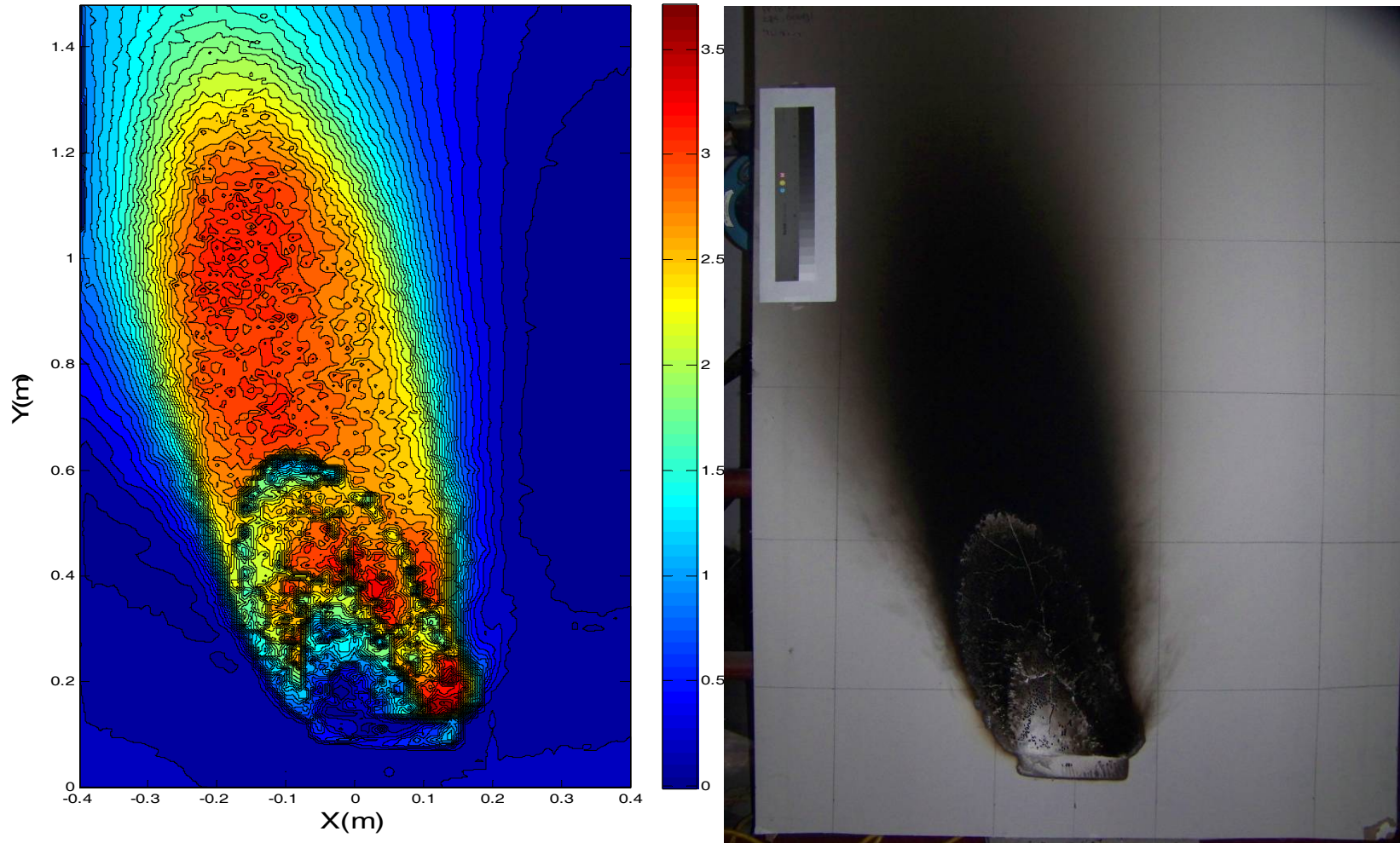
Figure A-11: 012810-T1, 8 x 8 PP (2400 seconds)
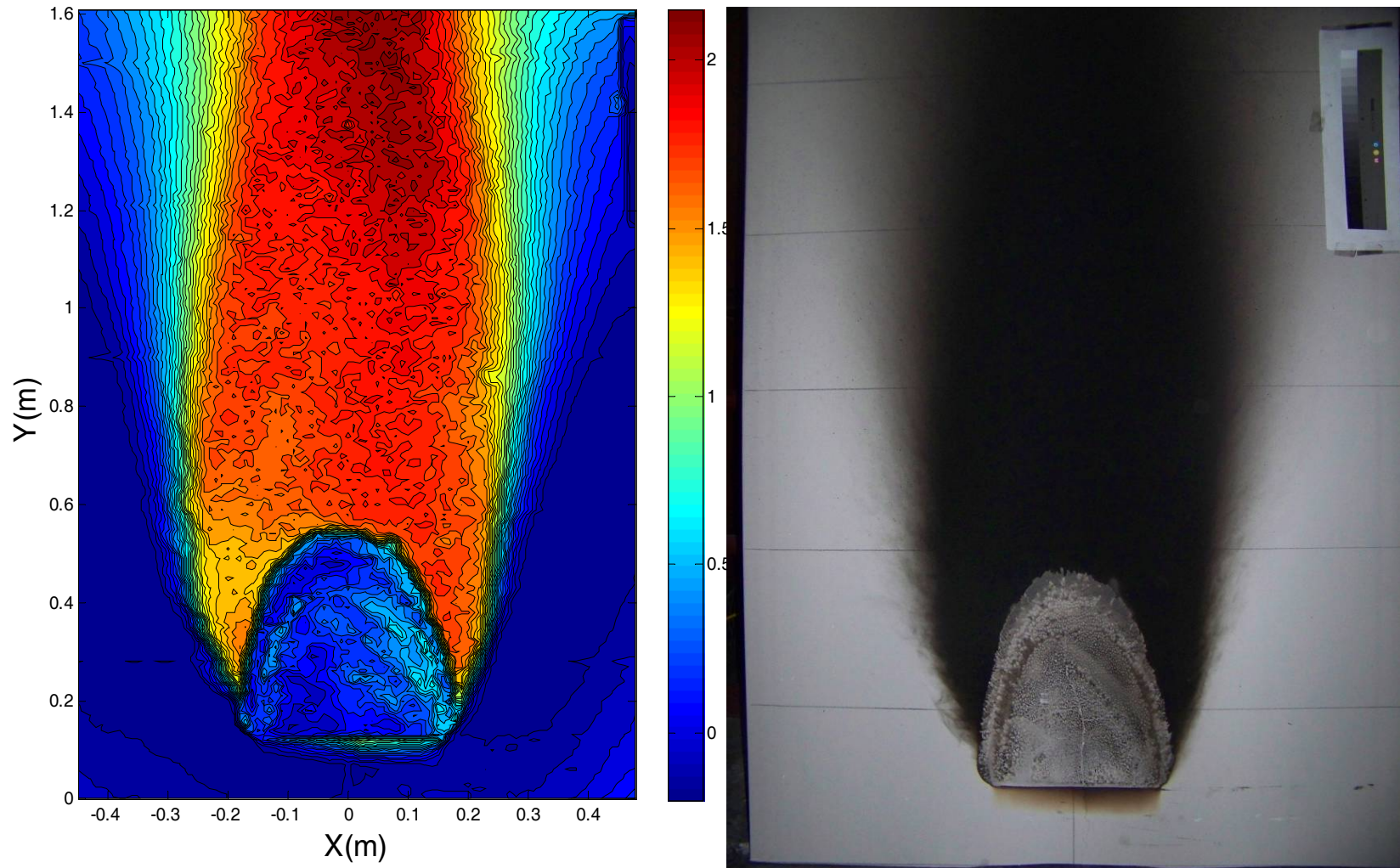
Figure A-12: 030810-T2, 8 x 8 ABS (1200 seconds)
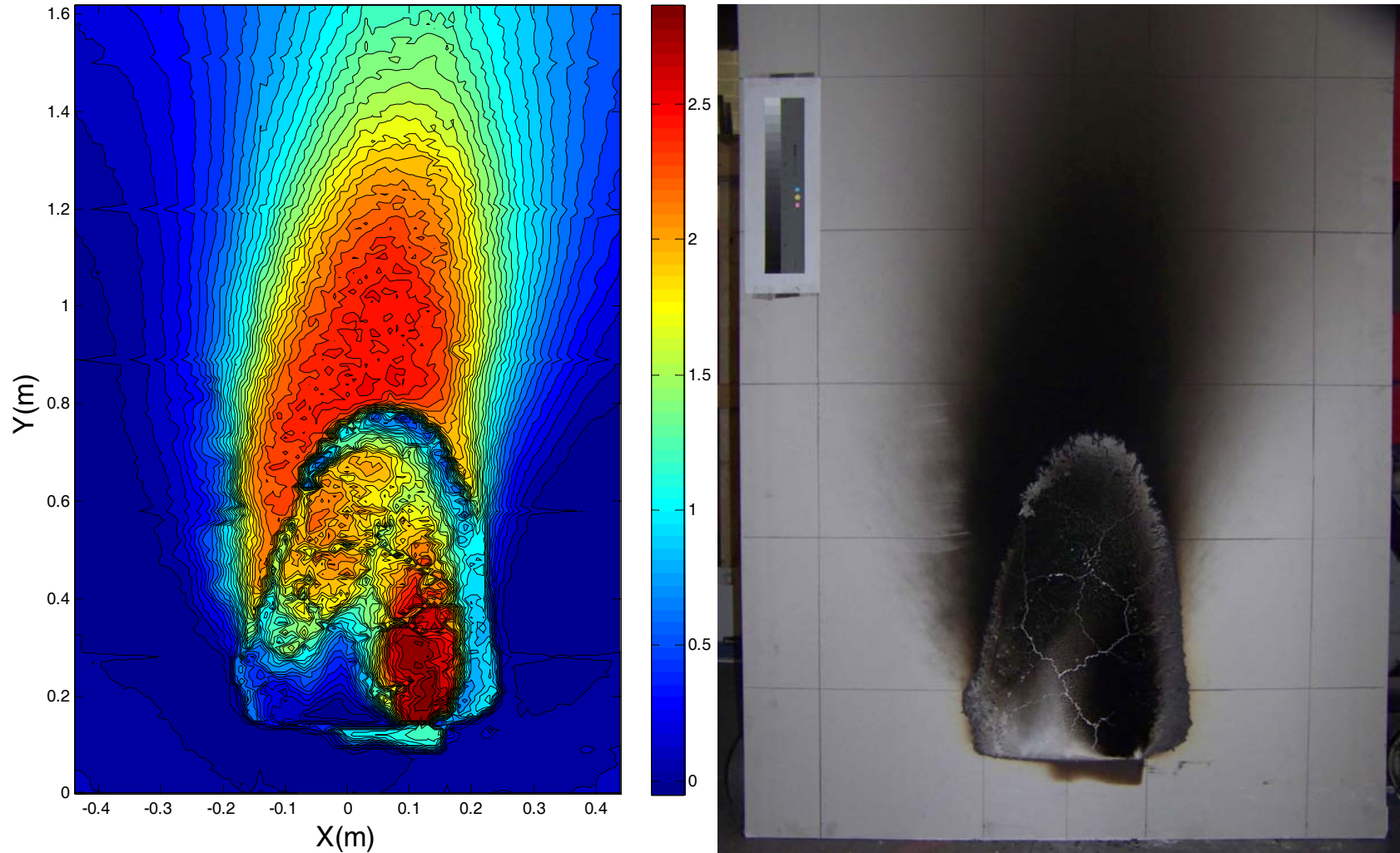
Figure A-13: 030510-T1, 12 x 12 PMMA (2700 seconds)
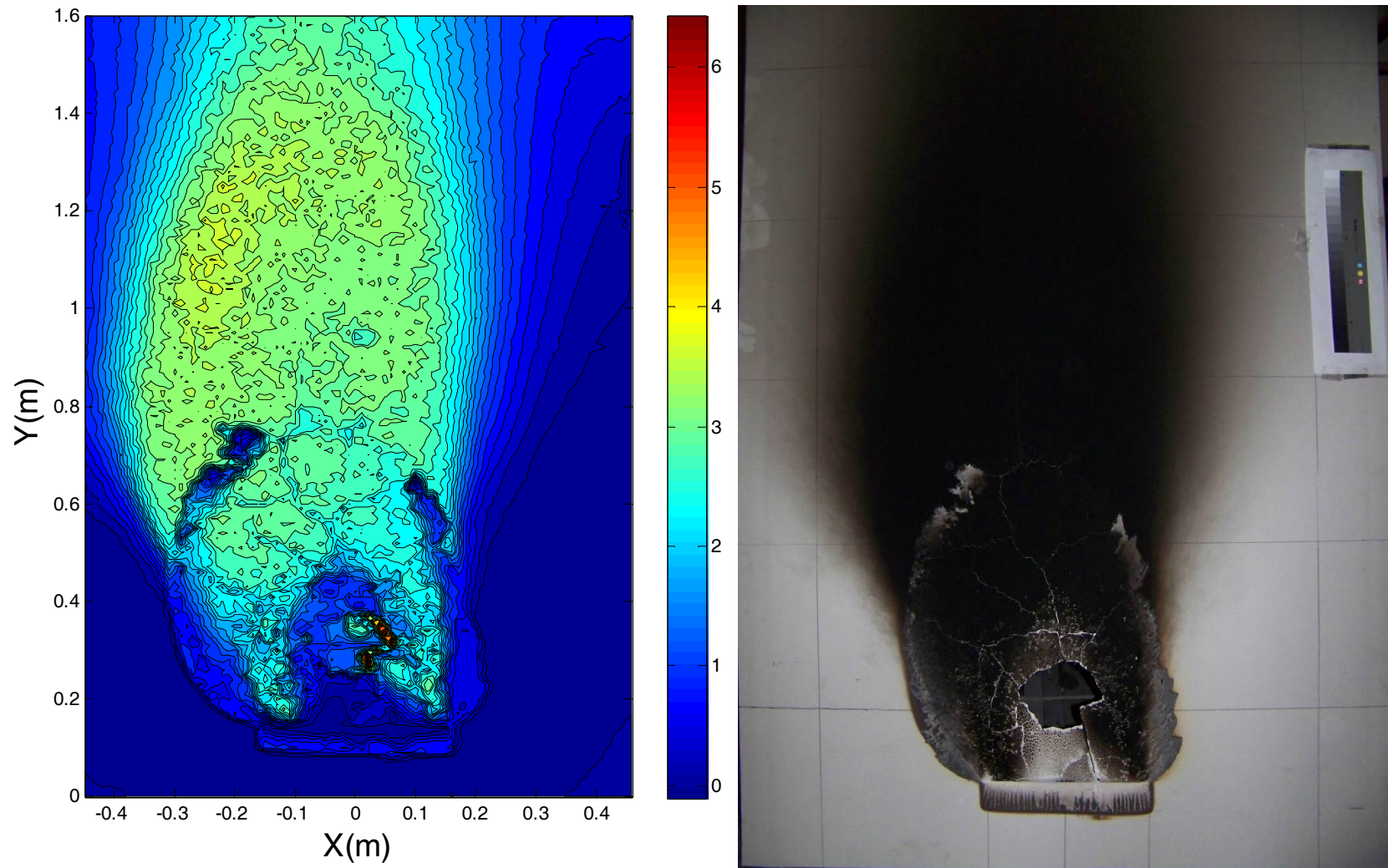
Figure A-14: 030510-T2, 12 x 12 PMMA (4400 seconds)
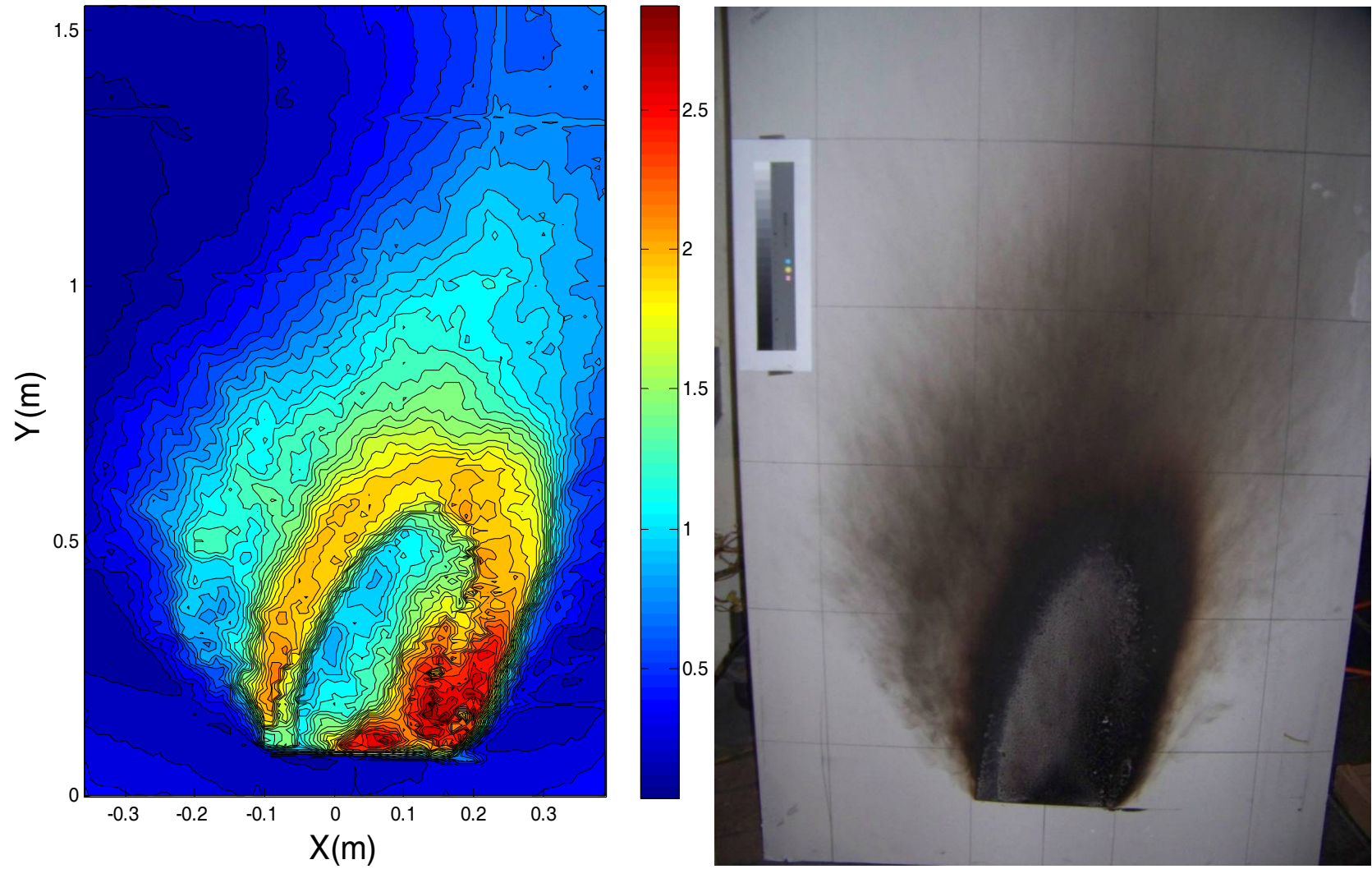
Figure A-15: 030310-T1, 12 x 12 gasoline (440 seconds)
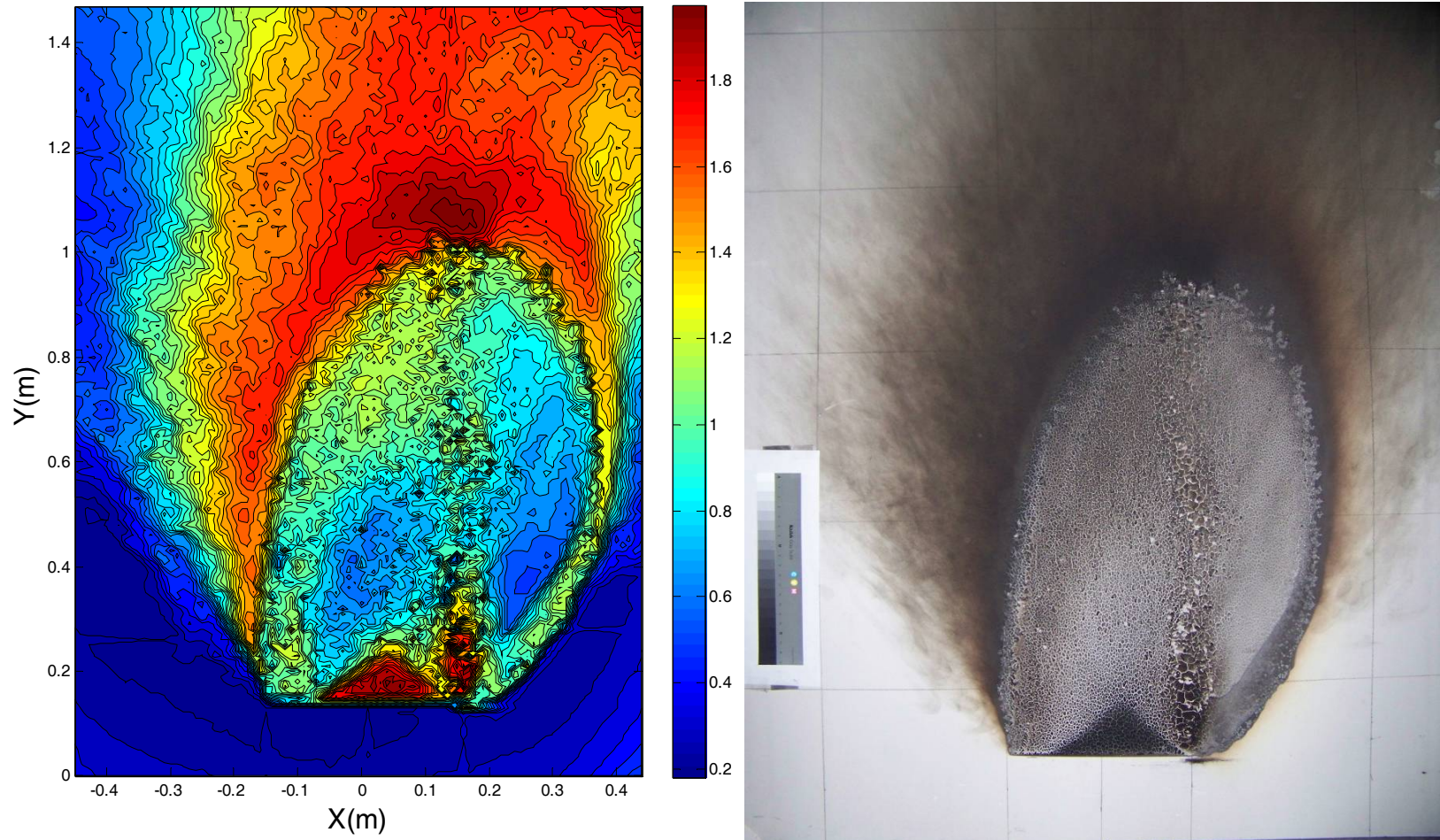
Figure A-16: 030310-T2, 12 x 12 gasoline (700 seconds)
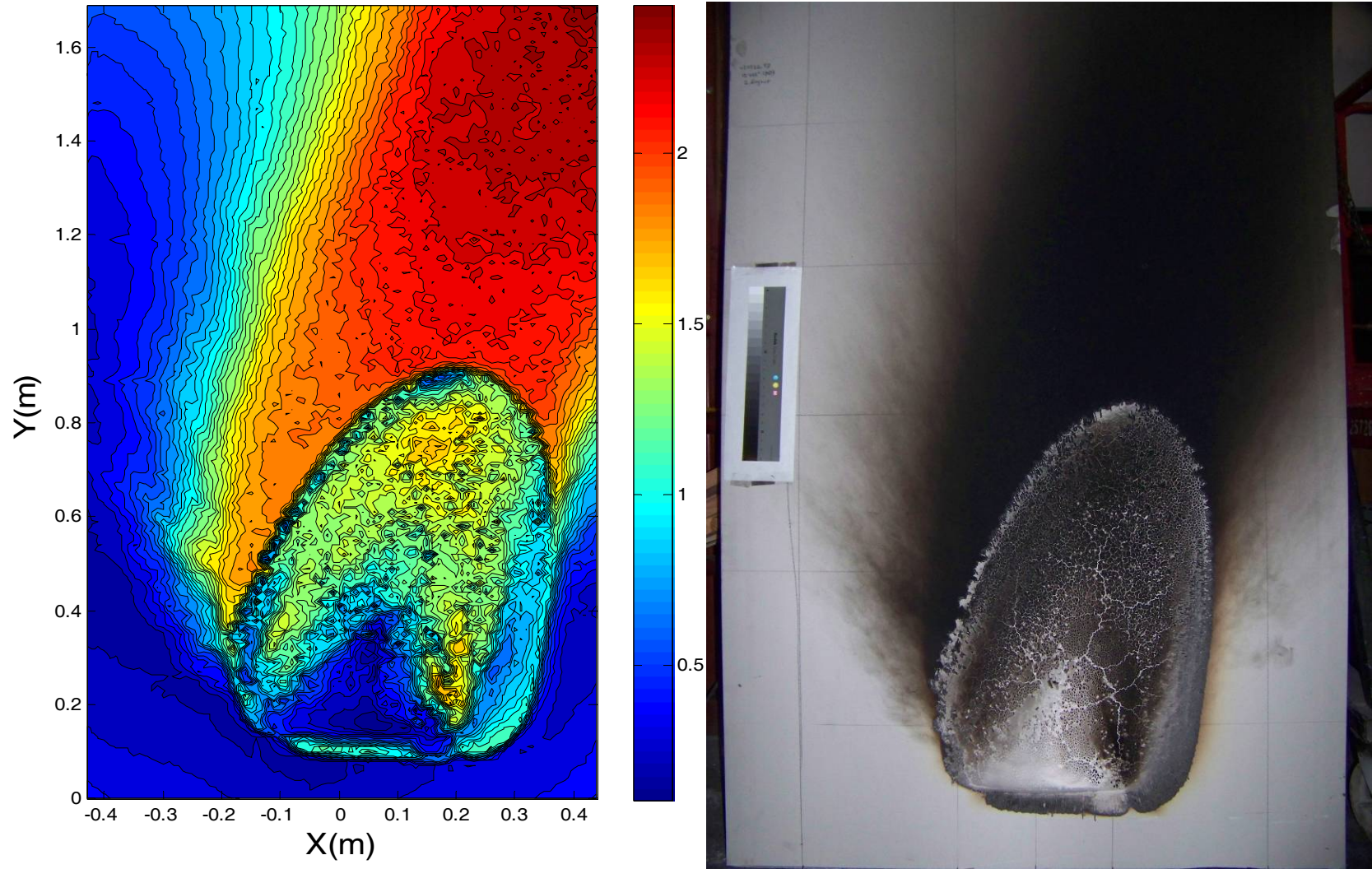
Figure A-17: 030310-T3, 12 x 12 PP (2100 seconds)
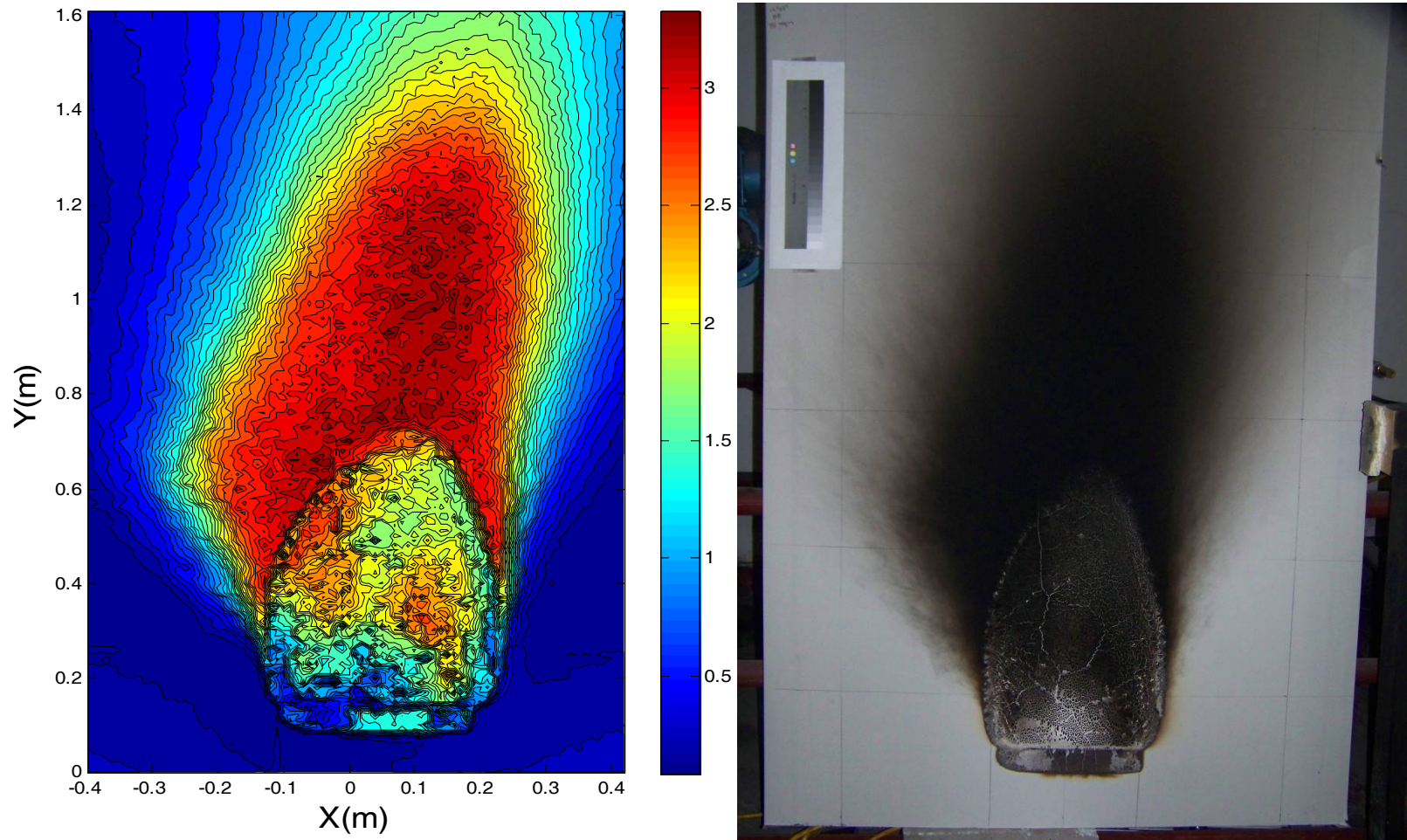
Figure A-18 : 020210-T1, 12 x 12 PP (2500 seconds)
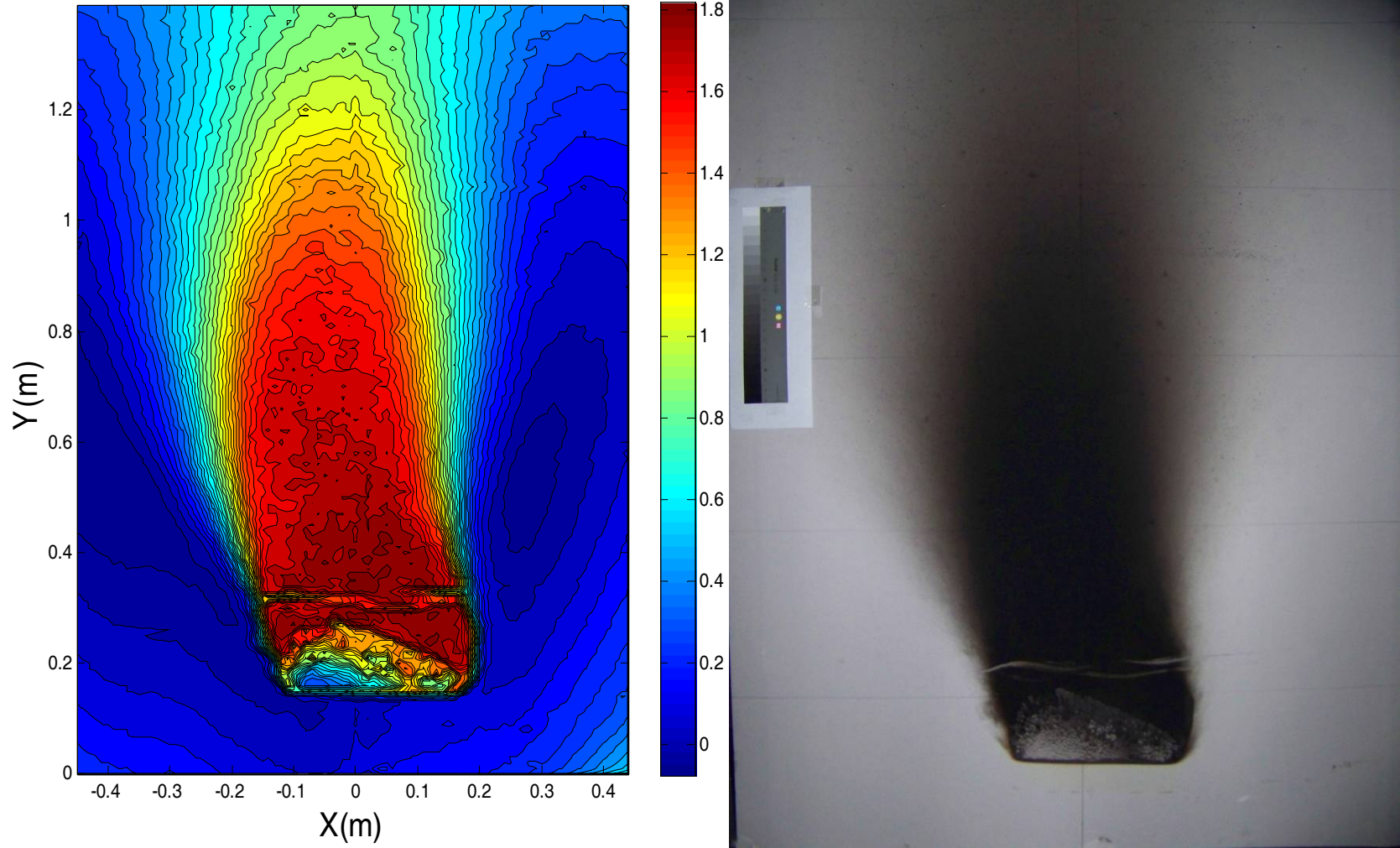
Figure A-19 : 031610-T2, 12 x 12 ABS (1000 seconds)

APPENDIX B –
CHEMICAL ANALYSIS OF FIRE SMOKES

Prof. JudithAnn Hartman
Department of Chemistry
U.S. Naval Academy
Annapolis, MD

B.1   Introduction

The chemical analyses of the fire smokes produced in this work were conducted to identify signatures of volatile organic carbons (VOC's) characteristic of the fuel that produced the smoke, and to characterize the smoke oxidation kinetics in support of prediction of the clean burn area of the smoke patterns.

B.2   Analytical Chemistry Methods

B.2.1 GC/MS Analysis

We analyzed the samples by extracting them into methanol for 30 minutes in a sonicator. Choroform and toluene were also used as the extraction solvent in some tests. After filtration, one microliter of the resulting extract was injected into the GC/MS apparatus. The NIST MS database was used to identify the chemical compounds.

B.2.2 Thermogravimetric Analysis (TGA)

Thermogravimetric analysis (TGA) was performed on a Thermal Analysis Model Q500 thermogravimetric analyzer. The instrument was calibrated with calcium oxalate. A representative soot sample of less than 3 mg was placed on an open platinum pan and heated from 80 to 750 °C using a linear heating rate of 10 K/min. Runs were conducted under dried air, 9.996% oxygen in nitrogen, or 1.996% oxygen in nitrogen with flow rates of 90 ml/min.

B.3   Chemical Analysis of Smoke

B.3.1   Soot from Full Scale Fire Experiments

In order to develop our chemical analysis protocol and results for the lab-generated soot, we analyzed soot samples from two full scale fire tests. Both tests were conducted in four compartment residential mockup. In the first test, the fuel was smoldering bedding. The second test was a flaming fire was started in the bedroom and spread to the kitchen full scale test. In both tests, samples were collected with methanol soaked cotton swabs in all four rooms from wallboard and glass surfaces. Interestingly, the samples from the smoldering test smelled strongly of smoke, while samples from the flaming test were essentially odorless (as were the samples we collected from the small-scale tests).

The results from the two tests were completely different from each other. The smoldering test resulted in dozens of organic chemicals in the GC/MS trace while the second test showed no detectable chemicals. The NIST MS database was used to identify the chemicals from the smoldering fire test and they were as expected (polyaromatic hydrocarbons and assorted functionalized aromatic compounds).

The results from the smoldering test confirm that we can find volatile organic chemicals in soot samples. The fact that no odor was detected in the samples from flaming test strongly suggests that we found no volatile organic chemicals in those samples because none were present. The major difference between the two tests is that the smoke in the first test was collected from smoldering bedding and the fire environment was relatively cool. The second test involved a flaming fire that spread from room to room so the soot was produced under much hotter conditions. It seems likely that volatile organics are not produced under these hotter flaming conditions.

B.3.2 Lab-generated Soot

The smoke from the combustion of ABS, fiberboard, gasoline, PMMA, and polypropylene was collected both from the wall mounted glass filters by mechanically pumping the hot gases through glass filter papers placed in the hot layer of the hood apparatus. No measurable quantities of any volatile organic chemicals (VOC's) were found in any of the samples, regardless of the fuel, sampling method, or extraction solvent. The absence of observable organic compounds suggests that the materials collected from the hood tests, like the smoke from the full scale flaming fire test described in the previous section, are primarily pure soot (inorganic carbon) that contains little condensed VOC's.

In order to confirm this hypothesis, the thermogravimetric analysis (TGA) data files for 21 tests were analyzed to look for volatile compounds (volatilization at 400 °C was used as the criteria for organic carbon). The TGA data for these tests showed less than 2% VOC's for ABS, gasoline, PMMA, and polypropylene, and 20% VOC's for the fiberboard. The kinetic parameters (Section 4) were consistent with this observation. They show that the smoke collected from burning ABS, gasoline, PMMA, and polypropylene all have an activation energy of combustion of approximately 224 kJ/mol (standard deviation = 17 kJ), thus indicating that the same product was produced in all fires. This activation energy is similar to that found by Ciambelli et al.[1] for amorphous carbon black (174 ± 13 kJ/mol) and by Stratakis et al.[2] for dry soot (190 ± 5 kJ/mol).

1. CiamBelli, P., Corbo P., Gambinbo, M., Palma, V., and Vaccaro, S. (1996), "Catalytic combustion of carbon particulate," *Catalysis Today*, **26** (1-2), pp. 99–106.
2. Stratakis, G.A. and Stamatelos, A.M. (2003), "Thermogravimetric analysis of soot emitted by a modern diesel engine run on catalyst-doped fuel," *Combustion and Flame*, **132** (1-2), pp. 157–169.

B.4   Kinetics of Smoke Oxidation

Arrhenius plots of the data were calculated based on the data between 10% and 90% decomposition as described below. The reaction of soot was assumed to be first order with respect to smoke mass, m, and nth order with respect to oxygen concentration (vol % oxygen).

$$-dm/dt = k \, m \, (Vol \, \%O_2)^n \quad \text{where } k = A \, e^{(-E/RT)}$$

If the concentration of oxygen is constant, this equation can be expressed as:

$$-dm/dt = A' \, e^{(-E/RT)} \, m$$

m: mass (g) of soot undergoing reaction

n: reaction order of oxygen

t: time (min)

k: specific rate constant

A: pre-exponential factor (1/s)

A': $A \, (Vol.\% \, O_2)^n$

E: activation energy

T: absolute temperature

R: molar gas constant

The logarithmic form of the equation in finite difference form gives:

$$Ln \, (-(\Delta m/\Delta t)/m) = ln \, A' - E/R(1/T)$$

E and A' are thus calculated from the linear regression of the plot of $Ln \, (-(\Delta m/\Delta t)/m)$ vs. 1/T. The Arrhenius constant (A) was calculated by analyzing data at different concentrations of oxygen (approximately 20%, 10%, and 2% oxygen).

B.5   Results

No difference was observed between the smoke oxidation from smokes produced from the different polymers. In all cases, less than 5% decomposition was observed for temperatures under 450 °C and in most cases less than 2% decomposition was observed. No change in shape of the curves was observed for the different oxygen concentrations, but the increased combustion

222

reaction rate caused by the increase in oxygen concentration let to a decrease in the temperature at 50% decomposition for the higher levels of oxygen. The 50% decomposition rates were approximately 600 °C for 20% oxygen, 625 °C for 10% oxygen, and 675 °C for 2% oxygen. Sample TGA results for PMMA samples run under the three different oxygen concentrations are shown in Figure B–1.
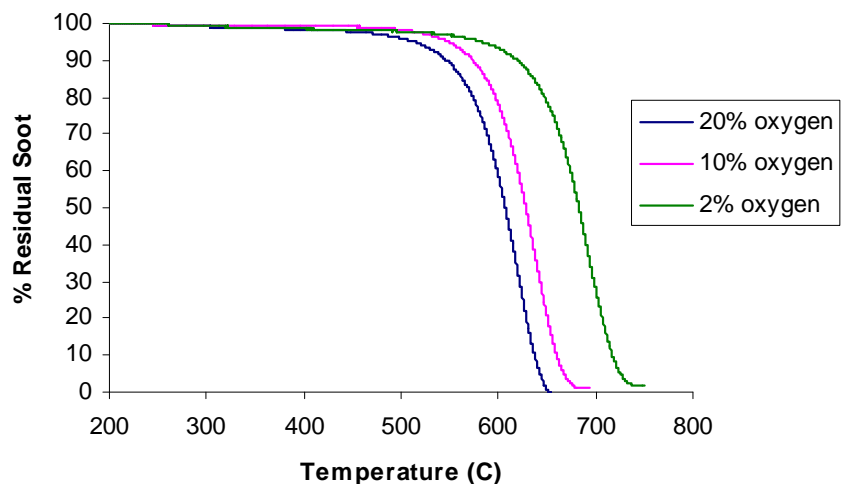
Figure B–1: TGA results for PMMA samples run under the three different oxygen concentrations

These data confirm the conclusion from the chemical analysis that the soot produced under our conditions contains essentially no VOC's. As a result, we were able to combine soot obtained from all of the fuels to calculate kinetic parameters. In total, eight runs were analyzed under each oxygen condition (duplicates runs for ABS, gasoline, PMMA, and PP) leading to a total of 24 experiments.

Although there have been many studies of soot oxidation, the observed kinetic equations have been found to vary widely, with activation energies ranging from 100 – 300 kJ/mol and the order of reaction of oxygen ranging from 0.6 – 1.[3] The magnitude of the activation energy depends on the composition of the soot, with flame soot having significantly higher activation

3. Kalogirou, M. and Samaras, Z. (2010), "Soot oxidation kinetics from TG experiments, Can they be reliably used in diesel particulate filter modeling tools?" *J. Ther. Anal. Calorim.*, **99**, pp. 1005–1010.

energy than diesel soot.[4] The order of the reaction with respect to oxygen appears to be dependent on the surface properties (i.e. site heterogeneity) of the soot and independent of the oxygen concentration during combustion.[5] In order to verify that the kinetic parameters for the combustion of soot generated under our conditions are independent of the oxygen concentration, we have analyzed all of the curves independently and averaged the results for each concentration of oxygen (Table B–1). The linear regressions for the PMMA data shown in Figure B-1 are summarized in Figure B–2 and the results for all of the experiments are summarized in Table B–1. The fact that the activation energies and the kinetic constants are within one standard deviation of each other confirms that the rate laws are not dependent on the concentration of oxygen and that we should be able to fit all 24 experiments together to get the most accurate kinetic constants.

Table B–1: Kinetic parameters from TGA data assuming a first order (n = 1) reaction with oxygen

Conditions	Activation Energy (Ea) ± Stand. Dev.	Pre-exponential Factor (A) ± Stand. Dev.
Air (20% oxygen)	224 ± 17 kJ/mol	$5.0 \times 10^{13} \pm 9 \times 10^{13}$ s−1
10% oxygen	230 ± 15 kJ/mol	$3.4 \times 10^{13} \pm 7 \times 10^{13}$ s−1
2% oxygen	240 ± 16 kJ/mol	$1.5 \times 10^{13} \pm 2 \times 10^{13}$ s−1

4. Kim, S. H., Fletcher, R. A., and Zachariah, M. R. (2005), "Understanding the difference in Oxidative Properties between Flame and Diesal Soot Nanoparticles: The Role of Metals," *Environ. Sci. Technol.*, **39**, pp. 4021–4026.
5. Hurt, R. H. and Haynes, B. S. (2005), "On the origin of power-law kinetics in carbon oxidation," *Proceedings of the Combustion Institute*, **30**, pp. 2161–2168.

PMMA soot in air
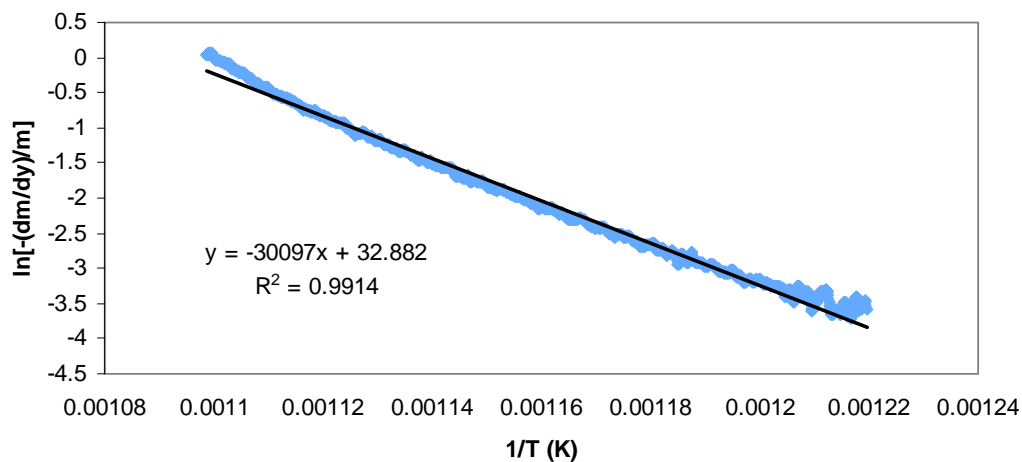
Figure B–2a: Linear regression analysis of PMMA soot combustion data in air. The data comprises 10% to 90% decomposition of the smoke.

PMMA soot 10% oxygen
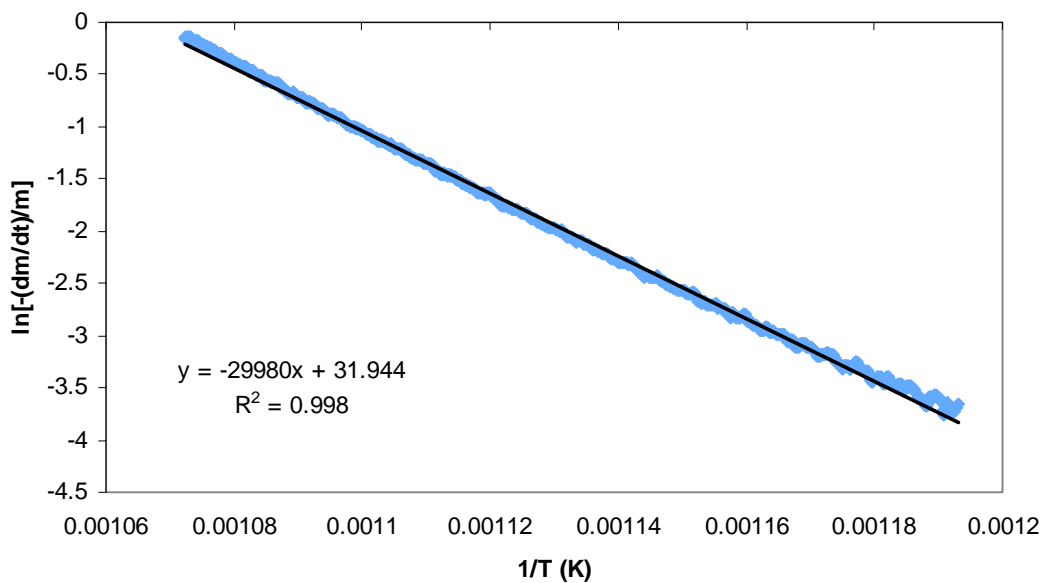
Figure B–2b: Linear regression analysis of PMMA soot combustion data in 10% oxygen concentration. The data comprises 10% to 90% decomposition of the smoke.

PMMA soot in 2% O2 121108_T2B
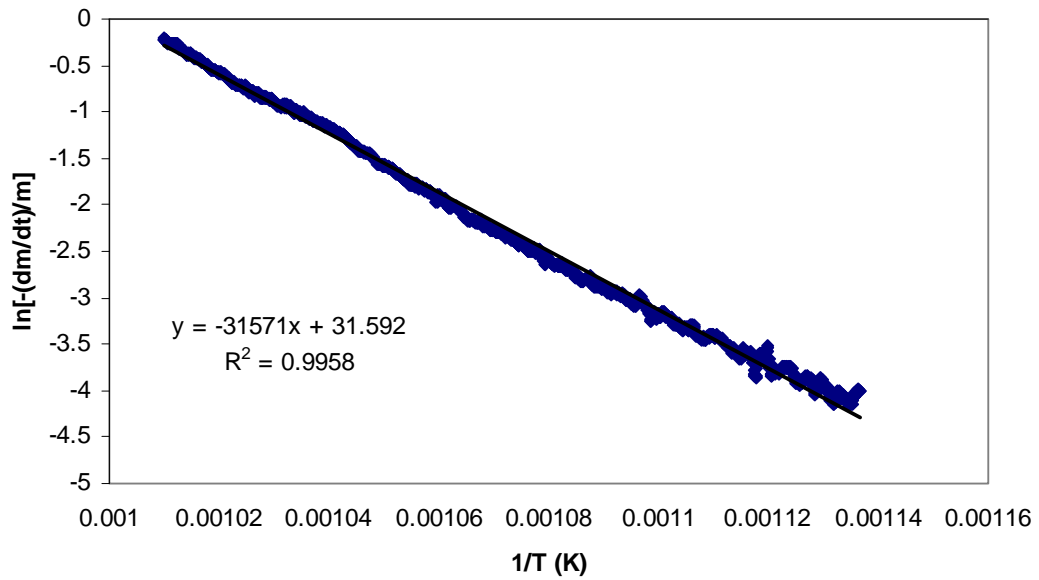
Figure B–2c: Linear regression analysis of PMMA soot combustion data in 2% oxygen concentration. The data comprises 10% to 90% decomposition of the smoke.

Kinetic parameters were calculated from fitting the combined data from all 24 experiments. Since the reaction order in oxygen for flame soot is poorly defined, we chose to fit the data using both the 0.83 as found by Du et al[6]. and 1.0 as found by Neeft et al.[7] A summary of the kinetic parameters are given in Table B–2 and the linear regressions are shown in Figure B–3.

Table B–2: Kinetic parameters from combined TGA data run under 20%, 10%, and 2% oxygen

Order of Oxygen	Activation Energy (Ea)	Pre-exponential Factor (A)	R^2 of fit
0.83	194 kJ/mol	$6.2 \times 10^9 \ s^{-1}$	0.879
1.0	211 kJ/mol	$4.7 \times 10^{10} \ s^{-1}$	0.971

Oxygen order of 0.83

$$y = -23273x + 22.543$$
$$R^2 = 0.9484$$
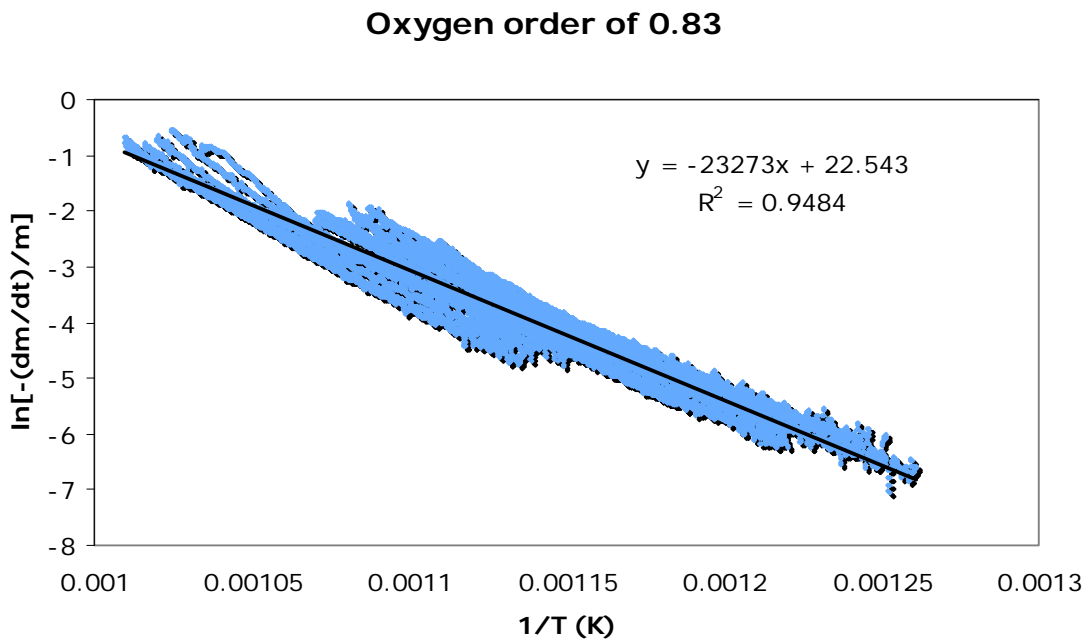
Figure B–3a: Linear regression analysis of smoke combustion data in air, 10%, and 2% oxygen concentrations for n=0.83. The data comprises 10% to 90% decomposition of the smoke.

6.   Du, Z., Sarofim, A. F., Longwell, J.P., and Mims, C. A. (1991), "Kinetic Measurement and Modeling of Carbon Oxidation" *Energy & Fuels*, **5**, pp. 214-221.
7.   Neeft, J. P. A., Nijhuis, T. X.,Smakman, E., Makkee, M., and Moulijn, J. A. (1997), "Kinetics of the oxidation of diesel soot" *Fuel*, **12**, pp. 1129-1136.

Oxygen order of 1.0
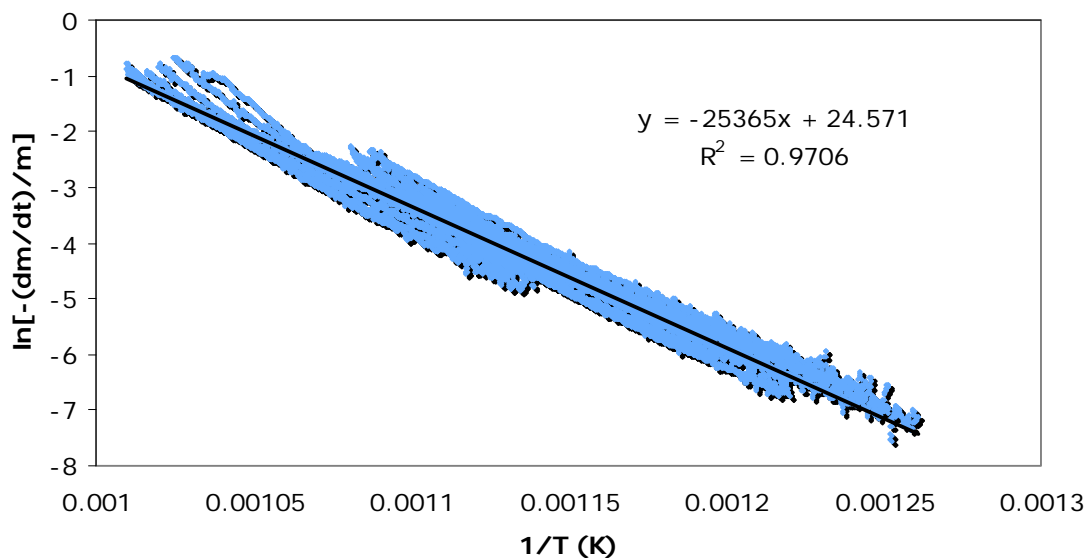
Figure B–3b: Linear regression analysis of smoke combustion data in air, 10%, and 2% oxygen concentrations for n=1. The data comprises 10% to 90% decomposition of the smoke.

The Figure B–3 shows that our data can be fit adequately using an oxygen reaction order of either 0.83 or 1.00, but an order of 1 appears to represent the better fit. This reaction order is on the high end of that typically observed[5] and is consistent with complete oxidation of the soot according to Du et al.[6] who determined that the experimental order of reaction was 0.77 for CO release and 1.0 for CO_2 release. The observed activation energies are also on the high side of observed values since most values are found to be between 140 and 210 kJ/mol.[2,8]

We have modeled these kinetic parameters as part of a larger project to be able to use soot patterns in the forensic analysis of fires. As a result, it is useful to use the parameters to calculate the half life of soot at different temperatures. The half life ($t_{1/2}$) of first order processes is related to the rate constant (k) by the expression $t_{1/2}$ = Ln 2/k. The relationship between half life and

---

8. Stanmore, B. R., Brilhac, J. F., and Gilot, P. (2001), "The oxidation of soot: a review of experiments, mechanisms, and models" *Carbon*, **39**, pp. 2247-2268.

temperature is summarized in Figure B–4. It can be seen that the smoke half life is very short at temperatures characteristic of the flame region.
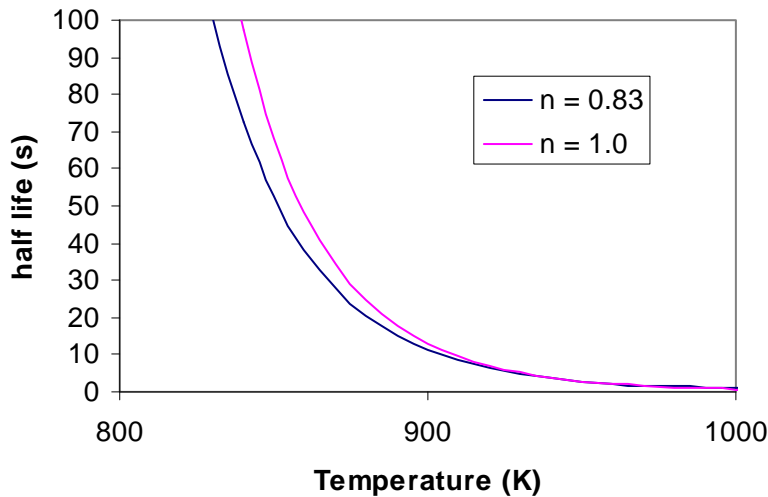
Figure B–4: Calculated half life of soot at 2% oxygen.

B.6   Conclusions

It was found that smokes from flaming fires are very dry, including negligible amounts of VOC's. As such, it is not possible to identify smoke VOC fingerprints that identify the fuel from which the smoke was produced.

Kinetic studies of the various smokes from flaming fires showed that the smokes were identical in terms of oxidation kinetics. Kinetics are consistent with the clean burn patterns found in the wall experiments.